

==== California ====

Cooperative Oceanic
Fisheries Investigations

==== Reports ====

VOLUME 60

DECEMBER 2019

**CALIFORNIA
COOPERATIVE
OCEANIC
FISHERIES
INVESTIGATIONS**

Reports

VOLUME 60
JANUARY 1 TO DECEMBER 31, 2019

Cooperating Agencies:

CALIFORNIA DEPARTMENT OF FISH AND WILDLIFE
UNIVERSITY OF CALIFORNIA, SCRIPPS INSTITUTION OF OCEANOGRAPHY
NATIONAL OCEANIC AND ATMOSPHERIC ADMINISTRATION, NATIONAL MARINE FISHERIES SERVICE

CALCOFI COORDINATOR John N. Heine
EDITOR John N. Heine

This report is not copyrighted, except where otherwise indicated, and may be reproduced in other publications provided credit is given to California Cooperative Oceanic Fisheries Investigations and to the author(s). Inquiries concerning this report should be addressed to CalCOFI Coordinator, Scripps Institution of Oceanography, La Jolla, CA 92038-0218.

EDITORIAL BOARD

John N. Heine
Brice Semmens

Printed and distributed December 2019, La Jolla, California
ISSN 0575-3317

CONTENTS

Scientific Contributions

State of the California Current 2018-19: a Novel Anchovy Regime and a New Marine Heat Wave? <i>Andrew R. Thompson, Isaac D. Schroeder, Steven J. Bograd, Elliott L. Hazen, Michael G. Jacox, Andrew Leising, Brian K. Wells, Jennifer Fisher, Kym Jacobson, Samantha Zeman, Eric Bjorkstedt, Roxanne R. Robertson, Mati Kahru, Ralf Goericke, Clare E. Peabody, Tim Baumgartner, Bertha E. Lavaniegos, Luis E. Miranda, Eliana Gomez-Ocampo, Jose Gomez-Valdes, Toby Auth, Elizabeth A. Daly, Cheryl A. Morgan, Brian J. Burke, John C. Field, Keith M. Sakuma, Edward D. Weber, William Watson, Jessica M. Porquez, Jane Dolliver, Don Lyons, Rachel A. Orben, Jeannette E. Zamon, Pete Warzybok, Jaime Jahncke, Jarrod A. Santora, Sarah Ann Thompson, Brian Hoover, William Sydeman, and Sharon R. Melin.</i>	1
Modeling Growth of the Pacific Sardine, <i>Sardinops caeruleus</i> , in the Gulf of California, Mexico, Using the Multimodel Inference Approach. <i>Manuel Otilio Nevárez-Martínez, Edgar Arnaldo Arzola-Sotelo, Juana López-Martínez, José Pablo Santos-Molina, María De Los Angeles Martínez-Zavala.</i>	66
Dynamic Habitat Use of Albacore and Their Primary Prey Species in the California Current. <i>Barbara Muhling, Stephanie Brodie, Owyn Snodgrass, Desiree Tommasi, Heidi Dewar, John Childers, Michael Jacox, Christopher Edwards, Yi Xu, Stephanie Snyder</i>	79
Distribution of Pelagic Thaliaceans, <i>Thetys vagina</i> and <i>Pyrosoma atlanticum</i> , During a Period of Mass Occurrence within the California Current. <i>Rebecca R. Miller, Jarrod A. Santora, Toby D. Auth, Keith M. Sakuma, Brian K. Wells, John C. Field, Richard D. Brodeur.</i>	94
Spatial Patterns in Nearshore Juvenile Fish Abundance throughout the California Network of Marine Protected Areas as Revealed by Seabird Foraging Rates. <i>Dan P. Robinette, Nadav Nur, Jaime Jahncke</i>	109
Rearing and Inducing Spawning in Captive Pacific Sardine (<i>Sardinops sagax</i>). <i>Emmanis Dorval, Beverly Macewicz, Patrick Appel, Megan Human, William Watson</i>	123
Instructions to Authors	135
CalCOFI Basic Station Plan	137

SCIENTIFIC CONTRIBUTIONS

STATE OF THE CALIFORNIA CURRENT 2018–19: A NOVEL ANCHOVY REGIME AND A NEW MARINE HEAT WAVE?

ANDREW R. THOMPSON*

National Marine Fisheries Service
Southwest Fisheries Science Center
8901 La Jolla Shores Drive
La Jolla, CA, 92037-1509
andrew.thompson@noaa.gov

ISAAC D. SCHROEDER^{1,2},
STEVEN J. BOGRAD¹, ELLIOTT L. HAZEN¹,
MICHAEL G. JACOX^{1,3}, ANDREW LEISING¹,
AND BRIAN K. WELLS⁴

¹Southwest Fisheries Science Center
National Marine Fisheries Service
99 Pacific Street, Suite 255A
Monterey, CA 93940-7200

²Institute of Marine Sciences
University of California
Santa Cruz, CA

and
Southwest Fisheries Science Center
NOAA
Monterey, CA

³Earth System Research Laboratory
NOAA
Boulder, CO 80305

⁴Southwest Fisheries Science Center
National Marine Fisheries Service
NOAA
Santa Cruz, CA 95064

JOHN LARGIER

Bodega Bay Marine Laboratory
University of California, Davis
Bodega Bay, CA 94923

JENNIFER L. FISHER^{1,2},
KYM C. JACOBSON², AND
SAMANTHA M. ZEMAN¹

¹Cooperative Institute for
Marine Resources Studies
Oregon State University
Hatfield Marine Science Center
Newport, OR 97365

²Northwest Fisheries Science Center
Hatfield Marine Science Center
Newport, OR 97365

ERIC P. BJORKSTEDT¹ AND
ROXANNE R. ROBERTSON²

¹Southwest Fisheries Science Center
National Marine Fisheries Service
NOAA
Santa Cruz, CA 95064

²Cooperative Institute for
Marine Ecosystems and Climate
Humboldt State University

MATI KAHRU
AND RALF GOERICKE

Scripps Institution of Oceanography
University of California, San Diego
La Jolla, CA 92093

CLARE E. PEABODY

National Marine Fisheries Service
Southwest Fisheries Science Center
8901 La Jolla Shores Drive
La Jolla, CA 92037-1509

TIMOTHY R. BAUMGARTNER,
BERTHA E. LAVANIEGOS,
LUIS E. MIRANDA,
ELIANA GOMEZ-OCAMPO,
AND JOSE GOMEZ-VALDES

Oceanology Division
Centro de Investigación Científica y
Educación Superior de Ensenada
Carretera Ensenada-Tijuana No. 3918
Zona Playitas C.P. 22860
Ensenada, Baja California, Mexico

TOBY D. AUTH¹,
ELIZABETH A. DALY²,
CHERYL A. MORGAN², AND
BRIAN J. BURKE³

¹Pacific States Marine Fisheries Commission
Hatfield Marine Science Center
2030 Marine Science Drive
Newport, OR 97365

²Cooperative Institute for
Marine Resources Studies
Oregon State University
Hatfield Marine Science Center
Newport, OR 97365

³Fish Ecology Division
Northwest Fisheries Science Center
National Marine Fisheries Service
National Oceanic and
Atmospheric Administration
2725 Montlake Boulevard E
Seattle, WA 98112

JOHN C. FIELD AND
KEITH M. SAKUMA

Southwest Fisheries Science Center
National Marine Fisheries Service
NOAA
Santa Cruz, CA 95064

EDWARD D. WEBER
AND WILLIAM WATSON

National Marine Fisheries Service
Southwest Fisheries Science Center
8901 La Jolla Shores Drive
La Jolla, CA 92037-1509

JESSICA M. PORQUEZ¹,
JANE DOLLIVER¹,
DONALD E. LYONS^{1,2}, AND
RACHAEL A. ORBEN¹

¹Department of Fisheries and Wildlife
Oregon State University
Hatfield Marine Science Center
Newport, OR 97365

²National Audubon Society
104 Nash Hall
Corvallis, OR 97331

JEANNETTE E. ZAMON
Northwest Fisheries Science Center
Point Adams Research Station
520 Heceta Place
Hammond, OR 97121

PETE WARZYBOK
AND JAIME JAHNCKE
Point Blue Conservation Science
3820 Cypress Drive, Suite 11
Petaluma, CA 94954

JARROD A. SANTORA¹,
SARAH ANN THOMPSON²,
BRIAN HOOVER², AND
WILLIAM SYDEMAN²
¹Department of
Applied Mathematics and Statistics
Center for Stock Assessment Research
University of California, Santa Cruz
Santa Cruz, CA 95060
²Farallon Institute for
Advanced Ecosystem Research
Petaluma, CA 94952

SHARON R. MELIN
National Marine Fisheries Service
Alaska Fisheries Science Center
Marine Mammal Laboratory
NOAA
7600 Sand Point Way N. E.
Seattle, WA 98115

ABSTRACT

The California Current Ecosystem (CCE) has been in a primarily warm state since 2014, and this pattern largely continued into 2019. The CCE experienced a mild El Niño from late 2018 into 2019, and basin-scale indicators reflected this condition (elevated Oceanic Niño Index and Pacific Decadal Oscillation; table 1). Despite the El Niño, spring upwelling was above average between southern California and Washington but below average in Baja California. Sea surface temperature (SST) was mostly near the long-term average between Washington and southern California, while surface chlorophyll *a* was above average in Oregon/Washington and slightly below average in most of California in spring/early summer 2019. SST changed dramatically by fall 2019, however, as a marine heat wave (MHW) that formed in May 2019 in the Gulf of Alaska impinged upon the West Coast of the United States. The expansion of the 2019 MHW followed a similar pattern to the 2014–15 MHW.

Off Oregon, the zooplankton assemblage was in a mixed state as southern copepods were close to average while northern copepod abundances were positively anomalous in 2019. Off northern California, *Euphausia pacifica* body size was smaller than average. Euphausiid abundances were well below average in both central and southern California in 2019.

In the north, winter 2019 larval fish abundances were high and dominated by offshore taxa that are associated with warm conditions; spring larval and post-larval biomass were close to average; and spring surface trawls observed record-high market squid (*Doryteuthis opalescens*) abundances. The single most important finding in 2019 was that northern anchovy (*Engraulis mordax*) adults and larvae were at record-high abundances in central and southern California. In central California, market squid and Pacific sardine (*Sardinops sagax*) were also abundant. In southern California warm-water mesopelagic fishes have been very abundant since 2014, and this trend continued into 2019.

Indicators for future salmon returns were mixed in 2019. The abundance of northern copepods, which correlate positively with returns, was high. However, abundances of yearling Chinook salmon (*Oncorhynchus tshawytscha*) and coho salmon (*O. kisutch*), which also correlate positively with returns, were slightly below average. Winter ichthyoplankton was comprised mostly of southern or offshore taxa, which bodes poorly for future salmon returns.

Seabird (common murre [*Uria aalge*]; Brandt's cormorant [*Phalacrocorax penicillatus*]; and pelagic cormorant [*Phalacrocorax pelagicus*]) productivity off Oregon was the highest in years in both 2018 and 2019. In 2018, common murre chicks in Oregon consumed large amounts

of young-of-the-year flatfish, a prey item known to be conducive to chick survival. Despite the prevalence of northern anchovy in central California, common murre and Brandt's cormorant production was low in Southeast Farallon Island as these birds were unable to feed optimally on northern anchovy, and there was a scarcity of more appropriate prey such as young-of-the-year flatfishes or rockfishes.

California sea lions (*Zalophus californianus*), by contrast, benefitted greatly from the large northern anchovy forage base. In 2018, live pup count, weight, and growth rate were anomalously high, and northern anchovy remains occurred in >85% of scat samples. Humpback whale (*Megaptera novaeangliae*) sightings were also very high in 2019, likely because humpback whales congregated near shore to feed on northern anchovy.

INTRODUCTION

The past 6 years were extraordinarily warm in the California Current Ecosystem (CCE) (Thompson et al. 2018). The warming began in the Gulf of Alaska in late 2013 when slack winds resulted in strong stratification and anomalous heating of surface waters. This “blob” of warm water expanded south throughout 2014 and impinged on the southern parts of the California Current by late 2014 (Bond et al. 2015). The warm pattern continued into 2015 when a strong El Niño brought warm water to both shallow and deep areas throughout the CCE (Jacox et al. 2016). Conditions remained warm throughout most of 2016, and 2014–16 turned out to be the warmest 3-year period in the CCE since records began in 1920 (Jacox et al. 2018a). This 3-year stretch was termed a “marine heat wave” (MHW) (Frölicher et al. 2018). Conditions in 2017 reverted to more of an average state, but many biological remnants of the MHW lingered throughout much of the CCE (Wells et al. 2017; Thompson et al. 2018). In 2018, oceanographic conditions north of Point Conception remained close to average, but anomalously warm water returned to the southern CCE in summer, and the single warmest daily water temperature since measurements began in 1931 occurred at the Scripps Pier on August 1, 2018 (Thompson et al. 2018). From a broad perspective, the Pacific Decadal Oscillation Index (PDO) was almost exclusively positive and the North Pacific Gyre Oscillation negative since 2014; both measurements are consistent with warm conditions in the eastern north Pacific (Thompson et al. 2018).

The post-2013 record-high water temperatures induced some major ecological surprises. For example, a near-paradigm based on data from roughly 1950 to 2002 was that Pacific sardine (*Sardinops sagax*; Sardine) thrive under warm and northern anchovy (*Engraulis mordax*) under cool ocean conditions (Chavez et al. 2003). However, northern anchovy recruitment was very high and

TABLE 1
 Overview of conditions throughout the California Current in 2019. For basin indices and physical conditions, blue font suggests that conditions are cool, pink font that conditions are moderately warmer than average, and red that conditions are much warmer than normal. For biological indices, green indicates that conditions are conducive for high production, pink moderately below average production, and red well below average.

Indicator	Basin	Oregon/ Washington	Central/Northern California	Southern California	Northern Baja California
ONI	slightly above average				
PDO	slightly above average				
NPGO	very, very low				
NPH	below average				
Upwelling (spring 2019)		above average	above average	above average	below average
Cumulative upwelling (2019)		average	average	average	
SST (spring 2019)		average	average	average	
SST (fall 2019)		far above average	far above average	far above average	
Chlorophyll <i>a</i> (spring 2019)		above average	slightly below average	slightly below average	
Copepods/krill		southern species above average; northern species above average	<i>Euphausia pacifica</i> smaller than average at Trinidad Head Line. Euphausiid abundances well below average in central CA.	Euphausiid abundance well below average.	
Forage fish and squid (2019)		larval fish abundance high in winter 2018 but dominated by southern taxa; larval fish abundance average in June 2019; post-larval biomass average in spring 2018	anchovy record high, market squid high, sardine high; juvenile rockfish, sanddabs, and hake low	anchovy record high; subtropical mesopelagics very high	
Salmon survival (2019)		yearling Chinook and yearling coho slightly below average; northern copepod biomass suggests better than average return; larval fish prey assemblage dominated by southern, offshore species which suggests poor salmon survival and adult return			
Seabird productivity (summer 2019)		above average reproductive success for murre, Brandt's cormorant and pelagic cormorant	below average production for murre and pelagic cormorant average production for Brandt's cormorant		
Seabird at-sea abundance (summer 2019)		sooty shearwater and common murre observations close to the long-term average	Brandt's cormorant, murre, pink-footed shearwater and sooty shearwater above average. black-footed albatross, and Cassin's auklet below average	Sabine's gull, Cook's petrel, pink-footed shearwater above average, sooty shearwater, murre and elegant tern slightly below average, black-footed albatross and Leach's storm petrel below average	
Sea lions (2018)				pup number, weight, and growth high	
Whales (2019)			high encounters of humpback		

sardine recruitment low during the 2014–16 MHW (Zwolinski et al. 2017). In addition, rockfishes (*Sebastes* spp.), which typically recruit highly during cool, productive conditions (Ralston et al. 2013), had very high recruitment from 2013–18 in central and southern California (Thompson et al. 2018; Schroeder et al. 2019). In

some cases, long-term fish abundance ~ environment correlations broke down during the past 6 years. For example, there was a highly significant, positive correlation between water oxygen concentration and larval abundance of many mesopelagic fishes between 1951 and 2008 but these mesopelagic fishes were very abun-

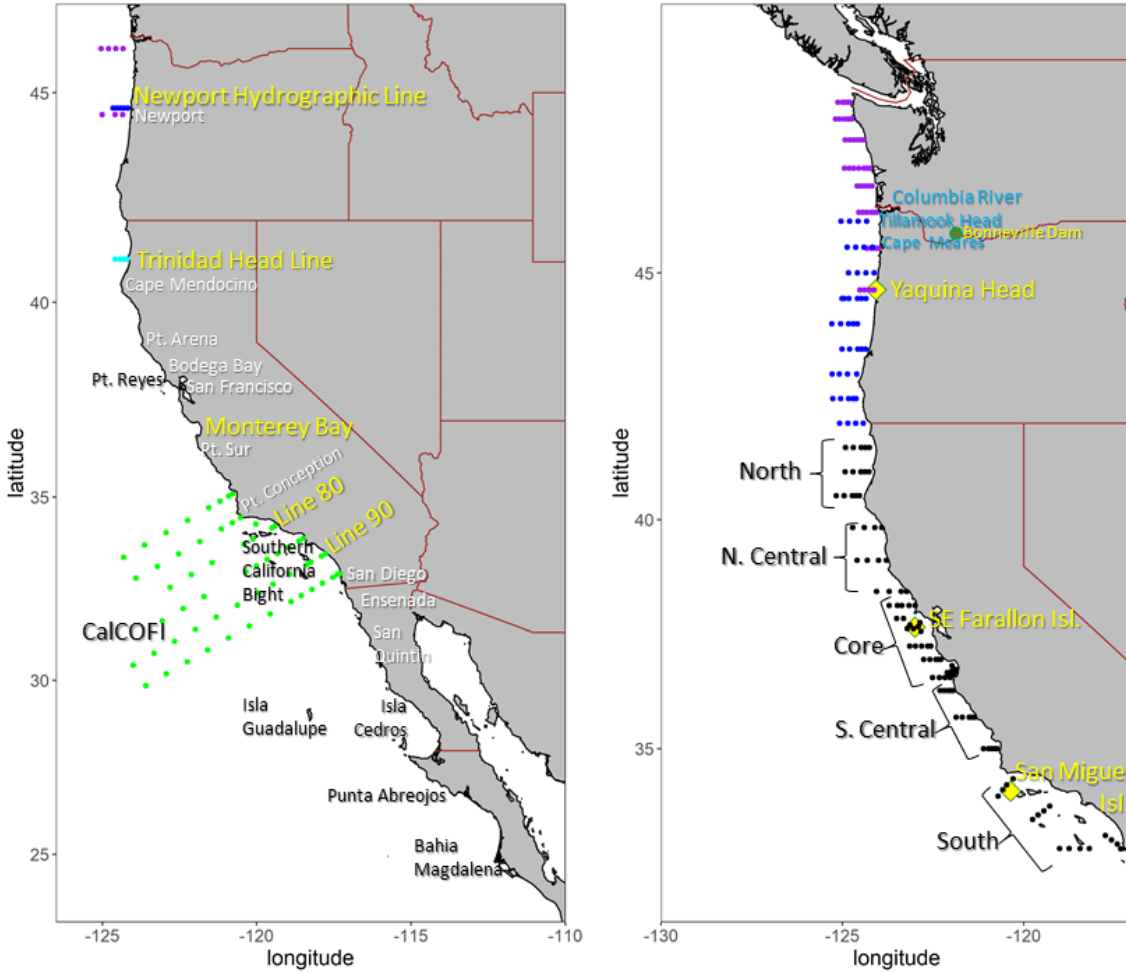


Figure 1. Maps depicting surveys that included bongo tows (left) versus rope trawls and fixed observations for birds or marine mammals (right). Left) Maps where bongo tows were conducted. From north, (purple) pre-larval surveys taken in summer, (blue) pre-larval survey from winter, (cyan) Trinidad head taken year-round, and (green) core CalCOFI stations sampled quarterly. Right) from north: (purple) Juvenile Salmon and Ocean Ecosystem Survey (JSOES) in the upper 20 m, (blue) post-larval midwater trawl, and (black) Rockfish Recruitment and Ecosystem Assessment Survey (RREAS); bracket define the five regions of the RREAS. Yellow diamonds define land-based locations of bird (Yaquina Head, Southeast Farallon Islands) and sea lion (San Miguel Island) surveys.

dant during the MHW even though mean oxygen was low (Koslow et al. 2019). Similarly, in the Pacific Northwest, returns of 1- or 2-year old salmon to the Columbia River correlated positively with the biomass of winter ichthyoplankton that juveniles encounter and consume when first leaving the river prior to the MHW (Daly et al. 2013). During the MHW, subsequent returns were low even though overall winter ichthyoplankton biomass was high (Daly et al. 2019). These and other unexpected events during the last six years challenged our capacity to understand mechanistically the processes that control population and assemblage dynamics in the CCE.

Three years past the 2014–16 MHW, it is possible that the proverbial MHW seeds would begin to bear fruit. For example, Northern Anchovy become sexually mature at one year old, reach peak maturity at ages 3–4, and typically do not live past 6 years (Schwartzlose et al. 1999). As such, larval abundance of northern

anchovy may be high in 2019. The high rockfish recruitment during the MHW may have also resulted in augmented adult populations by 2019. In this year’s State of the California Current, a variety of ongoing monitoring efforts are analyzed to evaluate how the extreme events of 2014–16, coupled with current oceanographic condition impact species at multiple trophic levels throughout the CCE (fig. 1).

BASIN-SCALE CONDITIONS

North Pacific Climate Indices

The Oceanic Niño Index¹ (ONI), a three-month running mean of SST anomalies averaged over 5°S–5°N and 120°W–170°W (NIÑO3.4 region), is a measure of El Niño–Southern Oscillation (ENSO) variability. The

¹The ONI, PDO, and NPGO indices can be downloaded at: <http://upwell.pfeg.noaa.gov/erddap/>.

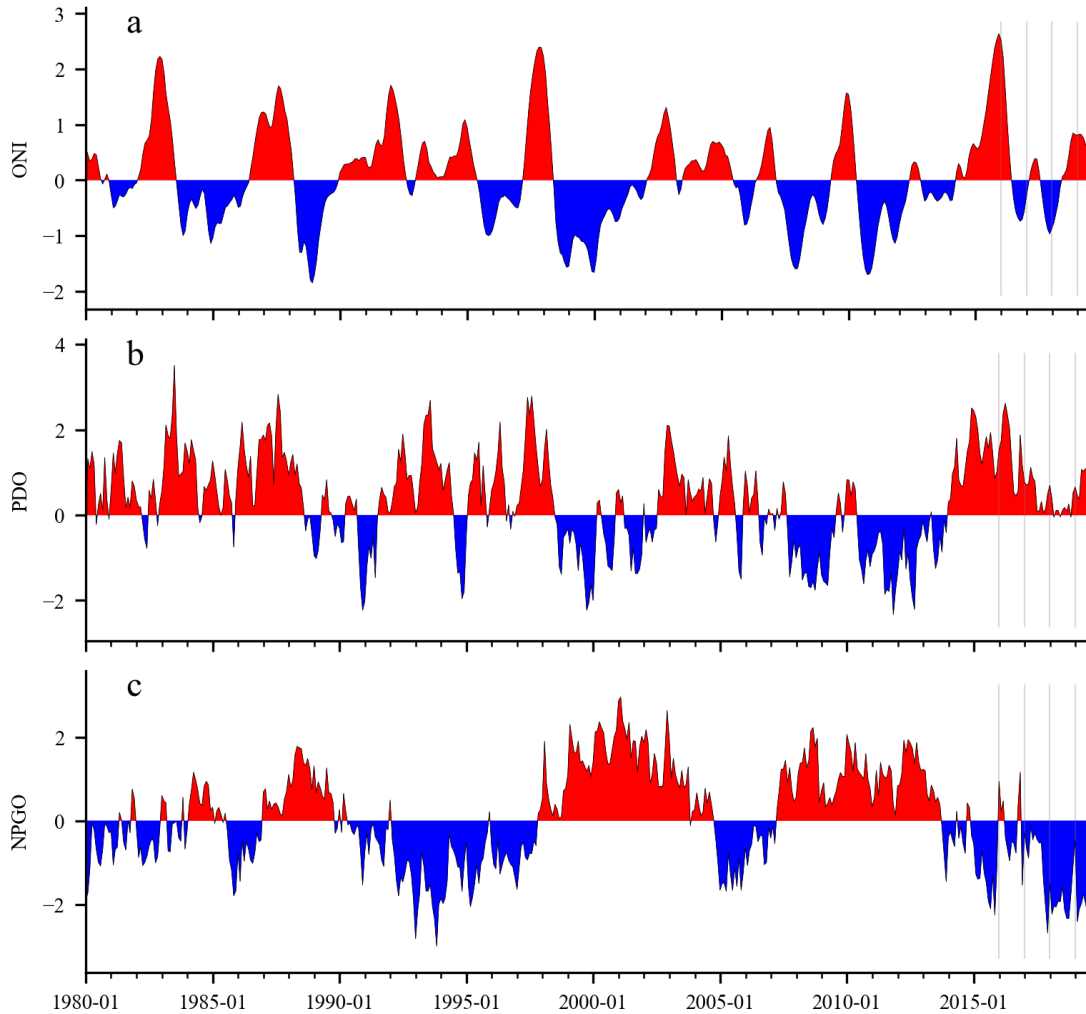


Figure 2. Time series of monthly values for three ocean indices especially relevant to the California Current: a) Oceanic Niño Index (ONI), b) Pacific Decadal Oscillation (PDO), and c) North Pacific Gyre Oscillation (NPGO). Vertical lines mark January 2016–19.

ONI marks an El Niño event when three-month averages reach a threshold of 0.5°C. The ONI indicated a transition from La Niña conditions during fall 2017 to winter 2017–18 to weak El Niño conditions over September 2018 to June 2019 (fig. 2a). The values of the ONI during the 2018–19 El Niño event only reached a high of 0.9°C, which is relatively low compared to the 2.6°C anomaly experienced during the strong 2015–16 El Niño event (fig. 2a). NOAA’s Climate Prediction Center (CPC) reported El Niño neutral conditions as of August 2019² and forecasted El Niño-neutral conditions to persist through spring 2020 (55%–60% chance). In general, El Niño impacts on the CCE include weaker upwelling (or stronger downwelling), lower nutrient supply from upwelled waters, warmer temperatures, and lower productivity (Jacox et al. 2015). However, there is considerable variability in the CCE response to

ENSO (Fiedler and Mantua 2017), and the CCE does not respond predictably to weak ENSO events (Jacox et al. 2018a).

The Pacific Decadal Oscillation (PDO) index describes the temporal evolution of dominant spatial patterns of SST anomalies over the North Pacific (Mantua et al. 1997). Positive PDO values are associated with a shallower upwelling cell in the northern CCE, resulting in less vertical mixing of nutrient-rich deep waters into the surface (Chhak and Di Lorenzo; 2007, Di Lorenzo et al. 2008). Since December 2018, the PDO exhibited positive values with values over 1 from April–June 2019 (fig. 2b). PDO values during 2019 were high, but not nearly as high as during past El Niño events of 1982, 1998, and 2016.

The North Pacific Gyre Oscillation (NPGO) is a low-frequency signal of sea surface height (SSH) variations across the North Pacific, indicating variations in the circulation of the North Pacific Subtropical Gyre and

²https://www.cpc.ncep.noaa.gov/products/analysis_monitoring/enso_advisory

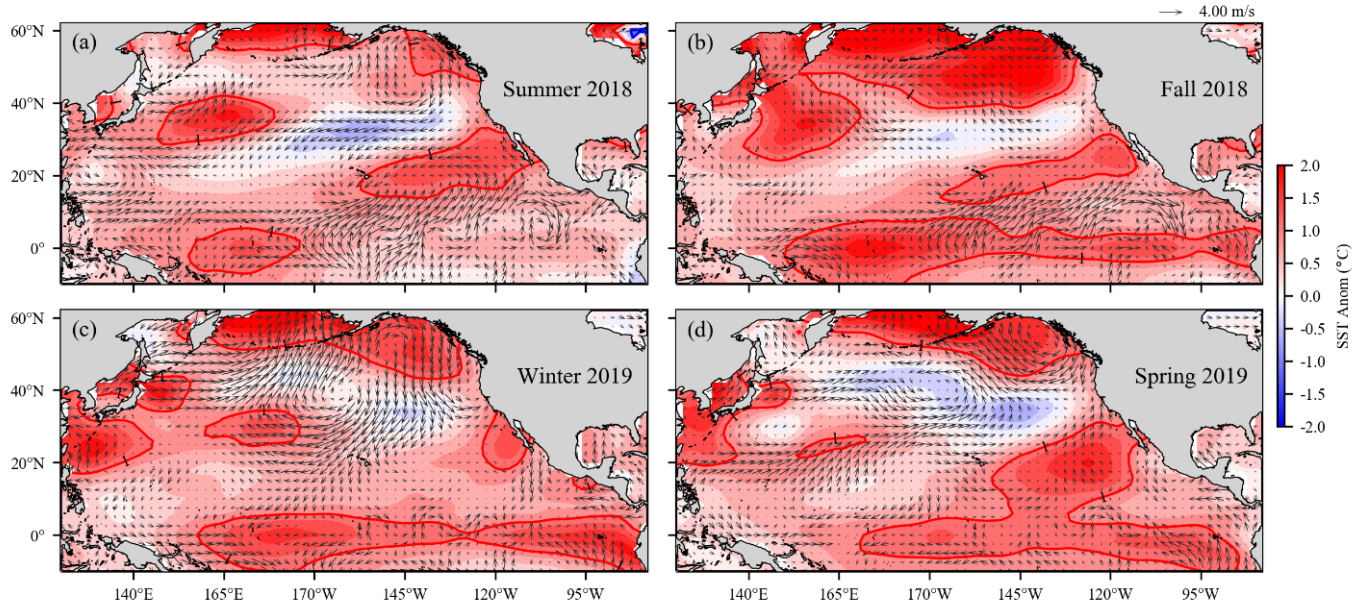


Figure 3. Anomalies of surface wind velocity and sea surface temperature (SST) in the North Pacific Ocean for summer (June–August) 2018, fall (September–November) 2018, winter (December–February) 2019, and spring (March–May) 2019. Arrows denote magnitude and direction of wind anomaly (scale arrow at top). Contours denote SST anomaly. Shading interval is 0.25°C and contour intervals at plus/minus 1°C are shown. Negative (cool) SST anomalies are shaded blue. Wind climatology period is 1968–96. SST climatology period is 1950–79.

Alaskan Gyre (Di Lorenzo et al. 2008). Positive NPGO values are linked with increased equatorward flow in the California Current, along with increased surface salinities, nutrients, and chlorophyll in the southern-central CCE (Di Lorenzo et al. 2009). Negative NPGO values are associated with a shallower upwelling cell in the southern CCE resulting in less vertical mixing of nutrient rich deep waters into the surface (Di Lorenzo et al. 2008). The NPGO during 2019 continued an extended period of negative values since December 2016 (fig. 2c). The negative NPGO values from October 2017 to June 2019, the NPGO reached some of the strongest negative values observed over the entire time-series (since 1950).

North Pacific Climate Patterns

A basin-scale examination of seasonal SST and surface wind anomalies³ allows for the interpretation of the spatial evolution of climate patterns and wind forcing over the North Pacific related to trends in the basin-scale and upwelling indices (fig. 3). From fall 2018 to spring 2019 El Niño conditions were present in the equatorial Pacific (fig. 2a), with temperature anomalies above 1°C in the Niño3.4 region (fig. 3). Since summer 2018, there has been a general expansion of positive 1°C anomalies in the Bering Sea and Gulf of Alaska (fig. 3), with the largest spatial extent of these anomalies occurring in fall 2018. In the eastern Pacific, north of Hawaii, negative ($\leq -0.5^\circ\text{C}$) to near-zero SST anomalies occurred over

the four seasons. Along the North American west coast, SST anomalies were slightly positive ($\leq 0.5^\circ\text{C}$) between Vancouver Island and the Southern California Bight, while coastal SST anomalies in the Gulf of Alaska and along the Baja Peninsula were over 1°C for the four seasons. The SST patterns of 2018–19 showed positive anomalies with spatial coverage similar to that seen during the 2015–16 El Niño event (McClatchie et al. 2016b), but the magnitude of the positive anomalies during 2015–16 were much higher, with some areas of seasonal anomalies over 2°C.

During the 2018–19 El Niño event, the trade winds over the western equatorial Pacific were weaker in fall 2018 and winter 2019, with westerly wind anomalies at 160°E (fig. 3). Spring 2019 trade winds strengthened with zero to positive easterly wind anomalies located between 165°E–120°W. Anticyclonic wind anomalies in the North Pacific and Gulf of Alaska were evident during summer 2018, winter 2019, and spring 2019. Along the West Coast, upwelling winds were near the climatological average for the four seasons, especially north of Point Conception.

COAST-WIDE CONDITIONS

Upwelling in the California Current

Anomalies of coastal SST⁴ (averaged from the coast to 100 km offshore), upwelling, and upwelled nitrate

³NOAA Extended Reconstructed SST V5 and wind NCEP/NCAR Reanalysis data were obtained from <http://www.esrl.noaa.gov>.

⁴Daily optimum AVHRR SST data obtained from <https://coastwatch.pfeg.noaa.gov/erddap/griddap/ncdcOisst2Agg>.

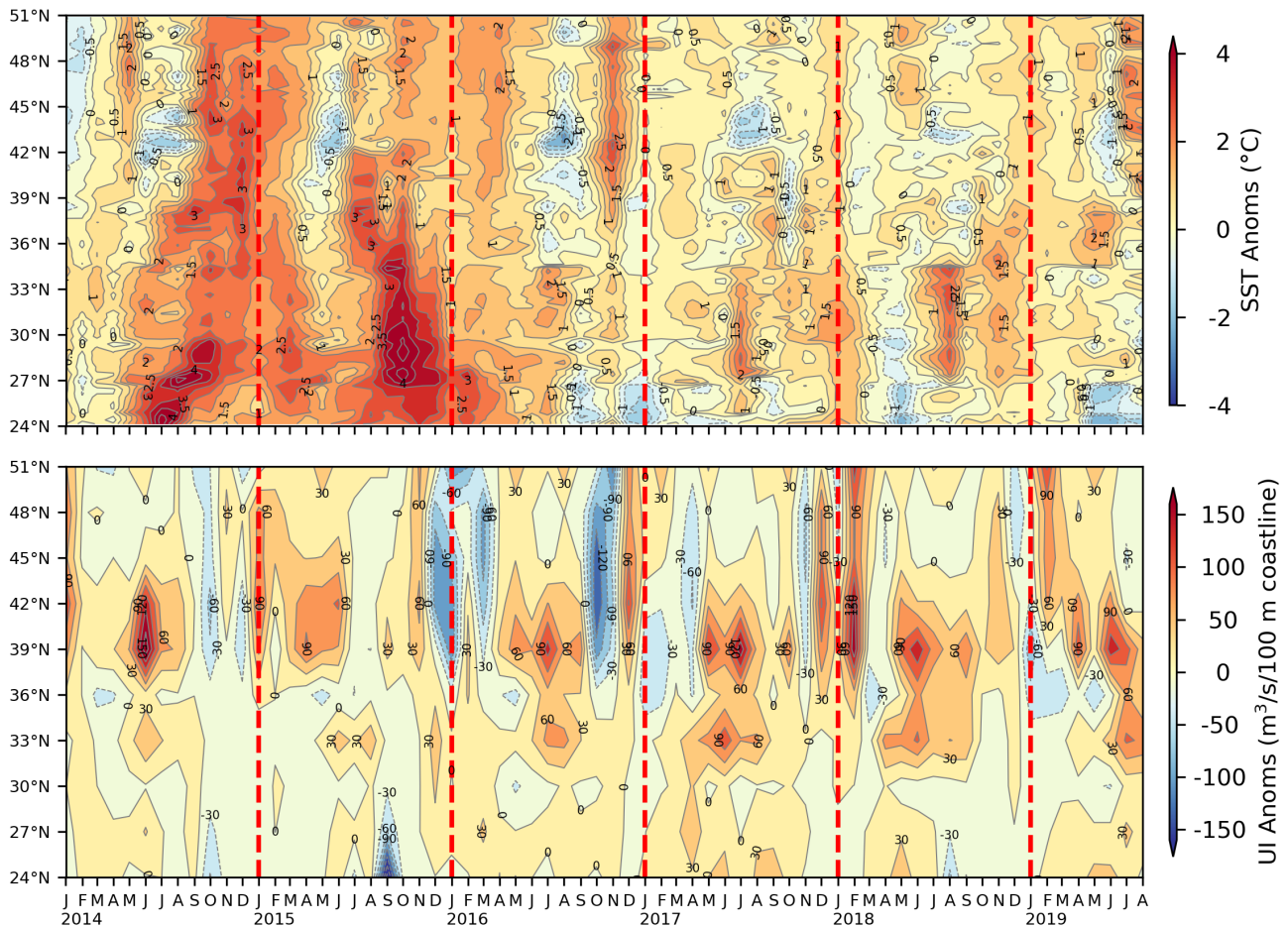


Figure 4. Monthly sea surface temperature (SST) anomalies (top) and Bakun upwelling index (UI) anomalies (bottom) for January 2014–August 2018. The SST anomalies were averaged from the coast to 75 km offshore. Positive and negative upwelling anomalies denote greater than average upwelling or downwelling (usually during the winter), respectively. Anomalies were relative to 1982–2010 monthly means.

were used to examine anomalous coastal upwelling conditions within the CCE from January 2014 to July 2019 (figs. 4, 5). Upwelling estimates came from two sources: the Bakun upwelling index⁵ (UI; fig. 4; Schwing et al. 1996) and the Coastal Upwelling Transport Index⁶ (CUTI; fig. 6; Jacox et al. (2018b)). In addition, The Biological Effective Upwelling Transport Index⁷ (BEUTI; fig. 5; Jacox et al. 2018b) gives estimates of vertical nitrate flux into the surface layer. Both CUTI and BEUTI were derived from a data-assimilative regional ocean model (Neveu et al. 2016). Multiple upwelling indices are evaluated as the UI has long been used in studies of the California Current, but in some places, particularly south of 39°N, it is a less reliable indicator of upwelling due to relatively poor estimation of the wind stress and modulation of upwelling by the cross-shore geostrophic flow

(Bakun 1973; Jacox et al. 2018b). In addition, the UI does not provide information on the nutrient content of upwelled water.

High SST anomalies during the 2014–16 marine heat wave (MHV) extended coastwide from fall 2014 to spring 2016, with anomalies exceeding 2°C (fig. 4). Since summer 2016, SST anomalies were generally weaker (with magnitude less than 1°C), and spatially dependent. However, during winter 2019, positive SST anomalies of 1°C occurred from 32° to 50°N. In May and June 2019 SST anomalies were large (>1°C) for Monterey Bay and Gulf of Farallones, though to the north, between 38° and 44°N, SST anomalies were negative (–0.5°C). This pattern reversed during July and August 2019, with positive anomalies (>1°C) in the north and negative anomalies (–0.5°C) in the south.

Despite warm temperatures during the 2014–16 MHW, spring upwelling in 2014 and 2015 was relatively strong, especially in the northern CCE (figs. 4, 5). Upwelling during winter 2015–16, during the El Niño event, was below average to average for latitudes

⁵Six-hourly upwelling index data obtained from <http://oceanview.pfeg.noaa.gov/erddap/tabledap/>.

⁶Data obtained from <http://upwell.pfeg.noaa.gov/erddap/>.

⁷SST output obtained from <https://oceanmodeling.ucsc.edu> and BEUTI from <https://oceanview.pfeg.noaa.gov/products/upwelling/>.

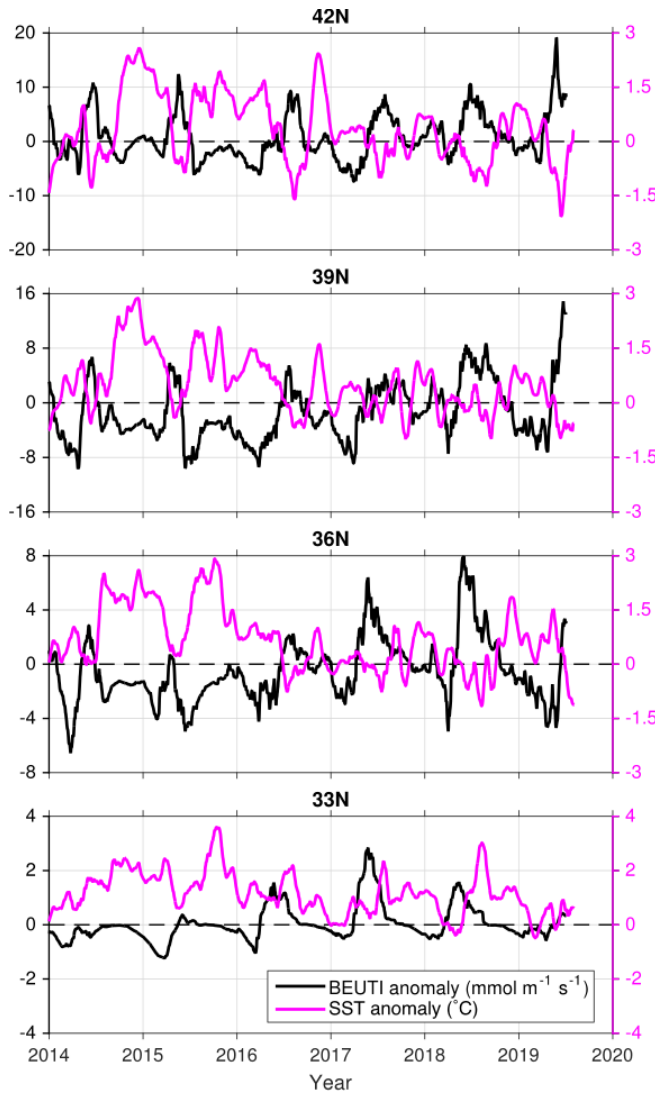


Figure 5. Daily anomalies over January 2014 to July 2019 of Biologically Effective Upwelling Transport Index (BEUTI; black) and sea surface temperature (SST; magenta) relative to 1980–2010 climatology, derived from a data assimilative ocean reanalysis of the California Current System at four latitudes off the US West Coast. Values were averaged from the coast to 75 km offshore. SST was smoothed with a 30-day running mean and BEUTI was smoothed with a 60-day running mean.

north of 39°N. Upwelling anomalies during the winter and spring of 2019 were mostly average to positive for latitudes north of 42°N. Slightly negative anomalies ($-30 \text{ m}^3/\text{s}/100 \text{ m}$ coastline) occurred in the Monterey Bay region (36.5°N), with lowest values during May 2019. During July and August 2018, upwelling anomalies north of 39°N were average to slightly negative, while positive upwelling anomalies occurred between 30° and 39°N.

Vertical nitrate fluxes during the MHW were extremely low as indicated by the negative BEUTI anomalies from fall 2014 to winter 2015–16, with the largest negative anomalies at 36°N and 39°N (fig. 5).

BEUTI values increased from 2016 to 2018 with higher values in each subsequent spring. This trend halted in spring 2019, which saw BEUTI values as low as during 2014–15, especially off central California. These low nitrate fluxes were the result of both weak upwelling and relatively low nitrate concentrations in upwelled waters. However, in June–July 2019 the highest BEUTI values in over a decade were observed near and to the north of Cape Mendocino (40°N), and, correspondingly, the cold, upwelled water produced strongly negative near-shore SST. This strong upwelling appeared to be keeping a thin strip of ocean next to the coast cool while there was a broad region of anomalously warm water farther offshore.

The cumulative Coastal Upwelling Transport Index (CCUTI) is the cumulative sum of daily CUTI values starting January 1 and ending December 31, and it provides an estimate of the net influence of upwelling on ecosystem structure and productivity over the course of the year (Bograd et al. 2009; Jacox et al. 2018b). In general, winter and spring upwelling was stronger during 2018–19 than the previous two years (fig. 6). Cumulative upwelling during 2016–17 was mostly average over the year for all latitudes except for the locations of 39°N and 42°N, which had low yearly values. Upwelling during 2019 was stronger in the north, with 45°N and 47°N experiencing strong upwelling in the spring. However, upwelling at 39°N was low, similar to 2018, with low CUTI values starting in January. The yearly range of upwelling at 33°N was not as large as the northern latitudes and the CCUTI values have been average over the past 4 years.

During winter, storm-driven mixing typically deepens the mixed layer and serves to elevate nutrient concentrations in surface waters, particularly in the northern CCS. However, in some years, periods of sustained calm and stratification (in the north) or even mild upwelling favorable winds (more so in the south) can occur in mid-to late-winter, and allow bursts of primary productivity and successful reproduction in copepod and krill populations well in advance of the typical spring transition (Feinberg and Peterson 2003; Feinberg et al. 2010). Such events serve to precondition the ecosystem for increased production in the spring (Schroeder et al. 2009; Black et al. 2010). The area of sea level atmospheric pressure associated with the North Pacific High (NPH)⁸ can be used as an index of this winter preconditioning (Schroeder et al. 2013). Since 2014 there has been a continually weak NPH during the winter (January–February; fig. 7). The 2019 area was similar to 2018, but the area was considerably smaller compared to high area years that were common from 1999–2013.

⁸Six-hourly data used to define the area of the NPH is located at <https://coastwatch.pfeg.noaa.gov/erddap/>.

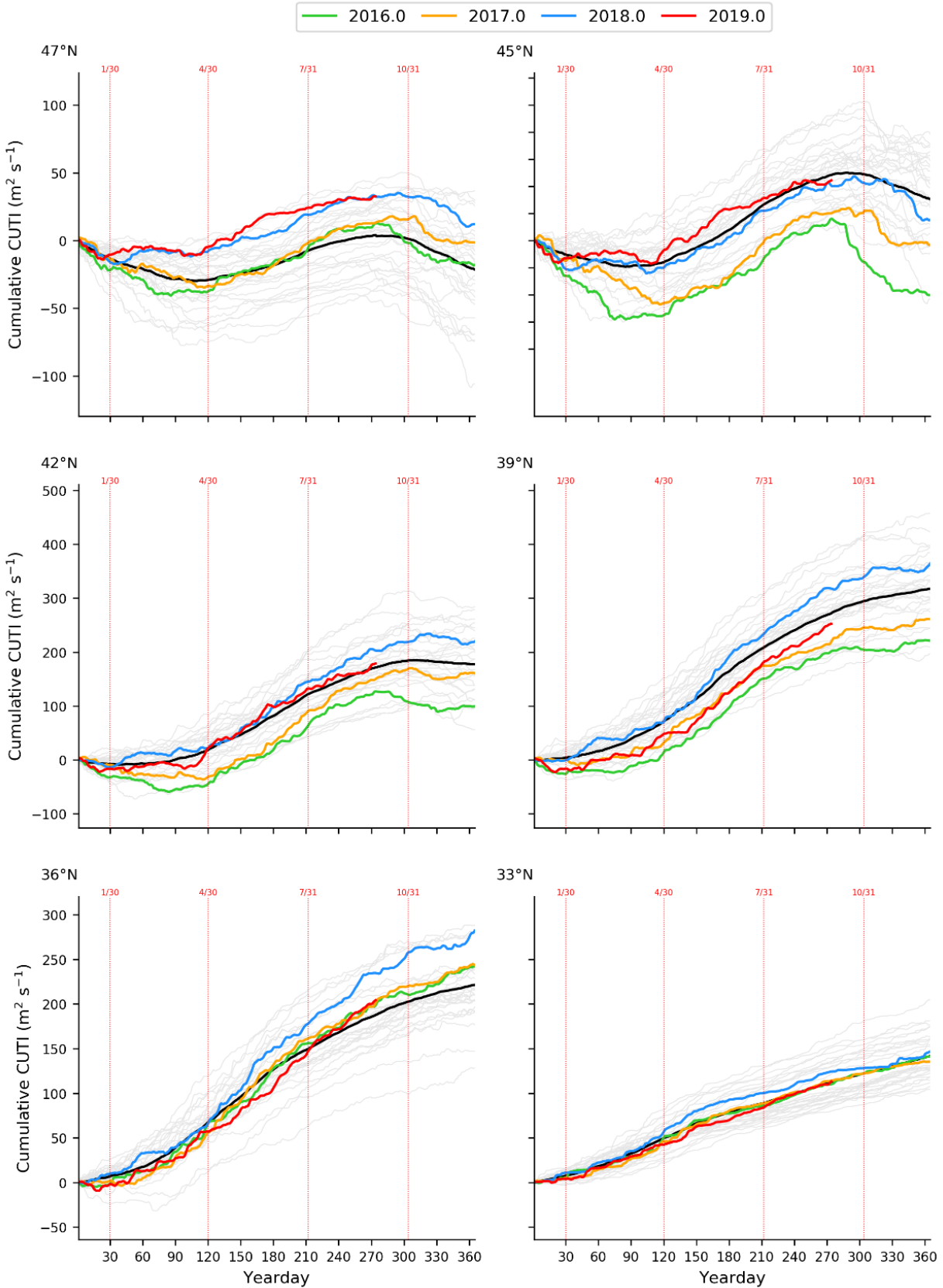


Figure 6. Yearly curves of the cumulative Coastal Upwelling Transport Index (CCUTI) starting on January 1 calculated from daily CUTI at locations along the west coast of North America. Grey lines are all yearly CCUTI for the years 1988–2015, colored curves are for the years 2016–19. The black line is the climatological mean. The red dashed vertical lines mark the end of January, April, July, and October.

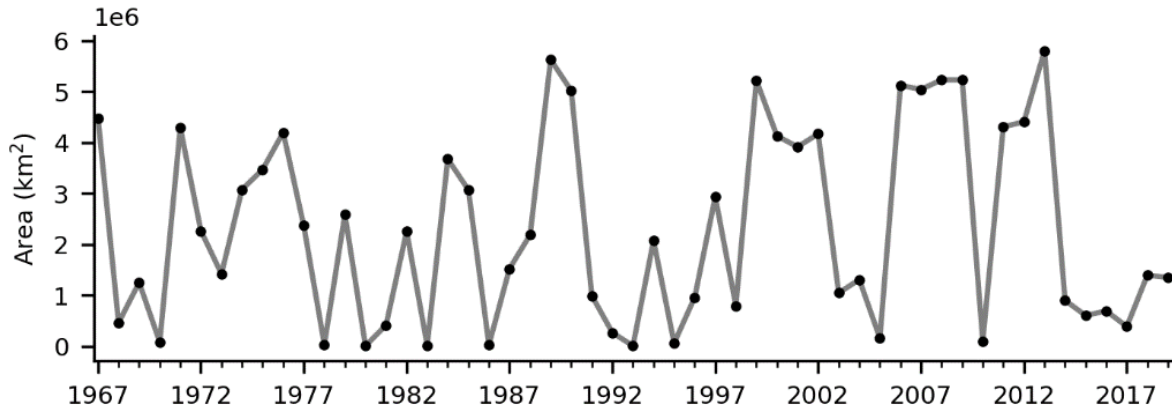


Figure 7. Area of high atmospheric pressure of the North Pacific High averaged over January and February each year. The area is the areal extent of the 1020 hPa isobar located in the eastern North Pacific.

Coastal sea surface and subsurface temperatures

Daily sea surface temperature (SST) time series, measured by National Data Buoy Center (NDBC) buoys⁹, showed periods of above temperatures over July 2018 to August 2019 (fig. 8). During this period, buoys in the Southern California Bight had the highest temperatures during summer and fall 2018, while buoys off Washington State had the highest temperatures over July to September 2019. However, temperature extremes over the last two years have not exceeded the magnitude and duration observed during the 2014–16 MHW. Alongshore winds during winter 2018–19 were similar to the 2015–16 El Niño event, with periods of strong downwelling winds (positive values of alongshore winds) especially during January 2019 (fig. 8). The two northern buoys (46041 and 46029) experienced strong northerly winds during May and June 2019, while the buoys to the south had weak upwelling during May 2019.

Subsurface ocean temperature anomalies derived from a data assimilative ocean reanalysis had the largest surface (0–50 m) positive anomalies during the 2014–15 marine heat wave (fig. 9). Positive anomalies extended from the surface down to 250 m during the two El Niño events of 2015–16 and 2018–19 for locations between 33°N–39°N. Cooling occurred by spring 2019, with negative temperature anomalies ranging from the surface to below 100 m; this cooling started several weeks earlier for locations 39°N and 42°N.

Primary production in the CCE

Spring (April–May) averages of chlorophyll *a* anomalies during 2019 showed a general pattern of northern (north of Monterey Bay) positive anomalies and southern negative anomalies (fig. 10). Positive anomalies spanned coastal areas between 43°–44°N and north of Pt. Reyes during 2019.

⁹Data provided by NOAA NDBC, <http://www.ndbc.noaa.gov/>.

Currents in the CCE

During spring 2018, surface currents were predominantly southward throughout the domain, including within the Southern California Bight¹⁰. In general, currents continued southward through summer, however there were marked offshore orientations, specifically between Point Sur and Point Conception, and poleward currents in the Santa Barbara Channel (fig. 11). In fall 2018, alongshore flow was variable with weak means throughout the domain, with the persistence of offshore-orientated surface currents. In winter 2019, flows were predominantly poleward, specifically north of Point Reyes and well organized north of Cape Blanco. Persistent mesoscale eddies were not observed in 2018–19, but enhanced offshore flows near headlands (Point Conception, Point Arena, Cape Mendocino) were observed as in prior years due to separation of alongshore flows.

A new marine heat wave

Although the coastal region remained relatively cool¹¹ during spring and early summer of 2019 (fig. 9), a new, large MHW formed off the Gulf of Alaska in mid-May 2019 (fig. 12). By late August 2019, this MHW extended to the coast of Washington, Oregon, and central and northern CA where surface temperatures were up to 3°C above average. In mid-September 2019, anomalously warm water impinged most of the coast north of Monterey Bay and was seaward of the shelf break off southern California and Baja California (fig. 13). In mid-

¹⁰Data on surface currents were obtained from high frequency (HF) radar, with vectors calculated hourly at 6 km resolution using optimal interpolation. Real-time displays can be viewed at www.sccoos.org/data/hfrnet/ and www.cencoos.org/sections/conditions/Google_currents/. HF-radar data are available thanks to the initial investment of the State of California in establishing the array in California and to the National Science Foundation for establishing elements of the array in Oregon and California. NOAA-IOS and participating universities (listed at <http://cordc.ucsd.edu/projects/mapping/>) provide ongoing funds/support for operation and management.

¹¹SST anomaly data from 1982–Aug 2019 NOAA OISST: <https://www.ncdc.noaa.gov/oisst>.

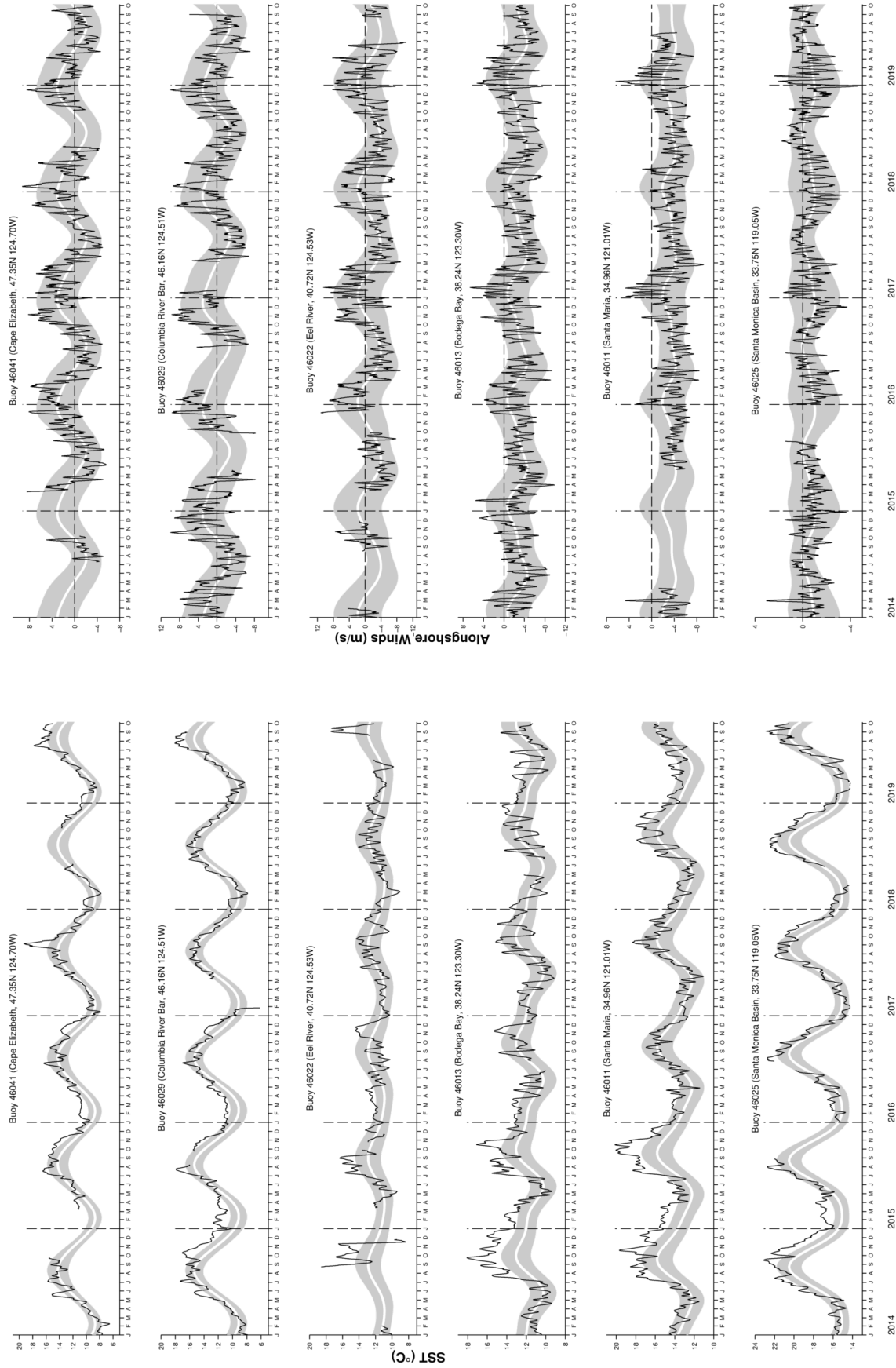


Figure 8. Time series of daily sea surface temperatures (left) and alongshore winds (right) from various National Data Buoy Center (NDBC) coastal buoys along the CCS for January 2014 to September 2019. The wide white line is the biharmonic annual climatological cycle at each buoy. Shaded areas are the standard errors for each Julian day. Series were smoothed with a 7-day running mean.

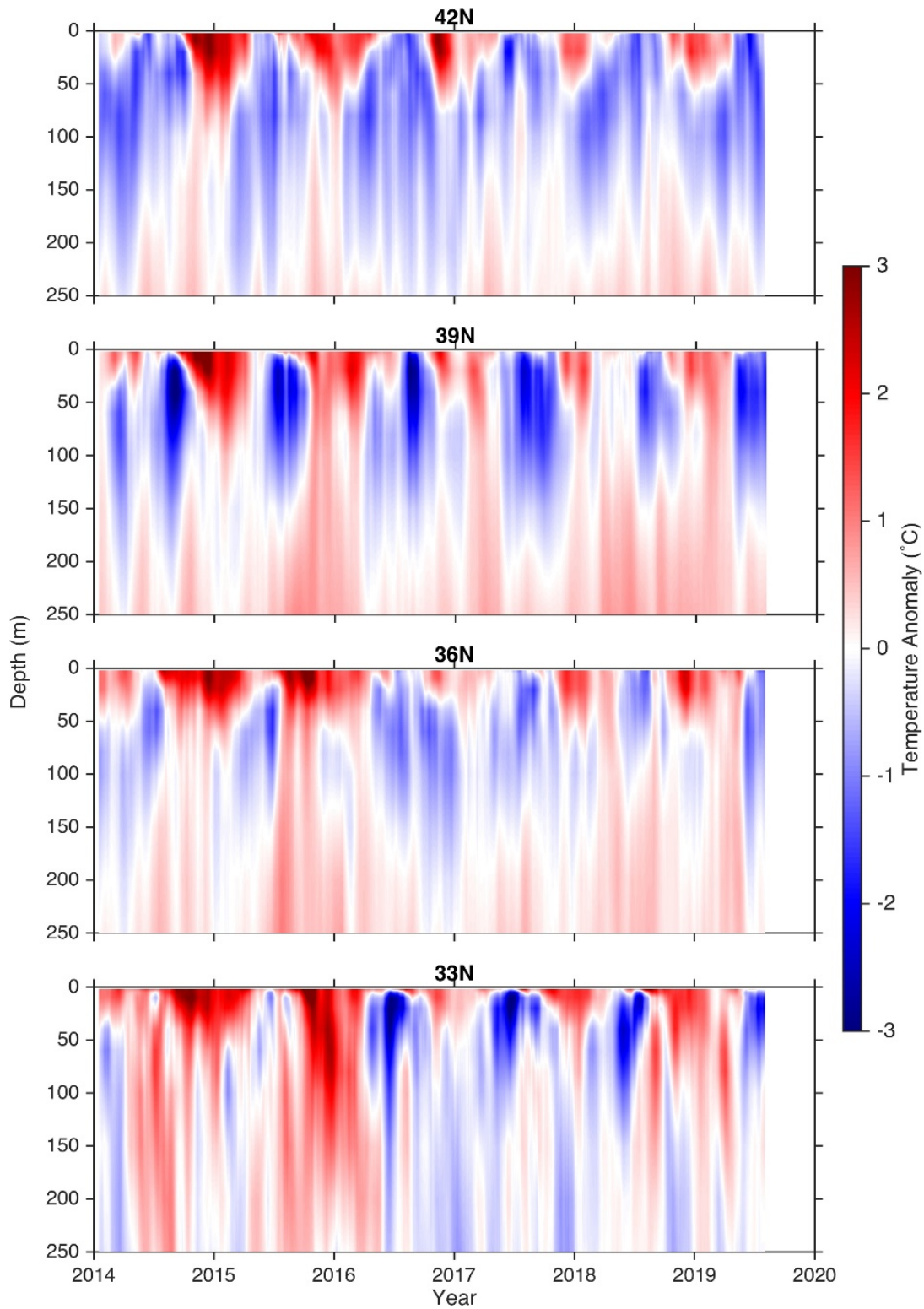


Figure 9. Temperature anomalies relative to the 1999–2011 climatology, derived from a data assimilative ocean reanalysis of the California Current System at four latitudes off the US West Coast. Temperatures were averaged from the coast to 75 km offshore and smoothed with a 30-day running mean.

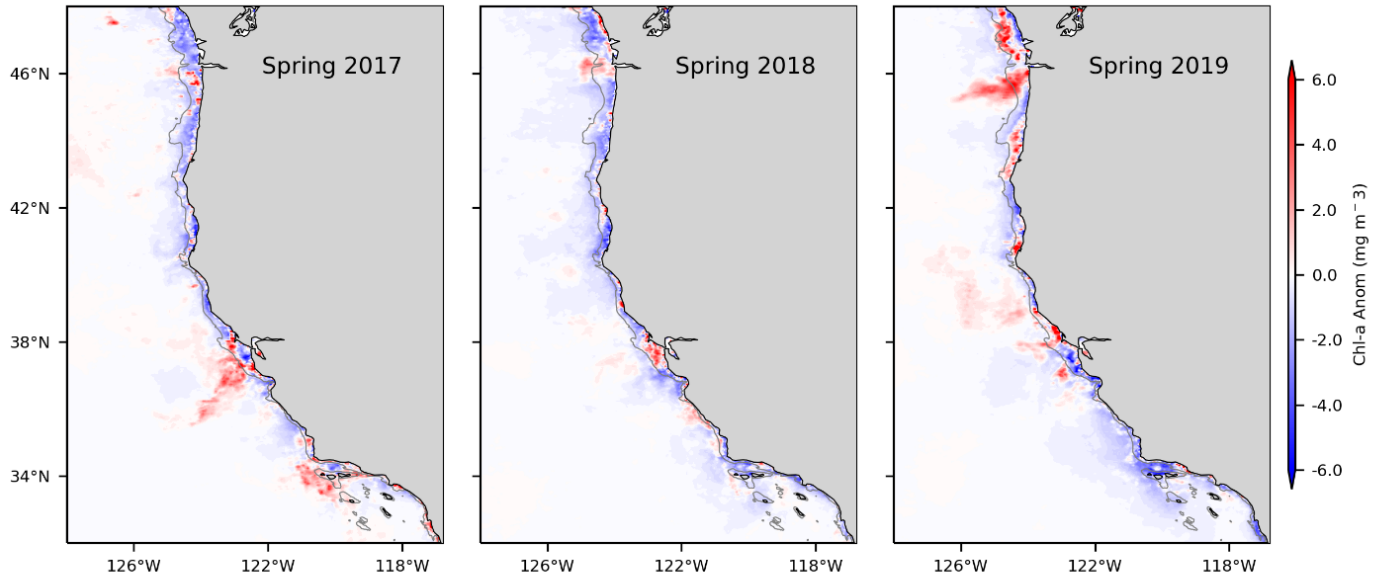


Figure 10. Chlorophyll a anomalies from Aqua MODIS over spring (March–May) 2017–19. Monthly anomalies were averaged onto a $0.1^\circ \times 0.1^\circ$ grid and the climatology was based on the 2003–19 period.

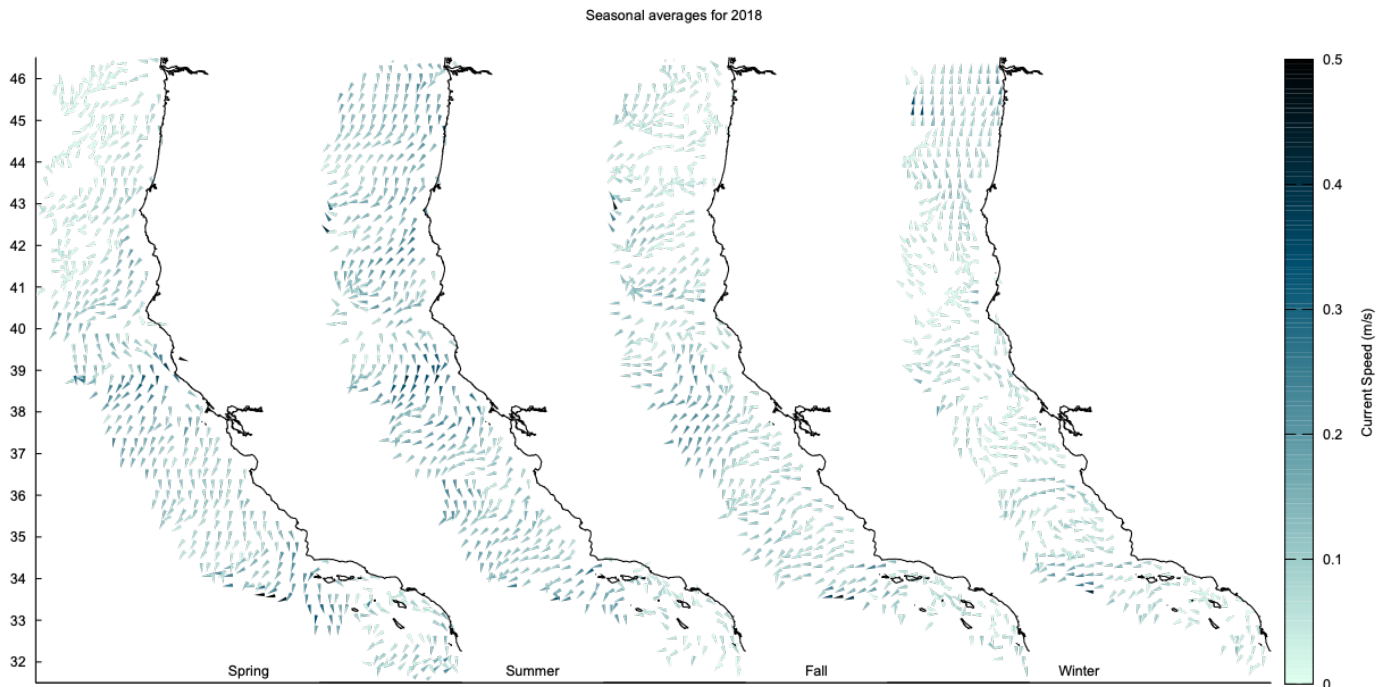


Figure 11. Seasonal mean surface currents observed in the CCE with HF radar. From left to right, the panels present data for spring (March–May 2018), summer (June–August 2018), fall (September–November 2018), and winter (December–February 2019). Current speed is indicated by shading and direction given by orientation of arrow extending from observation location. Currents are displayed with spatial resolution of 0.25° (i.e., nearshore flows are not well represented here).

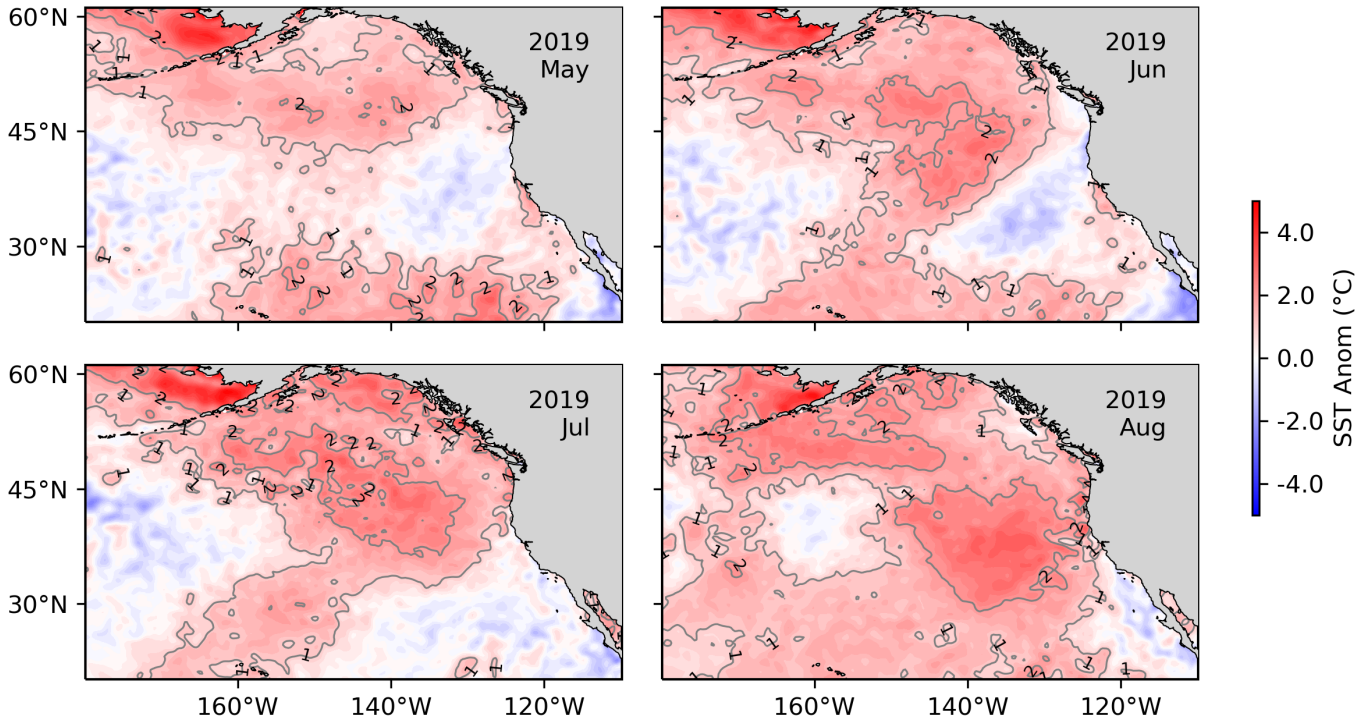


Figure 12. Monthly sea surface temperature anomalies from May to August 2019 relative to 1982–2010 climatology. Contour intervals depict 1°C and 2°C values.

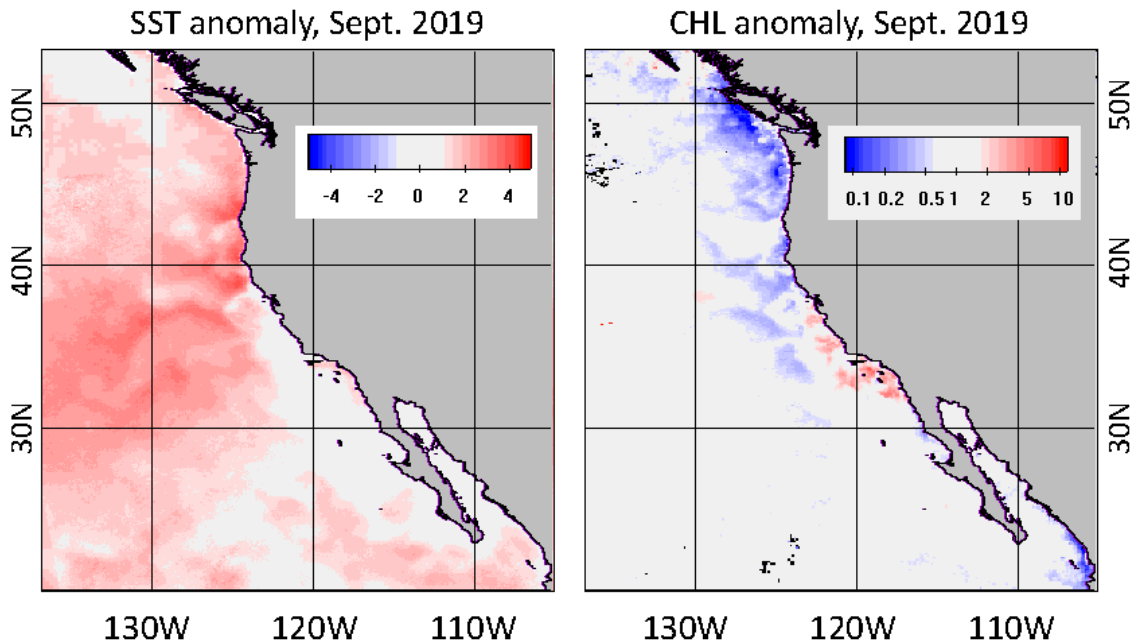


Figure 13. Spatial patterns of September, 2019 anomalies in SST and chlorophyll a. The SST anomaly was computed as difference from the long-term mean (1981–2019) in °C. The chlorophyll a anomaly was expressed as ratio to the long-term mean (1996–2019).

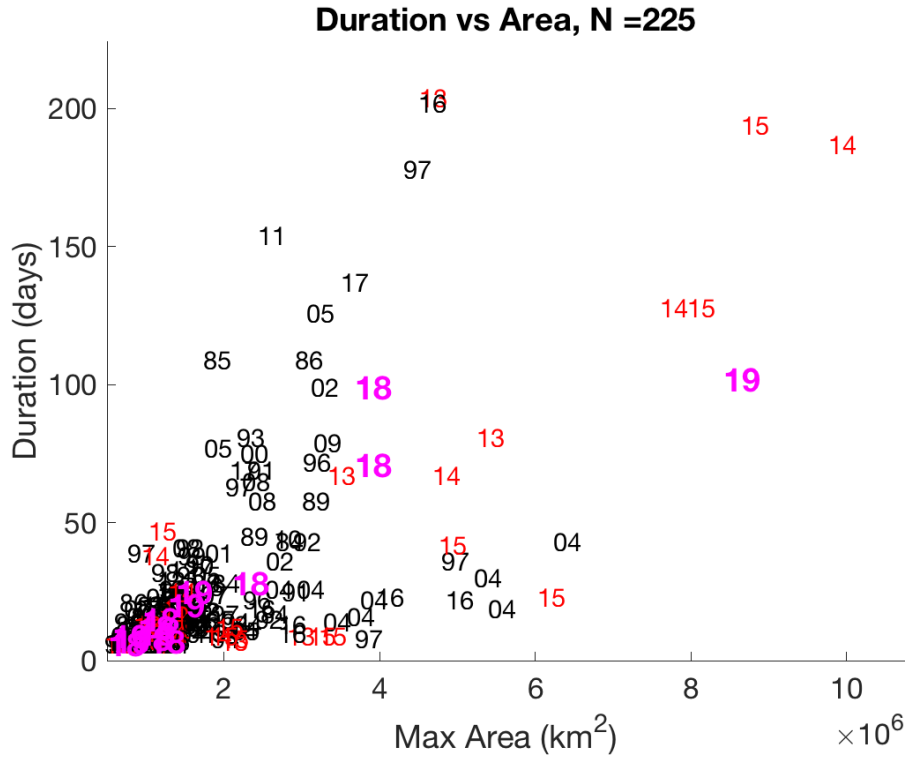


Figure 14. Duration of all marine heat waves (MHW) >5 days long vs maximum area of each MHW, with the year of the feature initiation labeled. Highlighted are the main “blob” years of 2013–14 in red, and the most recent MHW of 2018 and 2019 in magenta.

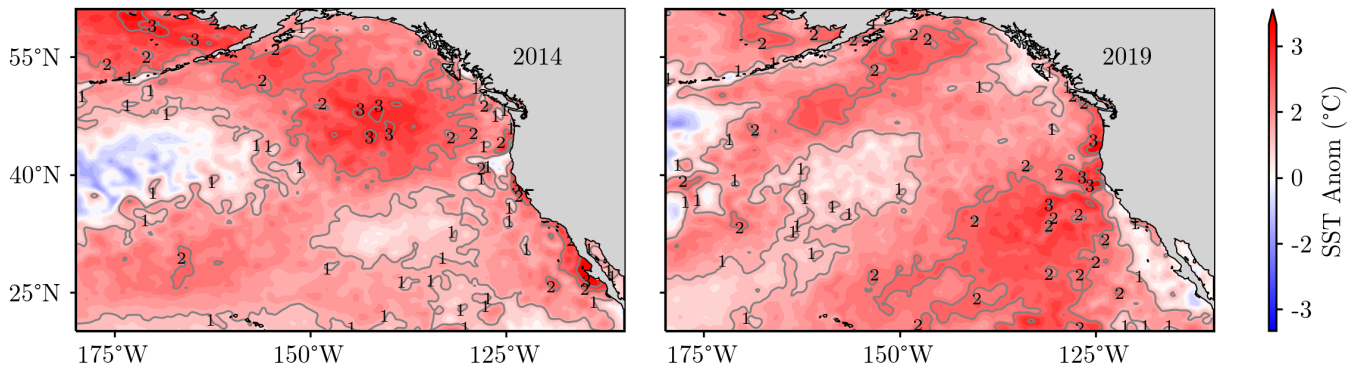


Figure 15. Monthly sea surface temperature anomalies from September 2014 (left) and September 2019 (right). Contour intervals depict 1°C and 2°C values.

September 2019, chlorophyll *a* was well above average in both central and southern California but below average off Oregon and Washington (fig. 13).

As of August 31, 2019, this large MHW, defined following criteria similar to those applied by Hobday et al. (2016), became the third-largest event out of 223 identified MHWs since 1982. The 2019 MHW lagged only slightly behind the MHWs tracked during 2014 and 2015. On August 31, 2019 the MHW was present for 104 days (fig. 14).

Comparison of SST anomalies towards the beginning

of the 2014–16 MHW in September 2014 versus September 2019 indicated that elevated SST were prevalent in many of the same areas between years (fig. 15). In both years, anomalously warm SST occurred in most of the offshore area off the United States, Baja California, and Canada. Similarly, SST was elevated close to shore in both years north of approximately Monterey Bay. However, while SST was anomalously high between Monterey Bay and southern Baja California in September 2014, SST was closer to average south of Monterey Bay in September 2019.

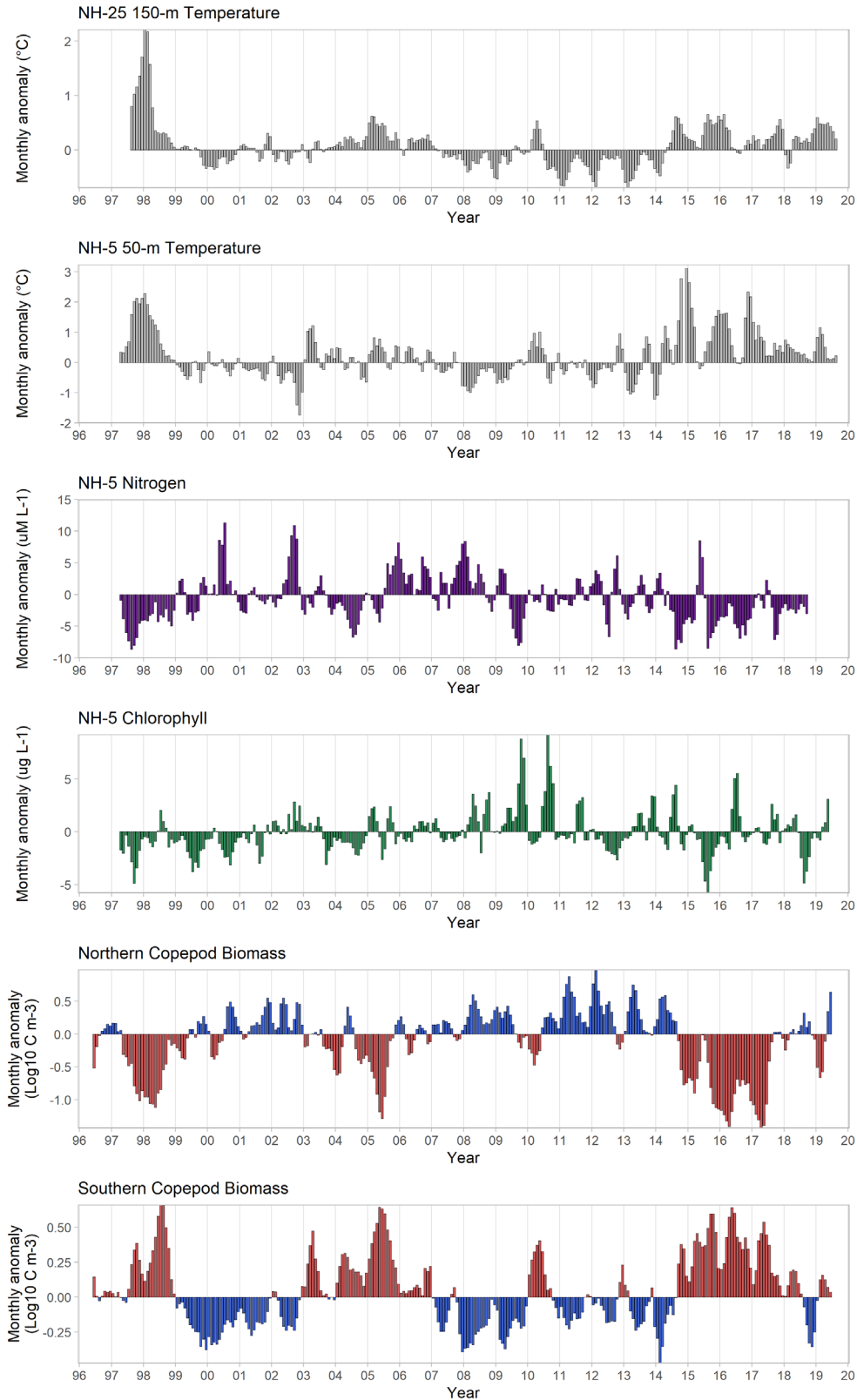


Figure 16. Time series plots of local physical and biological anomalies (monthly climatology removed) from 1996–present at NH-25 (Latitude: 44.6517 N Longitude: 124.65 W) and NH-5 (Latitude: 44.6517 N Longitude: 124.1770 W) along the Newport Hydrographic Line. Temperature and salinity are from 150 m and 50 at NH-25 and NH-5 respectively, NO₂ + NO₃ from the surface, and copepod biomass anomalies integrated over the upper 60 m. All data were smoothed with a 3-month running mean to remove high frequency variability.

REGIONAL OBSERVATIONS OF ENVIRONMENT AND LOWER TROPHIC LEVELS

Northern California Current:

Oregon (Newport Hydrographic Line)

Water temperature anomalies on the shelf (50 m) and slope (150 m) off Newport, Oregon (44.5°N, fig. 1), were strongly positive from the spring of 2014 until summer 2017 (fig. 16). During 2018 and 2019, temperature anomalies returned to weakly positive to near neutral on the shelf but remained strongly positive on the slope (fig. 16). The 2014–17 warm ocean conditions were associated with a southern copepod community, which persisted from fall 2014 through spring 2018 (Peterson et al. 2017)¹². The near-neutral temperature anomalies on the shelf during the summers of 2018 and 2019 were accompanied by an increased biomass of northern copepods, yet southern copepods were still abundant during that time, signaling a pelagic ecosystem still in flux. During September 2019, nearshore surface waters were +3°C above the long-term mean (figs. 13, 15), signaling the arrival of another MHW to continental shelf waters off Oregon.

In 2018 and 2019, the onset of upwelling followed the long-term mean. (figs. 4–6). Although the Bakun upwelling index indicated average upwelling during summer 2018, positive SST anomalies (+2.5°C) occurred for much of the summer, with brief periods of negative surface temperatures during the end of May, July, and the beginning of September (figs. 8, 16). Hypoxic oxygen concentrations below 1.4 ml/L were observed on the shelf from July–September 2018, and during August 2019 (data not shown). Following the upwelling season in 2018, positive temperature anomalies occurred on the shelf and slope (fig. 16). With the exception of two months during the 2015 and 2017 upwelling season, nitrogen concentrations on the shelf remained below average since fall 2015, and continued to be below average throughout 2018 (fig. 16). Chlorophyll *a* was well below average in mid-2018, became average in late 2018/early 2019, and was above average by mid-2019 (fig. 16).

The zooplankton community was dominated by southerly, lipid-poor species from September 2014 until the summer of 2017. The copepod community then transitioned to a more neutral state (fig. 16). During 2015 and 2016, the copepod community did not transition from a warm-water winter copepod community to a cold-water summer community (data not shown). This ecologically important biological transition to a lipid-rich, cold-water community also did not occur in 1998,

when warm ocean conditions occurred in the NCC. However, this transition did occur in late June 2017, 52 days later than the 21-year average. In 2018, this biological transition occurred in late May, 22 days later than the climatology. In 2019, the transition occurred on June 5, which is later than the long-term climatology, and similar to 2018.

During the spring and summer of 2018 and 2019, the abundance of southern copepods was still higher than average accompanied by positive biomass anomalies of the northern copepods, indicating that the pelagic ecosystem is in a state of flux between a warm copepod community and a cold upwelling community. During winter of 2018–19, negative biomass anomalies of northern copepods and positive anomalies of southern copepods occurred, signaling a warm water zooplankton community off central Oregon. In general, northern copepods have been scarce and southern copepods copious since mid-2014 off Newport (fig. 16).

Northern California Current:

Northern California (Trinidad Head Line: THL)

Coastal waters off THL in northern California (station TH02, 41°N, fig. 1) were relatively cool and salty throughout the first half of 2018, but warmed in response to relaxation from upwelling in late summer (fig. 17). Relatively high temperatures and low salinity persisted in shelf and near surface waters throughout early 2019 prior to the onset of moderate upwelling that cooled coastal waters in spring and early summer. Chlorophyll *a* concentrations were relatively high for a brief period in early summer, but otherwise remained low throughout the first half of 2019. There were no observed hypoxic events.

Throughout 2018, the euphausiid community continued to shift towards a composition similar to that observed prior to the 2014–16 marine heat wave, but this trend appears to have reversed in 2019 (fig. 18). Densities of adult *Thysanoessa spinifera* increased in abundance relative to the low abundances observed during the 2014–16 warm period (figure not shown). *Nyctiphanes simplex* (a warm-water species most commonly observed in the southern CC) were absent throughout 2018, but reappeared in early 2019 and persisted into April before disappearing with the intensification of spring upwelling. Likewise, *Euphausia recurva*, a warm-water species first detected in association with the arrival of “warm blob” waters in 2014, were again detected during winter 2019. Mean length of *Euphausia pacifica* adults continued to increase in 2018, reaching size distributions comparable to those observed prior to the warm anomaly, though still including a relatively high fraction of small adults (fig. 18). This trend appears to have reversed in 2019; the seasonal increase in mean length of

¹²Copepod data were based on samples collected with a 0.5 m diameter ring net of 202 µm mesh, hauled from near the bottom to the sea surface. A TSK flowmeter was used to estimate volume of water sampled.

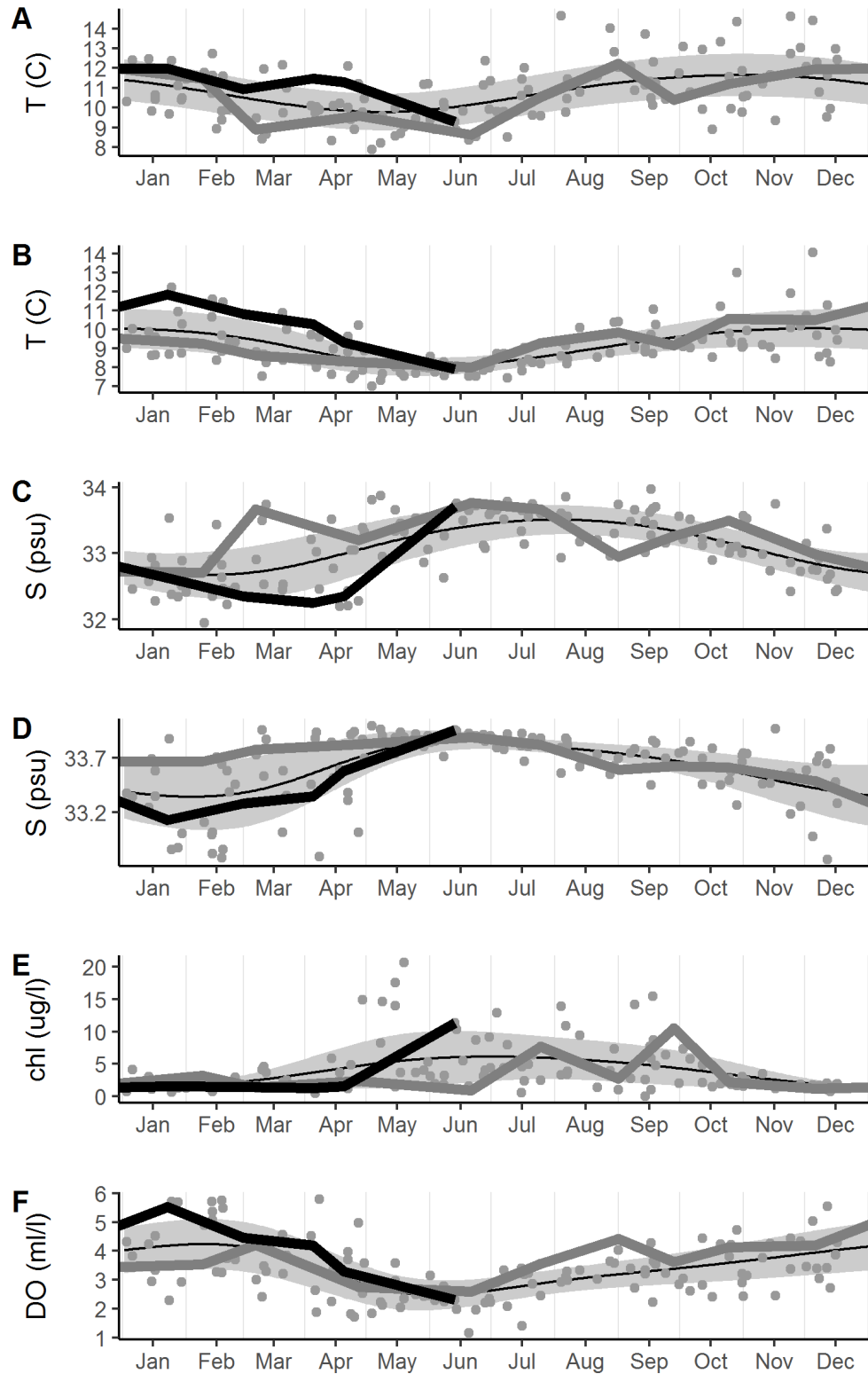


Figure 17. Hydrographic observations at station TH02 (mid-shelf) along the Trinidad Head Line in context of seasonal climatology. Panels from top to bottom show A) temperature at 15 m, B) temperature at 65 m, C) salinity at 15 m, D) salinity at 65 m, E) mean (uncalibrated) chlorophyll concentration from 2-30 m, and F) dissolved oxygen concentration at 65 m. Grey points indicate individual cruise observations. Thin black line indicates climatology derived from GAM of environmental parameter on day-of-year; light grey ribbon about this mean indicates range of mean residual around this climatology (based on GAM of absolute residuals on day of year). Dark grey line indicates observations during 2018. Black line indicates observations during 2019.

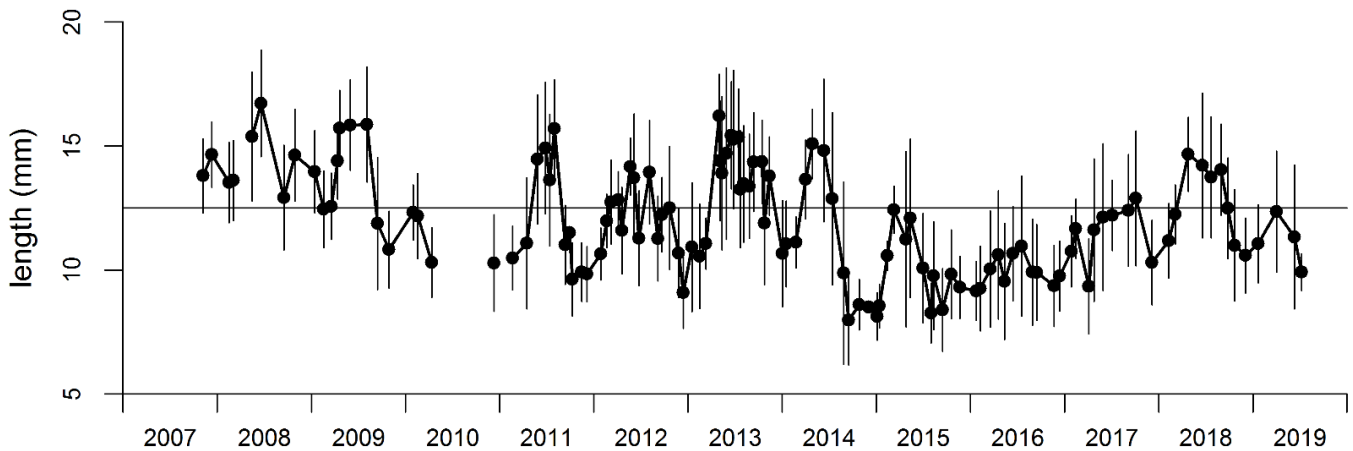


Figure 18. Density-weighted mean (points) and standard deviation (whiskers) of rostral-dorsal length of adult *Euphausia pacifica* collected along the Trinidad Head Line (aggregated over stations TH01 to TH05). Horizontal line indicates mean length taken over entire time series.

adult *E. pacifica* appears to have been cut short early in the year, so that mean lengths were comparable to during 2015–17 (fig. 18).

In conjunction with the observed shifts in euphausiid assemblage and size structure, pyrosomes (*Pyrosoma atlanticum*), which were prevalent in recent years (Brodeur et al. 2018), were absent during the first half of 2019.

Central and Southern California: Remotely Sensed SST and Chlorophyll *a*

After the period of extreme anomalies in 2014–16 that in many areas resulted in all-time highest SST and all-time lowest chlorophyll *a* (Kahru et al. 2018) and minima in the frequency of surface fronts, satellite readings¹³ revealed that the conditions in 2018 and the first half of 2019 were close to long-term averages. From 2017 to mid-2019, SST was mostly slightly above the long-term average (fig. 19). After the deep declines in 2014–16, chlorophyll *a* values in 2018 and in the first half of 2019 were close to the long-term averages (fig. 19). However, starting in July and particularly in August and September 2019, a new warm anomaly developed that produced SST anomalies about +2°C in offshore and transition zones (fig. 19, areas 1 and 2). In California the warm SST anomaly was primarily offshore and less

than +1°C in areas affected by upwelling (fig. 13). However, a separate narrow band of warm water developed along the coast of southern California. In contrast with the 2014–16 anomalies, warm SST in mid-2019 did not suppress chlorophyll *a* along the California coast. A steep decrease in chlorophyll *a*, however, was evident further north (e.g., off Vancouver Island (fig. 13).

Southern California: CalCOFI Survey

From spring 2018–spring 2019, mixed layer (ML) temperature anomalies averaged over the 66 standard CalCOFI stations¹⁴ (29°N to 35°N, fig. 1) were slightly, but significantly, above the long-term average (fig. 20a) except during fall 2018. Over the last two years, ML temperatures were similar to the 1984 to 1998 period. Mixed layer salinity increased rapidly from spring to summer 2018, peaked in winter 2019 and declined (but remained relatively high) in spring 2019 (fig. 20b). Temporal trends of ML salinity were similar in all four regions of the CalCOFI domain. Salinity maxima were observed during summer 2018 in the offshore and California Current regions¹⁵ (see footnote 14 for definition of which stations make up each region) and subsequently observed in the upwelling region and the Southern Cali-

¹³Time series of SST and chlorophyll *a* concentration were extended to September 20, 2019, using methods described in Kahru et al. (2018). SST data were derived from the version 2.0 daily data sets of optimally interpolated global blended AVHRR temperatures (Reynolds et al. 2007); https://podaac.jpl.nasa.gov/dataset/AVHRR_OI-NCEP-L4-GLOB-v2.0?ids=Platform&values=NOAA-18). High-resolution SST data were merged from MODIS-Terra, MODIS-Aqua, and VIIRS-SNPP. Chlorophyll *a* data were derived from the merged multisensor regionally optimized data set (Kahru et al. 2012; Kahru et al. 2015a; Kahru et al. 2015b); <http://www.wimsoft.com/CC4km.htm>). Anomalies were calculated relative to the long-term (1981–2019 for SST, 1996–2019 for chlorophyll *a*) mean monthly values. For SST these were difference anomalies; for chlorophyll *a* the anomalies were reported as ratio anomalies expressed as % (100*[Ratio - 1]). The time series is shown in six subareas, namely the offshore, transition and coastal zones of central and southern California (fig. 18).

¹⁴Methods used to collect and analyze samples from CalCOFI cruises were described in detail at calcofi.org/ccpublications/calcofi-methods.html. Results were presented as time series of properties averaged over all 66 standard CalCOFI stations covered during a cruise or as anomalies of such values with respect to the 1984–2012 period. The calculation of standard errors for such averages is not straightforward due to spatial autocorrelation of properties across the CalCOFI grid. To correct for this bias, standard errors for cruise means were calculated from the residuals of objectively mapped data and actual data.

¹⁵Averages from selected regions were based on a subset of the 66 standard CalCOFI stations. These regions (and corresponding CalCOFI stations) were: offshore (L77St100, L80St100, L83St100, L87St100–110, L90St90–120, L93St80–120), Southern California Current (L77St70–90, L80St70–90, L83St70–90, L87St70–90, L90St60–80), upwelling (L77St49–60; L80St51–60; St82.46, L83St51–60, L87St45–55) and Southern California Bight (L83St41–42, L87St33–40, L90St28–45, L93St27–45).

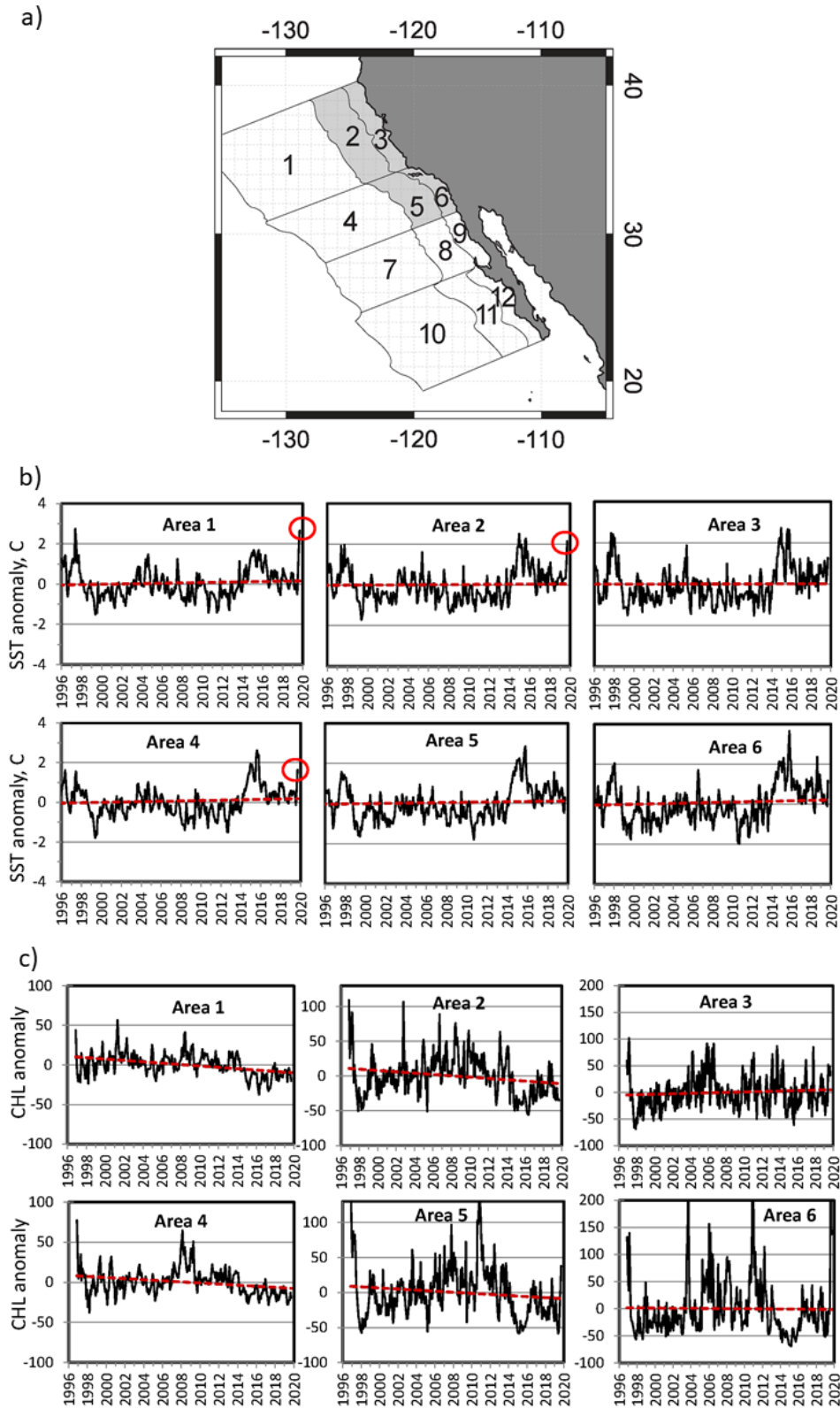


Figure 19. a) Map of the selected offshore (300–1000 km from coast, areas 1, 4), transition (100–300 km from coast, areas 2, 5) and coastal (0–100 km from coast, areas 3, 6) off central and southern California. b) Anomalies in monthly mean sea surface temperature off central and southern California. Anomalies were calculated relative to monthly means of Sept. 1981–September 2019. The dashed line is the long-term linear trend. Circles point to the +2 °C anomalies in August–September, 2019. Anomalies in monthly mean surface chlorophyll-a concentration off central and southern California (fig. 18a). Anomalies were calculated relative to monthly means from November 1996 to September 2019. The dashed line is the long-term linear trend.

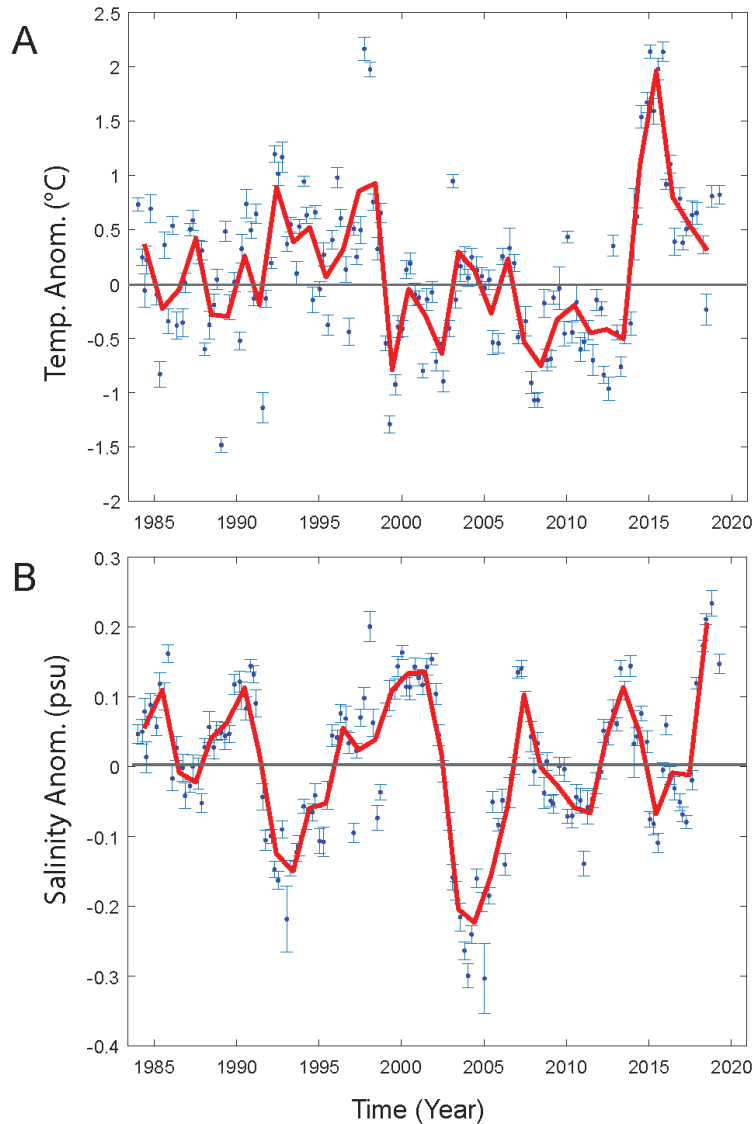


Figure 20. Cruise averages of ML temperature anomalies A) and ML salinity anomalies B) for the 66 standard CalCOFI stations (fig. 1) for 1984 to the spring of 2019. Whiskers indicate the 95% confidence intervals for the means. Red solid lines represent annual averages, grey horizontal lines the climatological mean, which is zero in the case of anomalies. Anomalies were based on the 1984 to 2012 period.

ifornia Bight in fall 2018, suggesting that the signal took no more than 3 months to propagate to those areas. Absolute changes of salinity were highest in the offshore and California Current regions that are closest to the likely source of the high salinity water, the open northeast Pacific (Thompson et al. 2018).

In 2017 and 2018, the σ -26.2 isopycnal, which has a long-term average depth of 151 m, shoaled by almost 20 m relative to the high values observed during the MHW of 2014–16 (fig. 21a). Over the last year, this isopycnal was only slightly deeper than its long-term average with the exception of the spring of 2019 when it was 19 m deeper than average, likely due to the effects

of the 2018–19 El Niño (fig. 21a). Patterns of spiciness (warm and salty versus cool and fresh) on the σ -26.2 isopycnal largely mirrored isocline depth during 2018–19 with values being close to average through winter 2019 and then rising by spring 2019 (fig. 21b). Oxygen on the isopycnal decreased significantly by about 10% between ~1995 and ~2005 (Bjorkstedt et al. 2012). Subsequent to 2005, however, oxygen on the isopycnal did not vary significantly over the long-term, and only short-term variations were observed (fig. 21c). A GAM fit to the data shows an increase of oxygen concentrations between 2010 and 2019, although this increase was not significant over the short time period. An analogous

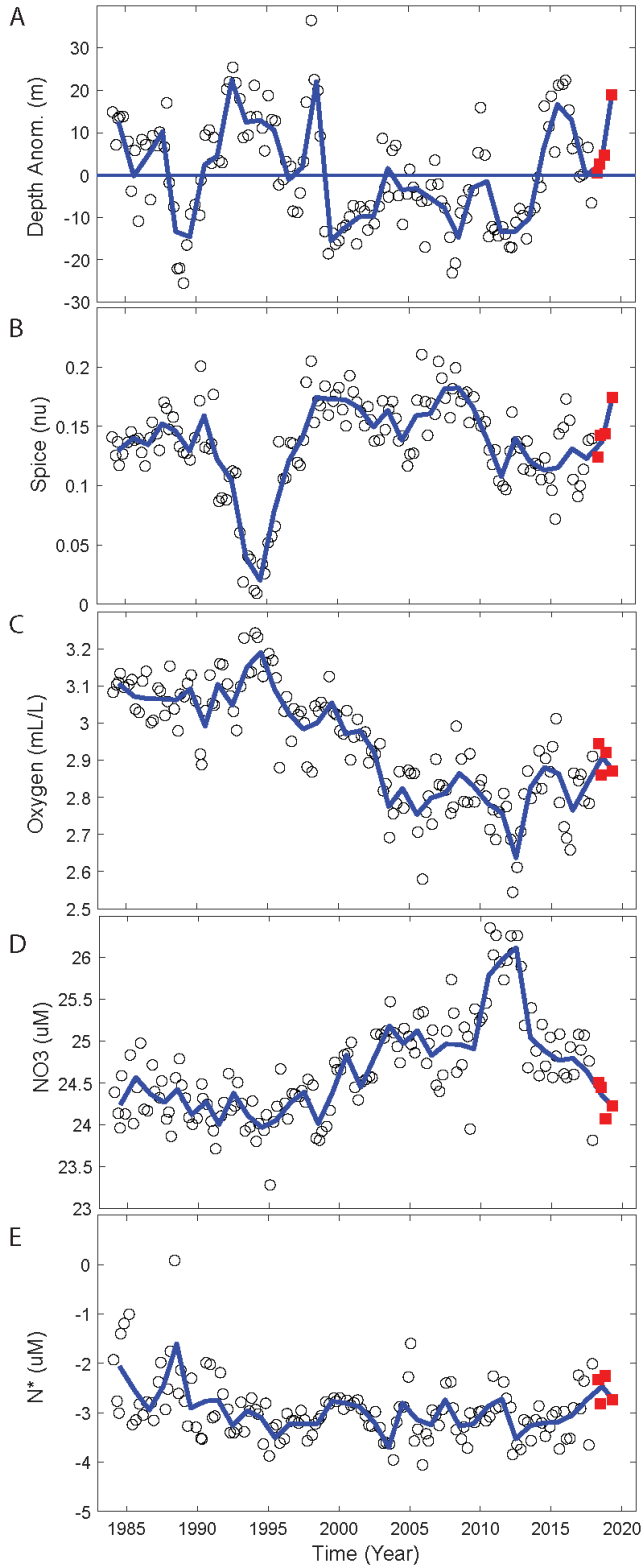


Figure 21. Anomalies of hydrographic properties at the σ_{θ} -26.2 isopycnal (open circles) averaged for each cruise over the 66 standard CalCOFI stations. Shown are anomalies of A) isopycnal depth, B) spiciness, C) oxygen, D) concentrations of nitrate and E) N^* , a biogeochemical indicator that reflects nitrate deficit relative to concentrations of phosphate. The solid blue line connects annual averages. Summer and fall 2018 and winter and spring 2019 cruises are in red.

analysis of oxygen in the CalCOFI domain at depths of 100 to 200 m yielded almost identical results, except that the oxygen increased significantly between 2010 and the present. Nitrate concentration on the isopycnal fell steadily since the 2015 peak, and this trend continued through spring 2018 (fig. 21d). By contrast, N^* , a biogeochemical indicator that reflects nitrate deficit relative to concentrations of phosphate (Gruber and Sarmiento 1997), on the isopycnal increased since 2014 (fig. 21e).

To determine if regional processes drove CalCOFI domain trends, region-specific concentrations of oxygen were analyzed at σ_{θ} -26.2 and the σ_{θ} -26.8 isopycnals. There was no evidence of region-specific trends as both isopycnals displayed patterns that were similar in all four regions over the past two decades (fig. S4). Oxygen at the σ_{θ} -26.2 isopycnal in all regions began declining significantly between 1995 and 2000 and continued to fall until about 2005. Oxygen did not decline significantly in any of the four regions after 2005; indeed, an increase of oxygen was observed for the California Current region. The patterns at the σ_{θ} -26.8 isopycnal, which is at a depth of 387 m on average, were similar in general, except that the large decline of oxygen lasted until about 2010, declining by 12% on average. Oxygen subsequently increased significantly in the California Current and upwelling regions.

Observations of oxygen dynamics are consistent with larger-scale analyses of oxygen in the North Pacific that show a rapid decline of oxygen concentrations at 300 m from about 1992 until 2003, stable oxygen from 2003 to 2013, and no significant long-term trend over the last 70 years (Schmidtko et al. 2017). These results do not support a hypothesis that global warming directly causes oxygen concentrations to decline in the CCE, nor do they suggest that this trend will continue monotonically over the coming decades. Concentrations of oxygen in the thermocline of the CCE are likely related to subsurface salinity variability in the North Pacific Current and controlled by ocean circulation dynamics linking the CCE to the North Pacific (Poza Buil and Di Lorenzo 2017). A modeling study suggest that anthropogenically-forced trends in oxygen at the σ_{θ} -26.5 isopycnal will be small in the CalCOFI domain and not detectable until decades from now (Long et al. 2016).

Mixed layer chlorophyll *a* was close to the long-term average over the last three years (fig. 22a); with values significantly lower than those observed during the 1999 to 2013 cool period. The exception was spring 2019 when chlorophyll *a* was as low as during the 2015–16 El Niño. These patterns were particularly strong in the California Current and upwelling regions (fig. S2). The depth distribution of chlorophyll *a* in the offshore and the California Current regions was similar to the warm period of 1984 to 1998, with subsurface maxima

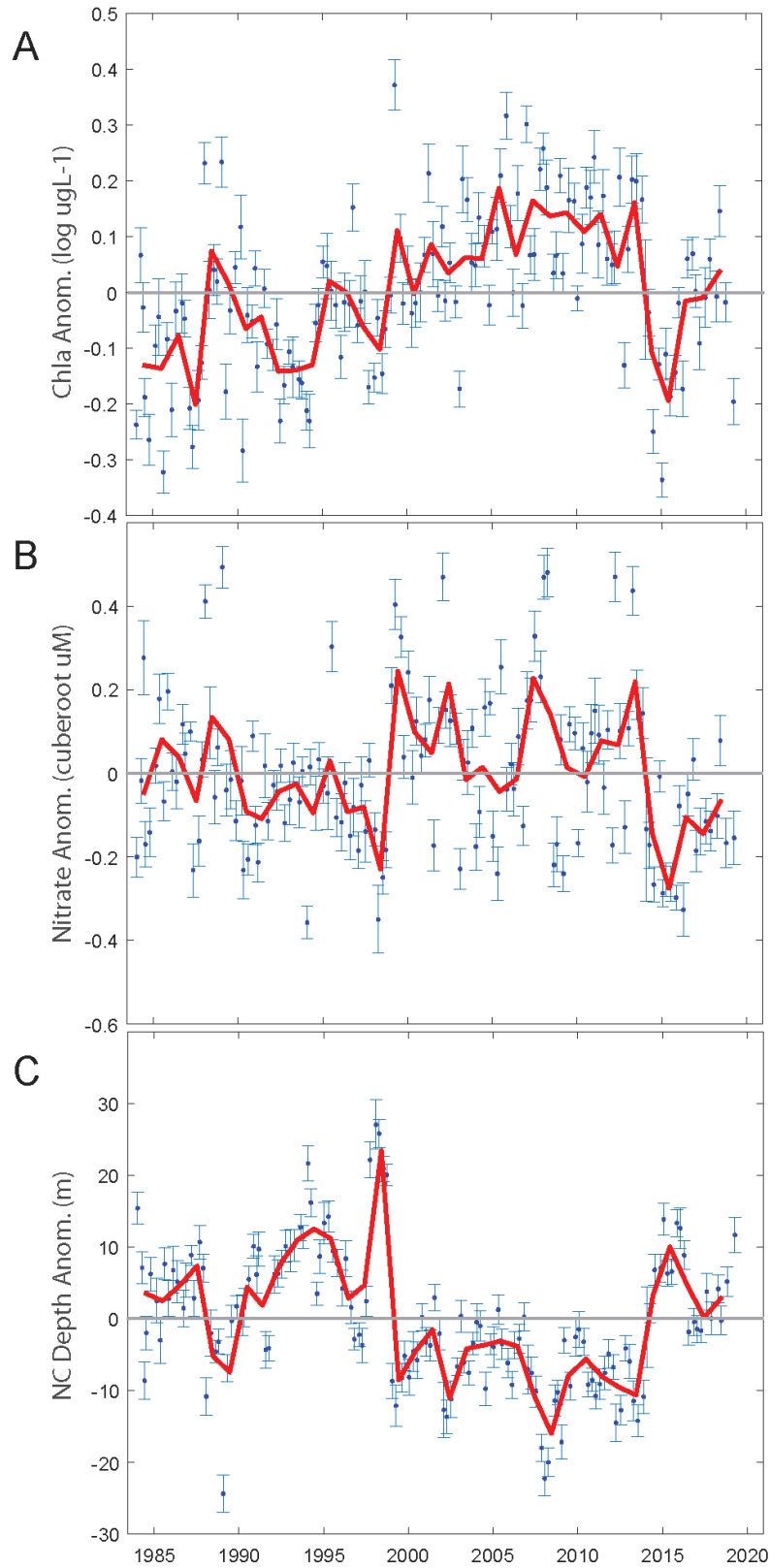


Figure 22. Cruise averages of mixed layer properties for the 66 standard CalCOFI stations. A) the \log_{10} of chlorophyll a, B) the cube root of nitrate, and C) nitracline depth.

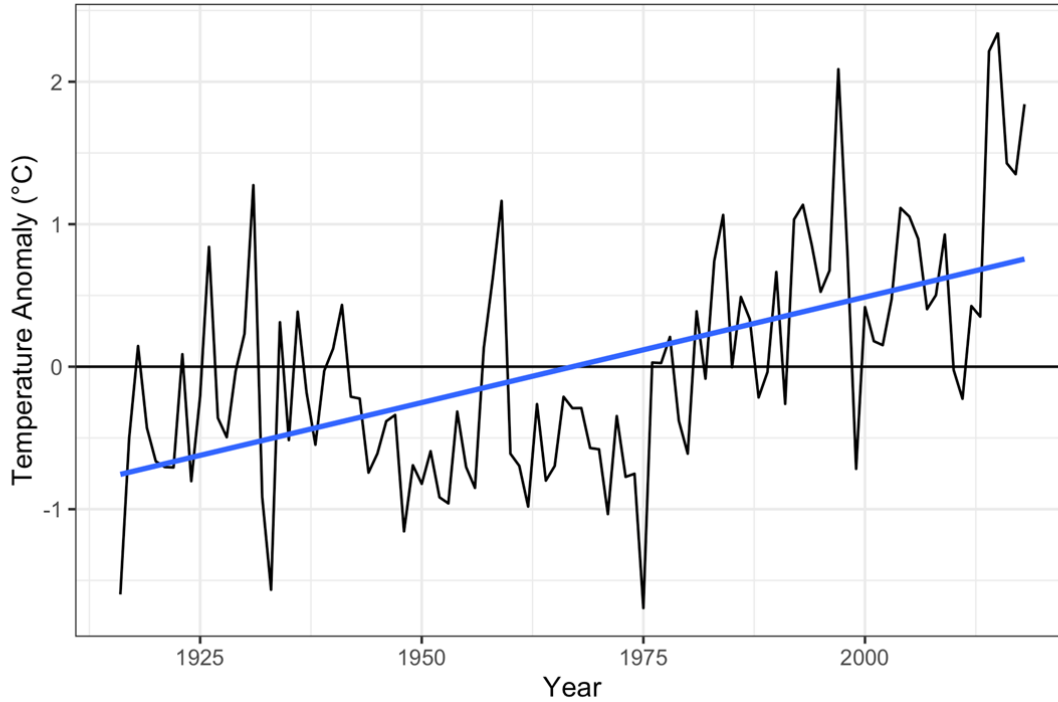


Figure 23. Annual mean SST anomalies taken from the Scripps Pier, La Jolla, California.

20 m below those observed during the 1999 to 2013 cool period.

Recent concentrations of mixed nitrate were significantly below long-term averages since the 2015–16 El Niño (fig. 22b). Nitracline depths¹⁶ mirror those of mixed layer nitrate: values over the last two years were close to long-term averages and significantly lower than during the 1999 to 2013 cool period (fig. 22c). The exception was the spring of 2019 with significantly higher nitracline depths. The changes of mixed layer chlorophyll *a* and nitracline depth in 2018–19 mirror each other. The anomalies observed during the spring of 2019 may well be due to El Niño conditions (fig. 2)

Overall, conditions over the last 12 to 36 months strongly resemble conditions observed during the 1984 to 1998 warm period and are unlike those observed during the 1999 to 2013 cool period. This statement holds for the mixed layer properties of temperature, chlorophyll *a*, nitrate and nitracline depth and the water column distribution of chlorophyll *a* (the subsurface chlorophyll *a* maximum shifted, fig. S2) and nitrate (fig. S3) in most regions of the study domain. It is unknown if these conditions will persist over the next decade as they did from 1984 to 1997.

¹⁶Nitracline depth was defined as the depth where concentrations of nitrate reach values of 1 μM , calculated from measurements at discrete depths using linear interpolation. Statistical analyses were carried out in Matlab except for trend analyses that were carried out using R's mgcv gam-package.

Southern California: Scripps Pier Water Temperature

Daily measurements of water temperature at the Scripps Pier in La Jolla, CA (32.5°N), began on August 22, 1916, and continue to the present¹⁷. On August 1, 2018, daily water temperature exceeded the previous record high from July 30, 1931 (Thompson et al. 2018). Water temperature continued to be anomalously warm through the remainder of 2018 as the mean annual temperature was $\sim 1.5^\circ$ above the long-term average (fig. 23). There was a significant trend ($r^2 = 0.30$) of rising water temperature through time with a $\sim 0.148^\circ\text{C}$ increase per year since 1916. Mean annual temperature was anomalously warm from 2012–18 and in 16 of 18 years since 2000 (fig. 23).

Baja California: Satellite Imagery for Summer 2018

SST¹⁸ ranged from 16° to 28°C and SST anomalies from -1.4° to 2.4°C throughout waters off Baja California (22.5°N to 32.3°N; fig. 22). SST anomalies were mostly positive in summer, 2018 but cooler water occurred off Punta Abreojos and just south of

¹⁷Scripps Pier temperature data was obtained from: <https://scripps.ucsd.edu/programs/shorestations/shore-stations-data/data-sio>. The Scripps Pier was lengthened in 1988 resulting in increased rip current transport of warmer water from the shore. Following (Checkley and Lindegren 2014), 0.45°C was subtracted from measurements taken after 1988.

¹⁸Temperature was obtained from https://podaac.jpl.nasa.gov/Multi-scale_Ultra-high_Resolution_MUR-SST.

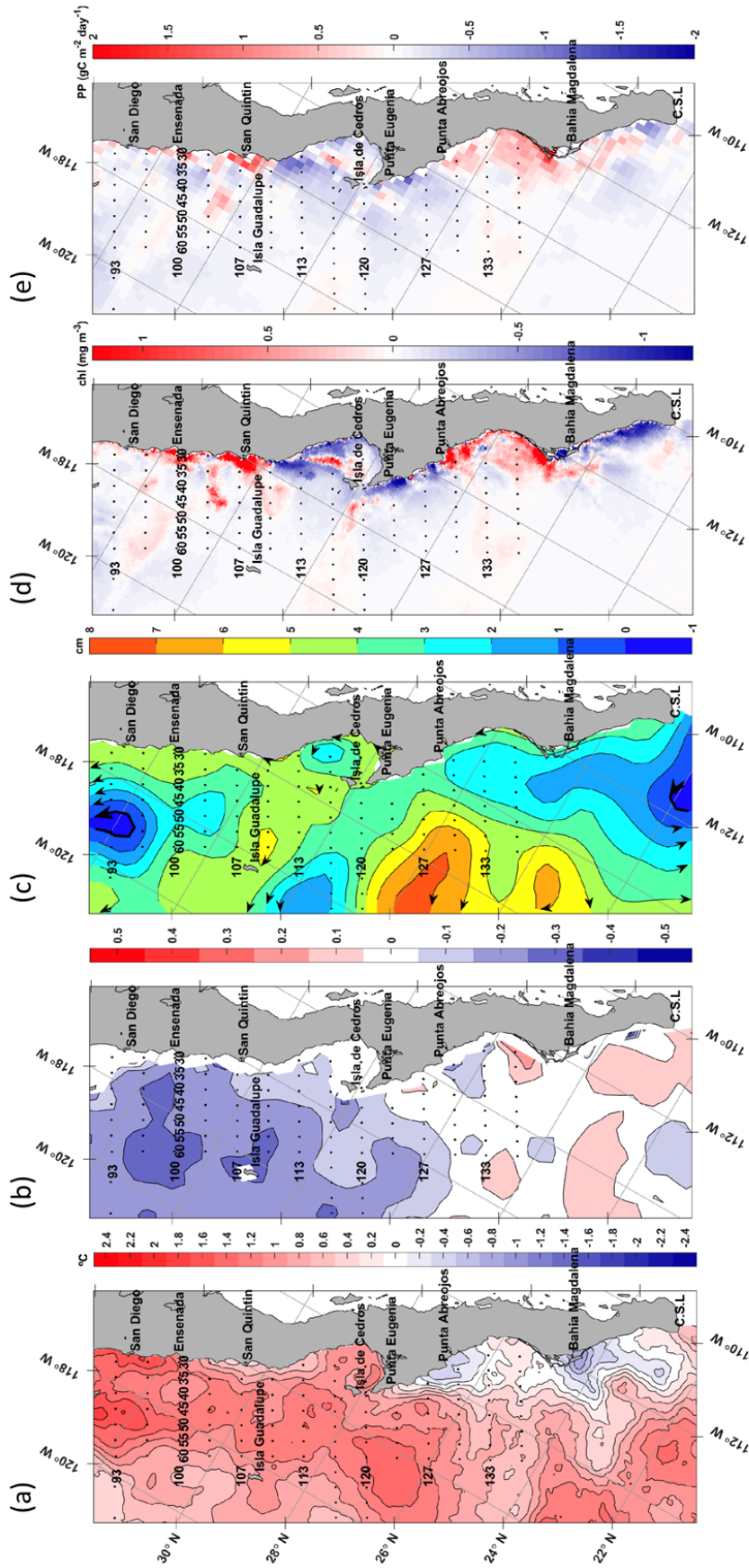


Figure 24. Satellite readings of a) SST, b) salinity, c) sea surface height, d) chlorophyll a and e) primary production off the coast of southern California and Baja California in summer 2018. Dots depict standard IMECCAL stations.

Bahia Magdalena (fig. 24a). This cool coastal water suggested high upwelling at these two sites. Surface salinity¹⁹ ranged from 33.4 to 35 and salinity anomalies from -0.5 to 0.2 (fig. 24b). Overall, salinity was negatively anomalous in northern Baja California and patchy to the south. Although upwelled water typically is relatively saline (McClatchie 2014), the spatial distribution of anomalously cool and anomalously saline water did not perfectly overlap. Rather, the cool water just south of Punta Abreojos was relatively fresh. South of Bahia Magdalena the cool water was mostly relatively saline.

SSH²⁰ anomalies (fig. 24c) ranged from -1 to just under 8 cm throughout the entire region. The SSH anomaly field depicted mesoscale eddies and gyres. There was a cyclonic gyre in the northern area, centered on line 93. This was the gyre of the Southern California Bight that extended southward roughly to a line between Isla Guadalupe and San Quintin. The cyclonic flow created a frontal system known as the Ensenada Front since it was generally most prominent off Ensenada (Peláez and McGowan 1986). The large anticyclonic eddy centered roughly 320 km southwest of Punta Eugenia measured approximately 7.5 cm in height, the highest point in the anomaly field. Further inshore, the flow reversed from generally equatorward to poleward (Lynn and Simpson 1987). This inshore poleward flow intruded from the south and was associated with broad cyclonic flow centered off Cabo San Lucas and stretching to Punta Abreojos (a distance of around 560 kilometers). The poleward flow appeared to be similar to that described by Durazo and Baumgartner (2002) in October 1997 at the beginning of the 1997–98 El Niño when warm, salty subtropical surface waters comprised much of the system.

Chlorophyll *a*²¹ concentrations during summer 2018 ranged from <0.1 to almost 10 mg m^{-3} and anomalies from approximately -1.2 to 1.2 mg m^{-3} (fig. 24d). The Ensenada Front was captured by a weak, offshore, positive anomaly between San Diego and Ensenada. There were strong, positive anomalies off Ensenada and San Quintin with filaments jutting offshore. Negative anomalies predominated south of San Quintin, from line 110 through line 127, with only patches of positive anomalies west and northeast of Isla Cedros. Positive anomalies from Punta Abreojos to just south of Bahia Magdalena mostly overlapped areas with cool water, suggesting that upwelling and production were high here in sum-

mer 2018. Primary production²² varied from <0.3 to roughly 6 gCm⁻²day⁻¹ with anomalies ranging between approximately -1.5 to 1.5 gCm⁻²day⁻¹ (fig. 24e). Primary production anomalies largely mirrored chlorophyll *a* anomalies with mostly positive anomalies from approximately San Diego to Isla Guadalupe, negative anomalies from Isla Guadalupe to Punta Abreojos, positive anomalies from Punta Abreojos to just south of Bahia Magdalena, and negative anomalies at the southern tip of the peninsula.

REGIONAL EPIPELAGIC MICRONEKTON AND SALMON OBSERVATIONS

Northern California Current

The Northwest Fisheries Science Center and Oregon State University have conducted multiple surveys over the last two decades to measure the status of various biota at multiple trophic levels. Although the main goal is to examine ocean conditions that correlate to salmon survival, other elements of the surveys examine prey composition, abundance, and availability, competitors, and predators of the salmon. Since these surveys target different life stages, they occur at different times of the year but are relatively consistent in timing among years. Each of these seasonal datasets represents a unique ecosystem state that, taken as a whole, can help us understand the phenology of the Northern California Current (NCC).

Winter salmon forage indicators in the northern California Current Juvenile Chinook salmon feed primarily on late-larval and early-juvenile fishes when they enter coastal waters (Daly and Brodeur 2015). The late-larval and early-juvenile life stage of most marine fishes is difficult to sample effectively (Brodeur et al. 2011), which led us to explore alternative indices of potential prey fish abundance. The majority of marine fishes in the NCC spawn in late winter and early spring (Brodeur et al. 2008). Winter-spawned fish larvae that grow and survive through spring provide a food base for juvenile steelhead and coho and Chinook salmon during their first marine summer. Therefore, winter ichthyoplankton biomass was used as a proxy for potential salmon food availability during the spring critical growth period. This biomass included five of the most commonly eaten fish prey (Daly et al. 2013). During cold and productive periods in October–December from 1997 to 2013, ichthyoplankton biomass was relatively high, and coastal fish larvae such as Pacific sand-lance (*Ammodytes personatus*), smelts (Osmeridae), and

¹⁹Salinity was obtained from https://podaac.jpl.nasa.gov/dataset/SMAP_JPL_L3_SSS_CAP_MONTHLY_V42.

²⁰Sea surface height anomalies were obtained at <https://www.aviso.altimetry.fr/en/data/products/sea-surface-height-products/global/gridded-sea-level-anomalies-mean-and-climatology.html>.

²¹Chlorophyll *a* concentration was obtained at <https://esa-oceancolour-cci.org/> and <https://rsg.pml.ac.uk/thredds/dods/CCI>.

²²Primary productivity was obtained from the VGPM model (Behrenfeld and Falkowski 1997) that is available from Oregon State University <https://www.science.oregonstate.edu/ocean.productivity/> using data from MODIS Aqua. The model estimates net primary production as a function of chlorophyll concentration, available light, and the temperature-dependent photosynthetic efficiency.

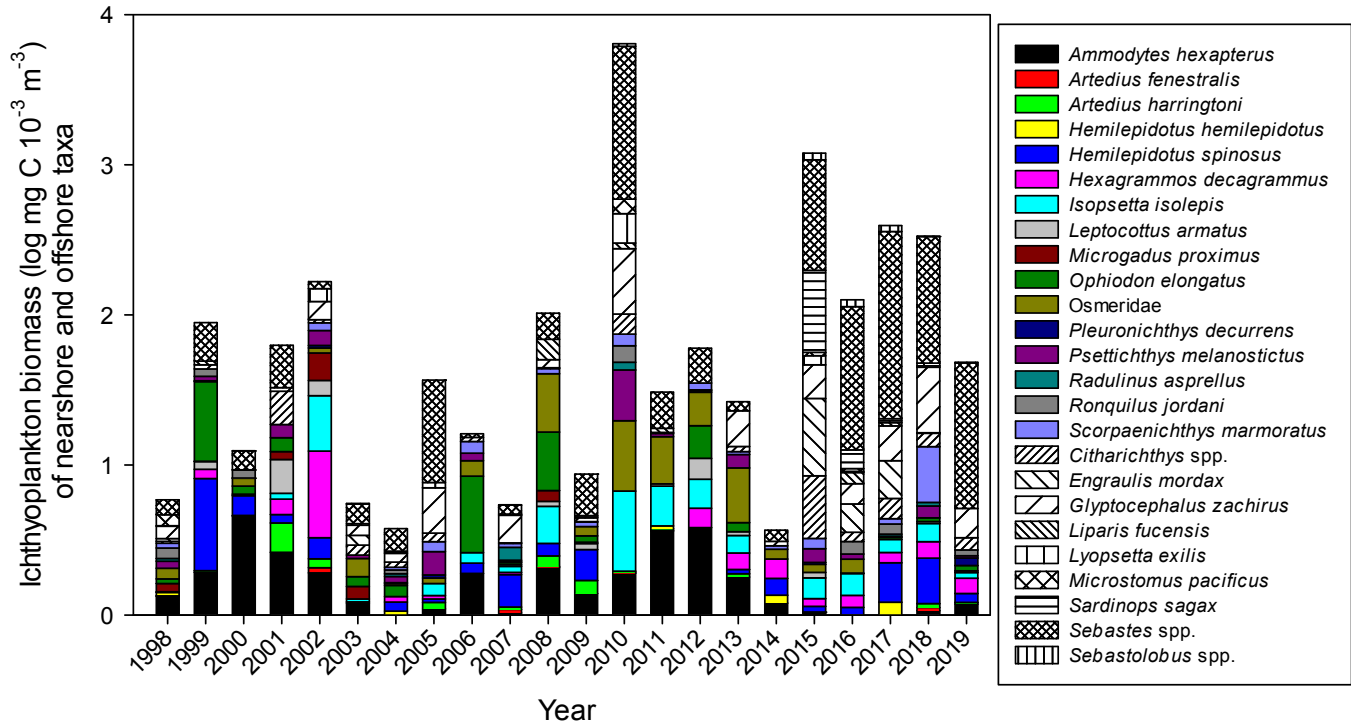


Figure 25. Annual average biomass of ichthyoplankton from winter (January–March) collected along the Newport Hydrographic Line (NH) line stations NH05–25. Taxa listed in color are coastal and make up the index of coastal prey biomass (ICPB). Taxa in black and white patterning reside offshore relative to the coastal taxa.

various sculpins (Cottidae) dominated the winter (January–March) fish communities (Daly et al. 2017). By contrast, when the ocean was relatively warm (coincident with onshore transport) in October–December of 1997 to 2013, overall winter ichthyoplankton biomass was low and dominated by offshore taxa such as rockfishes and winter-spawned northern anchovy (*Engraulis mordax*). Importantly, from 1997 to 2013, juvenile salmon survival was higher during the cold periods and lower during the warm periods.

The marine heat wave and El Niño of 2014–16 coincided with dramatic increases in SST temperatures throughout much of the northeast Pacific Ocean (+2.5°C; Bond et al. 2015), and this warming contributed to changes in the winter ichthyoplankton biomass and community not previously observed in the now 22-year time series (Auth et al. 2018). Specifically, there was a substantial increase in the observed cross-shelf differences in ichthyoplankton biomass (Daly et al. under review). Since 2015, the biomasses of offshore ichthyoplankton taxa increased significantly along the Newport Hydrographic Line (44.65°N, fig. 1), and juvenile salmon increasingly consumed these taxa (Daly et al. 2017). Moreover, the juvenile salmon that out-migrated in 2015–17, when there was a high biomass of offshore ichthyoplankton taxa, returned as adults to the Columbia River one to two years later in much reduced numbers compared to previous years²³.

In light of these changes, the winter ichthyoplankton biomass index based on winter ichthyoplankton samples from the Newport Hydrological Line²⁴ was modified from last year’s State of the California Current report (fig. 31 in Thompson et al. 2018) to include only taxa with cold-water affinity/coastal adult habitats (see fig. 25 for detailed list of the coastal [colored bars] and offshore [black and white bars] taxa). In addition, the number of taxa included in the new Index of Coastal Prey Biomass (ICPB) was expanded to include the coastal and offshore taxa beyond the top five fish prey of juvenile salmon that were analyzed previously (Thompson et al. 2018). Since 2014, the ICPB was below average with the exception of 2018 (which was more of an average year) and the coastal biomass index in 2019 was the third lowest in the 22-year time series (fig. 25). The community composition of ichthyoplankton in 2019 was once again dominated by offshore taxa, with the community indicator suggesting poor food conditions for piscivorous juvenile salmon that out-

²³Columbia River Data Access in Real Time [DART]; www.cbr.washington.edu/dart/query/adult_daily/; last accessed July 30, 2019.

²⁴Ichthyoplankton samples were collected from 5 stations spaced ~9 km apart along the Newport Hydrographic Line with a bongo net lowered to 100 m (or within 5 m of the bottom at shallow stations) and towed obliquely to the surface. Sampling was conducted approximately every 2 wk between January and March. Only samples from January–March were used, assuming that larvae collected during these months would have had sufficient time to grow to the average size of prey eaten by juvenile salmon in late spring and early summer (complete methods in Daly et al. 2017).

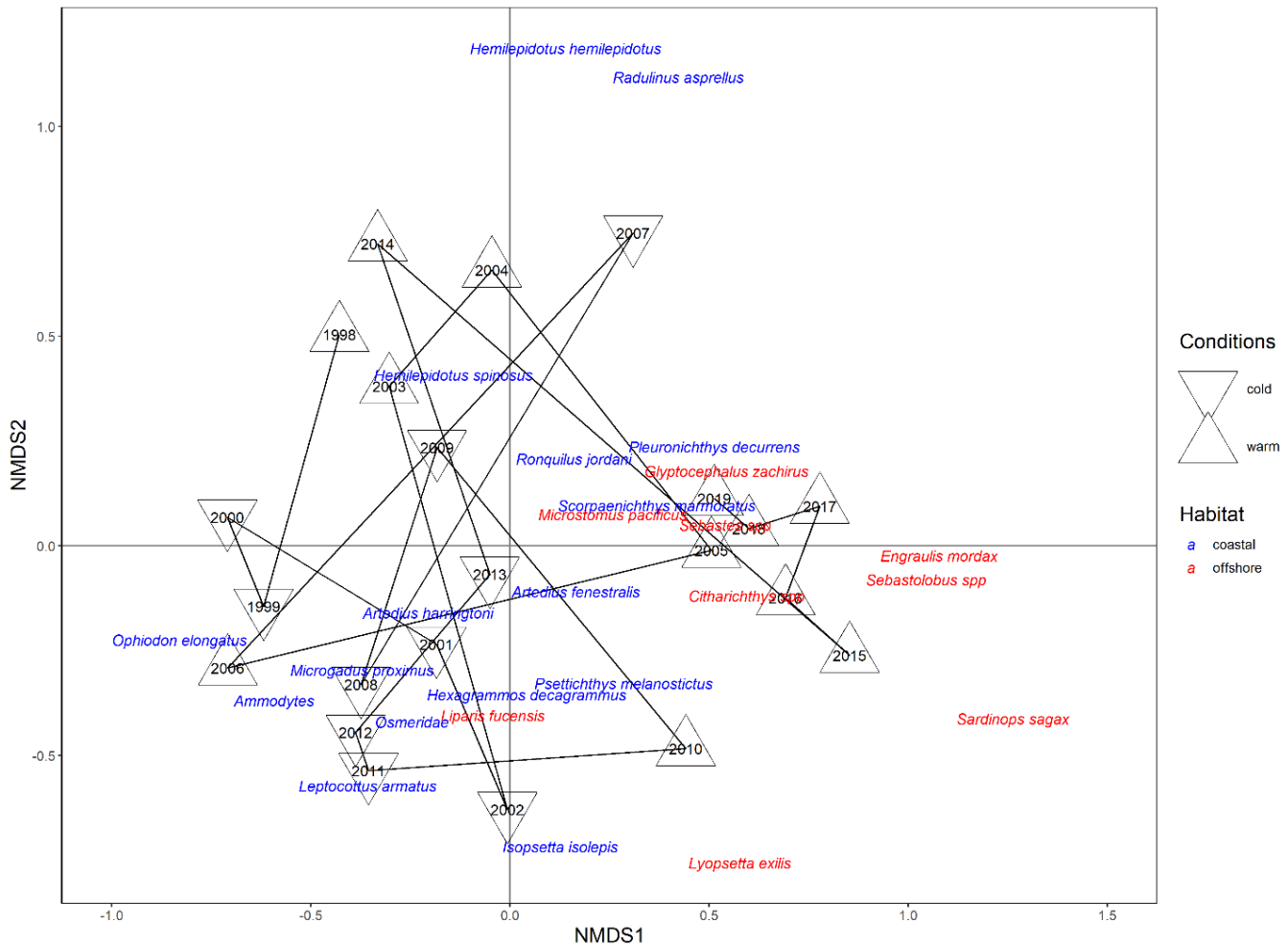


Figure 26. NMDS analysis of winter ichthyoplankton collected off the Newport Hydrographic line stations NH05-25. Taxa colored blue reside in coastal habitats as adults and those colored red live in offshore habitats as adults. Upward-facing triangles delineate warm years and downward-facing triangles cold years.

migrate into the ocean in 2019 (figs. 25, 26). Warm ocean conditions influence both the biomass and the community composition of winter ichthyoplankton in the NCC. Survival has uniformly been poor for juvenile salmon that out-migrated into the ocean since the marine heat wave of 2014–16. Ichthyoplankton biomass and species composition in 2019 were similar to those observed during 2015–18 (fig. 26), suggesting a continuation of the poor salmon returns for at least the next several years. Winter ichthyoplankton, especially the coastal taxa represented in the ICPB, are an important indicator of future food conditions for piscivorous juvenile salmon during a vulnerable and critical time in their life cycle.

Summer Pre-Recruit ichthyoplankton assemblage and micronekton assemblage In contrast to the winter findings described above, the composition and concentration of the summer ichthyoplankton assemblage along the central-northern coast of Oregon²⁵ in June 2019

was close to average relative to the previous 12 years (with the exception of the unusually high concentrations of northern anchovy in 2014 and 2016; fig. 27). Total mean larval concentration was the fourth highest in the 13-year time series. Larval myctophids in 2019 had the highest concentration of the time series, flatfish and “other” the second highest (although the “other” group still accounted for only 2% of the total mean larval concentration), and northern anchovy the fourth highest concentration. These observations are an indication that the larval fish community in the northern California Current was returning to a more “normal” or average state in the summer of 2019.

²⁵Ichthyoplankton samples were collected from 3–4 stations representing coastal (<100 m in depth), shelf (100–1000 m), and offshore (>1000 m) regions along both the Newport Hydrographic Line (44.65°N, 124.35–125.12°W) and Columbia River Line (46.16°N, 124.22–125.18°W) lines off the coast of Oregon during May–July in 2007–19. A bongo net lowered to 100 m (or within 5 m of the bottom for stations <100 m deep) and towed obliquely to the surface collected samples (complete methods in Auth (2011)).

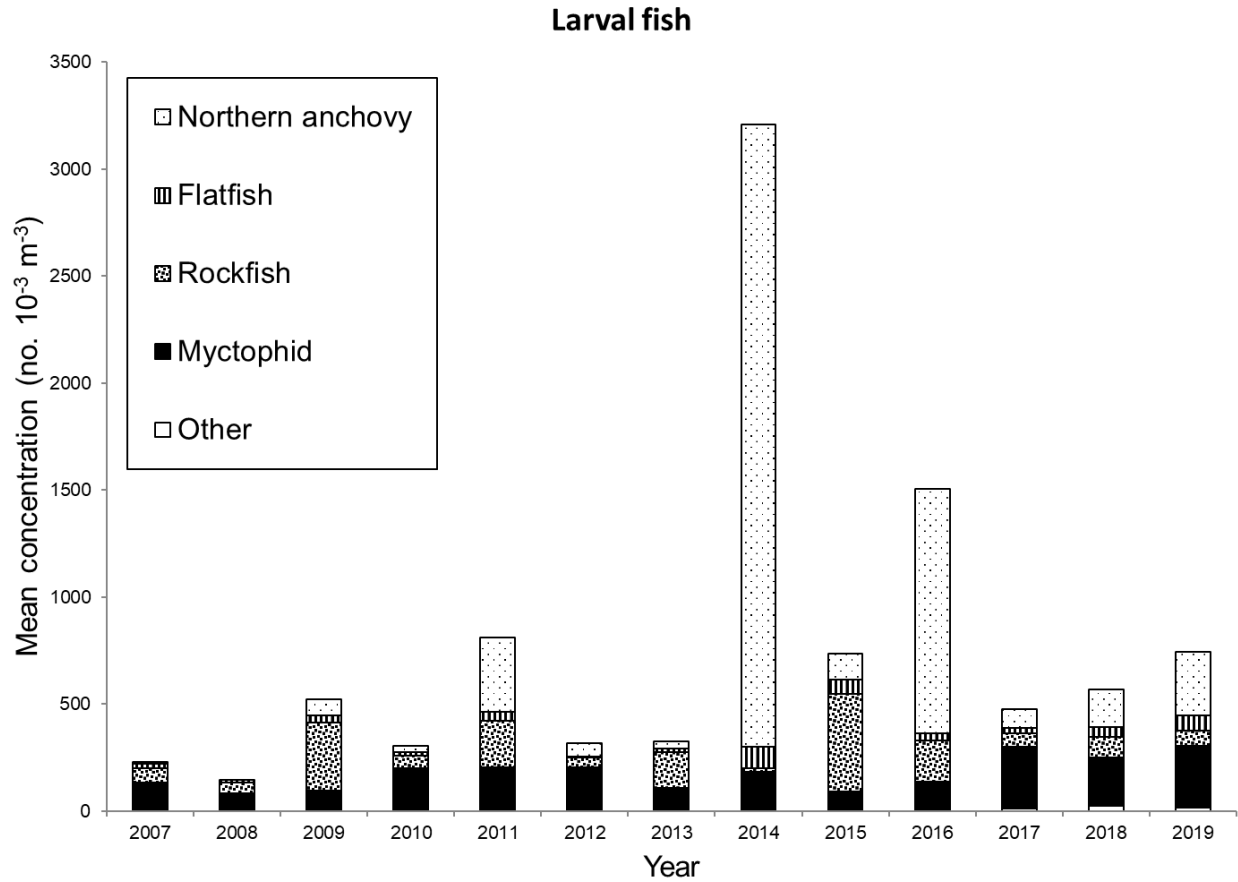


Figure 27. Mean concentrations (no. 10⁻³ m⁻³) of the dominant larval fish taxa collected during May–July in 2007–19 along the Newport Hydrographic (NH; 44.65°N, 124.35–125.12°W) and Columbia River (CR; 46.16°N, 124.22–125.18°W) lines off the coast of Oregon.

The summer micronekton assemblage²⁶, which consists of post-larval fish (i.e., juvenile and adult pelagic fish), in the NCC in June 2019 had average abundance for the eight-year time series, reversing the precipitous decline from 2016 to 2018 (fig. 28). The abundance of Clupeiformes and “other” taxa was the second lowest in the time series, while flatfish abundance was the highest. Rockfish abundance in 2019 was by far the highest for the time series (35 times the average rockfish abundance in 2011–18). High rockfish catch was primarily due to one large haul at the shelf-break station along the Columbia River line (46.0°N), where 7,474 juvenile rockfish were collected—mostly shortbelly rockfish (*Sebastes jordani*; n = 7343). Fourteen different taxa of rockfish were collected in 2019, with the dominant

species consisting of shortbelly (97% of total rockfish), widow (*S. entomelas*; 1.5%), and canary (*S. pinniger*; 0.7%). In addition, only one small pyrosome was collected in 2019, which was in sharp contrast to the extraordinarily high numbers throughout the sampling area in the previous three years (Brodeur et al. 2018). These observations are an indication that the pelagic juvenile/adult fish and tunicate communities in the northern California Current were returning to a more “normal” or average state in the summer of 2019.

In summary, the epipelagic ichthyoplankton and micronekton assemblages in the northern California current in 2019 exhibited different ecosystem states and spawning assemblages depending on the time of year the sampling occurred. In the NCC, the warm fall/winter SST conditions of 2018–19 induced low biomass of coastal ichthyoplankton taxa available in winter, as well as a predominance of fish taxa associated with warm water and offshore distributions. In contrast, by summer both the summer ichthyoplankton assemblage and the micronekton assemblages showed a return in both abundance and community composition to resemble an average ocean year. In addition to the seasonal difference

²⁶Post-larval (i.e., juvenile and some adult) fish were collected using a modified-Cobb midwater trawl (MWT) with a 26 m headrope and a 9.5 mm codend liner fished for 15 min at a headrope depth of 30 m and ship speed of ~2 kt. MWT collections were made at 3–6 evenly spaced, cross-shelf stations representing coastal, shelf, and offshore regions along nine half-degree latitudinal transects between 42.0 and 46.0°N latitude in the northern California Current region during May–July in 2011–19 (although no sampling was conducted in 2012). Sampled volume was assumed to be uniform for all hauls. All fish collected were counted and identified to the lowest taxonomic level often onboard, although pre-recruit rockfish were frozen and taken back to the lab for identification using precise meristic and pigmentation metrics.

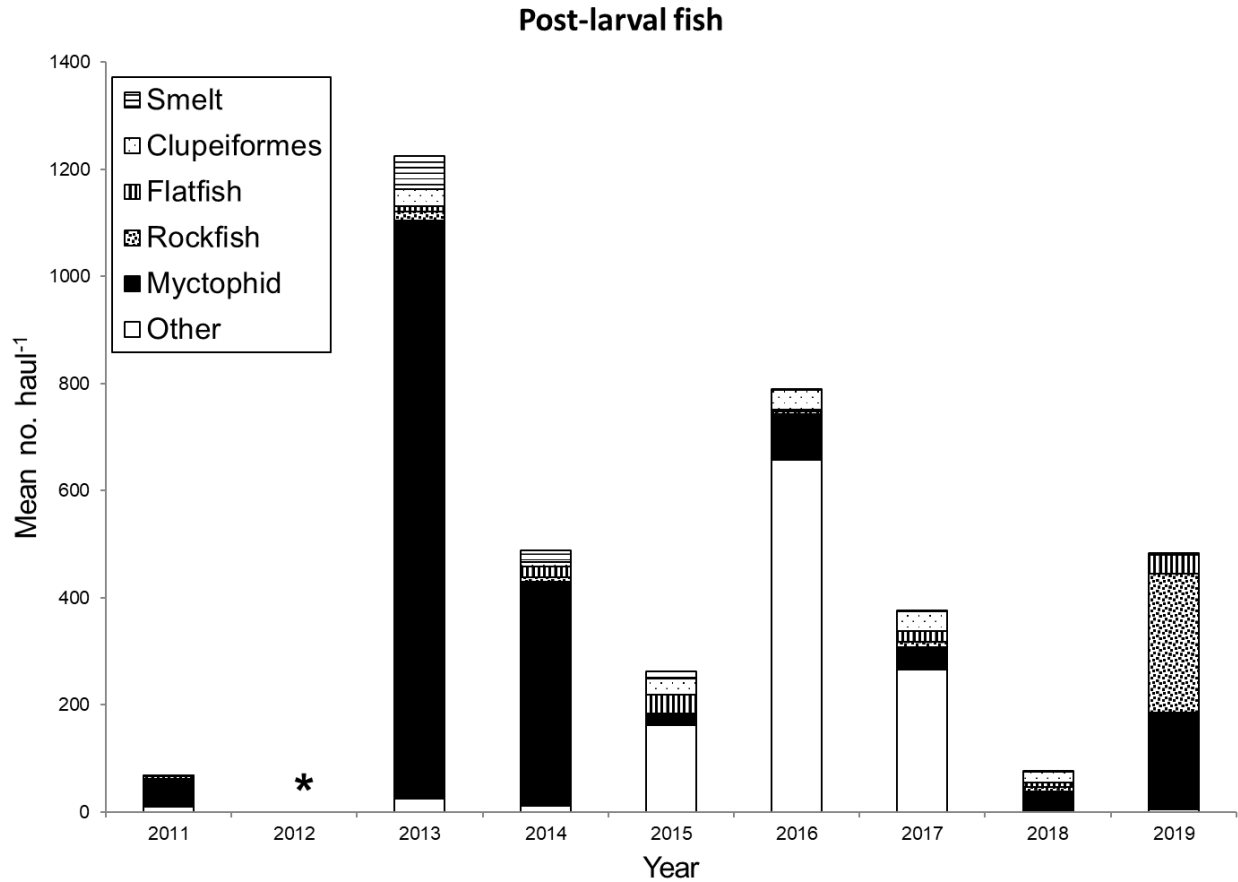


Figure 28. Mean catches (no. haul⁻¹) of the dominant post-larval fish taxa collected during May–July in 2011–19 along nine half-degree latitudinal transects between 42.0 and 46.0°N latitude in the northern California Current region. * = no samples were collected in 2012.

in when these ichthyoplankton data sets were collected, there were also differences in the spatial extent of sampling, suggesting that the differences between the two metrics could be either ecological change over time or simply representations of different ecosystems.

Juvenile Salmon and Ocean Ecosystem Survey (JSOES)

The fish and invertebrate assemblage from trawls in the upper 20 m off Oregon and Washington²⁷ in June 2018 and 2019 was less anomalous than during the preceding three years (fig. 29). During 2015–17, the NCC was dominated by taxa such as pyrosomes, Pacific mackerel (*Scomber pacificus*), and jack mackerel (*Trachurus sym-*

metricus) that typically reside in warmer waters to the south of the study area. An NMS ordination clearly showed that the 2015–17 assemblages were outliers, distinct not only from the 1999 La Niña assemblages, but also from the assemblage sampled during the 2005 warm event (Brodeur et al. 2006) in the NCC (fig. 29).

In 2018 and 2019, taxa such as Pacific pompano (*Pep-tilus simillimus*), which are typically only caught during warm years, were still present. Additionally, more California market squid (*Doryteuthis opalescens*) were captured in 2019 than any other year in the 22-year time series. Other common taxa in 2018 and 2019 included gelatinous species, yearling Chinook (*Oncorhynchus tshawytscha*), coho (*O. kisutch*), and juvenile chum (*O. keta*) salmon, and Pacific herring (*Clupea pallasii*). Pyrosomes, that were first captured in 2017 and still present in 2018, were absent in 2019.

Beginning in 2015, the jellyfish community off Washington and Oregon was quite different from previous years (fig. 30). Prior to 2015, the large, cool-water scyphozoan species, sea nettle (*Chrysaora fuscescens*), was numerically dominant. However, during the warm ocean years of 2015–16 and 2018, the more offshore-oriented

²⁷The JSOES has been conducted by the Northwest Fisheries Science Center (NWFS) in late June every year between 1998 and 2019. Sampling occurred along 11 east–west transect lines off Washington and Oregon (fig. 1), ranging from approximately 45° to 48°N. Trawls were conducted at 6 to 8 stations on each transect from the shallowest bottom depth possible (~30 m) out to ~50 km from shore, often extending beyond the continental shelf (Brodeur et al. 2005; Barcelo et al. 2018). Sampling was conducted during daytime in the upper 20 m of the water column at every station using a pelagic rope trawl with the headrope at about 1 m, that had a 336 m² mouth opening with variable mesh sizes (162.6 cm at mouth to 8.9 cm at cod end). To retain catches of small nekton, a 6.1 m long, 0.8 cm mesh knotless liner was sewn into the cod end. The rope trawl was towed for 30 minutes at a speed over ground of approximately 6 km h⁻¹.

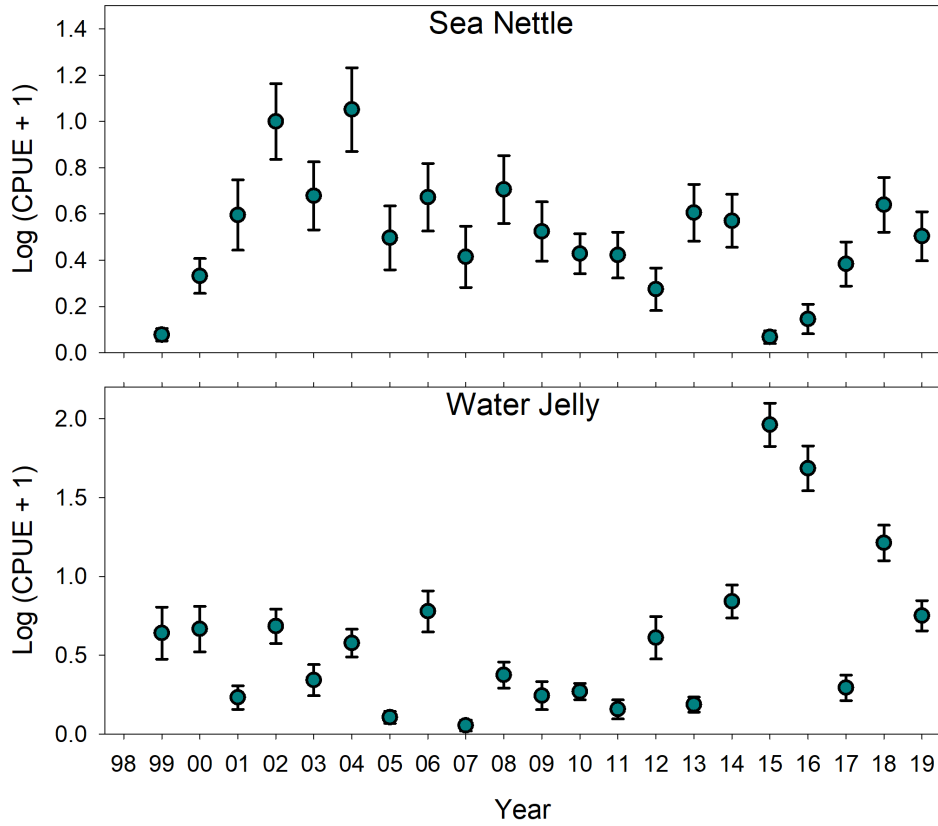


Figure 30. Catch per unit effort for common jellyfish by the Juvenile Salmon and Ocean Ecosystem Survey off Oregon and Washington.

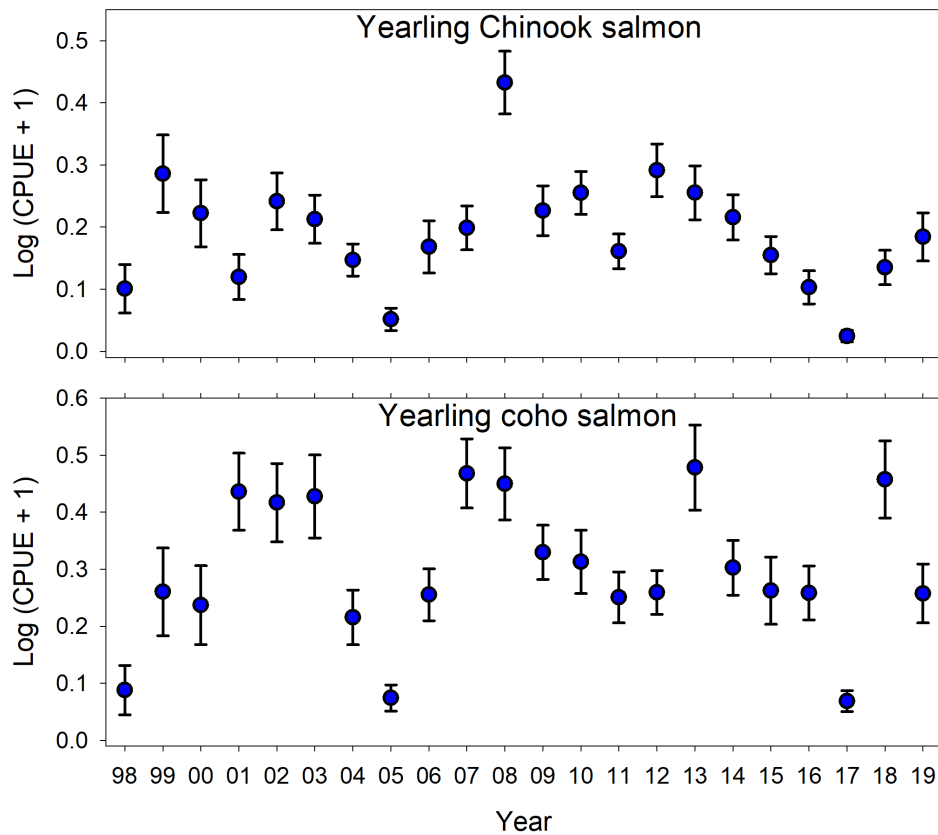


Figure 31. Catch per unit effort for yearling coho and Chinook salmon by the Juvenile Salmon and Ocean Ecosystem Survey off Oregon and Washington.

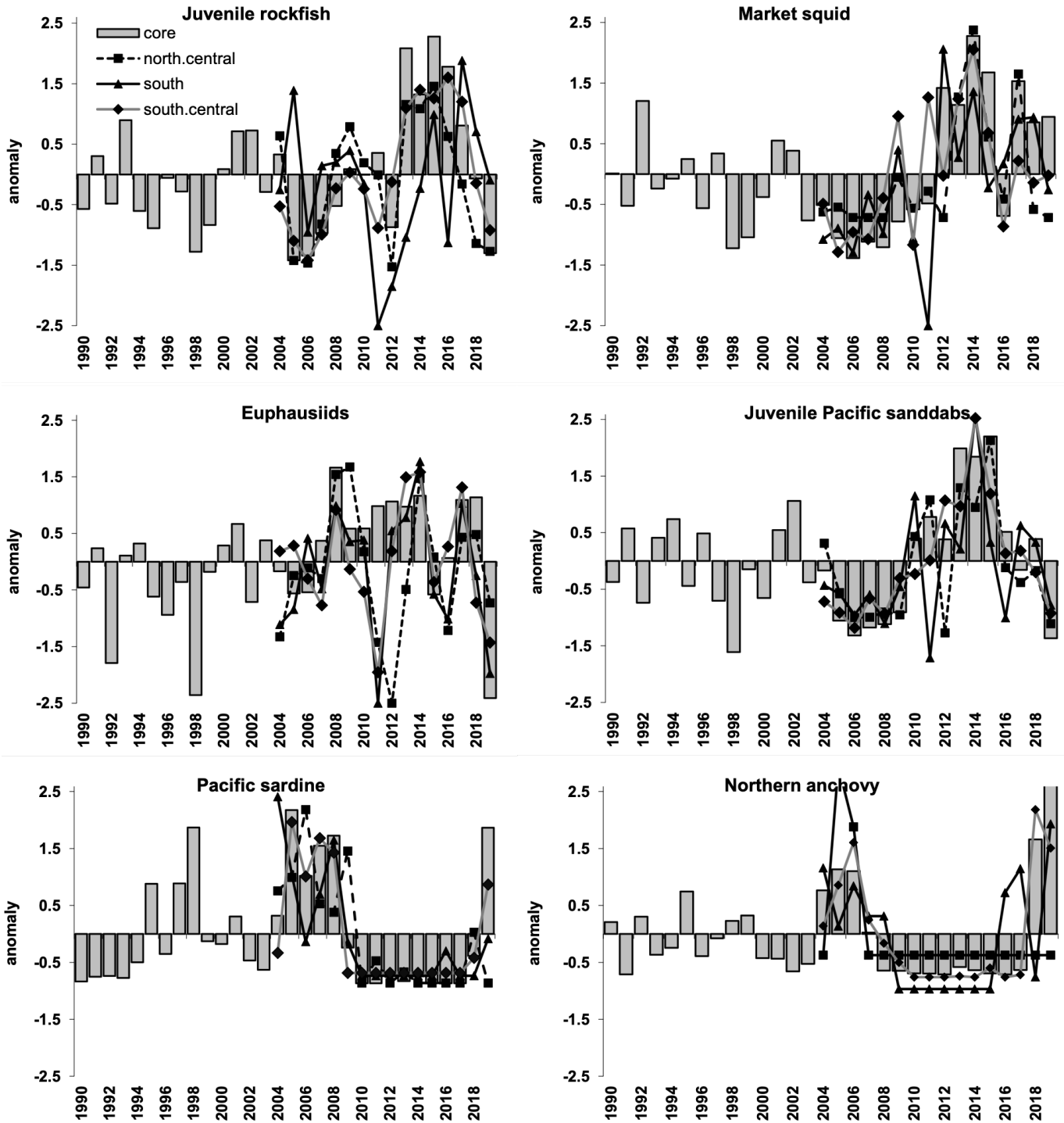


Figure 32. Standardized anomalies (of average $\ln(\text{catch}+1)$) catches for key forage taxa sampled by the Rockfish Recruitment and Ecosystem Assessment Survey.

and sanddabs (*Citharichthys* spp.), with strongly negative anomalies following near-average levels in 2018 and very high abundances from 2013–17 (fig. 32). Abundance of YOY rockfishes was greatest again in the Southern California Bight, where catches were close to the long-term average. YOY Pacific hake (*Merluccius productus*, not

shown) were at low abundance in central California, although this species was fairly abundant in the Southern California Bight. No YOY lingcod (*Ophiodon elongatus*) were captured in 2019.

The high abundance of adult northern anchovy in the core and south central regions continued in 2019

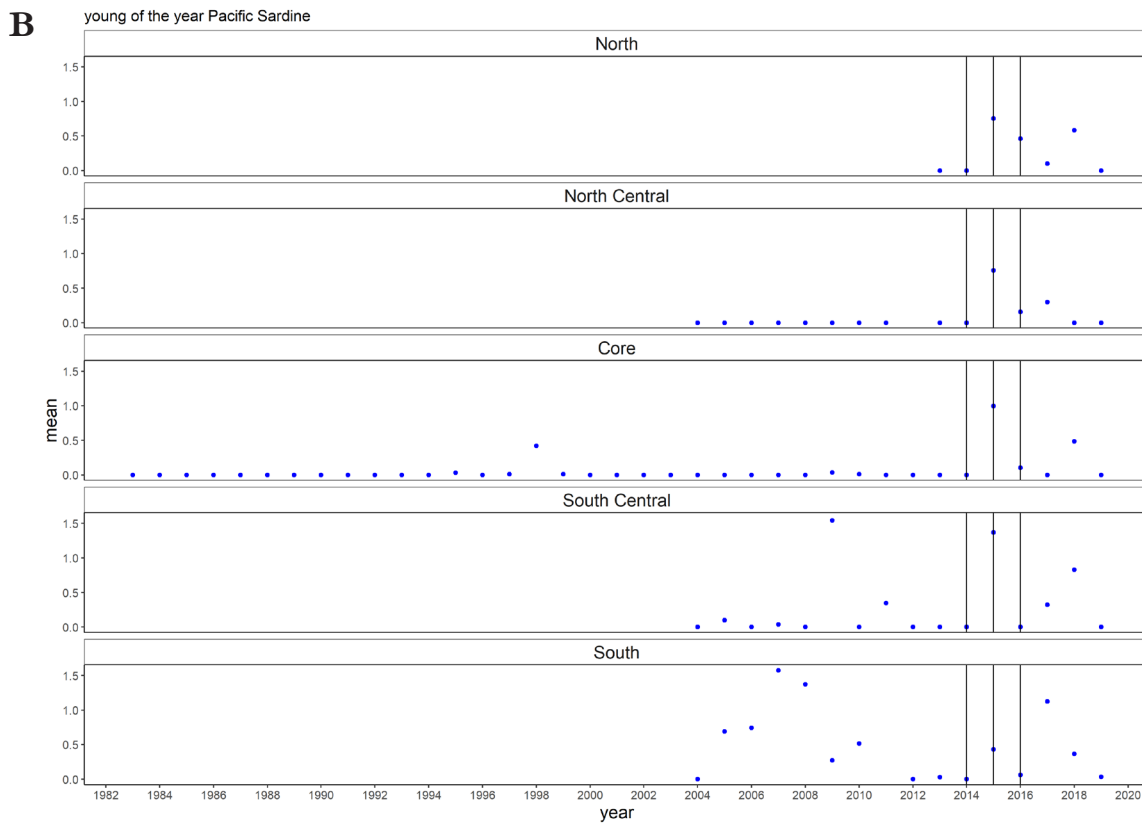
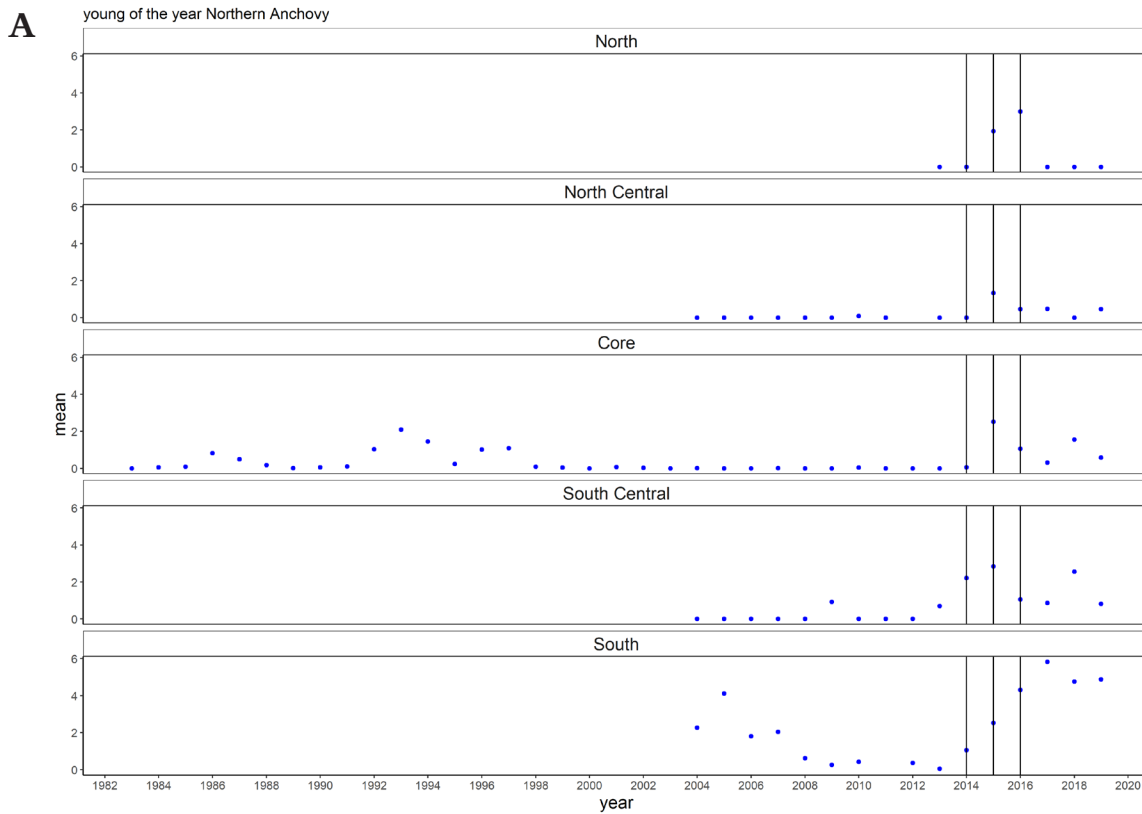


Figure 33. $\ln(\text{catch}+1)$ average catch for (A) young-of-the-year northern anchovy and (B) young of the year Pacific sardine from the RREAS in 5 regions off California.

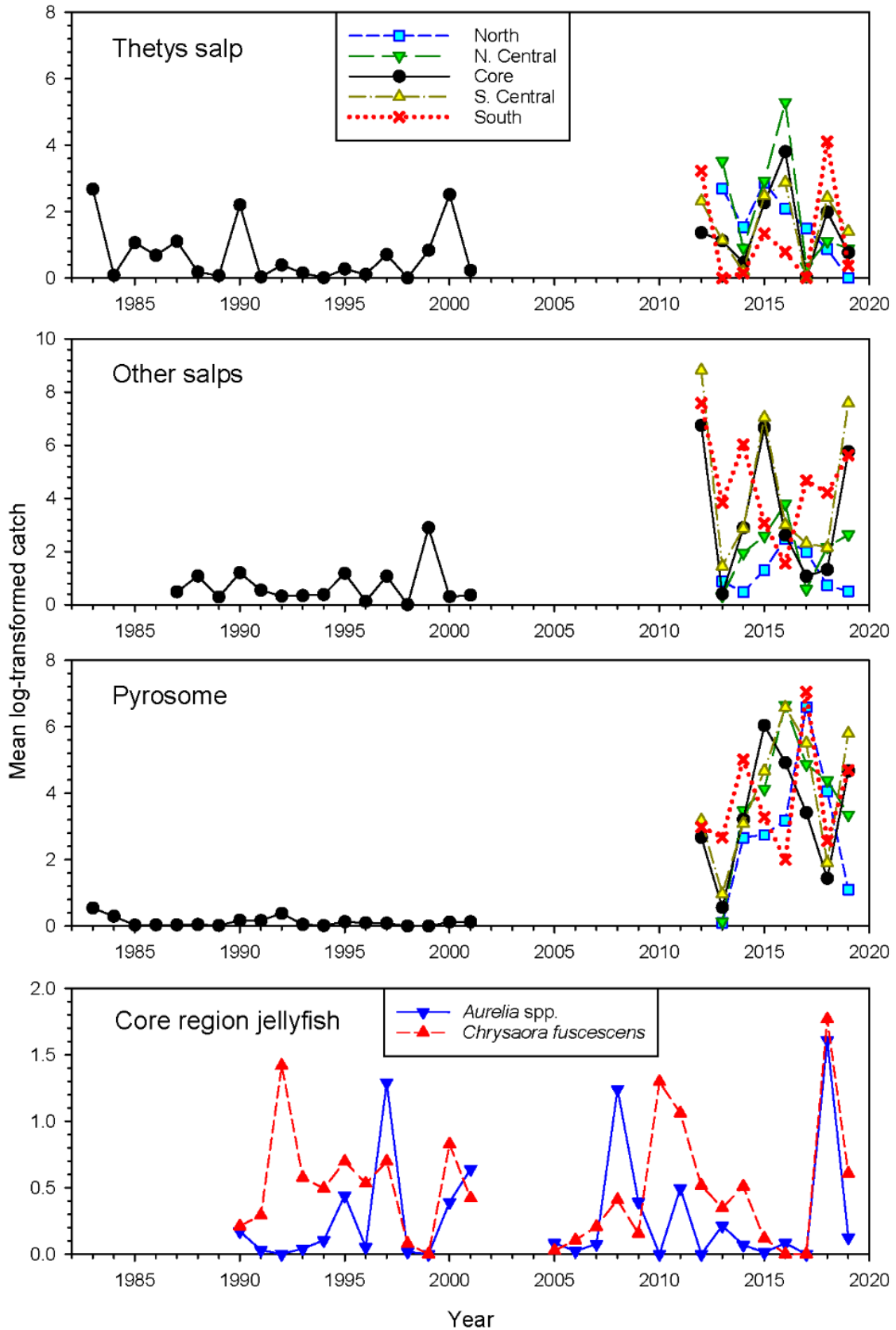


Figure 34. Standardized catches of and pelagic tunicates (*Thetys* salps, other salps, and pyrosomes) and jellyfish (*Aurelia* spp. and *Chrysaora fuscescens*) in the core and expanded survey regions.

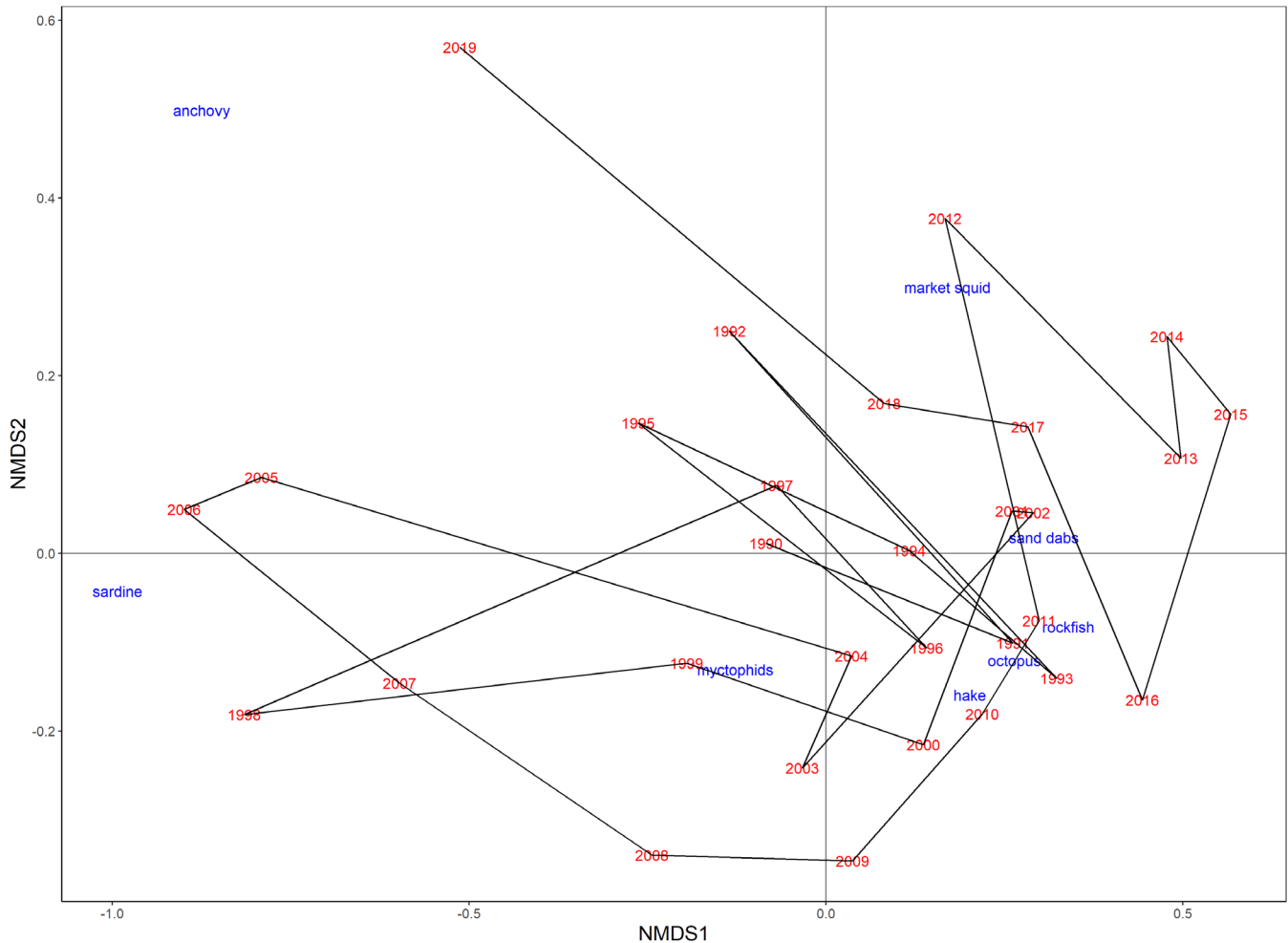


Figure 35. NMDS graph for the nine key taxonomic groups of forage species sampled in the central California core region in the 1990–2019 period.

(fig. 32). In fact, the relative abundance of adult anchovy in the core area was higher in 2019 than any previous year in the survey (extending back to 1983). Adult Pacific sardine were more abundant than in roughly the last ten years but still at low abundance relative to the late 1990s and early 2000s.

In 2015, YOY northern anchovy were at the highest level on record in each region with the exception of the south where abundance was second-highest only to 2005 (fig. 33). YOY northern anchovy remained high in 2016 in the north, south central and core regions in 2016. In 2019, YOY northern anchovy (fig. 33a) were at low levels throughout the survey area in, with the exception of the Southern California Bight, where abundances have been very high since 2015 (fig. 33a). YOY Pacific sardine abundance was also high in 2015 relative to prior years (fig. 33b). Subsequent to 2015, YOY Pacific sardine abundance was high in select regions and years (2018 in the north, core and south central; 2017 in the south), but was uniformly low in 2019. Overall, YOY northern anchovy were

much more abundant than YOY Pacific sardine (note that scales differ between panels in fig. 33a and b).

There were substantial declines in krill, particularly in the core region where abundance was comparable to 1998 (the lowest value in the 1990–2019 time series), a pattern which extended throughout most California waters (fig. 32). However, market squid were at fairly high abundance levels in the core region, and closer to average or just below average levels in other regions. Pelagic red crab (*Pleuroncodes planipes*, not shown) also continued to be encountered in the southern California Bight, albeit with a slow decline since the 2015 peak.

Shifts in the abundance of various gelatinous organisms showed reversals for 2019 relative to recent years (fig. 34). Catches of salps in the genus *Thetys* were low in 2019 relative to recent years; however, catches of other salps and pyrosomes were higher in 2019 than 2018, reflecting sustained high abundance of pelagic Thalacians in California waters (despite the tremendous drop in pyrosome abundance off Oregon and Washington). There

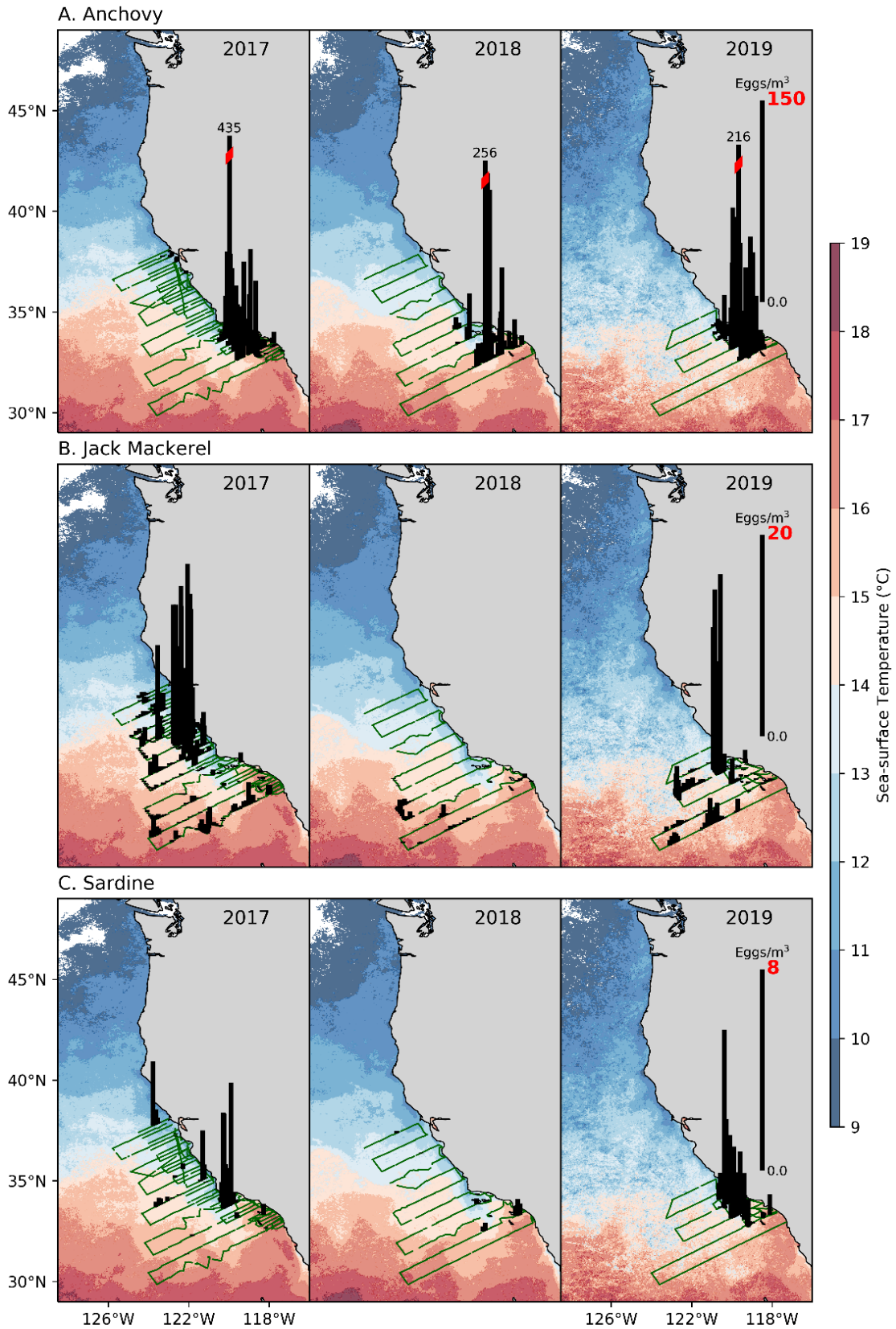


Figure 36. Density of eggs of anchovy (A), jack mackerel (B), and sardine (C) collected with the continuous underway fish egg sampler (CUFES) during the spring 2016–18 CalCOFI cruises. Data were overlaid on satellite-derived sea surface temperatures (AVHRR 1.4-km resolution; °C). Note that scales differ among species.

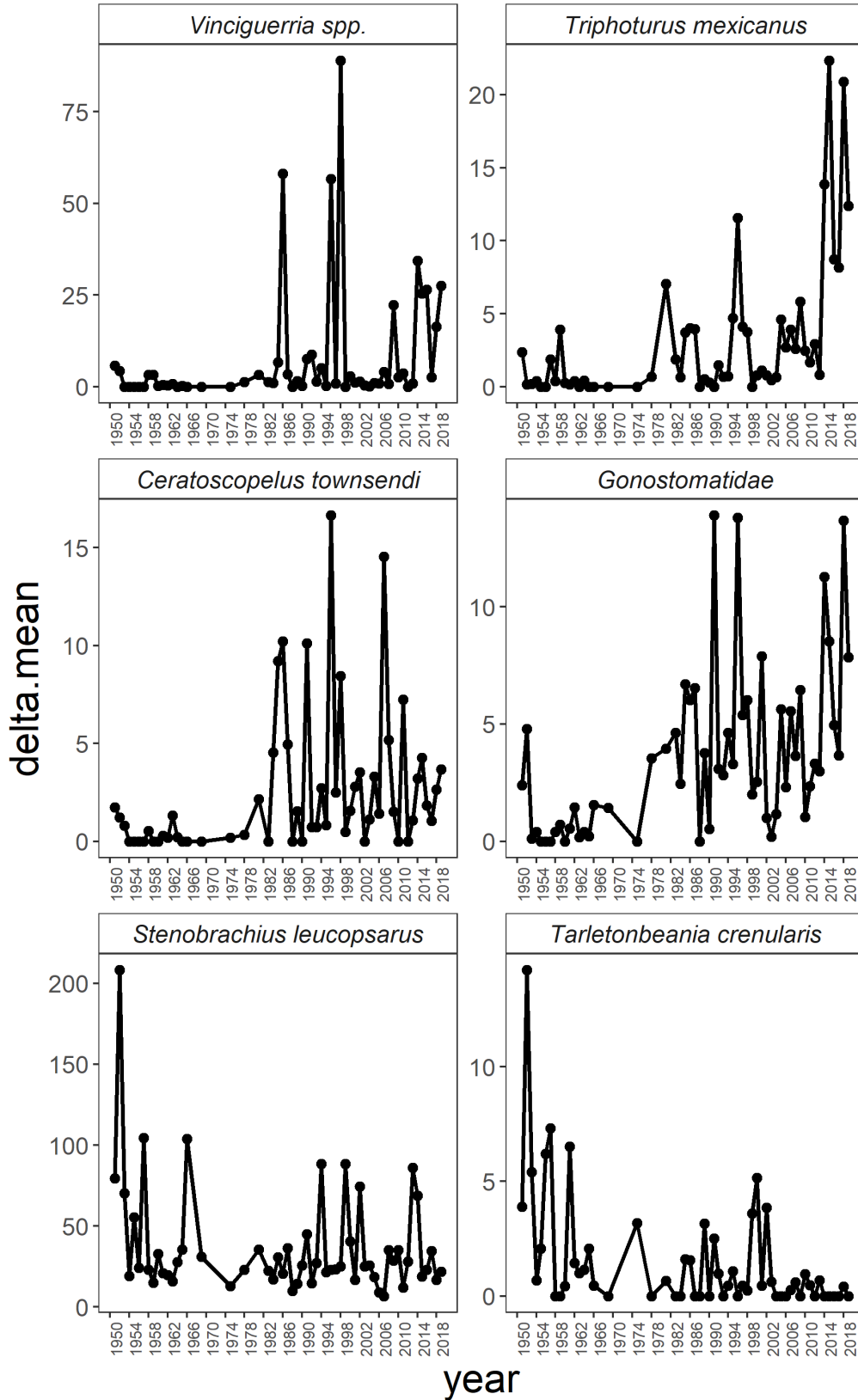


Figure 37. Mean abundances (calculated using the delta method of Nelson (2016), which accounts for zero inflation) of ichthyoplankton of mesopelagic taxa with warm (*Vinciguerria* spp., *Triphoturus mexicanus*, *Ceratoscopelus townsendi* and *Gonostomatidae*) and cool (*Stenobrachius leucopsarus*, *Tarletonbeania crenularis*) water affinities collected in spring on CalCOFI lines 80 and 90.

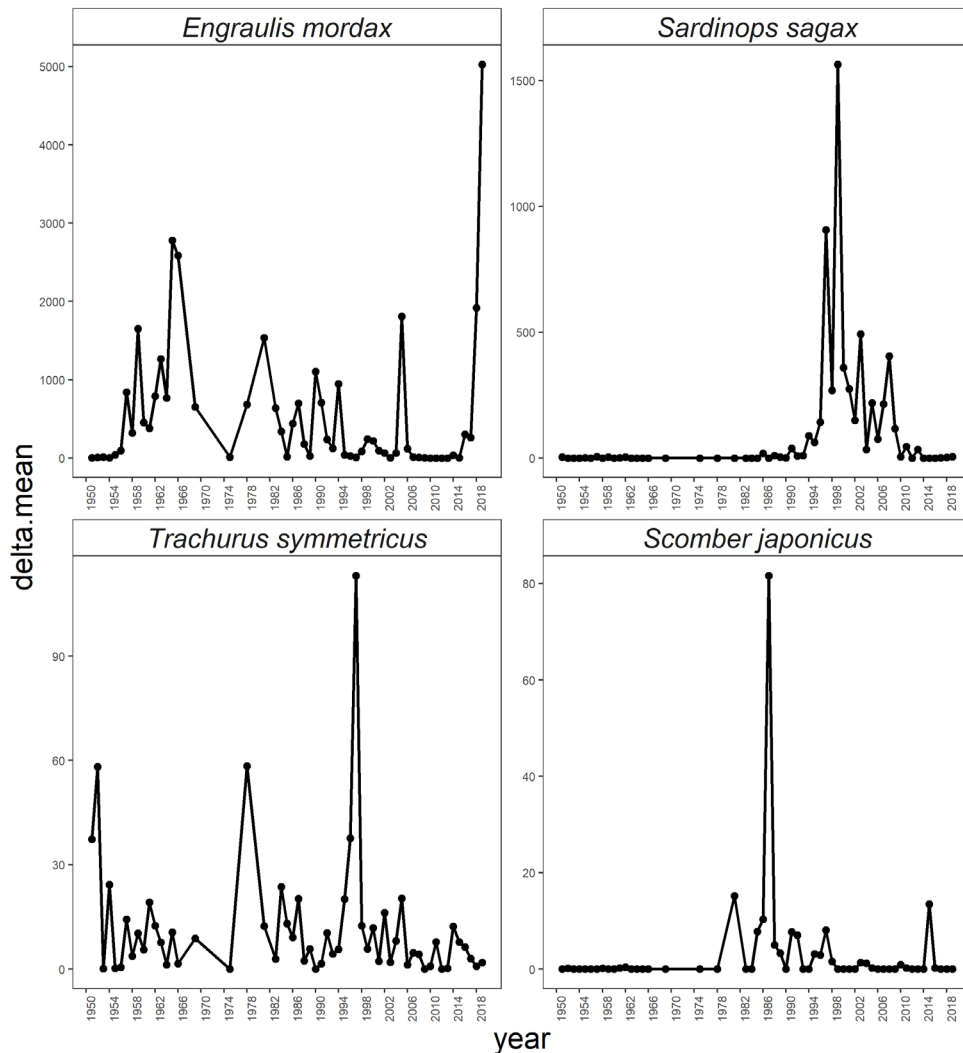


Figure 38. Mean delta abundances of ichthyoplankton from coastal pelagic species collected in spring on CalCOFI lines 80 and 90.

was a sharp reversal of the very high catches of scyphozoan jellyfish (primarily *Aurelia* spp. and *Chrysaora fuscescens*) from 2018, when both species were encountered at high abundance levels, although catches of *C. fuscescens* was close to long-term average levels.

NMDS analysis based on mean log catch of the fish and cephalopod community from the core RREAS region between 1990 and 2019 reflected the unprecedented dominance of adult northern anchovy the increase in Pacific sardine, and the scarcity of rockfishes and sanddabs (fig. 35). NMDS axis 2 correlated positively with anchovy and market squid abundance, and negatively with YOY Pacific hake and myctophids; the 2019 NMDS 2 value was the highest in the time-series. NMDS axis 1 correlated negatively with both northern anchovy and Pacific sardine abundance and positively with YOY rockfishes and sanddabs, and the 2019 NMDS axis

1 value was also relatively low, reflecting a reversal of the positive values observed over the preceding decade.

CalCOFI Continuous Underway Fish Egg Sampling (CUFES) Egg abundance of northern anchovy, jack mackerel, and Pacific sardine in spring 2019²⁹ was greatest in the northwest portion of the Southern California Bight and off Point Conception in waters with sea-surface temperatures of about 13.5–15°C (fig. 36). Although the spring CalCOFI survey often extends north to San Francisco, the spatial coverage of 2019 sampling was limited to the core CalCOFI area (fig. 1).

Northern anchovy was the most abundant species sampled in 2019. Northern anchovy egg abundances

²⁹Water was continuously pumped onto the ship from a depth of 3 m while the ship was underway. Water samples were filtered on the ship and collected sequentially at regular (5–30 minutes) intervals. Detailed methods in Checkley et al. (1997).

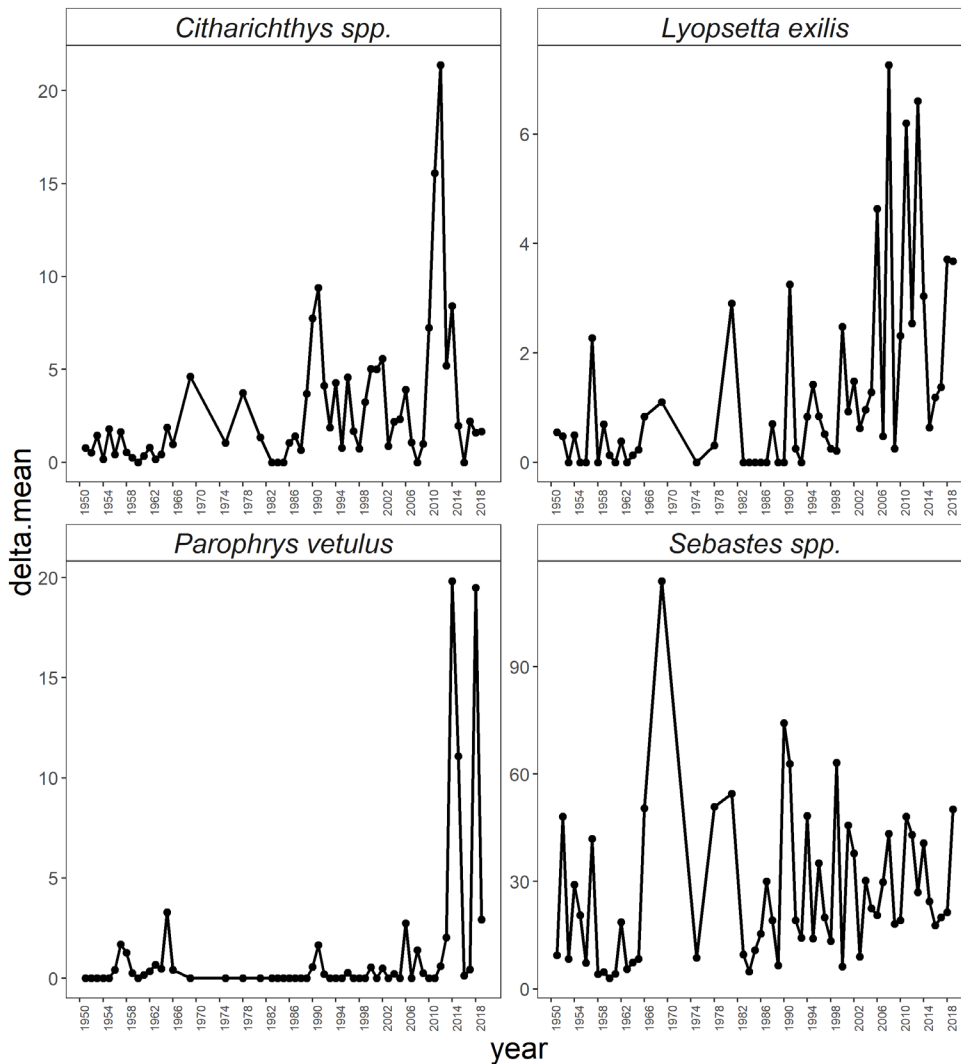


Figure 39. Mean delta abundances of ichthyoplankton from groundfishes collected in spring on CalCOFI lines 80 and 90.

have been some of the greatest in the CUFES time series (1996–present) for the three-year period 2017–19, following a period of very low abundance from 2009–16. The distribution pattern of anchovy eggs was similar in 2019 to that of the previous 2 years (fig. 36a).

Jack mackerel egg abundance was greater in 2019 than the extremely low-abundance year of 2018 (fig. 36b; note that scales differ by species). Overall, jack mackerel egg abundance was high relative to the last decade but generally less than that of the early and mid-2000s. Relatively large catches of jack mackerel eggs occurred near Point Conception but eggs were captured as well throughout the core CalCOFI sampling area.

Pacific sardine egg abundance also increased somewhat in 2019 following the lowest abundances recorded in the CUFES data set in 2018 (fig. 36c). However,

Pacific sardine egg densities remained very low relative to the 2000s, as they have been since 2014.

CalCOFI Ichthyoplankton The larval fish assemblage³⁰ from CalCOFI lines 80 (~34°N, fig. 1) and 90 (~32.5°N, fig. 1) in spring 2019 revealed the continued high abundance of mesopelagic species with warm-water, southern affinities such as Panama lightfish (*Vinciguerria lucetia*), Mexican lampfish (*Triphoturus mexicanus*), dogtooth lampfish (*Ceratoscopelus townsendi*) and bristlemouths (Gonostomatidae—mostly *Cyclothone signata*) (fig. 37). Although the abundance of these taxa was lower than the peak years subsequent to 2013, abundances were still very high relative to pre-MHW years. By contrast, mesopelagic species with cool-water affini-

³⁰Bongo nets lowered to 210 m (or 10 m from the bottom in shallow sites) and towed obliquely to the surface collected ichthyoplankton. See Thompson et al. (2019) for detailed methods.

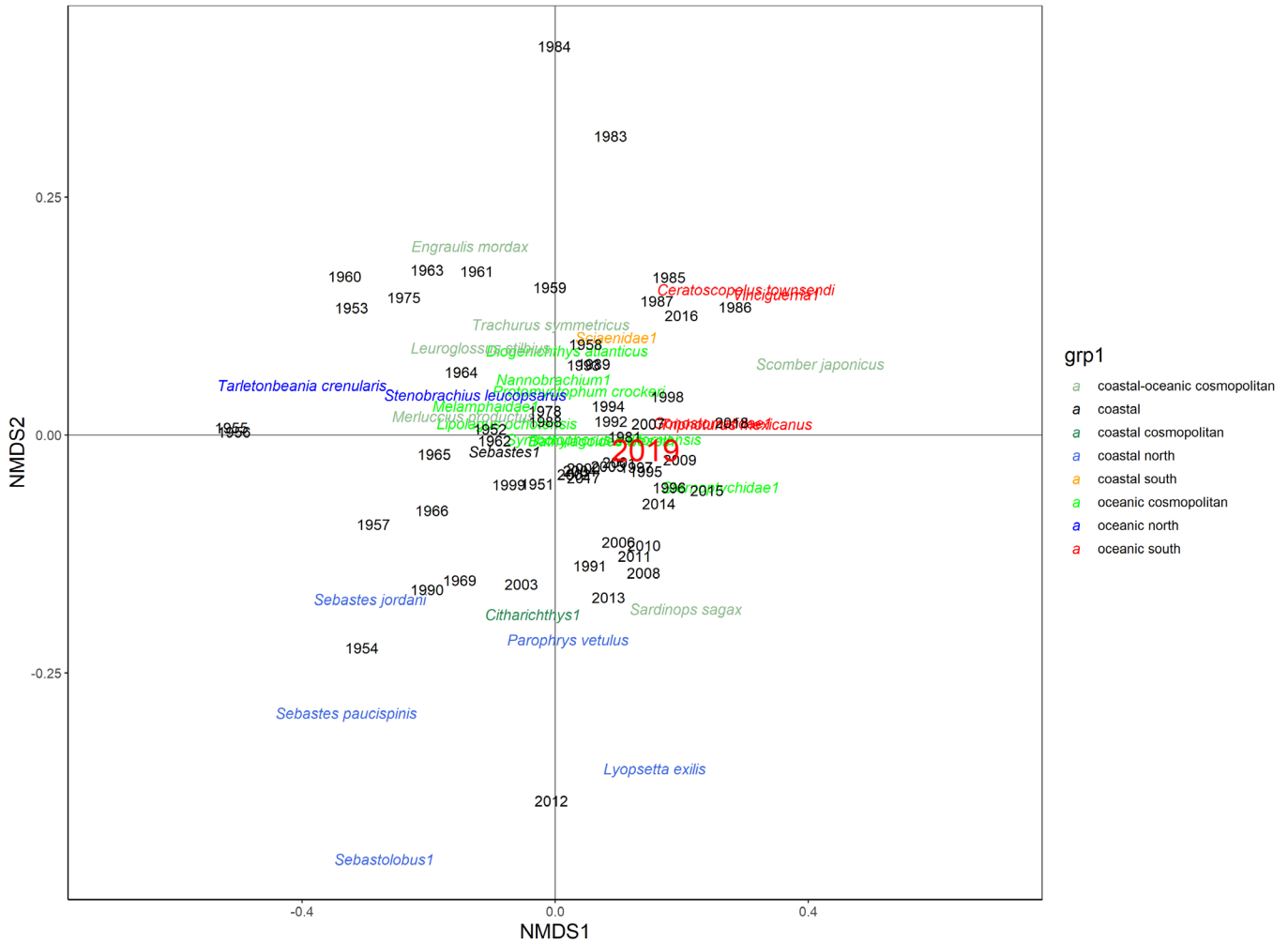


Figure 40. NMDS plot of the ichthyoplankton assemblage from CalCOFI lines 80 and 90 in spring. Adult habitat affinity defines taxa colors. 2019 is demarcated by the yellow circle to the right of the plot center.

ties (northern lampfish [*Stenobranchius leucopsarus*]) and blue lampfish [*Tarletonbeania crenularis*] remained near historically low abundances in 2019 (fig. 37).

Coastal pelagic species provided the most anomalous finding in the larval fish assemblage in 2019 (fig. 38). Whereas Pacific sardine, jack mackerel and Pacific mackerel remained at low levels, northern anchovy larvae were the most abundant in the history of CalCOFI. Indeed, 2019 northern anchovy values were nearly double the prior record high from the 1960s.

Among groundfishes, sanddabs abundances were low relative to prior years (fig. 39). Slender sole (*Lyopsetta exilis*), English sole (*Parophrys vetulus*) and rockfishes were close to long-term averages.

From a multivariate perspective, NMDS axis 1 separated assemblages dominated by warm water versus cool water taxa (fig. 40), and NMDS axis 2 mainly separated northern anchovy from rockfishes, slender sole, Pacific sardine, and English sole. The larval fish assemblage from

2014–18 loaded heavily and positively on NMDS axis 1, reflecting high abundances of warm mesopelagics. In 2019, these warm water mesopelagics were still abundant, but northern anchovy were by far the most abundant species over all. In fact, 2018 and 2019 were the only years when both northern anchovy and the mesopelagics were all top 5 in yearly abundance. The 2019 NMDS value likely reflected the competing influence of northern anchovy and warm water mesopelagic taxa. Whereas the 2019 value still aligned with the warm water mesopelagics, it was closer to the center than 2018, likely reflecting the influence of northern anchovy.

REGIONAL PATTERNS IN BIRDS

Northern California Current: Yaquina Head, Oregon

Common murre (*Uria aalge*) at Yaquina Head (44.4°N, fig. 1) experienced moderate reproductive success in

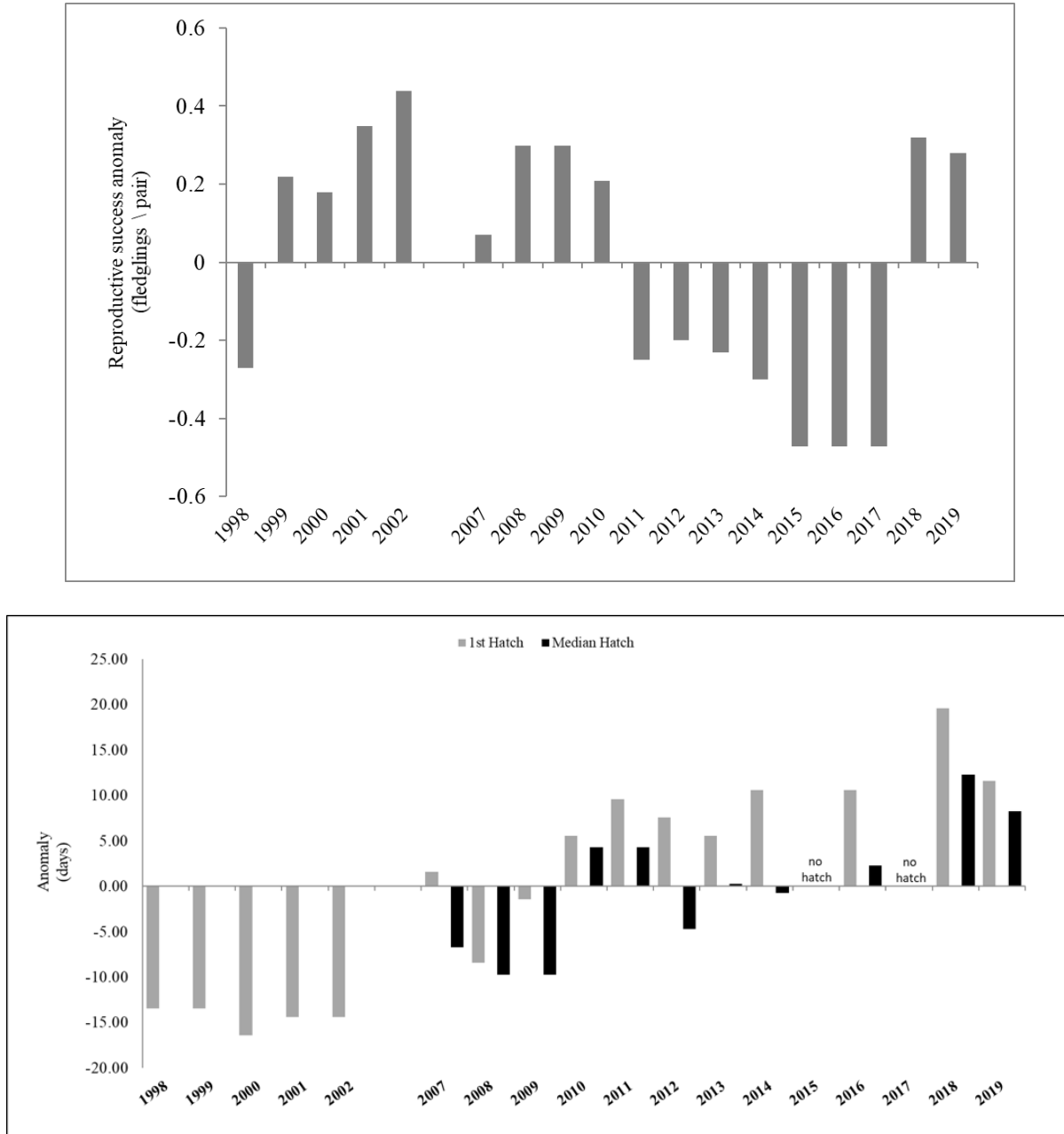


Figure 41. Anomalies of reproductive success (top), and first and median chick hatch dates (bottom) for common murres nesting at Yaquina Head, Oregon, 1998–2019. 2019 was the second year of reproductive success following consecutive years of near or total failure (2014–17).

both 2018 and 2019 following a sustained period of near or total failure from 2014–17 (fig. 41 top). Median hatch dates were later than the mean from 1998 to 2017 in both years: July 15 (2018), and July 9 (2019; fig 41 bottom). In 2018, overall hatching success was 51% and 79% of these chicks successfully fledged. In 2019, there was higher hatching success (69.7%), and 79% of these chicks successfully fledged. These were the most successful years for common murre since productivity at Yaquina Head began a steady decline in 2010.

As in previous years, both top-down predation and bottom-up prey availability affected common murre reproductive success at Yaquina Head. Bald eagles (*Haliaeetus leucocephalus*) prey on adult common murre, often leading to colony disturbances that allow secondary predators access to eggs and chicks (Horton 2014). Notably, in 2018, egg (0.78 eggs/hr) and chick (0.04 chicks/hr) depredation was the lowest since 2009 despite average rates of disturbance (0.39 disturbances/hour; long-term mean: 0.38 disturbances/hour). Ninety

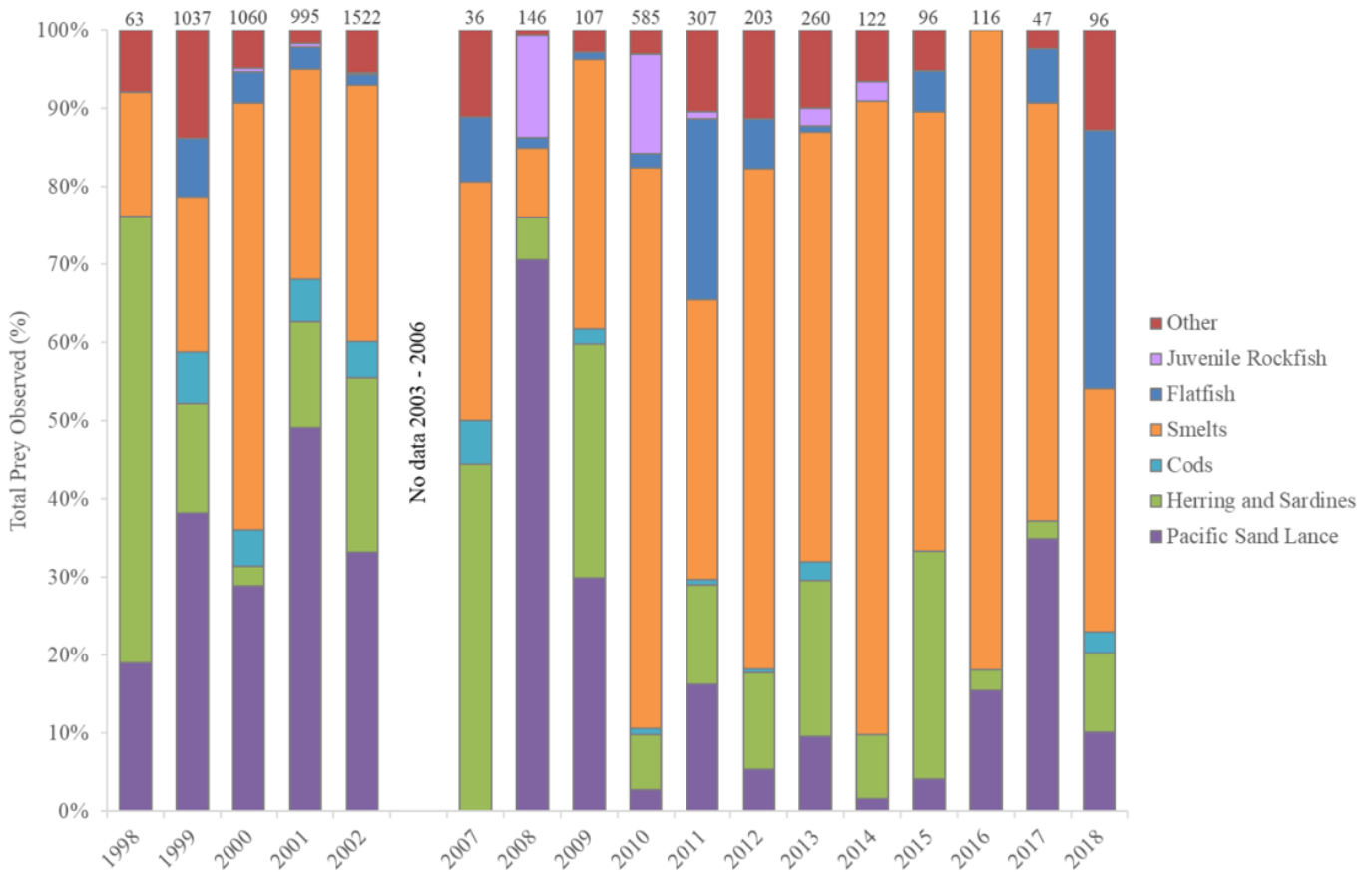


Figure 42. Prey composition of common murre diets at Yaquina Head 1998–2018 with annual sample size of identified prey items indicated above each bar. Proportions were highly variable year to year, and smelts typically appeared as the majority of diet composition (particularly 2010–17).

percent of all observed disturbances in 2018 occurred prior to the first observed chick hatch (July 7). Common murre appeared less likely to flush and abandon eggs than in years of reproductive failure (2015–17). In 2019, the frequency of predator disturbance events was the lowest of the past 10 years (0.15 disturbances/hr). From 2013–19, the “Flat Top” subcolony experienced near or complete failure, while the largest subcolony, Colony Rock, appeared to be more resilient (experienced failure 2015–17). Consistent with this, Colony Rock had medium-to-high rates of productivity in both 2018 (68% of nests hatched chicks, 47% of chicks successfully fledged) and in 2019 (91% of hatched chicks, 86% successfully fledged).

Common murre³¹ diets at Yaquina Head were highly dynamic between 1998 and 2018 (fig. 42). In 2018, the rate of flat fish provisions was the highest in the data set. Although smelts typically represented a large portion of the diet there appears to be a negative correlation between the proportion of smelt in common murre

diet and reproductive success (figs. 41, 42). Diet observations were collected in 2019, but prey identification is forthcoming.

In 2018, overall reproductive success increased for Brandt’s cormorant (*Phalacrocorax penicillatus*) and pelagic cormorant (*Phalacrocorax pelagicus*) (fig. 43). Both species were similarly successful in rearing and fledging chicks in 2019. Brandt’s reproductive success in 2018 was high (1.69 fledglings/nest), and in 2019 was the highest (1.89 fledglings/nest) in the time series (2008–19; fig. 43). Median hatch date for Brandt’s cormorants was later in 2018 (July 10) than in 2019 (July 5, fig. 44).

Northern California Current: JSOES Cape Flattery, Washington to Newport, Oregon

The JSOES (44.4°N to 48.3°N, fig. 1) has sampled at-sea seabird distribution and density patterns for the northern domain of the California Current during June from 2003–19. Data from 2019 indicated this region returned to more typical (near-median) summer seabird densities and distributions compared to the extremely low densities observed in 2017 (fig. 45). Mean total bird density in the 2019 survey was the 9th highest reported

³¹Diet data were collected 2-5 days per week during the chick-rearing period. Single prey items carried in the bill of adult murre were digitally photographed for identification.

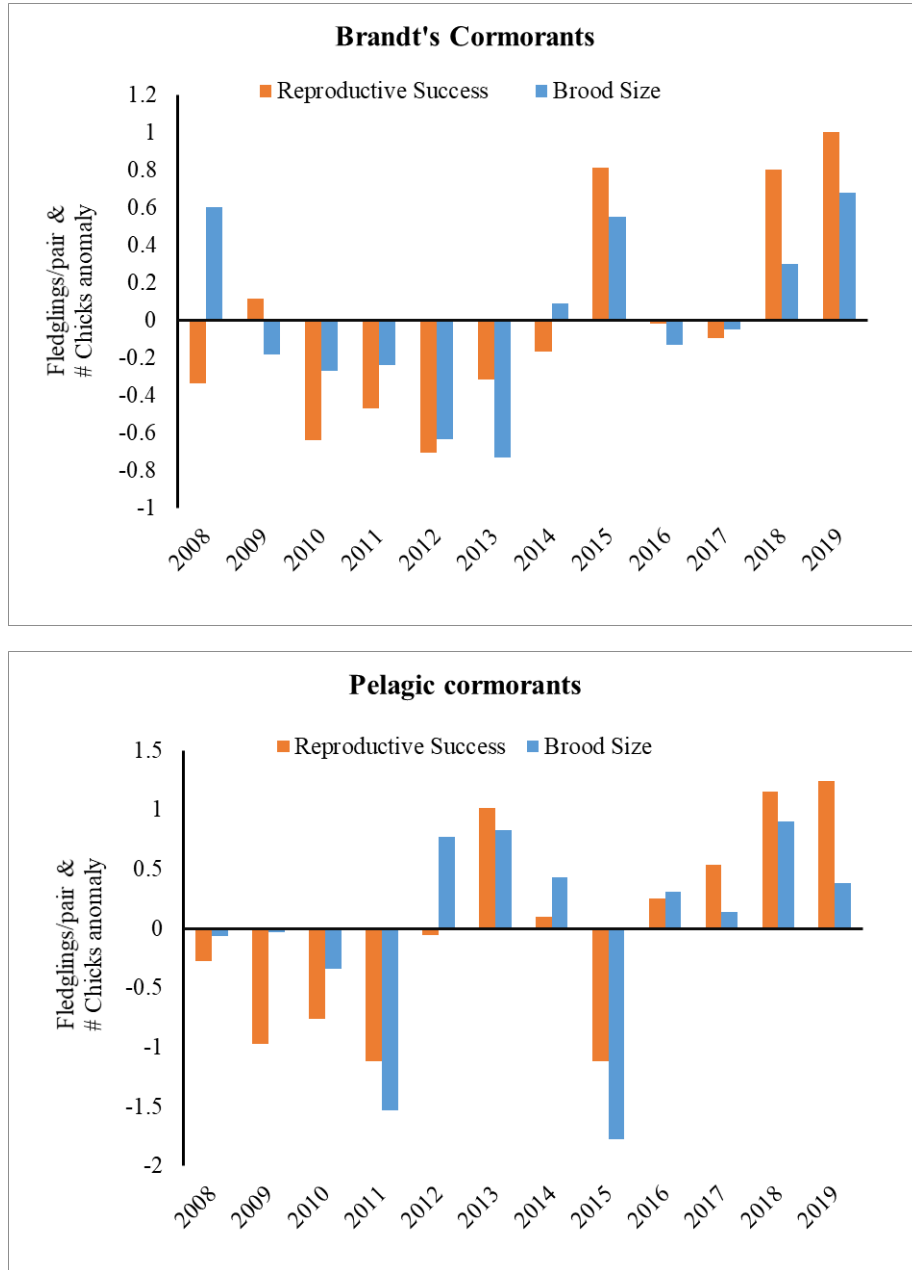


Figure 43. Anomalies of reproductive success and brood size for cormorants nesting at Yaquina Head, Oregon, 2008–19. In both 2018 and 2019, cormorants had above average reproductive success and brood size. Over the time series, average reproductive success and brood size for Brandt’s is 0.89, and 1.78 respectively; for pelagic cormorants average reproductive success is 1.12 and brood size is 1.86.

in the 15-year JSOES data set (41.1 birds per km² compared to a median value of 42.9 birds per km²). The majority of birds observed in 2019 were either sooty shearwater (*Ardenna grisea*, 55%) or common murre (34%). Sooty shearwater abundance was the 7th highest (22.4 birds per km², compared to the time-series median of 20.3 birds per km²) (fig. 45). This species was aggregated on the Grays Harbor, WA, transect (47°N) where 70% of all individuals observed during in 2019. This

distribution pattern was consistent with previous findings showing that during May and June, sooty shearwaters were observed in large numbers near the northern boundary of ocean waters affected by freshwater discharge from the Columbia River (Zamon et al. 2014; Phillips et al. 2017; Phillips et al. 2018). This region overlaps with distribution centers of dominant forage fish species such as northern anchovy, Pacific herring, Pacific sardine, and smelts (Phillips et al. 2017).

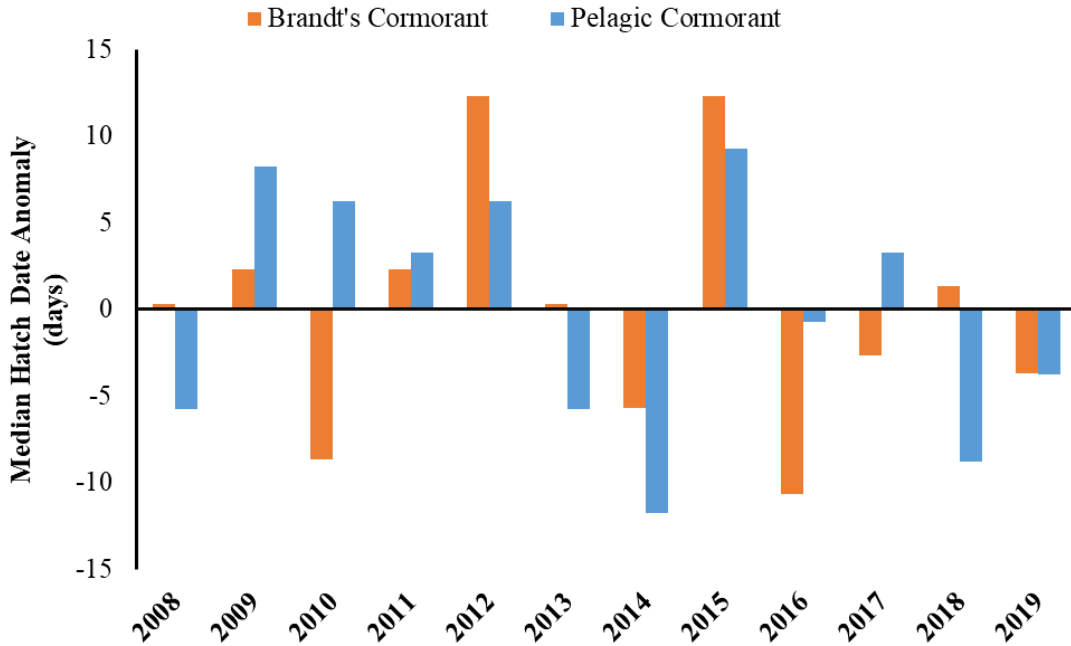


Figure 44. Anomalies of median hatch dates for Brandt's and pelagic cormorants at Yaquina Head, Oregon 2007-19. Over the time series, median hatch date is July 9 for Brandt's and July 15 for pelagic cormorants.

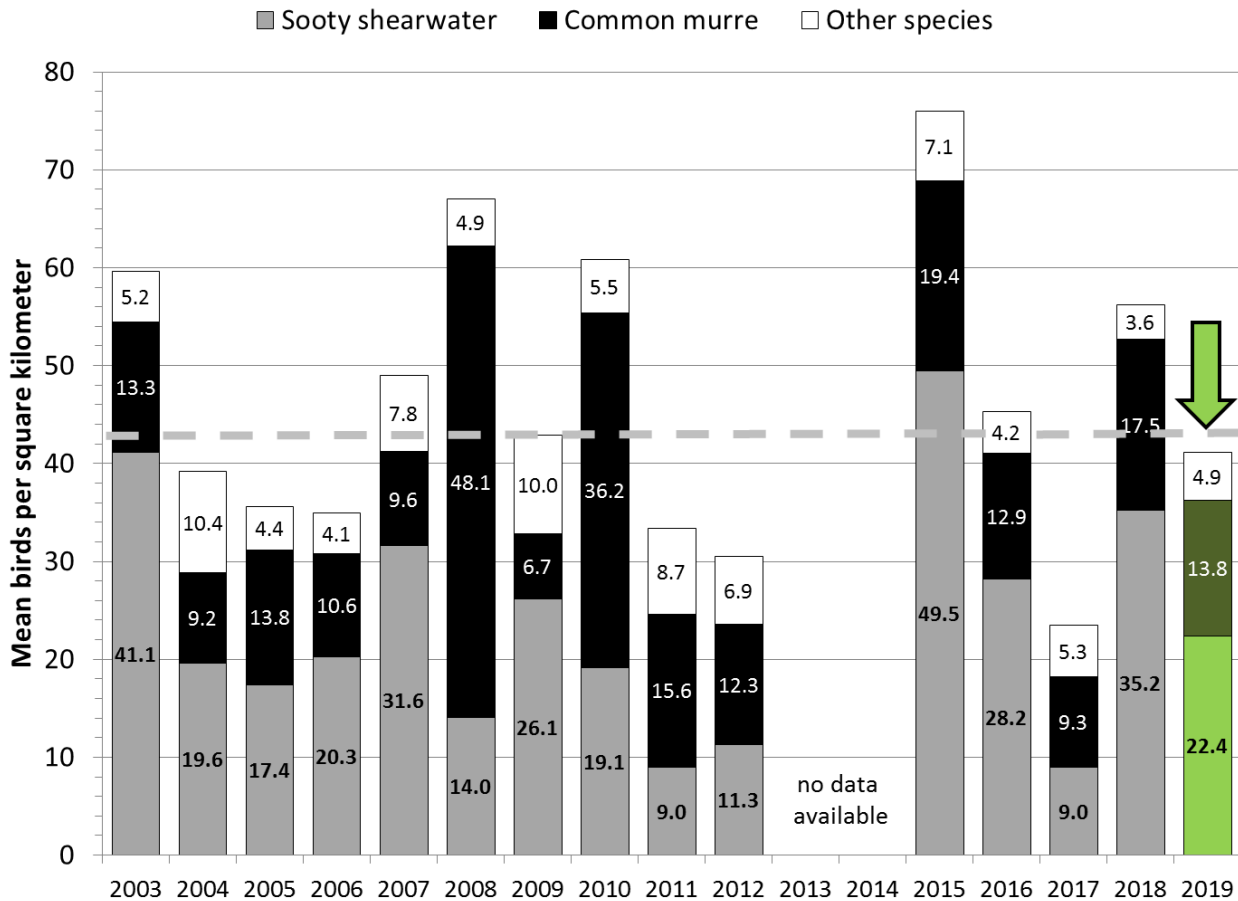


Figure 45. Mean seabird density observed on the continental shelf between Cape Flattery, WA (48.23°N) and Newport, OR (44.67°N) during annual JSOES surveys during late June. Data for 2019 are indicated with green; overall median seabird density for the survey time series (42.9 birds per km²) is shown with the gray dashed line.

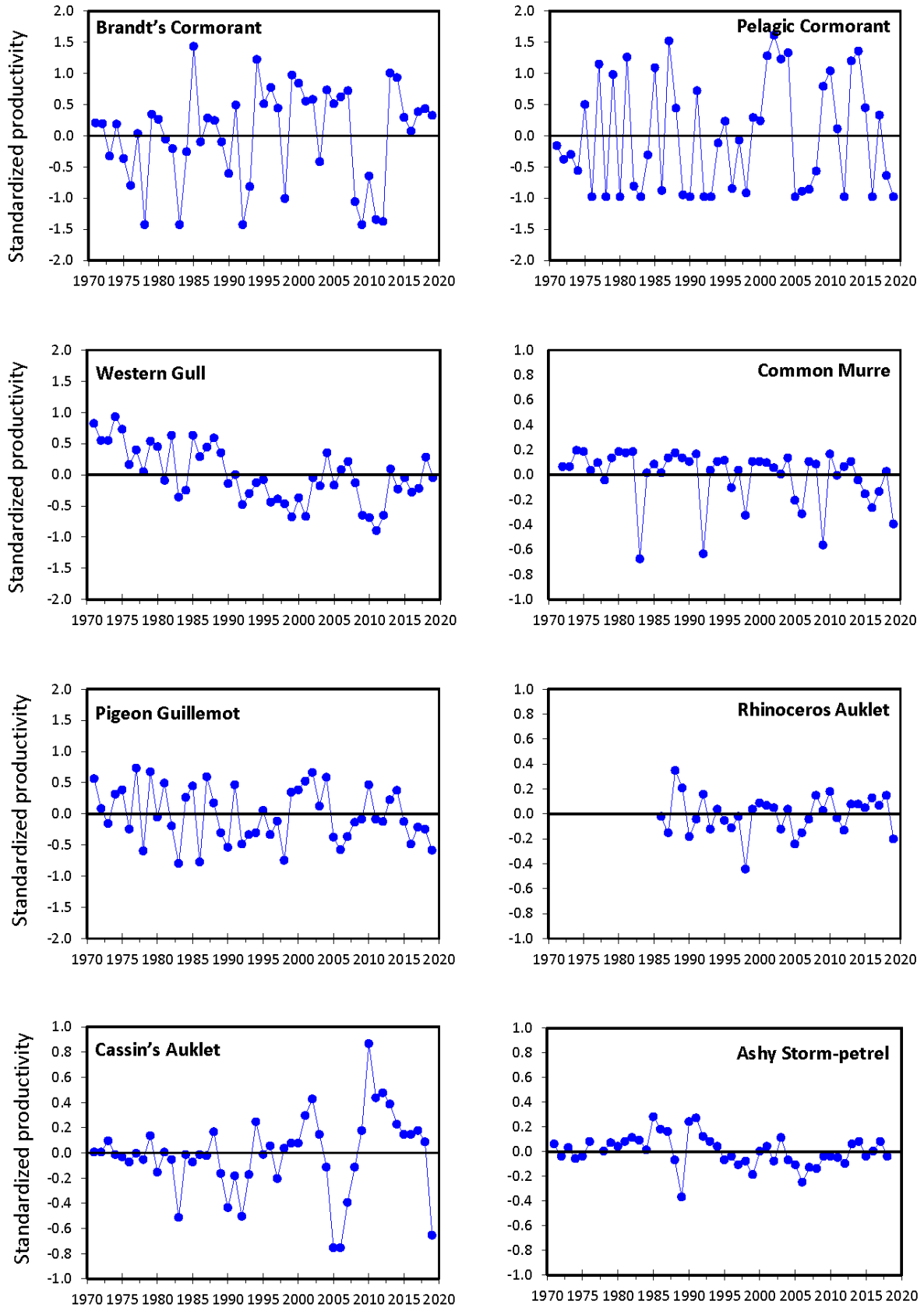


Figure 46. Standardized productivity anomalies for sea birds from Southeast Farallon Island.

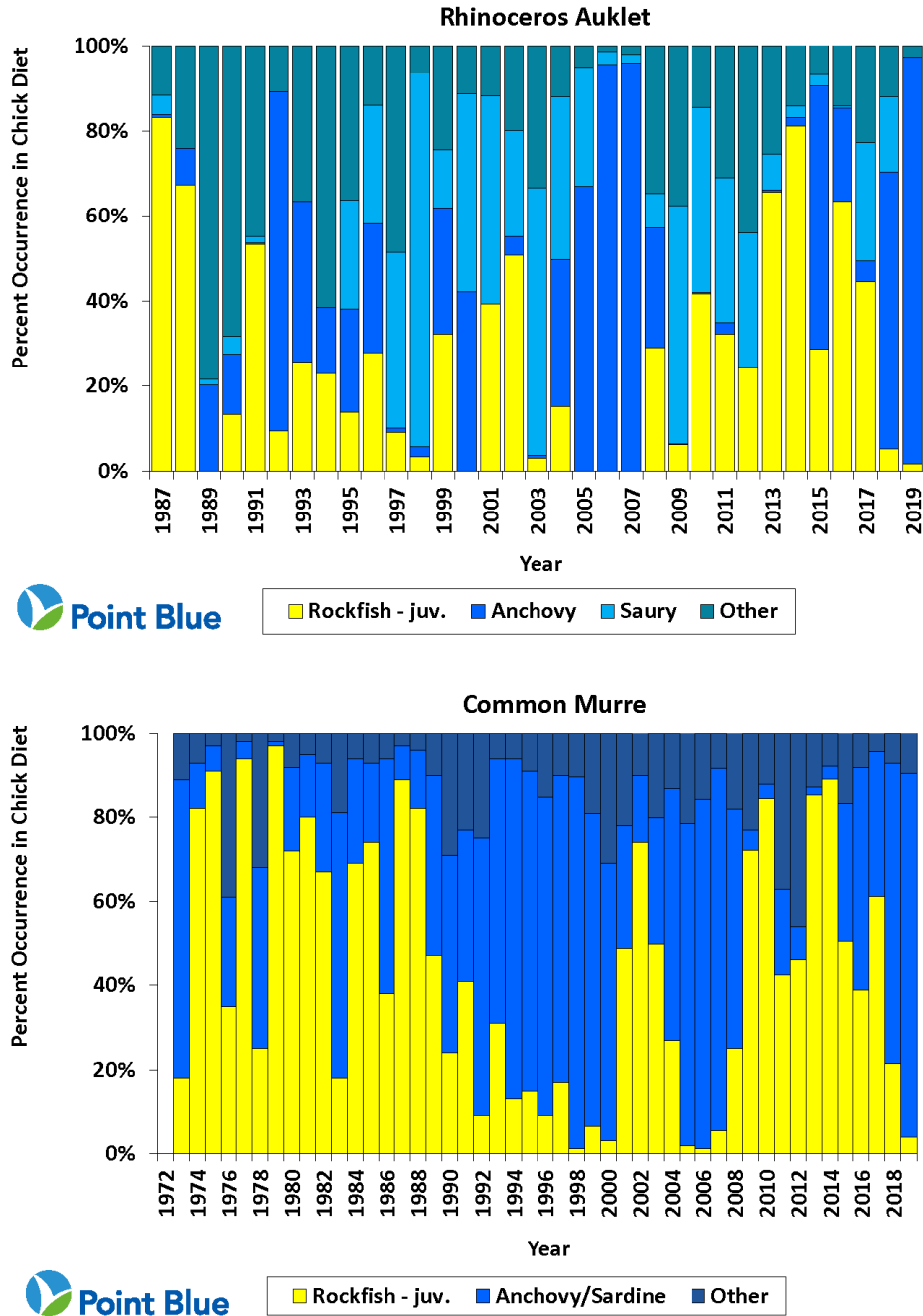


Figure 47. Percent of rhinoceros auklet (top) and common murre (bottom) chick diet comprised of juvenile rockfishes, anchovy/sardine or other fishes at Southeast Farallon Island.

Similar to sooty shearwater, common murre abundance was the sixth highest on record (13.8 birds per km², compared to the median of 13.4 birds per km²). Common murre was most abundant in the area directly affected by freshwater discharge from the Columbia River, with 66.8% of all individuals observed on the three transects closest to the Columbia River (from Cape Meares, OR 45.48°N to Willapa Bay, WA 46.67°N). Common Murre were also abundant near the Newport,

OR, colony (44.67°N; 23.7% of observations). This pattern of June common murre abundance being high near colonies and in areas affected by the Columbia River plume was consistent with past findings in the northern domain of the California Current (Zamon et al. 2014; Phillips et al. 2017; Phillips et al. 2018; Loredó et al. 2019; Phillips et al. 2019).

JSOES surface trawls in 2019 sampling nekton on the same transects where seabird density was surveyed

(fig. 25) indicated that prey species potentially available to fish-eating seabirds in the northern domain of the California Current included a mix of cool water (e.g., Pacific herring) and warmer water taxa (e.g., Pacific pompano and market squid). It is worth noting that market squid were more abundant than in any previous survey, continuing a recent upward trend in the occurrence of this species in daytime surface trawls. Whether this represented a short vs. longer-term shift in nekton community composition was not clear. It was also unclear if changes in squid abundance correlated with changes in squid consumption by seabird predators. The few studies on sooty shearwaters and common murre diets in the northern domain of the California Current indicated that these birds do not typically consume squid (Varoujean and Matthews 1983; Thompson et al. 2018). Regardless of diet information, distribution and density data from June 2019 continued to support the hypothesis that the Columbia River plume impacts trophic interactions between seabirds and fish in this region of the California Current (Adams et al. 2012; Zamon et al. 2014; Phillips et al. 2017; Phillips et al. 2018; Loredó et al. 2019; Phillips et al. 2019).

Central California: Southeast Farallon Island

In contrast with Yaquina Head, common murre production at Southeast Farallon Island (37.4°N, fig. 1) was low in 2019 and the fourth lowest since 1970 (fig. 46). In addition, pelagic cormorant, pigeon guillemot (*Cephus columba*), rhinoceros auklet (*Cerorhinca monocerata*) and Cassin's auklet (*Ptychoramphus aleuticus*) reproduction was quite low in 2019. Brandt's cormorant production was slightly above the long-term mean, while western gull (*Larus occidentalis*) and ash storm petrel (*Oceanodroma homochroa*) were close to average. The northern anchovy surge was reflected in the diets of rhinoceros auklet and common murre as northern anchovy constituted >90% of the diet of both species (fig. 47).

Central and Southern California: RREAS and CalCOFI

Seabird distribution and abundance anomalies from the RREAS core region in spring 2019 covered the region from Point Sur to Bodega Bay (36.18°N to 38.2°N, fig. 1). Observation efforts yielded a total of 15 survey days, resulting in 1,356 km (area surveyed 402 km²) of trackline sampled, and detection of 35 seabird species with an overall density of 74.6 seabirds per km². The RREAS typically encounters higher concentrations of resident breeding species within the Gulf of the Farallones, as well as the influx of trans-hemisphere migratory species and migrants from Hawaii. During 2019, resident breeders such as common murre and Brandt's cormorant displayed positive density anomalies, while

Cassin's auklet had negative density anomalies (fig. 48). Furthermore, the trans-hemisphere migrants, pink-footed shearwater (*Puffinus creatopus*) and sooty shearwater, also showed large positive anomalies (first time for pink-footed shearwater since 2009), with the anomaly for sooty shearwater being the highest ever recorded in the time series. The positive density anomalies for common murre, Brandt's cormorant and shearwaters may in part reflect the observed increased aggregation intensity of these species, attributed to the very high positive anomaly of adult northern anchovy observed by the RREAS in 2019 (fig. 32). The negative anomaly for Cassin's auklet may reflect the low numbers of euphausiids reported by the RREAS, although the anomalies for this species have been low since 2013. The migrant black-footed albatross (*Phoebastria nigripes*) densities continued to show negative anomalies since 2015.

A total of 15 days of survey effort covering 1,602 km (area surveyed 481 km²) of ocean habitat was recorded on the spring CalCOFI survey off southern California between lines 76.7 and 93.3, resulting in the detection of 36 seabird species and an overall total density of 4.2 seabirds per km². Spring CalCOFI seabird density anomalies may be correlated with water temperature variability as well as other factors such as prey availability (Sydeman et al. 2015) or population trends or range shifts in breeding or wintering distributions (Velarde et al. 2015). Anomalies of seabird density within southern California indicated mixed responses within warm and cool-water affinity species in 2019. For cool-water species, Sabine's gull (*Xema sabini*) was well above average while sooty shearwater and common murre were slightly below average (fig. 49). The upswing in Sabine's gull may indicate that this species' migration or conditions in the sub-Arctic (where this species breeds) was impacted by the spring ocean-climate conditions. The continued negative anomaly of common murre in southern California is likely a continued repercussion of the 2014–16 marine heat wave. Comparison of sooty shearwater between central and southern California indicate that sooty shearwater aggregations were less concentrated in southern California compared to central California (fig. 48, 49).

Among the warm-water species off southern California, Cook's petrel (*Pterodroma cookie*) and pink-footed shearwater were above average, Elegant Tern (*Thalasseus elegans*) was close to average, and black-footed albatross and Leach's storm petrel (*Oceanodroma leucorhoa*) were below average (figs. 49, 50; (Hyrenbach and Veit 2003; Santora and Sydeman 2015)).

A positive density anomaly of pink-footed shearwater was linked previously to the onset of warm-water conditions and this pattern held in 2019 (Hyrenbach and Veit 2003). The 2019 positive anomalies in pink-footed

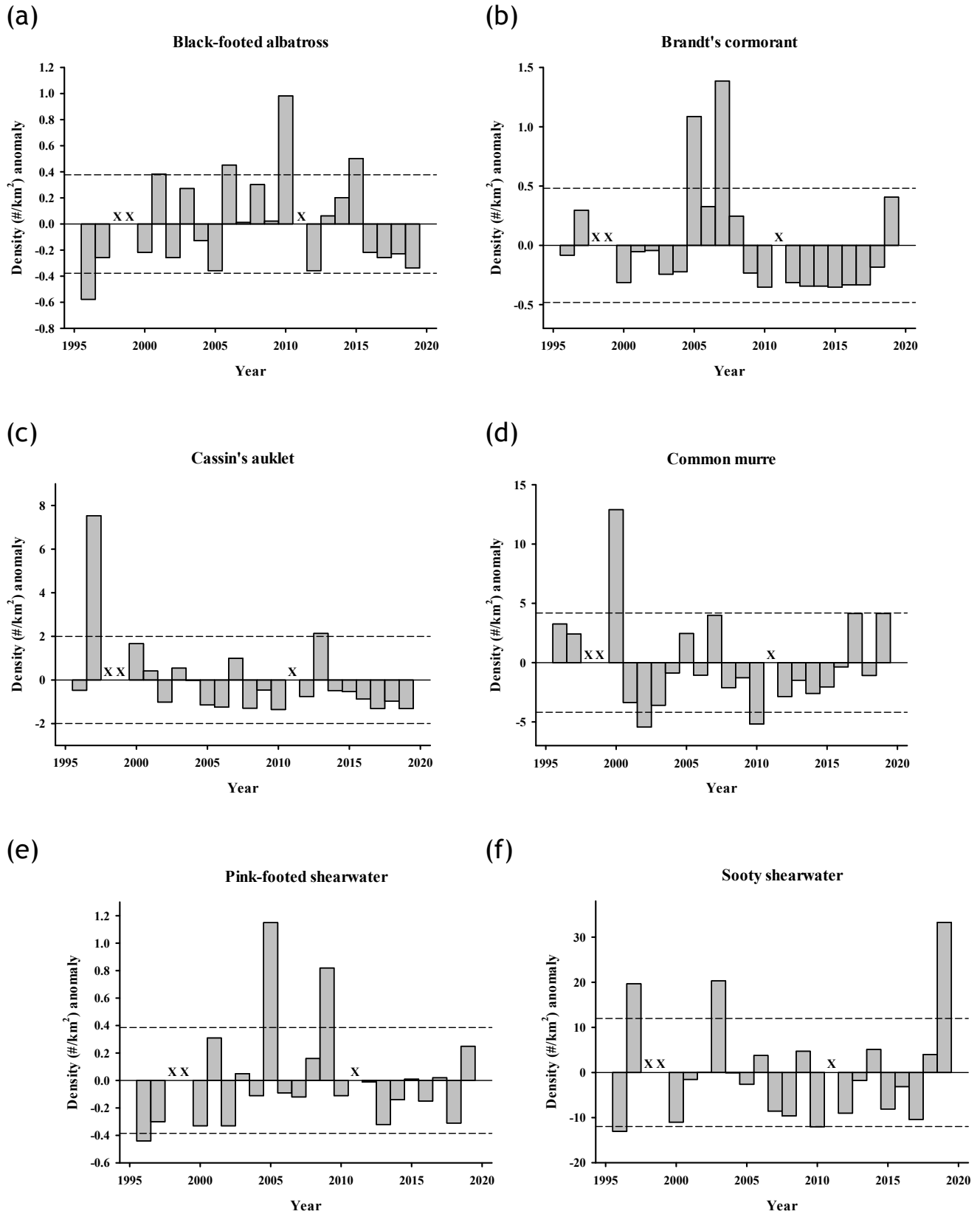


Figure 48. Density (number/km²; expressed as anomalies) over time from RREAS central California core area surveys, 1996–2019: (a) black-footed albatross, (b) Brandt's cormorant, (c) Cassin's auklet, (d) common murre, (e) pink-footed shearwater, (f) sooty shearwater; dashed lines indicate ± 1 s.d. of the long-term mean, and "x" indicates years when no survey was conducted.

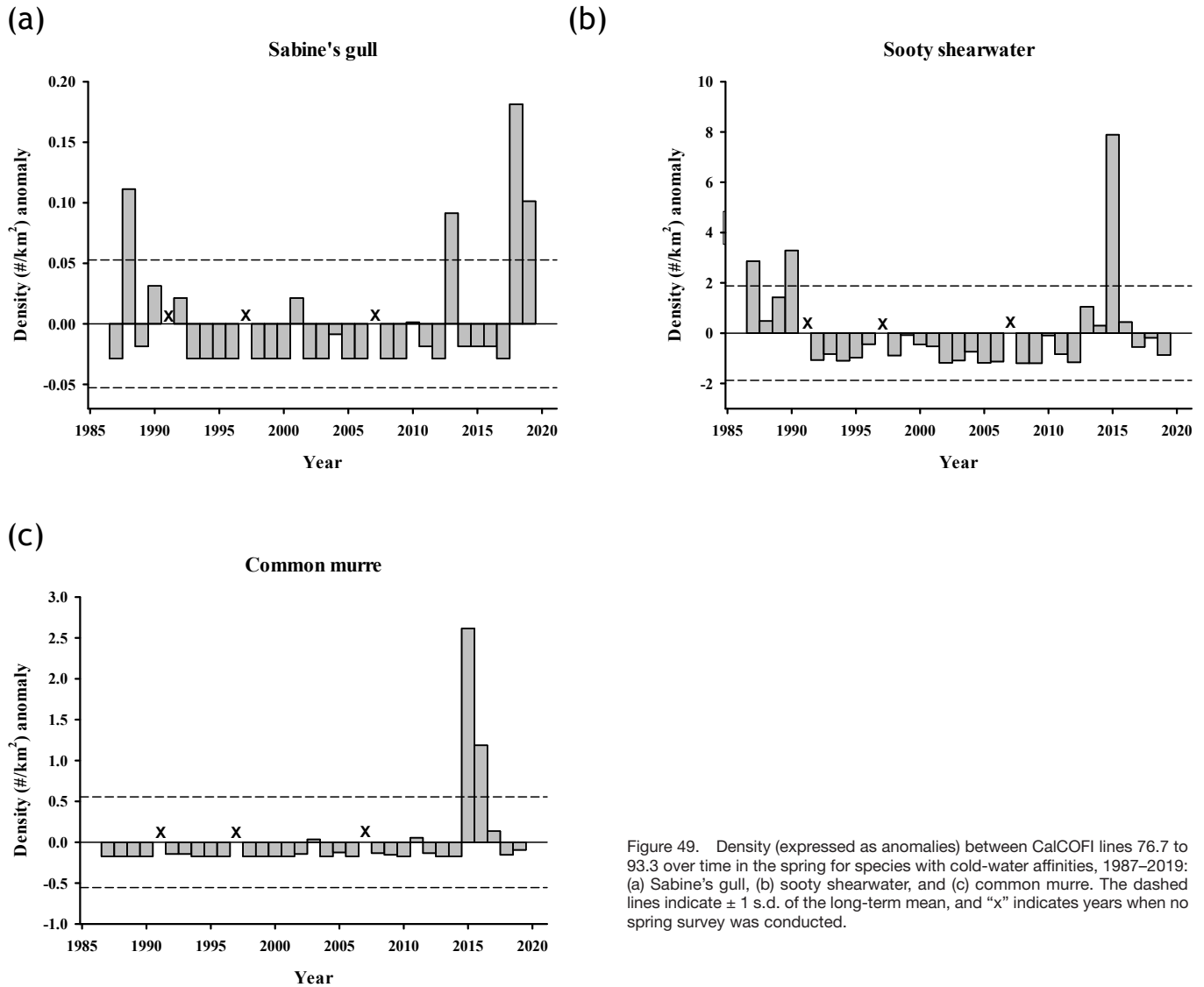


Figure 49. Density (expressed as anomalies) between CalCOFI lines 76.7 to 93.3 over time in the spring for species with cold-water affinities, 1987–2019: (a) Sabine’s gull, (b) sooty shearwater, and (c) common murre. The dashed lines indicate ± 1 s.d. of the long-term mean, and “x” indicates years when no spring survey was conducted.

shearwater and Cook’s petrel were similar to their sustained strong positive anomalies during 2014–16 (fig. 50). The decline in black-footed albatross may be related to the overall decline of their populations in Hawaii and elsewhere in the North Pacific (fig. 50).

MARINE MAMMALS

Central CA: Humpback Whales

Marine mammal surveys from the RREAS within central California continue to report increasing encounter rates for humpback whales (*Megaptera novaeangliae*) encounter rate continued to increase over the past decade (fig. 51). In 2019, humpback whale were regularly observed in high concentrations on the shelf feeding on northern anchovy (Jarrod Santora, personal observation). These observations continued to indicate

that humpback whale populations are likely increasing and that foraging conditions (e.g., availability of krill and northern anchovy aggregations) have been favorable for concentrating whales off central California in spring.

Southern CA: California Sea Lions at San Miguel Island, California

California sea lions (*Zalophus californianus*) are an indicator species to quantify the status of upper trophic level species in the CCE because they live, feed and breed in the CCE year round (Melin et al. 2012). The population breeding at San Miguel Island (34°N) is one of the largest in the world (about 45% of the US breeding population) and has been monitored for decades. Since 1997, four indices were used to measure trends in the population: 1) live pup census, 2) pup condition at 4 months of age, 3) pup growth rates during

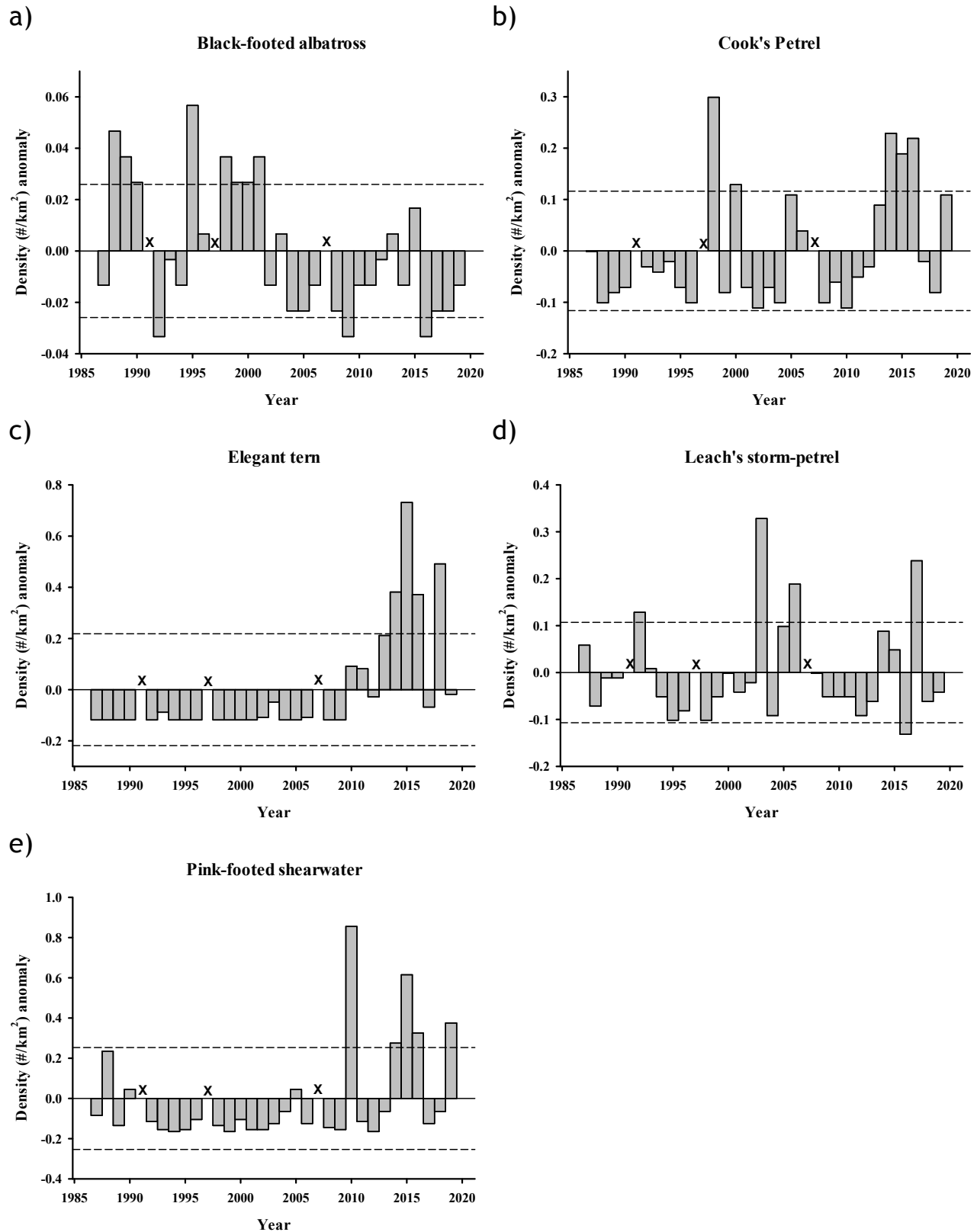


Figure 50. Density (expressed as anomalies) between CalCOFI lines 76.7 to 93.3 over time in the spring for species with warm-water affinities, 1987-2019: (a) black-footed albatross, (b) Cook's petrel, (c) elegant tern, (d) Leach's storm petrel, and (e) pink-footed shearwater. The dashed lines indicate ± 1 s.d. of the long-term mean, and "x" indicates years when no spring survey was conducted.

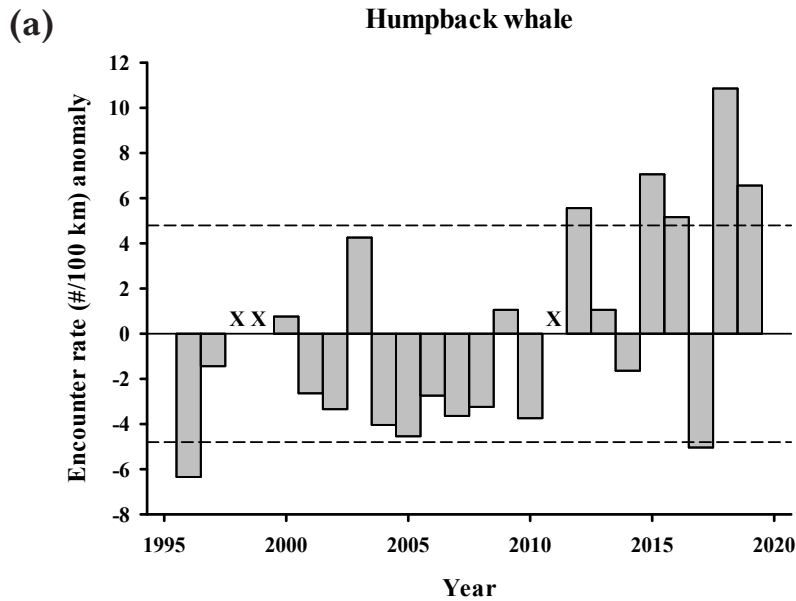


Figure 51. Encounter rate (number/100 km; expressed as anomalies) over time from RREAS central California core area surveys, 1996–2019, of (a) humpback whale; dashed lines indicate ± 1 SD of the long-term mean, and ‘x’ indicates years when no survey was conducted.

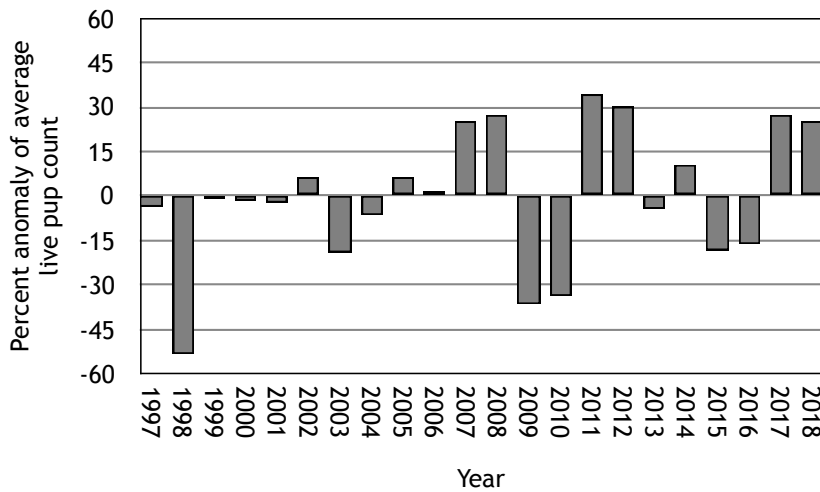


Figure 52. The percent anomaly of live California sea lion pup counts at San Miguel Island, California, based on a long-term average of live pup counts between 1997 and 2018 in late July when surviving pups were about 6 weeks old.

the period of maternal nutritional dependence, and 4) nursing female diet during the maternal care period³². The live pup census is a measure of successful births and is an indicator of prey availability to and nutritional status of nursing females from October to the following June. Pup condition and growth rates during the period of nutritional dependence measure the transfer of energy from the mother to the pup through lacta-

³²The number of pups alive were counted in late July and the average weights of pups at 4 months and 7 months of age. The number of live pups in late July represents the number of pups that survived from birth to about 6 weeks of age. Live pups were counted after all pups were born (between 20 and 30 July). A mean of the number of live pups was calculated from the total number of live pups counted by each observer. A long-term average live pup count was used to create annual anomaly percentages. Between 200 and 500 pups were weighed per year when about 4 months old. Pups were sexed, weighed, tagged, branded, and released. Up to 60 pups were captured in February and weighed and measured at 7 months of age. Of the 60 pups captured in February, up to 30 pups were branded which provided a longitudinal data set for estimating a daily growth rate between 4 months and 7 months old.

tion between June and the following February that is dependent on prey available to nursing females during that time. The frequency of occurrence of prey in the diet of nursing females provides a relative measure of the available forage community during the period of pup nutritional dependence.

Three indices of California sea lion population showed improvement in 2018, representing the third consecutive year of average or above average values following 2015, the worst year in the 1997–2018 time series. In 2018, pup births declined 2% from 2017 but were still 24% above the long-term average (fig. 52). Pup weights at 3 months of age were similar to 2017 (fig. 53). Although pup growth rates at 7 months of age were lower than 2017 they were still above the long-term average (fig. 54). Continued improvement in the population indices coincides with a shift in the frequency of occurrence

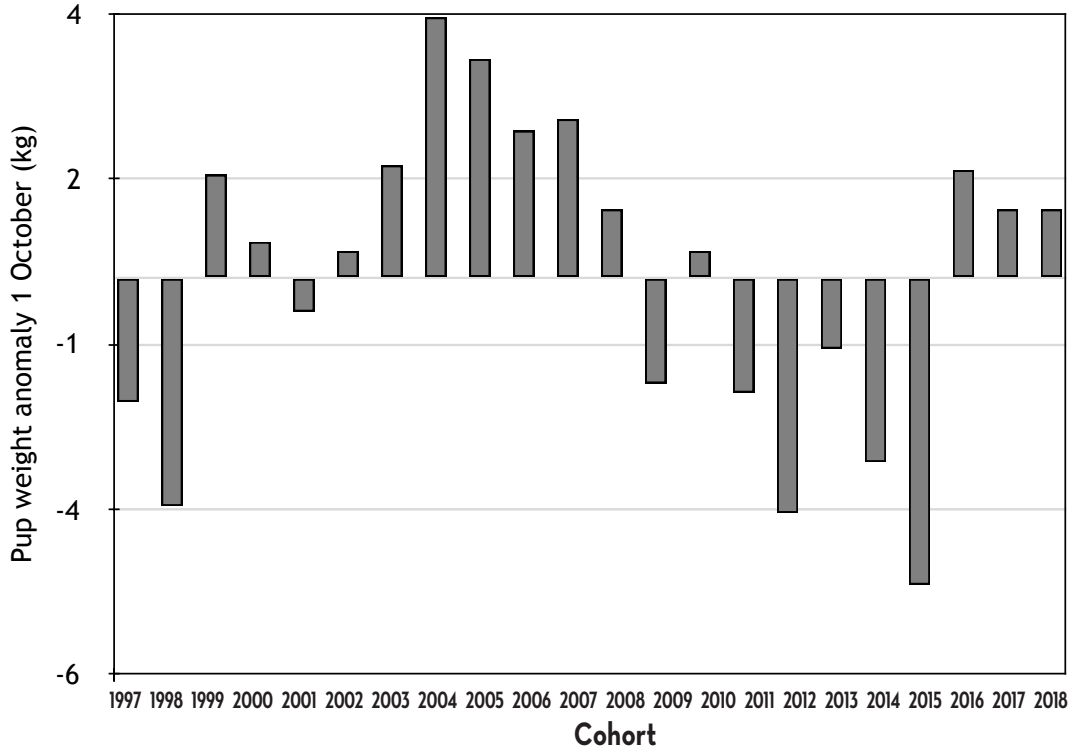


Figure 53. Average pup weight anomaly (kg) from predicted average weights of 4-month-old female California sea lion pups at San Miguel Island, California, from the long-term average between 1997 and 2018.

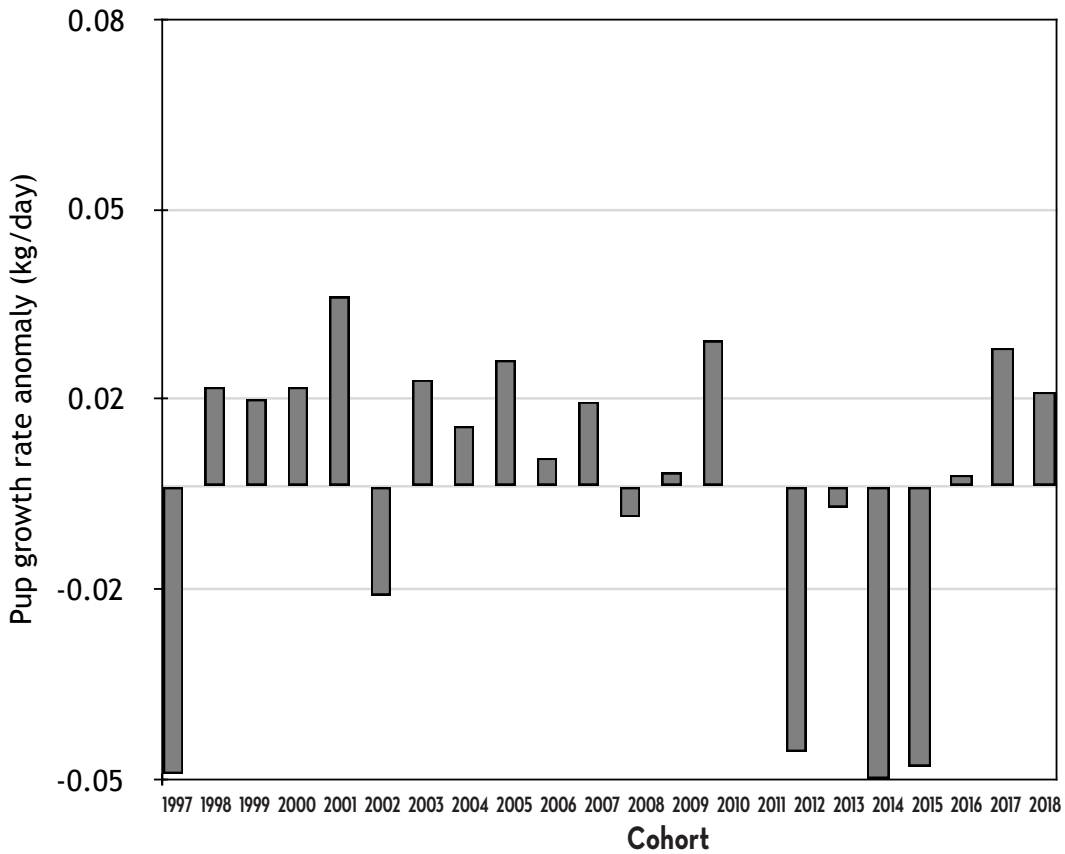


Figure 54. Average daily growth rate anomaly of female California sea lion pups from 4 and 7 months old at San Miguel Island, California, from the long-term average between 1997 and 2018.

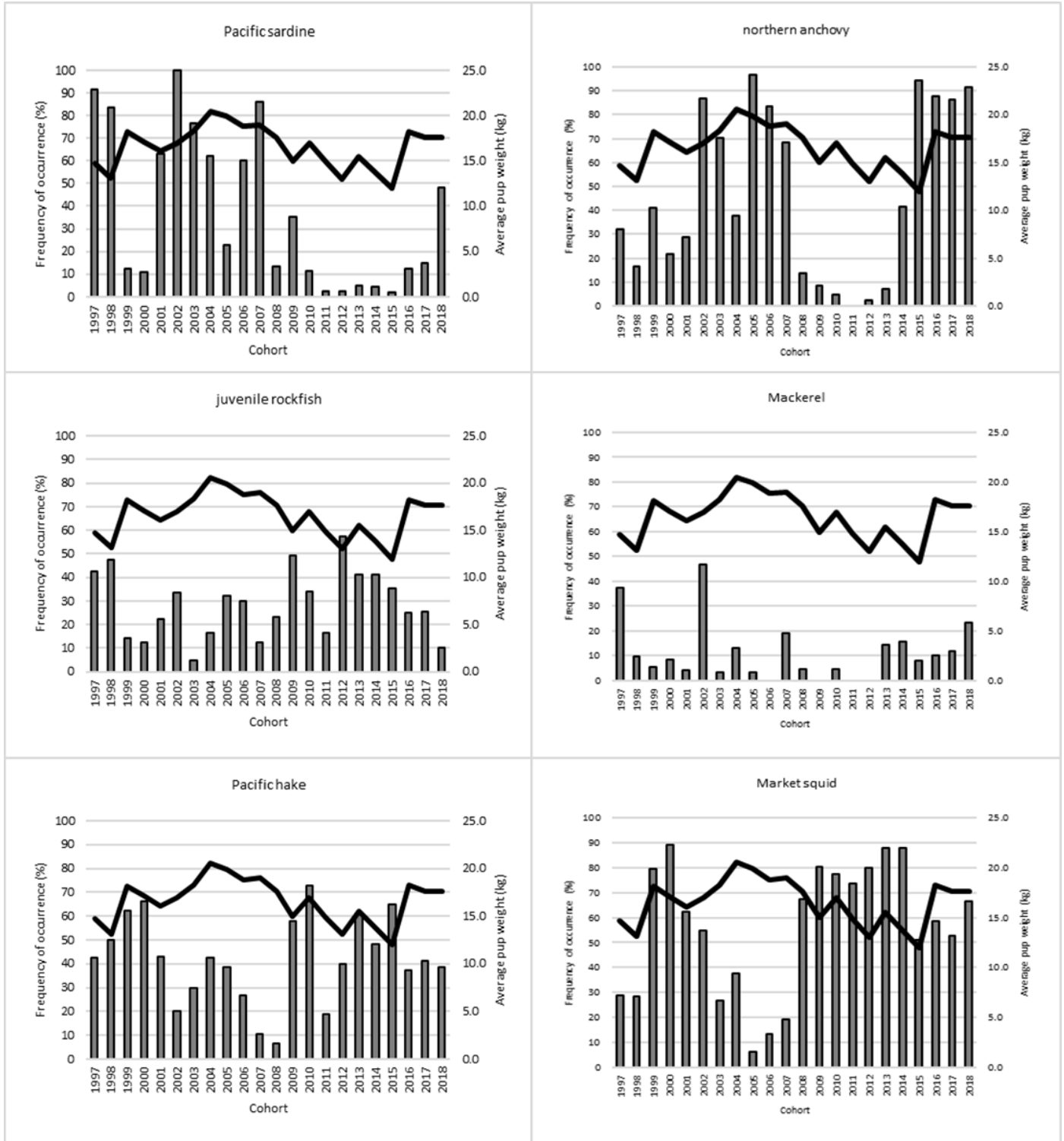


Figure 55. Frequency of occurrence of prey taxa (bars) identified from nursing female fecal samples collected at San Miguel Island during the first 4 months of lactation and average California sea lion female pup weight at 4 months old (line), 1997–2018.

(FO) of the primary prey in the nursing female diet³³. More favorable ocean conditions for northern anchovy and Pacific sardine resulted in the return of northern anchovy as the most frequently occurring prey (>85%) in the past four years, and the resurgence of Pacific sardine in the diet in 2018 (48%; fig. 55). Pacific hake, market squid and mackerel (Pacific and jack) also had high FO in 2018 resulting in a diverse diet of high quality prey for nursing females that likely contributed to the positive trends in the population indices.

DISCUSSION

A novel anchovy regime?

Northern anchovy larval abundances were the highest in the 70-year history of CalCOFI and adult northern anchovy catches the greatest in the 36-year history of the RREAS in 2019. Taken together, this provides strong evidence that the overall northern anchovy population size is as high as it has been since the onset of quantitative marine monitoring in the CCE. The surge in northern anchovy appears to be the product of an extremely high recruitment class in 2016 fueled by high survival of larvae or juveniles spawned in 2015 (Zwolinski et al. 2017; Stierhoff et al. 2019; Zwolinski et al. 2019).

The high recruitment of 2016 and subsequent rapid increase in population size qualifies as an ecological surprise (Lindenmayer et al. 2010). Indeed, analysis of northern anchovy stock size from 1951–2011 suggested that the population was near an all-time low from 2009–11 (MacCall et al. 2016), and subsequent analysis showed that the population remained depressed through 2015 (Thayer et al. 2017). Although some relatively small but dense aggregations remained in patches that were missed by CalCOFI and other marine sampling programs (McClatchie et al. 2018), analyses examining data sources outside of the core CalCOFI region failed to turn up significant numbers of northern anchovy (Davison et al. 2017). By every indication, overall northern anchovy population size was quite low in the CCE entering 2015.

The resurgence of northern anchovy in 2015 points out that there is not a complete mechanistic understanding of the forces that drive northern anchovy population dynamics in the CCE. Indeed, the picture is not as clear as suggested by previous correlative time-series analysis showing that northern anchovy thrive in cold regimes and Pacific sardine in warm regimes (Chavez et al. 2003; McClatchie 2012). A critical question that thus emerged

from observation of the CCE since 2014 is: What went right for northern anchovy in 2015–16?

Wild fluctuations in populations sizes is a hallmark of coastal pelagic species worldwide (Dickey-Collas et al. 2014; Peck et al. 2014), and understanding the causes of these fluctuations has often been elusive (Houde 1987, 2008). In the CCE, Reuben Lasker and colleagues conducted years of research on the causes of northern anchovy population fluctuation in the 1970s and 1980s (Lasker et al. 1970; Lasker 1975; Scura and Jerde 1977; Lasker 1978, 1981, 1985). Lasker's premise, based on seminal work by Hjort (Hjort 1914, 1926), was that recruitment classes are set during a "critical period" that occurs after the yolk sack is absorbed in a larval fish. Once the yolk sack runs out, a fish must rapidly begin to feed or starve to death. Based on lab and field experiments and CalCOFI observations, Lasker's stable ocean hypothesis essentially concluded that to induce high recruitment the right species of larval prey must be available, the prey must be dense, and the ocean must be non-turbulent such that young, poor swimming larvae can catch the prey (Lasker 1985).

The stable ocean hypothesis may help explain the very successful recruitment class of 2016. There was an unusual mixture of high production coupled with high stratification in 2015, potentially creating the type of conditions conducive for larval survival identified by Lasker. Analysis of ocean conditions in areas where northern anchovy larvae were found in 2015 using Regional Ocean Modeling System (Schroeder et al. 2019) should determine if ocean conditions were stable enough to foster larval feeding. Aside from lacking turbulence, the stable ocean hypothesis states that the right type of prey at high density has to be present to feed larvae. Indeed, laboratory experiments evaluating larval northern anchovy growth demonstrated that a high proportion of larvae fed the dinoflagellate *Gymnodinium splendens* survived after 10 days while there was no survival when fed a different dinoflagellate, *Gonyaulax polyedra* (Scura and Jerde 1977). Despite the major effect of prey type on northern anchovy survival, northern anchovy did not discriminate among the two dinoflagellate species when exposed to both (Scura and Jerde 1977). Quantifying the prey available to larvae is therefore likely an important factor for mechanistically understanding drivers of larval survival and recruitment. Environmental DNA (eDNA) (Goodwin et al. 2017) holds the potential to quantify the larval prey field. eDNA analysis involves sequencing DNA from multiple species using primers that target various trophic levels. For water collected in the CCE, primers exist to enumerate the amount of DNA in bacterial, phytoplankton, zooplankton, and fish communities. Whereas the DNA from higher trophic level species such as fish

³³Fecal samples were collected from haulout areas on San Miguel Island, California where California sea lions nursed their pups. Samples were collected between late May and September each year 1997–2018. Prey taxa were identified from hard parts recovered from the samples, and frequency of occurrence (FO) was calculated using methods described in Lance et al. (2001) and Orr et al. (2003).

probably comes from sloughed cells, DNA from bacteria and phytoplankton is more likely to come directly from the entire species. Hence, eDNA has the potential to accurately characterize the amount of different phytoplankton species available to larval fishes. eDNA has been collected regularly on CalCOFI cruises since 2014, and comparison of phytoplankton assemblages between 2015 and other years could lend insight as to the type of prey that fosters larval northern anchovy survival.

In addition to living past first feeding, fish must survive later stages to recruit into the adult population, and it is possible that conditions experienced at later stages also affect year class strength (Houde 2008). For example prey for late larvae and juveniles can significantly influence survival. As northern anchovy larvae grow, zooplankton prey becomes important (Scura and Jerde 1977). eDNA can be a useful tool for assessing the prey field of older larvae and juveniles as universal primers exist to characterize the zooplankton assemblage in the California Current (Goodwin et al. 2017). Comparison of the zooplankton assemblage between 2014, when there were relatively few young-of-the-year northern anchovy in southern California, and 2015–19 when abundances were very high, could deduce if optimal prey for older larvae and juveniles became more abundant during and subsequent to the MHW.

Given the hyper-abundance of adult northern anchovy in 2018 (Thompson et al. 2018) and 2019, another question that arises is whether the CCE is currently in a new “anchovy regime.” Northern anchovy were scarce when CalCOFI began in 1949 but increased beginning in the 1960s and stayed abundant through the late 1980s (MacCall et al. 2016). Because most northern anchovy do not live past 6 years, the most recent ~30-year northern anchovy regime included multiple strong recruitment classes. Results from Southwest Fisheries Science Center coast-wide acoustic-trawl survey detected very large numbers of young northern anchovy in 2016, indicating that a high proportion of larvae spawned in 2015 survived into 2016 (Stierhoff et al. 2019). Ocean conditions in 2015 had surface water warming that originated in late 2013 in the Gulf of Alaska, impinged the coast of California by late 2014, and persisted into 2015 during the peak northern anchovy spawning period. A relatively strong El Niño during late 2015 and most of 2016 also affected the CCE (Jacox et al. 2016). Given that a strong MHW developed during summer 2019, reflecting ocean conditions that are similar and second in magnitude only to the event in 2014–15, and that young-of-the-year northern anchovy abundance was high in southern California in 2019, it is possible that conditions will be primed for high northern anchovy recruitment in 2020. Ultimately, getting a mechanistic

understanding of what controls recruitment variation in northern anchovy is the only way to predict whether this novel “regime” will last.

A new blob?

During summer 2019, another large MHW reminiscent of “the blob” of 2014–15 (Leising et al. 2015) developed in the Gulf of Alaska. This event reached its peak area in late August, but then showed a slight decline through September. The magnitude of this event is rivaled only by the 2014–15 event, with most other events over the past 38 years coming in a distant third (fig. 14). Beyond the potential impacts on small pelagics such as northern anchovy (discussed above), this new MHW is likely to impact other portions of the CCE. This new MHW reached the Washington coast in July, and then much of the Oregon coast in August. Continued upwelling in patches along the California coast, however, kept the 2019 MHW mostly offshore in much of the California region. Unlike the 2014–15 event, the early phases of the 2019 MHW did not penetrate as deeply into the water column, nor did it include secondary, strongly anomalous warm area in the further offshore regions of southern California. These are two important differences between the 2019 MHW and the “blob” of 2014–15, and thus the impacts may be different than noted before.

Even with its noted physical differences, the MHW of 2019 is still a highly unusual event in terms of its size and magnitude, and is thus likely to have many effects. The impacts of the 2014–15 event included coast-wide harmful algal blooms, shifts in species distributions, changes in planktonic community structure, increased large marine mammal entanglements, decreased salmon survival, and seabird and marine mammal die-offs and strandings (Leising et al. 2015; Cavole et al. 2016; Daly et al. 2017). Given that the 2019 MHW was present from May–September 2019 in the Pacific Northwest, it is likely that salmon returns will be low in subsequent years. Fortunately for marine mammals, the lack of the southern California offshore warming, and offshore position of this MHW for much of the rest of California, is likely to have less impact on this group than the previous event if these conditions persist. It is still too early to tell exactly how the 2019 MHW will evolve; if this event does end up proceeding more similarly to the 2014–15 event, then its impact will be apparent in 2020.

Implications for predators: winners and losers

Although the California Current broadly defines much of the marine ecosystem from Baja California, Mexico, to Washington State, USA, regional differences in population dynamics are often found within the CCE (Thompson et al. 2014; Thompson et al. 2019).

In 2018–19, south of approximately San Francisco, predators that thrive on northern anchovy were highly productive while those that require prey items other than northern anchovy tended to have low productivity. Sea lions benefited from the abundance of northern anchovy. Female sea lions give birth to a pup in May or June and undergo foraging trips ranging between the Channel Islands in the south and Monterey Bay in the north (Melin et al. 2008). In years when adequate prey is available, females produce enough milk to nourish pups, but when females are malnourished milk supply is limited and pups can starve (Melin et al. 2010). Pup condition was very poor in 2014–15, leading to the declaration of an “unusual mortality event” (McClatchie et al. 2016b). In 2016, the number of pups born was low, but pup condition improved greatly relative to 2015. The augmented pup condition of 2016 likely resulted from the female sea lions beginning to exploit the strong 2016 northern anchovy year class (adult northern anchovy abundance was positively anomalous in southern California in late spring, 2016, fig. 33). All measures of pup condition were positively anomalous in 2017 and 2018, again probably due to the high abundance of northern anchovy. Whereas many long-standing ecological patterns need to be reconsidered in light of the 2014–16 MHW (Daly et al. 2017; Koslow et al. 2019), the strong, positive correlation between summed northern anchovy/Pacific sardine abundance and sea lion pup condition (McClatchie et al. 2016a) appears to be holding strong.

Whereas sea lions overwhelmingly responded positively to the northern anchovy surge, the story varied for sea birds in California. On Southeast Farallon Island, Cassin’s auklet, common murre, pelagic cormorant, pigeon guillemot, and rhinoceros auklet exhibited historically low productivity, suggesting that prey other than northern anchovy are needed for these species to thrive. This pattern mostly fits well with Santora et al. (2014) who found positive correlations between availability of krill and production of common murre, rhinoceros auklet, and Brandt’s cormorant; juvenile rockfish availability to Cassin’s auklet and pelagic cormorant production and sanddab to pigeon guillemot production. Life history traits of these birds explains their inability to thrive on northern anchovy. Common murre and rhinoceros auklet feed chicks whole prey items and because the northern anchovy population was comprised almost exclusively of adults, the available northern anchovy were simply too large to feed the chicks. Indeed, adult northern anchovy lying next to nests, but untouched by chicks, were common in 2019 (Peter Warzybok, personal observation). Pelagic cormorants and pigeon guillemots, by contrast, forage very close to shore where northern anchovy are typically unavailable and rely on benthic fishes such as

juvenile rockfishes and sanddabs. Finally, Cassin’s auklet rely on krill (Jones et al. 2018), which, in addition to juvenile rockfishes and sanddabs, were historically scarce off central California in 2019 (fig. 33). Brandt’s cormorant, which feed their chicks partially digested regurgitation, was the only species that had above average productivity at Southeast Farallon Island. Hence, adult Brandt’s cormorant adults directly consumed adult northern anchovy and were able to translate this prey into nourishment for the chicks. Overall, 2019 was unusual given that northern anchovy were hyperabundant but many other common prey species were scarce. This dynamic had direct and predictable effects on sea bird productivity.

North of the Farallon Islands in Yaquina Head, Oregon, common murre reproductive success was positively anomalous in 2018 and 2019 following seven consecutive years of very low production. The uptick in common murre productivity was also likely affected by different prey availability in recent years. In 2018, there was a large increase in the percent of flatfish, and a decrease in the percent of smelts, in common murre chick diets. In addition to common murre, both Brandt’s cormorants and pelagic cormorants exhibited record production in 2018 and/or 2019. This enhanced production was probably also a result of the availability of abundant and appropriate prey species as well as lower predation on eggs and chicks by avian predators such as bald eagles.

Distribution shifts

The 2014–16 MHW induced northward shifts to many marine species. Prior to 1977, mesopelagic fishes such as Panama lightfish were uncommon in southern California in winter and spring, but following the 1977 regime shift, taxa inhabiting similar habitats as Panama lightfish were frequently encountered in southern California ichthyoplankton samples throughout the year (Peabody et al. 2018). Subsequent to 2014, however, these fishes became some of the most common in the ichthyoplankton assemblage. Mexican lampfish, for example, had higher springtime abundances in 2014, 2015, 2018, and 2019 than any year prior to 2014 (fig. 37). Most of these warm-water mesopelagic species vertically migrate to the epipelagic or surface at night and therefore would be available as prey to higher trophic level species such as sea lions. Indeed, Mexican lampfish otoliths were identified in sea lion scat in 2015 (Mark Lowry, personal communication). Understanding the energetic contributions of these taxa, therefore, is likely important for elucidating drivers in ecosystem dynamics.

To the north, taxa associated with warm-water conditions continued to be prevalent, and those with cool-water conditions were relatively uncommon, near shore off Oregon and Washington in 2019. Reduced survival

of yearling salmon is one ecosystem implication of the elevated abundance of warm-water prey species (Daly and Brodeur 2015; Daly et al. 2017). Shortbelly rockfish, a semi-pelagic, diminutive rockfish with a biogeographic center of distribution off central California, was also hyper-abundant near the shelf break in Oregon and Washington. Although there is not a directed fishery for shortbelly rockfish, this species sometimes is caught as bycatch by the commercial hake fishery. Hence, the Pacific Fisheries Management Council (PFMC) set an annual catch limit (ACL) for shortbelly rockfish off Oregon and Washington. Because shortbelly rockfish historically did not occur in large numbers in the Pacific Northwest, the ACL was set low and the surge in abundance resulted in the hake fishery exceeding the ACL very early in the fishing season in both 2018 and 2019 (PFMC 2019b). To avoid shutting down the hake fishery the PFMC increased sixfold the shortbelly rockfish ACL (PFMC 2019a). The northern movement of species, therefore, has the potential to affect both ecosystem dynamics and ecosystem-based management.

SUMMARY

Warm conditions largely persisted into 2019 in the CCE (table 1). Whereas temperatures were close to the long-term average in early 2019, a new MHW formed in the Gulf of Alaska in May and impinged on most of the coast by September 2019. Despite the warm conditions, productivity was above average in most of the CCE. In the Pacific Northwest, fish and invertebrate assemblages included taxa associated with both warm and cool conditions. In California, northern anchovy abundance from both larval and midwater surveys was the highest in recorded history while many common forage fish (e.g., juvenile rockfishes, sanddabs) and krill were very low. This unique forage base had clear and predictable effects on predators. In Oregon, seabird productivity was the highest in years, as juvenile flatfish comprised a large portion of chick diet. In central California, production of seabirds such as Cassin's auklet, common murre, and pelagic cormorant was very low as these species could not feed chicks adult northern anchovy and smaller, more appropriate prey was mostly unavailable. Sea lions, by contrast, preyed copiously on northern anchovy and translated this energy source into successfully rearing pups. The main questions going into 2020 are: 1) Will the 2019 MHW will persist into 2020 in a manner similar to the 2014 MHW or dissipate? and 2) Are we in a novel anchovy regime that will last for years to come?

ACKNOWLEDGEMENTS

We thank with all sincerity the crews of ships that helped collect samples and the researchers that conducted land-based surveys of sea birds and marine mam-

als. The manuscript benefitted greatly from reviews by Greg Williams and Noelle Bowlin.

LITERATURE CITED

- Adams, J., C. MacLeod, R. M. Suryan, K. D. Hyrenbach, and J. T. Harvey. 2012. Summer-time use of west coast US National Marine Sanctuaries by migrating sooty shearwaters (*Puffinus griseus*). *Biological Conservation* 156:105–116.
- Auth, T. D. 2011. Analysis of the spring–fall epipelagic ichthyoplankton community in the northern California Current in 2004–09 and its relation to environmental factors. *California Cooperative Oceanic Fisheries Investigations Reports* 52:148–167.
- Bakun, A. 1973. Coastal upwelling indices, west coast of North America, 1946–71. US Department of Commerce NOAA Technical Report NMFS-SSRF 671:1–103.
- Barcelo, C., L. Ciannelli, and R. D. Brodeur. 2018. Pelagic marine refugia and climatically sensitive areas in an eastern boundary current upwelling system. *Global Change Biology* 24:668–680.
- Behrenfeld, M. J., and P. G. Falkowski. 1997. Photosynthetic rates derived from satellite-based chlorophyll concentration. *Limnology and Oceanography* 42:1–20.
- Bjorkstedt, E. P., R. Goericke, S. McClatchie, E. Weber, W. Watson, N. Lo, W. T. Peterson, R. D. Brodeur, T. Auth, J. Fisher, C. Morgan, J. Peterson, J. Largier, S. J. Bograd, R. Durazo, G. Gaxiola-Castro, B. Lavanigos, F. P. Chavez, C. A. Collins, B. Hannah, J. Field, K. Sakuma, W. Satterthwaite, M. O'Farrell, S. Hayes, J. Harding, W. J. Sydeman, S. A. Thompson, P. Warzybok, R. Bradley, J. Jahncke, R. T. Golightly, S. R. Schneider, R. M. Suryan, A. J. Gladics, C. A. Horton, S. Y. Kim, S. R. Melin, R. L. DeLong, and J. Abell. 2012. State of the California Current 2011–12: ecosystems respond to local forcing as La Niña wavers and wanes. *California Cooperative Oceanic Fisheries Investigations Reports* 53:41–76.
- Black, B. A., I. D. Schroeder, W. J. Sydeman, S. J. Bograd, and P. W. Lawson. 2010. Wintertime ocean conditions synchronize rockfish growth and seabird reproduction in the central California Current ecosystem. *Canadian Journal of Fisheries and Aquatic Sciences* 67:1149–1158.
- Bograd, S. J., I. D. Schroeder, N. Sarkar, X. M. Qiu, W. J. Sydeman, and F. B. Schwing. 2009. Phenology of coastal upwelling in the California Current. *Geophysical Research Letters* 36.
- Bond, N. A., M. F. Cronin, H. Freeland, and N. Mantua. 2015. Causes and impacts of the 2014 warm anomaly in the NE Pacific. *Geophysical Research Letters* 42:3414–3420.
- Brodeur, R. D., E. A. Daly, C. A. Benkwitt, C. A. Morgan, and R. L. Emmett. 2011. Catching the prey: Sampling juvenile fish and invertebrate prey fields of juvenile coho and Chinook salmon during their early marine residence. *Fisheries Research* 108:65–73.
- Brodeur, R. D., J. P. Fisher, R. L. Emmett, C. A. Morgan, and E. Casillas. 2005. Species composition and community structure of pelagic nekton off Oregon and Washington under variable oceanographic conditions. *Marine Ecology Progress Series* 298:41–57.
- Brodeur, R. D., I. Perry, J. Boldt, L. Flostrand, M. Galbraith, J. King, J. Murphy, K. M. Sakuma, and A. R. Thompson. 2018. An unusual gelatinous plankton event in the NE Pacific: The Great Pyrosome Bloom of 2017. *PICES Press* 26:22–27.
- Brodeur, R. D., W. T. Peterson, T. D. Auth, H. L. Soulen, M. M. Parnel, and A. Emerson. 2008. Abundance and diversity of coastal fish larvae as indicators of recent changes in ocean and climate conditions in the Oregon upwelling zone. *Marine Ecology Progress Series* 366:187–202.
- Cavole, L. M., A. M. Demko, R. E. Diner, A. Giddings, I. Koester, C. M. S. Pagnello, M. L. Paulsen, A. Ramirez-Valdez, S. M. Schwenck, N. K. Yen, M. E. Zill, and P. J. S. Franks. 2016. Biological impacts of the 2013–2015 warm-water anomaly in the northeast Pacific: winners, losers, and the future. *Oceanography* 29:273–285.
- Chavez, F. P., J. R. Ryan, S. E. Lluch-Cota, and M. Niquen. 2003. From anchovies to sardines and back: Multidecadal change in the Pacific Ocean. *Science* 299:217–221.
- Checkley, D. M., and M. Lindegren. 2014. Sea Surface Temperature Variability at the Scripps Institution of Oceanography Pier. *Journal of Physical Oceanography* 44:2877–2892.
- Checkley, D. M., P. B. Ortner, L. R. Settle, and S. R. Cummings. 1997. A continuous, underway fish egg sampler. *Fisheries Oceanography* 6:58–73.

- Chhak, K., and E. Di Lorenzo. 2007. Decadal variations in the California Current upwelling cells. *Geophysical Research Letters* 34:L14604.
- Daly, E. A., T. D. Auth, R. D. Brodeur, and K. C. Jacobson. 2019. Changes in juvenile salmon prey fields associated with a recent marine heat wave in the northern California Current. NPAFC Technical Report 15:in press.
- Daly, E. A., T. D. Auth, R. D. Brodeur, and W. T. Peterson. 2013. Winter ichthyoplankton biomass as a predictor of early summer prey fields and survival of juvenile salmon in the northern California Current. *Marine Ecology Progress Series* 484:203–217.
- Daly, E. A., and R. D. Brodeur. 2015. Warming Ocean Conditions Relate to Increased Trophic Requirements of Threatened and Endangered Salmon. *PLoS One* 10:e0144066.
- Daly, E. A., R. D. Brodeur, and T. D. Auth. 2017. Anomalous ocean conditions in 2015: impacts on spring Chinook salmon and their prey field. *Marine Ecology Progress Series* 566:169–182.
- Davison, P., W. J. Sydeman, and J. A. Thayer. 2017. Are there temporal or spatial gaps in recent estimates of anchovy off California? *California Cooperative Oceanic Fisheries Investigations Reports* 58:1–13.
- Di Lorenzo, E., J. Fiechter, N. Schneider, A. Bracco, A. J. Miller, P. J. S. Franks, S. J. Bograd, A. M. Moore, A. C. Thomas, W. Crawford, A. Pena, and A. J. Hermann. 2009. Nutrient and salinity decadal variations in the central and eastern North Pacific. *Geophysical Research Letters* 36:L14601.
- Di Lorenzo, E., N. Schneider, K. M. Cobb, P. J. S. Franks, K. Chhak, A. J. Miller, J. C. McWilliams, S. J. Bograd, H. Arango, E. Curchister, T. M. Powell, and P. Riviere. 2008. North Pacific Gyre Oscillation links ocean climate and ecosystem change. *Geophysical Research Letters* 35:L08607.
- Dickey-Collas, M., G. H. Engelhard, A. Rindorf, K. Raab, S. Smout, G. Aarts, M. van Deurs, T. Brunel, A. Hoff, R. A. M. Lauerburg, S. Garthe, K. H. Anderson, F. Scott, T. van Kooten, D. Beare, and M. A. Peck. 2014. Ecosystem-based management objectives for the North Sea: riding the forage fish rollercoaster. *ICES Journal of Marine Science* 71:128–142.
- Durazo, R., and T. R. Baumgartner. 2002. Evolution of oceanographic conditions off Baja California: 1997–1999. *Progress in Oceanography* 54:7–31.
- Feinberg, L. R., and W. T. Peterson. 2003. Variability in duration and intensity of euphausiid spawning off central Oregon, 1996–2001. *Progress in Oceanography* 57:363–379.
- Feinberg, L. R., W. T. Peterson, and C. Tracy Shaw. 2010. The timing and location of spawning for the Euphausiid *Thysanoessa spinifera* off the Oregon coast, USA. *Deep Sea Research Part II: Topical Studies in Oceanography* 57:572–583.
- Fiedler, P. C., and N. J. Mantua. 2017. How are warm and cool years in the California Current related to ENSO? *Journal Geophysical Research Oceans* 122:5936–5951.
- Frölicher, T. L., E. M. Fischer, and N. Gruber. 2018. Marine heat waves under global warming. *Nature* 560:360–364.
- Goodwin, K. D., L. R. Thompson, B. Duarte, T. Kahlke, A. R. Thompson, J. C. Marques, and I. Caçador. 2017. DNA Sequencing as a Tool to Monitor Marine Ecological Status. *Frontiers in Marine Science* 4:107.
- Gruber, N., and J. L. Sarmiento. 1997. Global patterns of marine nitrogen fixation and denitrification. *Global Biogeochemical Cycles* 11:235–266.
- Hjort, J. 1914. Fluctuations in the great fisheries of Northern Europe viewed in the light of biological research. *Rapports et Procès-Verbaux des Réunions* 20:1–228.
- Hjort, J. 1926. Fluctuations in the year classes of important food fishes. *Journal du Conseil / Conseil Permanent International pour l'Exploration de la Mer* 1:5–38.
- Hobday, A. J., L. V. Alexander, S. E. Perkins, D. A. Smale, S. C. Straub, E. C. J. Oliver, J. A. Benthuisen, M. T. Burrows, M. G. Donat, M. Feng, N. J. Holbrook, P. J. Moore, H. A. Scannell, A. Sen Gupta, and T. Wernberg. 2016. A hierarchical approach to defining marine heat waves. *Progress in Oceanography* 141:227–238.
- Horton, C. A. 2014. Top-down influences of Bald Eagles on Common Murre populations in Oregon. MS. Thesis. Oregon State University.
- Houde, E. 2008. Emerging from Hjort's shadow. *Journal of the Northwest Atlantic Fisheries Science* 41:53–70.
- Houde, E. D. 1987. Fish early life dynamics and recruitment variability. *Transactions of the American Fisheries Society* 2:17–29.
- Hyrenbach, D. K., and R. R. Veit. 2003. Ocean warming and seabird communities of the Southern California Current System (1987–98): response at multiple temporal scales. *Deep Sea Research II* 50:2537–2565.
- Jacox, M. G., M. A. Alexander, N. J. Mantua, J. D. Scott, G. Hervieux, R. S. Webb, and F. E. Werner. 2018a. Forcing of multiyear extreme ocean temperatures that impacted California current living marine resources in 2016. *Bulletin of the American Meteorological Society* 99:S27–S33.
- Jacox, M. G., C. A. Edwards, E. L. Hazen, and S. J. Bograd. 2018b. Coastal upwelling revisited: Ekman, Bakun, and improved upwelling indices for the U.S. west coast. *Geophysical Research Letters* 123:7332–7350.
- Jacox, M. G., J. Fiechter, A. M. Moore, and C. A. Edwards. 2015. ENSO and the California Current coastal upwelling response. *Journal Geophysical Research Oceans* 120:1691–1702.
- Jacox, M. G., E. L. Hazen, K. D. Zaba, D. L. Rudnick, C. A. Edwards, A. M. Moore, and S. J. Bograd. 2016. Impacts of the 2015–2016 El Niño on the California Current System: Early assessment and comparison to past events. *Geophysical Research Letters* 43:7072–7080.
- Jones, T., J. K. Parrish, W. T. Peterson, E. P. Bjorkstedt, N. A. Bond, L. T. Balance, V. Bowes, J. M. Hipfner, H. K. Burgess, J. E. Dolliver, K. Lindquist, J. Lindsey, H. M. Nevins, R. R. Robertson, J. Roletto, L. Wilson, T. Joyce, and J. Harvey. 2018. Massive Mortality of a Planktivorous Seabird in Response to a Marine Heat wave. *Geophysical Research Letters* 45:3193–3202.
- Kahru, M., M. G. Jacox, and M. D. Ohman. 2018. CCE1: Decrease in the frequency of oceanic fronts and surface chlorophyll concentration in the California Current System during the 2014–2016 northeast Pacific warm anomalies. *Deep Sea Research Part I: Oceanographic Research Papers* 140:4–13.
- Kahru, M., R. M. Kudela, C. R. Anderson, and B. G. Mitchell. 2015a. Optimized merger of ocean chlorophyll algorithms of MODIS-Aqua and VIIRS. *IEEE Geoscience and Remote Sensing Letters* 12:11.
- Kahru, M., R. M. Kudela, M. Manzano-Sarabia, and B. G. Mitchell. 2012. Trends in the surface chlorophyll of the California Current: Merging data from multiple ocean color satellites. *Deep Sea Research II* 77–80:89–98.
- Kahru, M., Z. Lee, R. M. Kudela, M. Manzano-Sarabia, and B. G. Mitchell. 2015b. Multi-satellite time series of inherent optical properties in the California Current. *Deep Sea Research II* 112:91–106.
- Koslow, J. A., P. Davison, E. Ferrer, S. Rosenberg, G. Aceves-Medina, and W. Watson. 2019. The evolving response of mesopelagic fishes to declining midwater oxygen concentrations in the southern and central California Current. *ICES Journal of Marine Science* 76:626–638.
- Lance, M. M., A. J. Orr, S. D. Riemer, M. J. Weise, and J. L. Laake. 2001. Pinniped food habits and prey identification techniques protocol. Alaska Fisheries Science Center Processed Report 2001–04.
- Lasker, R. 1975. Field criteria for survival of anchovy larvae: The relation between inshore chlorophyll maximum layers and successful first feeding. *Fishery Bulletin* 73:453–462.
- Lasker, R. 1978. The relation between oceanographic conditions and larval anchovy food in the California Current: Identification of factors contributing to recruitment failure. *Rapports et Procès-verbaux des Réunions. Conseil International pour l'Exploration de la Mer* 173:212–230.
- Lasker, R. 1981. Factors contributing to variable recruitment of the northern anchovy (*Engraulis mordax*) in the California Current: Contrasting years 1975 through 1978. *Rapports et Procès-verbaux des Réunions. Conseil International pour l'Exploration de la Mer* 178:375–388.
- Lasker, R. 1985. What limits clupeoid production. *Canadian Journal of Fisheries and Aquatic Sciences* 42:31–38.
- Lasker, R., H. M. Feder, G. H. Theilacker, and R. C. May. 1970. Feeding, growth, and survival of *Engraulis mordax* larvae reared in the laboratory. *Marine Biology* 5:345–353.
- Leising, A. W., I. D. Schroeder, S. J. Bograd, J. Abell, R. Duranzo, G. Gaxiola-Castro, E. P. Bjorkstedt, J. C. Field, K. M. Sakuma, R. R. Robertson, R. Goericke, W. T. Peterson, R. D. Brodeur, C. Barcelo, T. D. Auth, E. A. Daly, R. M. Suryan, A. J. Gladics, J. M. Porquez, S. McClatchie, E. D. Weber, W. Watson, J. A. Santora, W. J. Sydeman, S. R. Melin, F. C. Chavez, R. T. Goightly, S. R. Schneider, J. Fisher, C. A. Morgan, R. Bradley, and P. Warybok. 2015. State of the California Current 2014–15: Impacts of the warm-water “Blob”. *California Cooperative Oceanic Fisheries Investigations Reports* 56:31–68.
- Lindenmayer, D. B., G. E. Likens, C. J. Krebs, and R. J. Hobbs. 2010. Improved probability of detection of ecological “surprises.” *Proceedings of the National Academy of Sciences* 107:21957–21962.
- Long, M. C., C. Deutsch, and T. Ito. 2016. Finding forced trends in oceanic oxygen. *Global Biogeochemical Cycles* 30:381–397.
- Loredo, S. A., R. A. Orben, R. M. Suryan, D. E. Lyons, J. Adams, and S. W. Stephenson. 2019. Spatial and temporal diving behavior of non-breeding common murres during two summers of contrasting ocean conditions. *Journal of Experimental Marine Biology and Ecology* 517:13–24.

- Lynn, R. J., and J. J. Simpson. 1987. The California Current System: The seasonal variability of its physical characteristics. *Journal of Geophysical Research* 92:12947–12966.
- MacCall, A. D., W. J. Sydeman, P. Davison, and J. A. Thayer. 2016. Recent collapse of northern anchovy biomass off California. *Fisheries Research* 175:87–94.
- Mantua, N., S. R. Hare, Y. Zhang, J. M. Wallace, and R. C. Francis. 1997. A Pacific decadal climate oscillation with impacts on salmon. *Bulletin of the American Meteorological Society* 78:1069–1079.
- McClatchie, S. 2012. Sardine biomass is poorly correlated with the Pacific Decadal Oscillation off California. *Geophysical Research Letters* 39.
- McClatchie, S. 2014. Regional fisheries oceanography of the California Current System and the CalCOFI program. Springer.
- McClatchie, S., J. C. Field, A. R. Thompson, T. Gerrodette, M. Lowry, P. C. Fiedler, W. Watson, K. M. Nieto, and R. D. Vetter. 2016a. Food limitation of sea lion pups and the decline of forage off central and southern California. *Royal Society Open Science* 3:150628.
- McClatchie, S., R. Goericke, A. Leising, T. D. Auth, E. Bjorkstedt, R. R. Robertson, R. D. Brodeur, X. Du, E. A. Daly, C. A. Morgan, F. P. Chavez, A. J. Debich, J. Hildebrand, J. C. Field, K. M. Sakuma, M. G. Jacox, M. Kahru, R. Kudela, C. Anderson, B. E. Lavanigos, J. Gomes-Valdes, S. P. A. Jimenez-Rosenberg, R. McCabe, S. R. Melin, M. D. Ohman, L. M. Sala, B. Peterson, J. L. Fisher, I. D. Schroeder, S. J. Bograd, E. L. Hazen, S. R. Schneider, R. T. Golightly, R. M. Suryan, A. J. Gladics, S. Lored, J. M. Porquez, A. R. Thompson, E. D. Weber, W. Watson, V. Trainer, P. Warzybok, R. Bradley, and J. Jahncke. 2016b. State of the California Current 2015–16: Comparisons with the 1997–98 El Niño. *California Cooperative Oceanic Fisheries Investigations Reports* 57:5–61.
- McClatchie, S., R. D. Vetter, and I. L. Hendy. 2018. Forage fish, small pelagic fisheries and recovering predators: managing expectations. *Animal Conservation* 21:445–447.
- Melin, S. R., R. L. DeLong, and D. B. Sniff. 2008. The effects of El Niño on the foraging behavior of lactating California sea lions (*Zalophus californianus californianus*) during the nonbreeding season. *Canadian Journal of Zoology* 86:192–206.
- Melin, S. R., A. J. Orr, J. D. Harris, J. L. Laake, and R. L. DeLong. 2012. California sea lions: An indicator for integrated ecosystem assessment of the California Current System. *California Cooperative Oceanic Fisheries Investigations Reports* 53:140–152.
- Melin, S. R., A. J. Orr, J. D. Harris, J. L. Laake, R. L. DeLong, F. M. Gulland, and S. Soudt. 2010. Unprecedented mortality of California sea lion pups associated with anomalous oceanographic conditions along the central California coast in 2009. *California Cooperative Oceanic Fisheries Investigations Reports* 51:182–194.
- Morgan, C. A., A. M. Baptista, B. R. Beckman, R. D. Brodeur, B. J. Burke, E. A. Daly, K. C. Jacobson, E. M. Phillips, D. M. Van Doornik, and J. E. Zamon. 2019. Ocean Survival of Salmonids RME, 1/1/2018–12/31/2018. Annual Report, 1998-014-00. 54pp. Available at: <https://www.cbfish.org/Document.mvc/Viewer/P164449>.
- Neveu, E., A. M. Moore, C. A. Edwards, J. Fiechter, P. Drake, W. J. Crawford, M. G. Jacox, and E. Nuss. 2016. An historical analysis of the California Current circulation using ROMS 4D-Var: System configuration and diagnostics. *Ocean Modelling* 99:133–151.
- Orr, A. J., J. L. Laake, M. I. Dhruv, A. S. Banks, R. L. DeLong, and H. R. Huber. 2003. Comparison of processing pinniped scat samples using a washing machine and nested sieves. *Wildlife Society Bulletin* 31:253–257.
- Pacific Fisheries Management Council. 2019a. Agenda Item H.6 2020 Harvest Specifications for Cowcod and Shortbelly rockfish. https://www.pcouncil.org/wp-content/uploads/2019/09/H6_CouncilAction_SEPT-2019.pdf.
- Pacific Fisheries Management Council. 2019b. Groundfish Management Team Report on 2020 Harvest Specifications for Shortbelly Rockfish. Agenda Item H.6.a, Supplemental GMT Report 1, September 2019 https://www.pcouncil.org/wp-content/uploads/2019/09/H6a_Sup_GMT_Rpt1_SEPT2019BB.pdf.
- Peabody, C. E., A. R. Thompson, D. F. Sax, R. E. Morse, and C. T. Perretti. 2018. Decadal regime shifts in southern California's ichthyoplankton assemblage. *Marine Ecology Progress Series* 607:71–83.
- Peck, M. A., S. Neuenfeldt, T. E. Essington, V. M. Trenkel, A. Takasuka, H. Gislason, M. Dickey-Collas, K. H. Anderson, L. Ravn-Jensen, N. Vestergaard, S. F. Kvamsdal, A. Gardmark, J. Link, and J. C. Rice. 2014. Forage fish interactions: a symposium on “Creating tools for ecosystem-based management of marine resources.” *ICES Journal of Marine Science* 71:1–4.
- Peláez, J., and J. A. McGowan. 1986. Phytoplankton pigment patterns in the California Current as determined by satellite. *Limnology and Oceanography* 31:927–950.
- Peterson, W. T., J. L. Fisher, P. T. Strub, X. Du, C. Risien, J. Peterson, and C. T. Shaw. 2017. The pelagic ecosystem in the Northern California Current off Oregon during the 2014–2016 warm anomalies within the context of the past 20 years. *Journal of Geophysical Research: Oceans* 122:7267–7290.
- Phillips, E. M., M. H. Horn, J. Adams, and J. E. Zamon. 2018. Selective occupancy of a persistent yet variable coastal river plume by two seabird species. *Marine Ecology Progress Series* 594:245–261.
- Phillips, E. M., J. K. Horne, and J. E. Zamon. 2017. Predator-prey interactions influenced by a dynamic river plume. *Canadian Journal of Fisheries and Aquatic Sciences* 74:1375–1390.
- Phillips, E. M., J. K. Horne, J. E. Zamon, J. J. Felis, and J. Adams. 2019. Does perspective matter? A case study comparing Eulerian and Lagrangian estimates of common murre (*Uriaaalge*) distributions. *Ecology and Evolution* 9:1–15.
- Pozo Buil, M., and E. Di Lorenzo. 2017. Decadal dynamics and predictability of oxygen and subsurface tracers in the California Current System. *Geophysical Research Letters* 44:4204–4213.
- Ralston, S., K. Sakuma, and J. Field. 2013. Interannual variation in pelagic juvenile rockfish (*Sebastes* spp.) abundance—going with the flow. *Fisheries Oceanography* 22:288–308.
- Reynolds, R. W., T. M. Smith, C. Liu, D. B. Chelton, K. S. Casey, and M. G. Schlax. 2007. Daily High-resolution Blended Analyses for sea surface temperature. *Journal of Climate* 20:5473–5496.
- Sakuma, K. M., J. C. Field, B. B. Marinovic, C. N. Carrion, N. J. Mantua, and S. Ralston. 2016. Anomalous epipelagic micronekton assemblage patterns in the neritic waters of the California Current in spring 2015 during a period of extreme ocean conditions. *California Cooperative Oceanic Fisheries Investigations Reports* 57:163–183.
- Santora, J. A., I. D. Schroeder, J. C. Field, B. K. Wells, and W. J. Sydeman. 2014. Spatio-temporal dynamics of ocean conditions and forage taxa reveal regional structuring of seabird-prey relationships. *Ecological Applications* 24:1730–1747.
- Santora, J. A., and W. J. Sydeman. 2015. Persistence of hotspots and variability of seabird species richness and abundance in the southern California Current. *Ecosphere* 6:214.
- Schmidtke, S., L. Stramma, and M. Visbeck. 2017. Decline in global oceanic oxygen content during the past five decades. *Nature* 542:335–339.
- Schroeder, I. D., B. A. Black, W. J. Sydeman, S. J. Bograd, E. L. Hazen, J. A. Santora, and B. K. Wells. 2013. The North Pacific High and wintertime pre-conditioning of California Current productivity. *Geophysical Research Letters* 40:541–546.
- Schroeder, I. D., J. A. Santora, S. J. Bograd, E. L. Hazen, K. M. Sakuma, A. M. Moore, C. A. Edwards, B. K. Wells, and J. C. Field. 2019. Source water variability as a driver of rockfish recruitment in the California Current Ecosystem: implications for climate change and fisheries management. *Canadian Journal of Fisheries and Aquatic Sciences* 76:950–960.
- Schroeder, I. D., W. J. Sydeman, N. Sarkar, S. A. Thompson, S. J. Bograd, and F. B. Schwing. 2009. Winter pre-conditioning of seabird phenology in the California Current. *Marine Ecology Progress Series* 393:211–233.
- Schwartzlose, R. A., J. Alheit, A. Bakun, T. R. Baumgartner, R. Cloete, R. J. M. Crawford, W. J. Fletcher, Y. Green-Ruiz, E. Hagen, T. Kawasaki, D. Lluch-Belda, S. E. Lluch-Cota, A. D. MacCall, Y. Matsuura, M. O. Nevarez-Martinez, R. H. Parrish, C. Roy, R. Serra, K. V. Shust, M. N. Ward, and J. Z. Zuzunaga. 1999. Worldwide large-scale fluctuations of sardine and anchovy populations. *South African Journal of Marine Science* 21:289–347.
- Schwing, F. B., M. O'Farrell, J. M. Steger, and K. Baltz. 1996. Coastal Upwelling indices west coast of North America. NOAA Technical Report NMFS SWFSC NMFS SWFSC 231.
- Scura, E. D., and C. W. Jerde. 1977. Various species of phytoplankton as food for larval northern anchovy, *Engraulis mordax*, and relative nutritional value of the dinoflagellates *Gymnodinium splendens* and *Gonyaulax polyedra*. *Fisheries Bulletin* 75:577–583.
- Stierhoff, K. L., J. P. Zwolinski, and D. A. Demer. 2019. Distribution, biomass, and demography of coastal pelagic fishes in the California Current Ecosystem during summer 2018 based on acoustic-trawl sampling. U.S. Department of Commerce, NOAA Technical Memorandum NMFS-SWFSC-613.

- Sydeman, W. J., S. A. Thompson, J. A. Santora, J. A. Koslow, R. Goericke, and M. D. Ohman. 2015. Climate-ecosystem change off southern California: Time-dependent seabird predator-prey numerical responses. *Deep Sea Research II* 112:158–170.
- Thayer, J. A., A. D. MacCall, P. C. Davison, and W. J. Sydeman. 2017. California anchovy population remains low, 2012–16. *California Cooperative Oceanic Fisheries Investigations Reports* 58:69–76.
- Thompson, A. R., T. D. Auth, R. D. Brodeur, N. M. Bowlin, and W. Watson. 2014. Dynamics of larval fish assemblages in the California Current System: a comparative study between Oregon and southern California. *Marine Ecology Progress Series* 506:193–212.
- Thompson, A. R., C. J. Harvey, W. J. Sydeman, C. Barceló, S. J. Bograd, R. D. Brodeur, J. Fiechter, J. C. Field, N. Garfield, T. P. Good, E. L. Hazen, M. E. Hunsicker, K. Jacobson, M. G. Jacox, A. Leising, J. Lindsay, S. R. Melin, J. A. Santora, I. D. Schroeder, J. A. Thayer, B. K. Wells, and G. D. Williams. 2019. Indicators of pelagic forage community shifts in the California Current Large Marine Ecosystem, 1998–2016. *Ecological Indicators* 105:215–228.
- Thompson, A. R., I. D. Schroeder, S. J. Bograd, E. L. Hazen, M. G. Jacox, A. Leising, B. K. Wells, J. L. Largier, J. L. Fisher, K. Jacobson, S. Zeman, E. P. Bjorkstedt, R. R. Robertson, F. P. Chavez, M. Kahru, R. Goericke, S. McClatchie, C. E. Peabody, T. R. Baumgartner, B. E. Lavanigos, J. Gomez-Valdes, R. D. Brodeur, E. A. Daly, C. A. Morgan, T. D. Auth, B. J. Burke, J. C. Field, K. M. Sakuma, E. D. Weber, W. Watson, J. Cooates, R. Schoenbaum, L. Rogers-Bennett, R. M. Suryan, J. Dolliver, S. Lored, J. E. Zamon, S. R. Schneider, R. T. Golightly, P. Warzybok, J. Jahncke, J. A. Santora, S. A. Thompson, W. J. Sydeman, and S. R. Melin. 2018. State of the California Current 2017–18: Still not quite normal in the north and getting interesting in the south. *California Cooperative Oceanic Fisheries Investigations Reports* 59:1–66.
- Varoujean, D. H., and D. R. Matthews. 1983. Distribution, abundance, and feeding habits of seabirds off the Columbia River, May–June 1982. Report No. OIMB 83–1, University of Oregon Institute of Marine Biology, Charleston. 28 pp.
- Velarde, E., E. Ezcurra, M. H. Horn, and R. T. Patton. 2015. Warm oceanographic anomalies and fishing pressure drive seabird nesting north. *Science Advances* 1:e1400210.
- Wells, B. K., I. D. Schroeder, S. J. Bograd, E. L. Hazen, M. G. Jacox, A. Leising, N. Mantua, J. A. Santora, J. L. Fisher, W. T. Peterson, E. Bjorkstedt, R. R. Robertson, F. P. Chavez, R. Goericke, R. Kudela, C. Anderson, B. E. Lavanigos, J. Gomez-Valdes, R. D. Brodeur, E. A. Daly, C. A. Morgan, T. D. Auth, J. C. Field, K. M. Sakuma, S. McClatchie, A. R. Thompson, E. D. Weber, W. Watson, R. M. Suryan, J. K. Parrish, J. Dolliver, S. Lored, J. M. Porquez, J. E. Zamon, S. R. Schneider, R. T. Golightly, P. Warzybok, R. Bradley, J. Jahncke, W. J. Sydeman, S. R. Melin, J. A. Hildebrand, A. J. Debich, and B. Thayre. 2017. State of the California Current 2016–17: Still anything but “normal” in the north. *CalCOFI Reports* 58:1–55.
- Zamon, J. E., E. M. Phillips, and T. J. Guy. 2014. Marine bird aggregations associated with the tidally-driven plume and plume fronts of the Columbia River. *Deep Sea Research II* 107:85–95.
- Zwolinski, J. P., D. A. Demer, B. J. Macewicz, S. Mau, D. Murfin, D. Palance, J. S. Renfree, T. S. Sessions, and K. Stierhoff. 2017. Distribution, biomass and demography of the central-stock of Northern Anchovy during summer 2016, estimated from acoustic-trawl sampling. U.S. Department of Commerce NOAA-TM-NMFS-SWFSC-572.
- Zwolinski, J. P., K. L. Stierhoff, and D. A. Demer. 2019. Distribution, biomass, and demography of coastal pelagic fishes in the California Current Ecosystem during summer 2017 based on acoustic-trawl sampling. U.S. Department of Commerce, NOAA Technical Memorandum NMFS-SWFSC-610.

SUPPLEMENTAL FIGURES

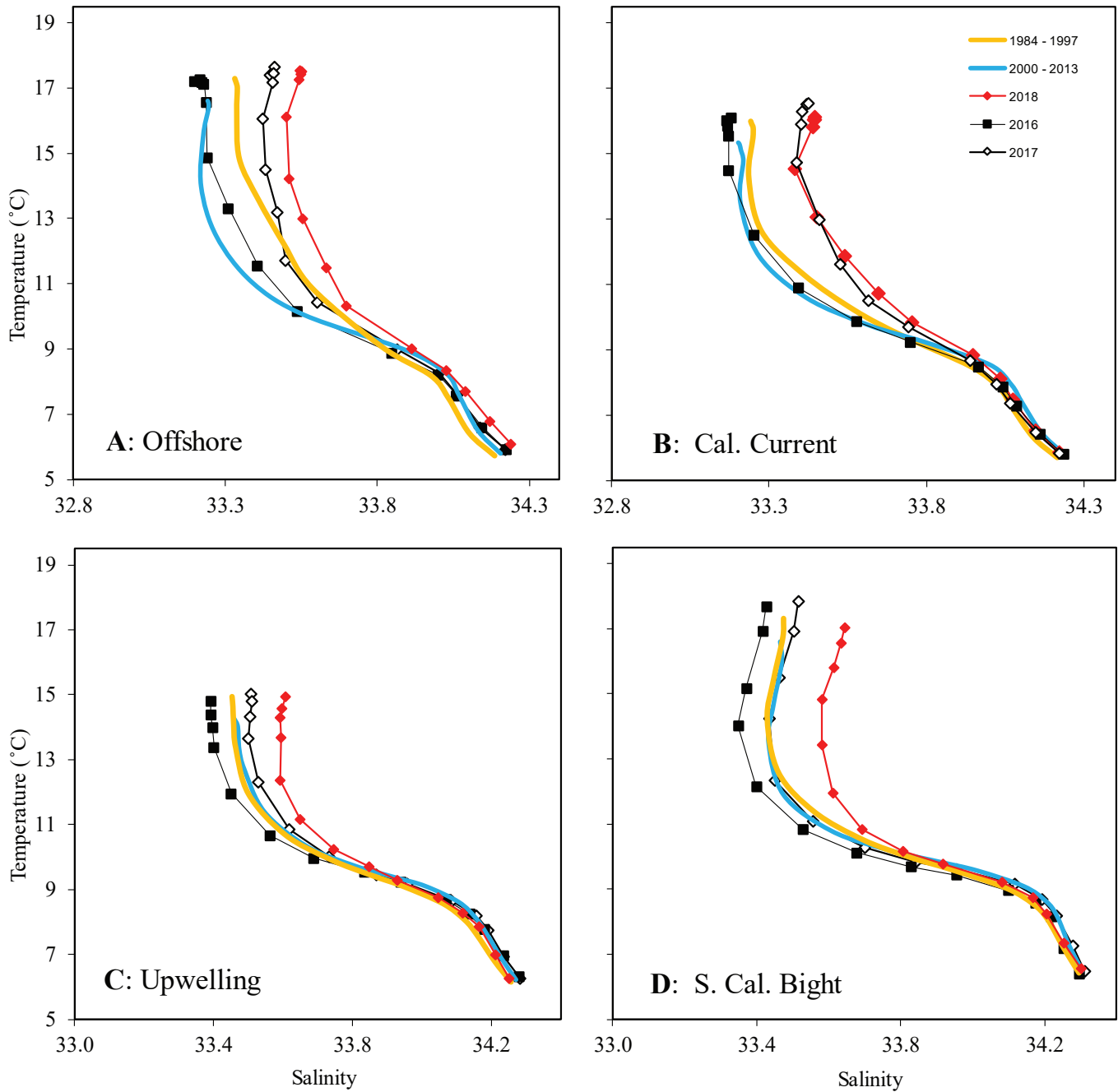


Figure S1. Annual average TS properties for representative areas of the CalCOFI region for different time periods, i.e. 1984 to 1997, 2000 to 2013, 2016, 2017 and 2018. Annual averages are based on ENSO years, i.e., the time from June of the target year until May of the target year plus one. The regions are: A: offshore (CalCOFI Lines 90-93, Stations ≥ 90 ; L87-77, St ≥ 100), B. California Current region (L90 St 60-80, L87-77 St 70-90), C. upwelling (L87 St 51-60, L82 St 47, L77-80 St ≤ 60), and D: Southern California Bight (L 90-93 St ≤ 45 , L87 St ≤ 40 , L83 St ≤ 42). Each data point represents the average TS characteristic of one standard depth level (0, 10, 20, 30, 50, 75, 100, 125, 150, 200, 250, 300, 400, and 500 m) for the specified time period and area.

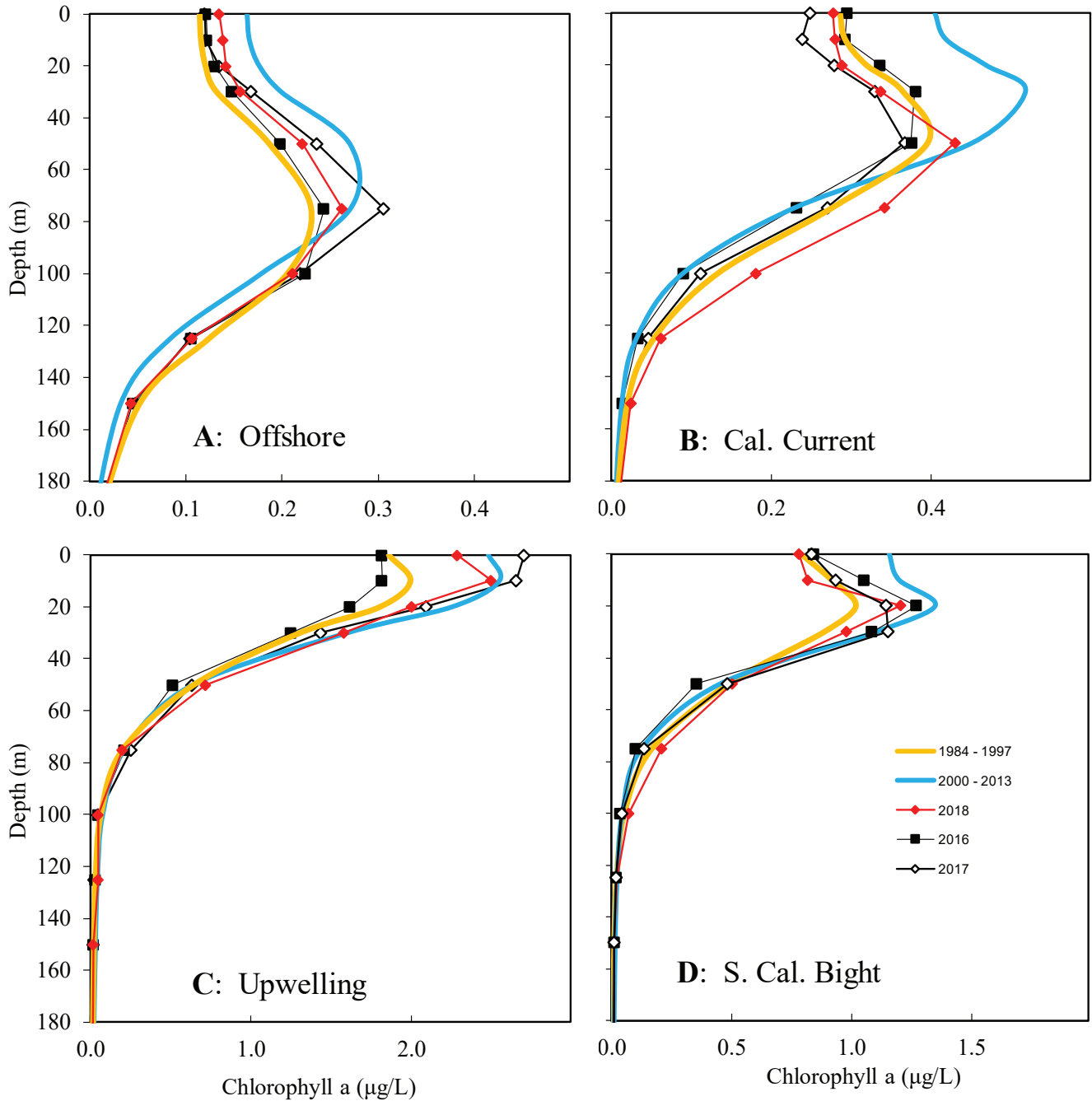


Figure S2. Depth profiles of Chl a for the times and four areas of the CalCOFI region that are defined in CalCOFI Fig. S1. Data were derived and are presented as described in CalCOFI Fig. S1.

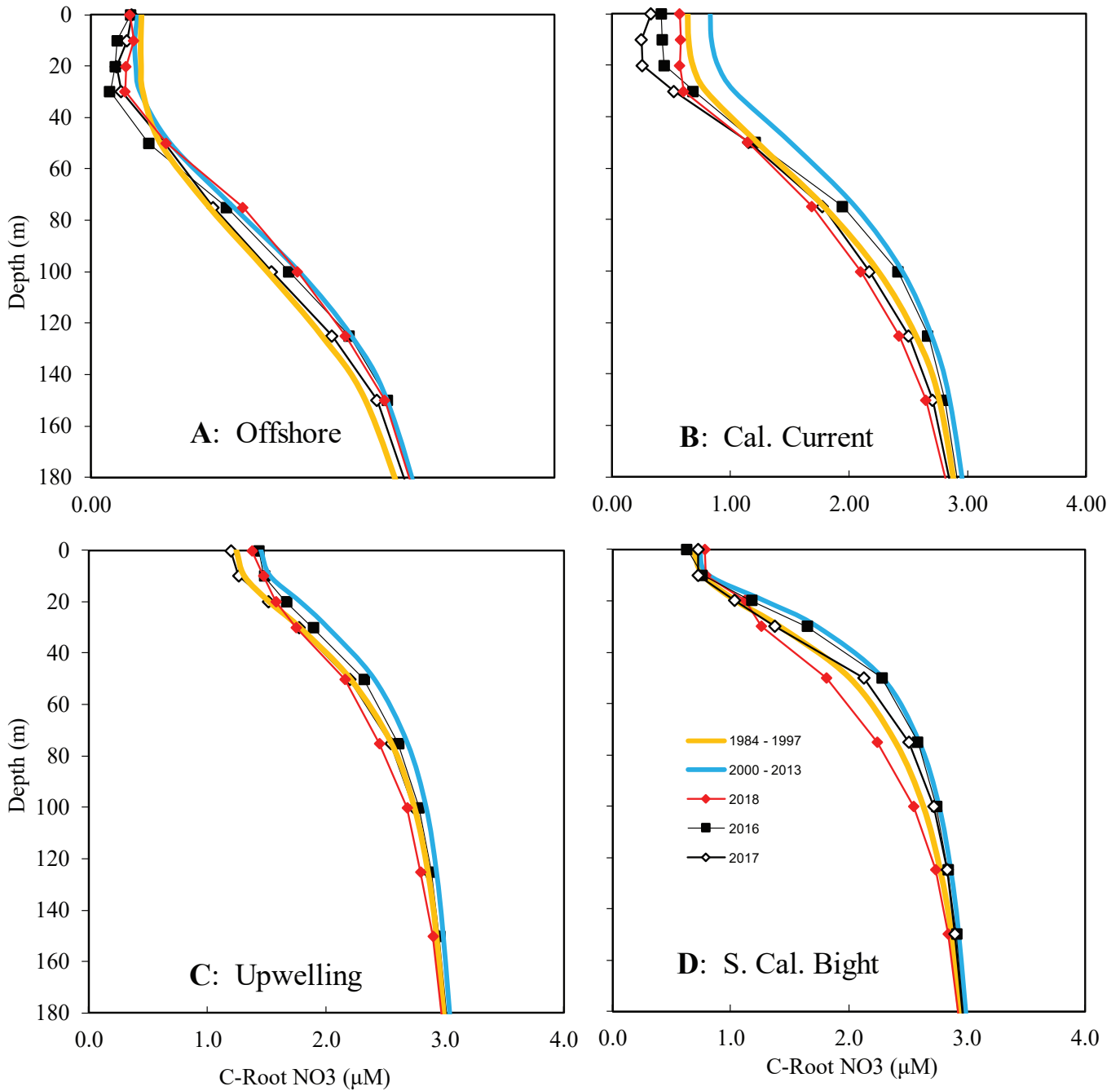


Figure S3. Depth profiles of cuberoot of nitrate for the times and four areas of the CalCOFI region that are defined in CalCOFI Fig. S1. Data were derived and are presented as described in CalCOFI Fig. S1.

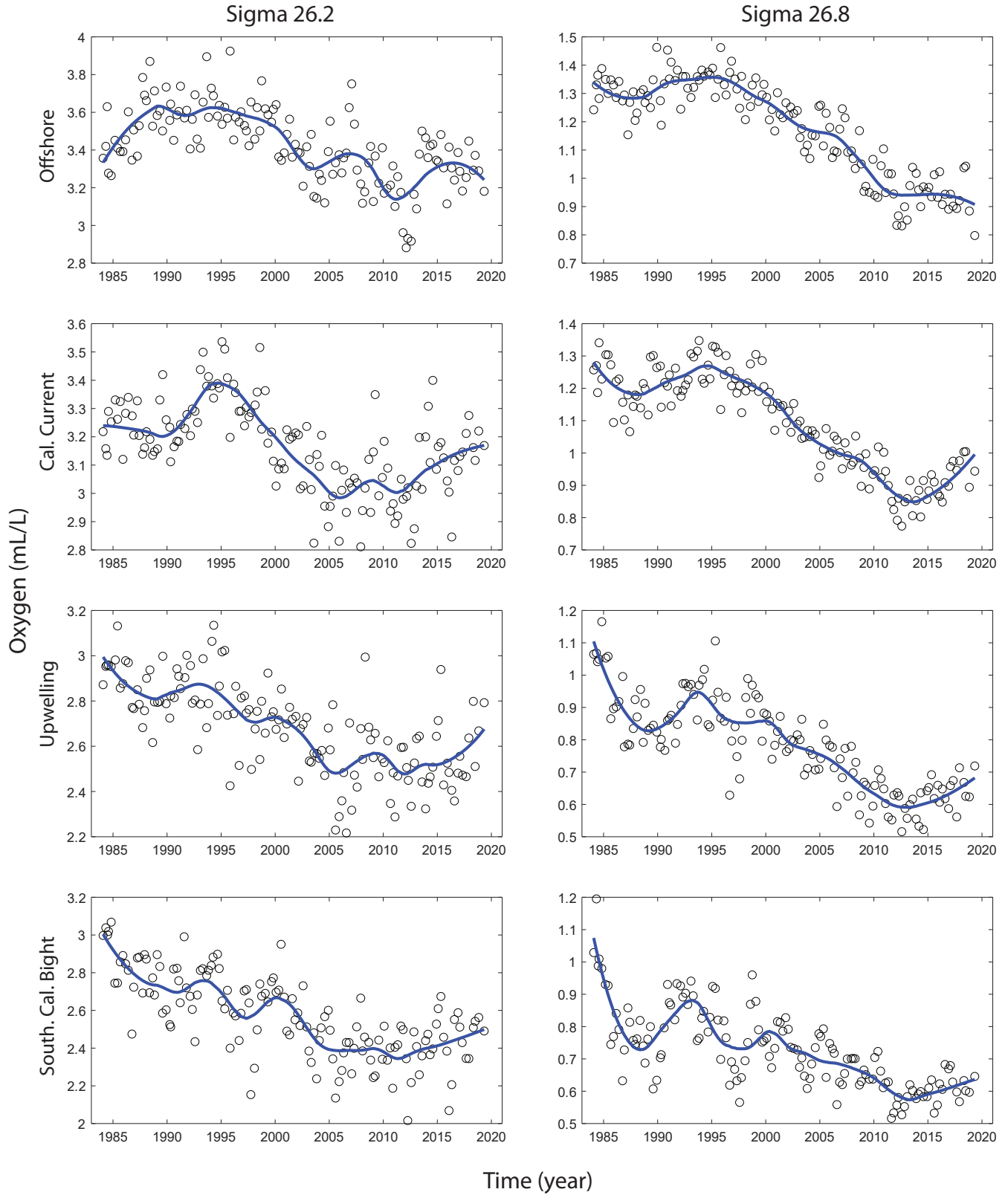


Figure S4. Oxygen concentration anomalies at the $\sigma_{26.2}$ and $\sigma_{26.8}$ isopycnals plotted as described in CalCOFI Fig. 2 for the four regions as defined in the legend of CalCOFI Fig. S1.

MODELING GROWTH OF THE PACIFIC SARDINE *SARDINOPS CAERULEUS* IN THE GULF OF CALIFORNIA, MEXICO, USING THE MULTIMODEL INFERENCE APPROACH

MANUEL OTILIO NEVÁREZ-MARTÍNEZ

Instituto Nacional de Pesca y Acuicultura
Centro Regional de Investigación Pesquera
Guaymas, Sonora, México
Calle 20 Sur 605, Colonia La Cantera
Guaymas, Sonora 85430, México

EDGAR ARNOLDO ARZOLA-SOTELO

Centro de Investigaciones Biológicas del Noroeste, S.C.
Km 2.35 Carretera a Las Tinajas, Colonia Tinajas
CP. 85460
Guaymas, Sonora, México

JUANA LÓPEZ-MARTÍNEZ

Centro de Investigaciones Biológicas del Noroeste, S.C.
Km 2.35 Carretera a Las Tinajas, Colonia Tinajas
CP. 85460
Guaymas, Sonora, México
ph: +52 (622) 221 2237
fax: +52 (622) 221 2238
jlopez04@cibnor.mx

JOSÉ PABLO SANTOS-MOLINA

Instituto Nacional de Pesca y Acuicultura
Centro Regional de Investigación Pesquera
Guaymas, Sonora, México
Calle 20 Sur 605, Colonia La Cantera
Guaymas, Sonora 85430, México

MARÍA DE LOS ÁNGELES MARTÍNEZ-ZAVALA

Instituto Nacional de Pesca y Acuicultura
Centro Regional de Investigación Pesquera
Guaymas, Sonora, México
Calle 20 Sur 605, Colonia La Cantera
Guaymas, Sonora 85430, México

ABSTRACT

To evaluate growth of the Pacific sardine in the Gulf of California, fish samples were collected from the commercial fleet during the 2010–11, 2011–12 and 2012–13 fishing seasons. Sardine samples were measured in standard length (SL) and age was determined based on counting opaque and hyaline growth increments in the otoliths. Four growth models were fitted to the age and length data: von Bertalanffy Growth Model (VBGM), Gompertz, Logistic, and Schnute, using a maximum likelihood algorithm. Confidence intervals of each parameter were calculated through likelihood profiles. The model that best explained the species growth kinetics was selected by Akaike information criteria and Akaike's weight (w_i), while growth parameter covariance was obtained by the likelihood contour method. The sardines obtained from catches ranged in age from 0.5–6 years; sizes varied from 98–218 mm (SL). The growth model that obtained the greatest weight was VBGM ($w_i = 73.11\%$) whose estimated parameters and confidence intervals (CI) for the Pacific sardine were $L_\infty = 201.28$ (200.70–201.80) mm SL, $K = 0.581$ (SD: 0.577–0.586) and $t_0 = -0.839$ (SD: -0.855 – -0.824), showing a more accelerated growth rate of the species in the Gulf of California compared to the same species inhabiting the coasts of Baja California and California.

INTRODUCTION

Small pelagic fish are part of one of the main fishery resources in Mexico because of their great catch volume (Cisneros-Mata et al. 1990; Nevárez-Martínez et al. 2014). The sardine fishery has contributed up to

30% annual landing weight mainly in the Gulf of California (GC), representing around 10% of national fishing economic value (Nevárez-Martínez et al. 2001; Nevárez-Martínez et al. 2014; DOF 2018). The main fishery target is the Pacific sardine (*Sardinops caeruleus* Girard 1856), which in some seasons has contributed up to 80% of the total small pelagic catches in the GC (Nevárez-Martínez et al. 2014; DOF 2018). Their distribution and abundance have been linked to environmental factors such as wind patterns (upwelling) and sea surface temperature (SST) (Nevárez-Martínez et al. 2001; Lanz-Sánchez et al. 2008; Dorval et al. 2015). Between Mexico and Canada, three stocks of Pacific sardine have been well identified with different approaches, including morphometrics, meristic, tagging, blood antigen, differentiated spawning areas and catch-sea temperature data (Clark and Jensen 1945; Clark 1947; Vrooman 1964; Mais 1972; Radovich 1982; Parrish et al. 1989; Félix-Uraga et al. 2004, 2005; Smith 2005; García-Rodríguez et al. 2011; Demer and Zwolinski 2014). The first one is the cold stock located off the northern coast of Baja California, México, to Canada; the second one is the temperate stock found in waters from southern California, U.S.A., to Bahía Magdalena, Baja California Sur, México; and the third stock and objective of this study is the one that inhabits the Gulf of California (Vrooman 1964; Smith 2005; Demer and Zwolinski 2014).

Biomass fluctuations and stock availability, within and out of the GC, depend on climate and environmental factors, which influence strongly high population variability in parameters such as cohort growth through time (Félix-Uraga et al. 2005; Dorval et al. 2015; Checkley Jr.

et al. 2017). Growth of the sardine *S. caeruleus* within the GC differed from that found in the Pacific, which may be due to the ecosystem dynamics of the GC compared to the Pacific (De Anda-Montañez et al. 1999).

Growth rate is one of the most important life history parameters of fish populations, particularly in commercially exploited species (Mercier et al. 2011; Lorenzen 2016). Growth estimation helps us to understand biological traits of the population that could be affected by overfishing (Ali et al. 2003) and determine long-term impacts deriving from fishing or environmental effects (Botsford 1981; Dorval et al. 2015). Furthermore, growth parameter values such as asymptotic length (L_{∞}) and growth rate coefficient (K) are used as seed values in multiple stock assessment models (Beddington and Kirkwood 2005; Haddon 2011).

In the Pacific sardine, most growth estimations performed until now have been based on using the von Bertalanffy (VBGM) model (Cisneros-Mata et al. 1990; Gallardo-Cabello et al. 1991; De Anda-Montañez et al. 1999; Martínez-Zavala et al. 2006) and Gompertz model for length-age data of juveniles in the GC (Quiñonez-Velázquez et al. 2000). The VBGM has been historically used in fisheries to assess fish growth (Katsanevakis and Maravelias 2008; Mercier et al. 2011; Lorenzen 2016); nonetheless, appropriate models should be selected on the indication of biological reality, statistical fit, and when the models applied are complex, also the parsimony (Burnham and Anderson 2002; Cailliet et al. 2006; Katsanevakis 2006). Thus, it was necessary to assess growth with more than one model and compare the fits among models to select the one that best described growth kinetics of the species through statistical information criteria (Burnham and Anderson 2002; Katsanevakis and Maravelias 2008; Beninger et al. 2012). Therefore, the objective of this study was to assess growth of the Pacific sardine *S. caeruleus* in the Gulf of California through the multimodel approach, including as candidate models VBGM, Gompertz, Logistics and Schnute for the sake of robustness in growth parameters estimation for this species.

MATERIALS AND METHODS

Sampling

The information analyzed for the Pacific sardine, *Sardinops caeruleus* Girard 1856, came from samples obtained from the commercial sardine fishery during the 2010–11, 2011–12 and 2012–13 seasons in the Gulf of California, Mexico (fig. 1); the fishing season starts in October and ends in July or August of the following year. Catch of this species was performed with purse seine nets, which consisted of large net walls that close and secure the bottom and then drag below sardine

schools (Lewison et al. 2004). Dimensions of this fishing gear depend on boat capacity (regularly greater than 100 tons); thus, purse seine net were between 366 and 640 m long and 40 to 100 m high with the same 25.1 mm mesh size for the entire net (DOF 2018).

Length structure and age determination

For the period that comprised the fishing seasons from 2010–11 to 2012–13, samples of the Pacific sardine *S. caeruleus* caught in the Gulf of California and landed at the ports of Guaymas and Yavaros (Sonora) were analyzed. Sampling was done in port where fishing landings were made; a sample of approximately 10 kg (from 80 to 120 sardines, depending on individual weight) was taken at random. All the sardines in the sample were measured in standard length (SL, precision of ± 1 mm), grouped into five-millimeter length intervals. Five sardines were selected from each length interval or if there were less than five, those that were in that interval were selected. This subsample of fish was measured for biological characteristics such as standard length (SL), total weight (TW, accuracy of ± 1 g), sex, and otoliths (*sagitta*) were extracted. The otoliths were rinsed with clean water to remove any remaining tissue, and then stored to dry in labeled gelatin capsules.

The age of the Pacific sardines was determined based on counting opaque and hyaline growth increments in the otoliths. For this purpose, otoliths were immersed in distilled water and observed under a stereoscopic microscope (16X and 40X), using reflected light on a dark background, which allowed observing the opaque increments in whitish color and the hyaline increments in dark color (Williams and Bedford 1974; Holden and Raitt 1974; Nevárez-Martínez et al. 1996; Yaremko 1996). The reading of growth increments in the otoliths was made by two independent readers that counted them at two different times; the results were compared and when discrepancies were reported, they were verified through a third reading. At the time of the readings, the readers did not have the information either of the size or sex. By means of a graphical analysis of the relative monthly frequency of otoliths with opaque and hyaline edges (Méndez-Da-Silveira 1987; Jiménez-Rodríguez 1991; Nevárez-Martínez et al. 1996), the periodicity of the formation of an opaque and a hyaline increment was defined. No assumption of birthdate was made. As such, the most distal of the opaque or translucent edges were counted as growth increments. Since the growth increment counts were not adjusted for the birthdate, the counted growth increments were equal to the age of the fish. For example, if the otoliths of a specific sardine were counted as three growth increments, one opaque, one hyaline, and the edge was undoubtedly opaque, this sardine was assigned an age of 1.5 years.

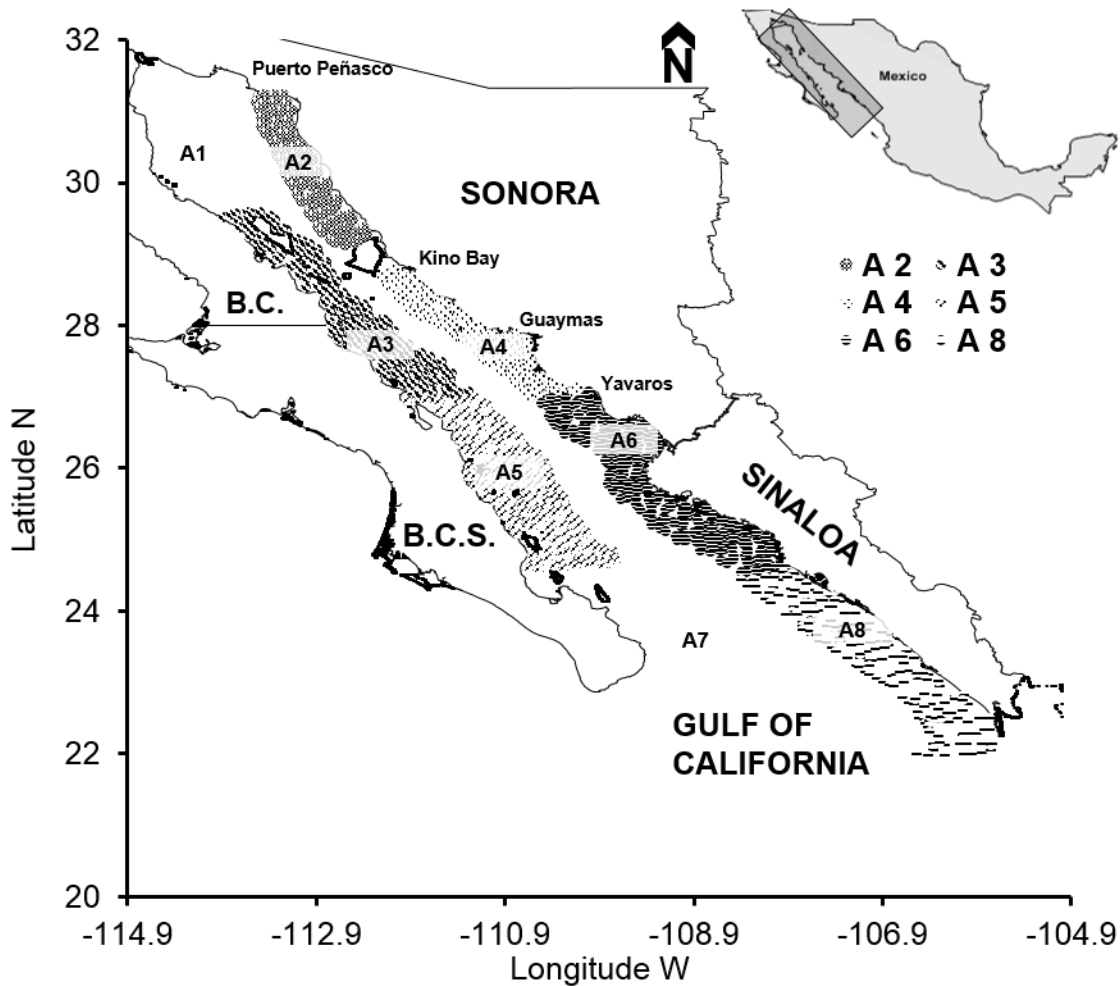


Figure 1. Total study area and regular fishing grounds or capture areas (A2 = Area 2; A3 = Area 3; A4 = Area 4; A5 = Area 5; A6 = Area 6 and A8 = Area 8) of the Pacific sardine *Sardinops caeruleus* in the Gulf of California during the seasons 2010-11 to 2012-13. Capture areas are among the states of Baja California (B.C.), Baja California Sur (B.C.S.), Sonora and Sinaloa, México.

Based on the assigned age and the standard length measured for each of the Pacific sardines sampled, a length-age key was constructed for growth modeling. Moreover, variability in length to age was estimated using that age-length key.

Growth modeling

Age in years and standard length data of the Pacific sardine were used for modeling individual growth by means of a multimodel inference approach (Katsanevakis 2006; Katsanevakis and Maravelias 2008). For this purpose, four growth models were used (table 1); von Bertalanffy (1938), Gompertz (1825), Logistic (Ricker 1975), and Schnute (1981). The Schnute model was used assuming that the parameters $a \neq 0$ and $b \neq 0$, as the required condition to denote asymptotic growth (Schnute 1981).

For parameter estimation, it was assumed that the residuals had a log-normal distribution around the

growth models. Growth parameters (θ) for all four candidate growth models were fitted using a maximum log likelihood approach, according to the next objective function (Neter et al. 1996; Haddon 2001):

$$LL_{(\theta | data)} = -\left(\frac{n}{2}\right) [\ln(2\pi) + 2 * \ln(\sigma) + 1], \quad (1)$$

Where $LL_{(\theta | data)}$ is the maximum log likelihood value; n is the number of observations; and σ is the standard deviation (SD), which was obtained by the following analytical equation (Haddon 2001):

$$\sigma = \sqrt{\frac{1}{n} \sum_{i=1}^n [\ln(SL_{obs(t)}) - \ln(SL_{est(t)})]^2}, \quad (2)$$

where $SL_{obs(t)}$ is the standard length observed (in mm) at age t (in years), and $SL_{est(t)}$ is the estimated standard length at age t . It was assumed that $L_{(t)}$ had a log-nor-

TABLE 1
 Candidate growth models for the Pacific sardine *Sardinops caeruleus* age-length data in the Gulf of California.

Model	Equation	Description
von Bertalanffy growth model (VBGM)	$L_{(t)} = L_{\infty} (1 - e^{-K(t-t_0)})$	$L_{(t)}$ is length at age t . L_{∞} is asymptotic length. K determines the rate of approach to L_{∞} (the curvature parameter).
Gompertz	$L_{(t)} = L_{\infty} e^{-e^{-K(t-t_0)}}$	t_0 in VBGM and Schnute models is the hypothetical age at which the sardines showed zero length (initial condition parameter). t_0 in Gompertz and Logistic models corresponds to an inflection point on the growth curve. t is age at size $L_{(t)}$.
Logistic	$L_{(t)} = \frac{L_{\infty}}{(1 + e^{-K(t-t_0)})}$	a is a relative growth rate (time constant). b is an incremental relative growth rate (incremental time constant).
Schnute (Solution case 1; $a \neq 0, b \neq 0$)	$L_{(t)} = \left[y_1^b + (y_2^b - y_1^b) \frac{1 - e^{-a(t-T_1)}}{1 - e^{-a(T_2-T_1)}} \right]^{\frac{1}{b}}$	T_1 is the lowest age in the data set.
To estimate τ_0 (t_0):	$\tau_0 = T_1 + T_2 - \frac{1}{a} \text{Ln} \left[\frac{e^{aT_2} y_2^b - e^{aT_1} y_1^b}{y_2^b - y_1^b} \right]$	T_2 is the highest age in the data set.
To estimate L_{∞} :	$L_{\infty} = \left[\frac{e^{aT_2} y_2^b - e^{aT_1} y_1^b}{e^{aT_2} - e^{aT_1}} \right]^{\frac{1}{b}}$	y_1 is the size at age T_1 . y_2 is the size at age T_2 .

mal distribution around the candidate growth models. The objective function was solved using Solver in Excel®.

Confidence intervals

The Pacific sardine growth parameters and their fitting values (LL) obtained by each growth model were used to calculate confidence intervals (CI) by means of profile likelihood construction, which is a robust way for construction of confidence regions (Venzon and Moolgavkar 1988; Hilborn and Mangel 1997). A likelihood interval by itself is not very informative and thus insufficient to indicate change in plausibility of the values of θ within the range. A likelihood interval must always be accompanied by the value of θ to give some idea of the symmetry of the likelihood function with respect to probable alternative values of θ , and in this sense show how plausibility changes within the interval. This estimation was made for all growth parameters and based on Chi-squared distribution (χ^2) with m degrees of freedom (Zar 1999) where confidence intervals were defined as all values θ that satisfied inequality:

$$2[LL_{(\theta|data)} - LL_{(\theta|best)}] < \chi^2_{1,1-\alpha}, \tag{3}$$

where $LL_{(\theta|best)}$ is the log likelihood of the most probable value of θ and $\chi^2_{1,1-\alpha}$ are the distribution values of χ^2 with one-degree freedom at a confidence level of $1 - \alpha$; thus, the confidence interval at 95% covered all values of

θ that were twice the difference between the log likelihood in the likelihood profile and the best estimate of θ . Those values less than 3.84 were included into confidence intervals (Haddon 2001; Pawitan 2001).

When considering more than one growth parameter, confidence intervals became wider, which only occurred if any correlation existed between parameters in growth models. The von Bertalanffy growth model had the asymptotic length and growth coefficient parameters correlated; therefore, in this case the solution was to compute the likelihood based confidence region estimated from contours of constant log-likelihood over the target surface. This procedure was applied to the L_{∞} and K parameters jointly to cope the problem of parameter correlation in describing individual growth of the Pacific sardine. In this case the equation above must satisfy the inequality associated with the χ^2 distribution with two degrees of freedom where the reference value was less than 5.99 for two parameters (Haddon 2001; Pawitan 2001).

Growth model selection

The Akaike information criterion (AIC) (Burnham and Anderson 2002; Katsanevakis 2006; Katsanevakis and Maravelias 2008) was used to select the best growth model for the Pacific sardine age and length data, according to the following equation:

$$AIC = (-2 * LL_{(\theta|data)}) + (2 * k), \tag{4}$$

TABLE 2
 Age-length key for the Pacific sardine *Sardinops caeruleus* obtained from commercial purse seine fishery
 in the Gulf of California during the seasons 2010–11 to 2012–13.

SL (mm) /	Age (years)												Total
	0.5	1	1.5	2	2.5	3	3.5	4	4.5	5	5.5	6	
98	19	0	0	0	0	0	0	0	0	0	0	0	19
103	19	0	0	0	0	0	0	0	0	0	0	0	19
108	4	0	0	0	0	0	0	0	0	0	0	0	4
113	0	1	0	0	0	0	0	0	0	0	0	0	1
118	0	5	0	0	0	0	0	0	0	0	0	0	5
123	0	8	0	0	0	0	0	0	0	0	0	0	8
128	0	11	2	0	0	0	0	0	0	0	0	0	13
133	0	24	4	0	0	0	0	0	0	0	0	0	28
138	0	41	7	3	0	0	0	0	0	0	0	0	51
143	0	34	15	14	0	0	0	0	0	0	0	0	63
148	0	28	23	22	0	0	0	0	0	0	0	0	73
153	0	12	16	46	4	0	0	0	0	0	0	0	78
158	0	0	16	51	8	2	0	0	0	0	0	0	77
163	0	0	5	52	24	3	0	0	0	0	0	0	84
168	0	0	0	39	34	11	1	0	0	0	0	0	85
173	0	0	0	20	45	21	5	0	0	0	0	0	91
178	0	0	0	9	35	32	14	5	0	0	0	0	95
183	0	0	0	1	18	37	30	13	4	0	0	0	103
188	0	0	0	0	6	26	21	29	11	3	0	0	96
193	0	0	0	0	0	4	14	22	20	13	7	3	83
198	0	0	0	0	0	0	4	8	18	21	15	10	76
203	0	0	0	0	0	0	0	1	4	6	12	15	38
208	0	0	0	0	0	0	0	0	1	1	1	2	5
	42	164	88	257	174	136	89	78	58	44	35	30	1195

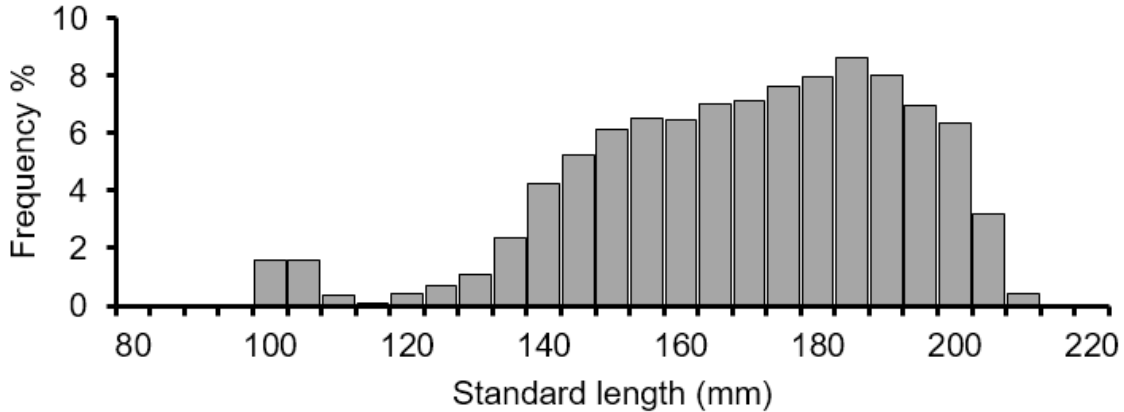


Figure 2. Standard length (mm) frequency distribution of the Pacific sardine in the Gulf of California during the study period (2010-11 to 2012-13).

where k is the number of parameters in each model, including σ (Burnham and Anderson 2002). The AIC differences (Δ_i) for each model were given by the following function:

$$\Delta_i = AIC_i - AIC_{min}, \tag{5}$$

where AIC_{min} represents the AIC for the best candidate growth model, and AIC_i is the AIC estimated for each growth model. Plausibility was estimated for candidate growth models (i) by means of the Akaike weight (w_i) given by (Burnham and Anderson 2002):

$$w_i = \frac{e^{(-0.5 * \Delta_i)}}{\sum_{i=1}^4 e^{(-0.5 * \Delta_i)}} \tag{6}$$

In accordance to the multimodel inference approach, an averaged was calculated for asymptotic length (\bar{L}_∞) taking into account predicted values for this parameter ($\hat{L}_{\infty,i}$) and w_i of all four models by the following equation (Burnham and Anderson 2002):

$$\bar{L}_\infty = \sum_{i=1}^4 w_i \hat{L}_{\infty,i} \tag{7}$$

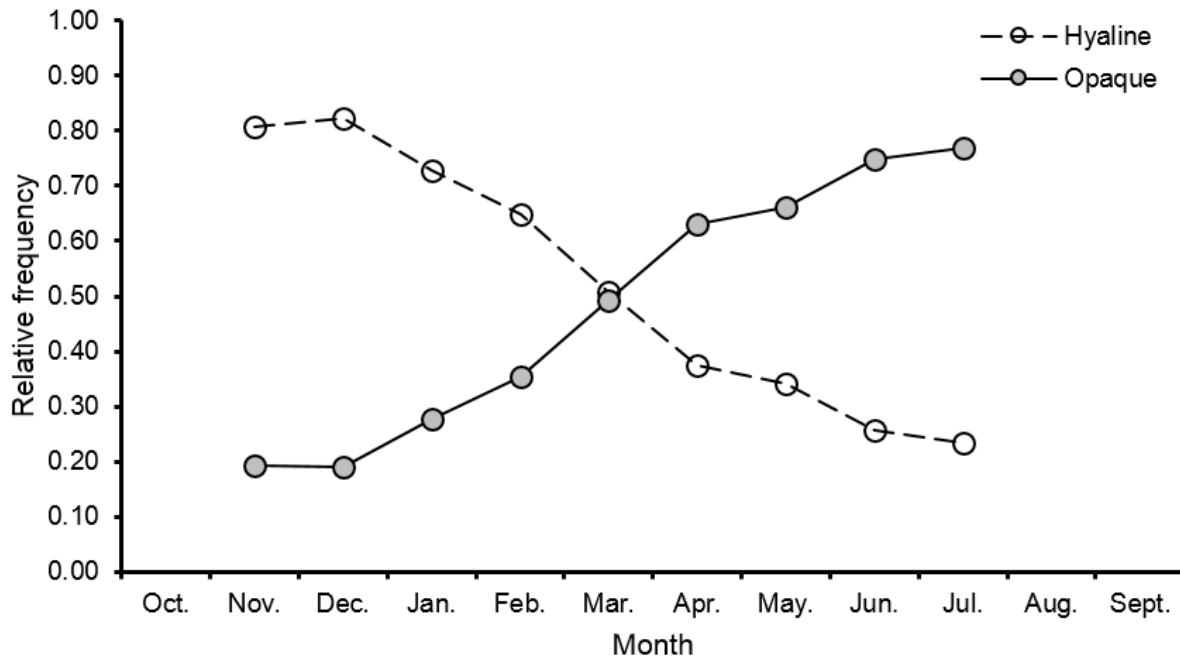


Figure 3. Monthly relative frequencies of otoliths with opaque edge (gray circle) and hyaline (white circle or empty circle) in the Pacific sardine of the Gulf of California. Period 2010–11 to 2012–13.

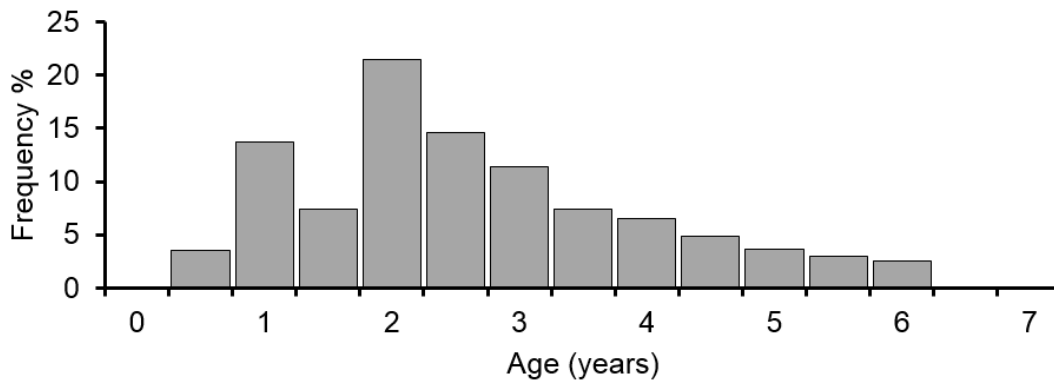


Figure 4. Age (years) frequency distribution of the Pacific sardine in the Gulf of California during the study period (2010–11 to 2012–13).

For all models, 95% confidence intervals for \hat{L}_∞ were estimated by means of t Student test with df degrees of freedom, using the following equation:

$$\hat{L}_\infty \pm t_{df,0.975}se(\hat{L}_\infty), \quad (8)$$

Here, $se(\hat{L}_\infty)$ is the asymptotic standard error.

The unconditional standard error of \bar{L}_∞ [$use(\bar{L}_\infty)$] was estimated as (Burnham and Anderson 2002):

$$use(\bar{L}_\infty) = \sum_{i=1}^4 w_i * [var(\hat{L}_{\infty,i} | g_i) + (\hat{L}_{\infty,i} - \bar{L}_\infty)^2]^{1/2}, \quad (9)$$

where $var(\hat{L}_{\infty,i} | g_i)$ is the variance of the estimated asymptotic length according to model g_i , conditional on the model.

RESULTS

A total of 1,195 Pacific sardine (*Sardinops caeruleus*) were measured and aged from the 2010–11 to the 2012–13 fishing seasons in the Gulf of California (table 2). SL frequency distribution (fig. 2) for the three seasons combined (2010–11, 2011–12 and 2012–13) showed a length range from 98 to 208 mm of SL, with average of 167.0 mm SL; and standard deviation was 23.56 mm.

The monthly relative frequency of otoliths with opaque and hyaline edges is shown in Figure 3. The percentage of opaque edges was low during autumn–winter and maximum in spring–summer while the translucent edges showed their maximum during autumn and winter and their lower values in spring–summer. This result indicates that in the course of one year an annuli (an

TABLE 3
Mean standard length (mm) and standard deviation
by age of the Pacific sardine *Sardinops caeruleus*
obtained during the study period (2010–11 to 2012–13)
in the Gulf of California. The value *n* indicates the
number of individuals observed for each age.

<i>n</i>	Age (years)	Mean standard length (mm)	Standard deviation
42	0.5	101.2	3.2
164	1.0	138.9	8.7
88	1.5	148.8	8.1
257	2.0	159.7	9.0
174	2.5	172.1	7.8
136	3.0	179.5	7.3
89	3.5	184.9	6.3
78	4.0	189.2	5.4
58	4.5	193.9	5.4
44	5.0	196.8	4.3
35	5.5	199.0	3.9
30	6.0	200.7	3.8

opaque edge plus a hyaline edge) is formed; in average growth increments (opaque or hyaline) occur in approximately half a year.

Ages of the Pacific sardine were integrated by fish from 0.5 years (one opaque edge) to 6.0 years (six opaque edges plus six translucent edges) of age (table 2); fish of age 0.5 years were in the range of 98–108 mm SL and those of age 6.0 years in the range of 193–208 mm SL. Age frequency distributions are shown in Figure 4; the highest frequency was observed at the age of two years. The average age was 2.64 years and standard deviation was 1.34 years. Table 3 shows the average standard length and standard deviation by age of the Pacific sardine.

The estimated growth parameter values, 95% confidence intervals and Chi-square probability for the

four candidate growth models are shown in Table 4. The highest asymptotic length ($L_{\infty} = 201.287$ mm SL) was estimated with VBGM, followed by Schnute model ($L_{\infty} = 199.480$ mm SL). A variation in K , the rate of approach to L_{∞} , among the candidate growth models was observed with minimum $K = 0.581$ (VBGM and Schnute model) and maximum $K = 0.822$ (Logistic model). The four growth models tested revealed a phase of rapid growth during the first two years of age (reached ~80% L_{∞} value), with the growth rate decreasing and reaching 95% L_{∞} value at age of four years (fig. 5).

The Akaike differences (Δ_i) showed that only the VBGM and Schnute models had a substantial support ($\Delta_i \leq 2$; table 5). According to the model selection criteria, the estimated AIC was the lowest for the VBGM ($AIC = -3610.87$) with Akaike weight, $w_i = 73.11\%$, followed by Schnute model with $AIC = -3608.87$ and $w_i = 26.89\%$ (table 5). According to the multi-model inference approach, it was calculated a $\bar{L}_{\infty} = 200.8$ mm (95% CI was 199.0–202.6 mm) (table 5).

The 95% confidence intervals for the best fitted model (VBGM), as well as likelihood profiles for L_{∞} , K and t_0 , are shown in Figure 6. The likelihood profiles for parameters of the Schnute growth model (the second best) are shown in Figure 7. The covariance of parameters L_{∞} and K of the VBGM and the highest likelihood values are shown by likelihood contours in Figure 8.

DISCUSSION

The periodicity validation of growth increment formation is a critical step for the use of hard parts for age and growth studies in aquatic animals (Beamish and McFarlane 1983). The analysis of the otolith edges used in this study indicated that the time a sardine requires

TABLE 4
Growth parameter values, 95% confidence intervals (95% CI) and Chi-squared probability (χ^2) for the
Pacific sardine in the Gulf of California. L_{∞} is asymptotic standard length; K is the growth coefficient, t_0 is the
hypothetical age at which the sardines showed zero length; a is relative growth rate; b is incremental relative
growth rate; Y_1 is the size at age T_1 and Y_2 is the size at age T_2 . Period 2010–11 to 2012–13.

Model	Parameter	Value	Lower 95% CI	Upper 95% CI	χ^2
VBGM	L_{∞} (mm)	201.287	200.700	201.800	0.032
	K_{annual}	0.581	0.577	0.586	0.090
	t_0 (years ⁻¹)	-0.839	-0.855	-0.824	0.016
Gompertz	L_{∞} (mm)	199.213	198.600	199.800	0.032
	K_{annual}	0.702	0.694	0.710	0.095
	t_0 (years ⁻¹)	-0.261	-0.277	-0.244	0.107
Logistic	L_{∞} (mm)	197.798	197.200	198.400	0.004
	K_{annual}	0.822	0.811	0.833	0.059
	t_0 (years ⁻¹)	0.161	0.142	0.178	0.050
Schnute	a	0.581	0.568	0.595	0.136
	b	1.002	1.001	1.003	0.292
	Y_1 (mm)	107.910	105.768	108.840	0.160
	Y_2 (mm)	195.737	195.050	196.400	0.128

For Schnute; $L_{\infty} = 199.480$ and $t_0 = -0.837$

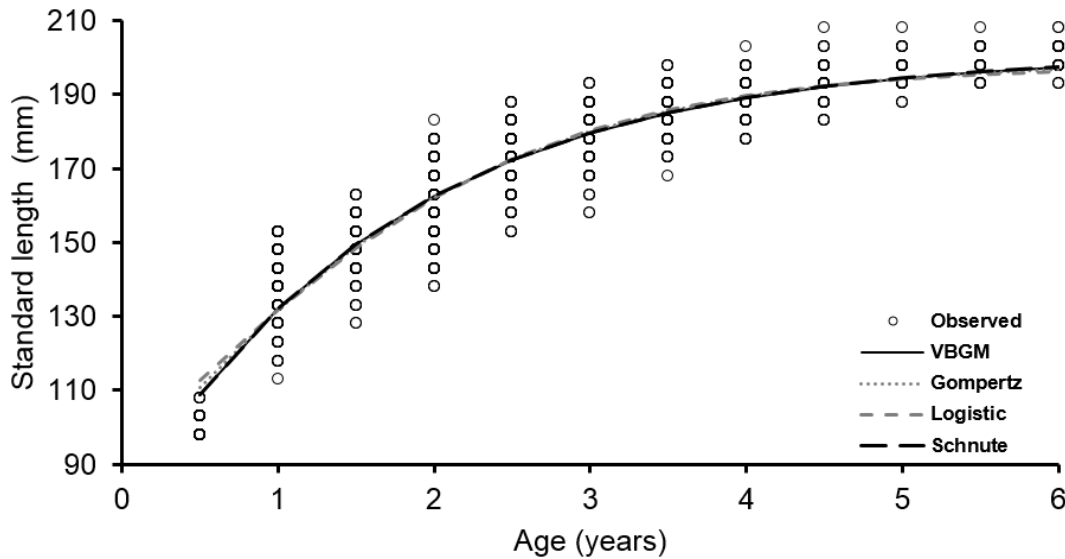


Figure 5. Growth models fitted to age-at-length data of Pacific sardine from Gulf of California (n=1,195). Period 2010–11 to 2012–13.

TABLE 5
Growth model selection for the Pacific sardine in the Gulf of California, where k is the number of parameters; LL is the maximum likelihood; AIC is the Akaike's information criterion; Δ_i is Akaike's differences, w_i is Akaike's weight for each model; and S.E. is the standard error.

Models	k	LL	AIC	Δ_i	$w_i\%$	L_∞ (mm)	S.E.
VBGM	4	1808.43	-3610.87	0.00	73.11	201.29	0.05
Gompertz	4	1781.74	-3557.49	53.38	0.00	199.21	0.05
Logistic	4	1758.31	-3510.63	100.24	0.00	197.80	0.06
Schnute	5	1808.43	-3608.87	2.00	26.89	199.48	0.05
Averaged multi-model						200.80	0.71

to form an opaque or a hyaline zone, on average, is approximately half a year, and showed that over a year, one opaque band plus one hyaline band were formed. Our results coincide with what was found in previous studies on the age of the Pacific sardine (Barnes and Foreman 1994; Nevárez-Martínez et al. 1996; Quiñonez-Velázquez et al. 2002).

The results of this study have demonstrated that the Pacific sardine of the GC was found in a relatively wide range of sizes (98–208 mm of SL) that corresponded to specimens from 0.5–6.0 years of age. Ages that contributed mainly to the catch were 1.0 to 3.0 years, which jointly meant almost 69% of the analyzed individuals.

The results showed that, except at a younger age, a greater variability of length at age was observed and as age increased, variability with respect to length decreased. The standard deviation was 8.19–9.03 mm in ages 1.0 to 2.0, decreasing gradually until the oldest sardine reached 3.88 mm (age 6.0). According to Parma and Deriso (1990) and Vincenzi et al. (2016), growth variability in populations results both from environmental disturbances and intrinsic differences in the maximum lengths observed in the analyzed specimens. In this case,

as the greatest variability occurred in young adults, it was probable that the environmental effects operated strongly in defining growth velocity in these age groups while older adults reached almost the same asymptotic size.

Among the growth models tested in the Pacific sardine, VBGM was the one that showed the highest asymptotic SL value ($L_\infty = 201.287$ mm) while the Logistic model was the one that obtained the lowest one ($L_\infty = 197.79$ mm). The value of K obtained both by VBGM and by Schnute (a) model were the lowest (0.581) within the candidate models while Gompertz (0.72) and Logistic (0.82) were higher. These differences in values estimated by each of the models confronted could be explained by their ability to represent growth of the Pacific sardine reliably, given the observed data. According to the AIC and w_i values obtained by the VBGM and Schnute models, they could represent better the growth kinetics of the Pacific sardine, especially the VBGM that showed a value $w_i = 73.11\%$; however, the Gompertz and Logistic models have a null Akaike weight ($w_i = 0.00\%$), that is, given the data used, apparently they have none supported to explain the growth of this species in the Gulf of California. If w_i represents the probability

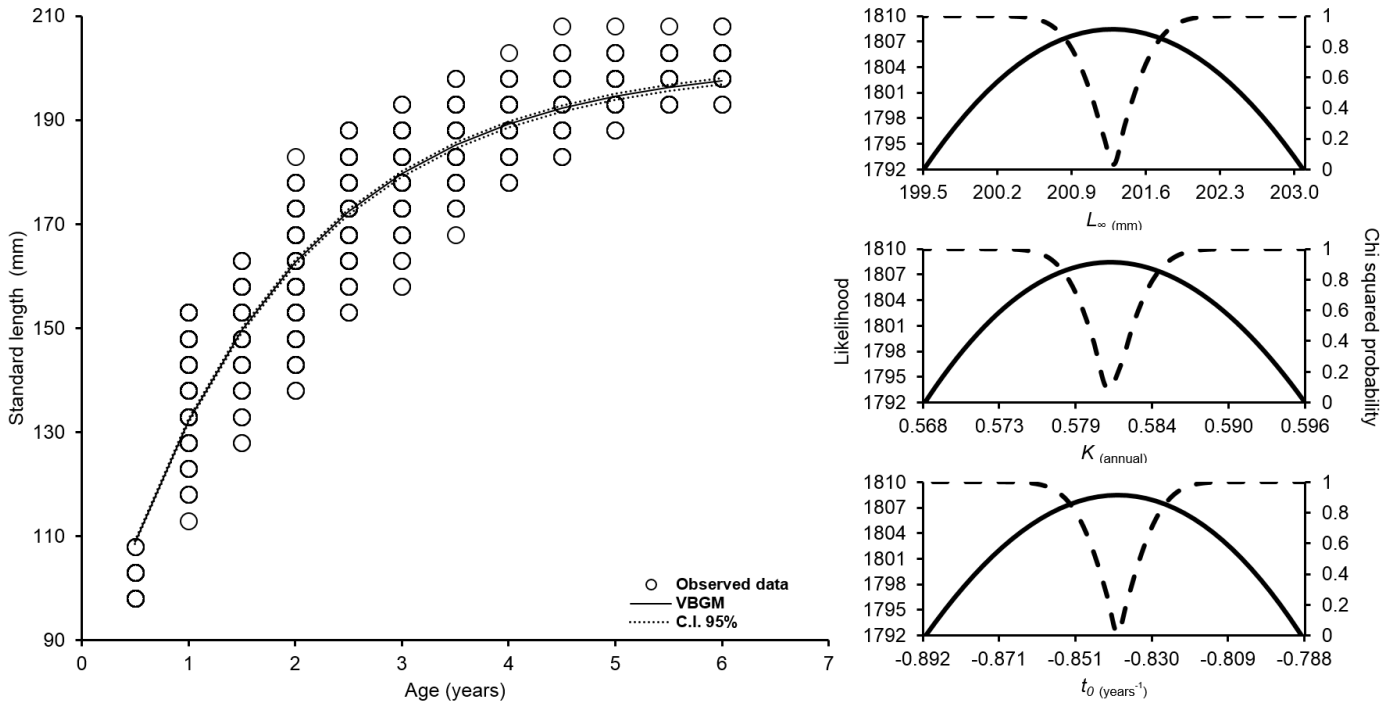


Figure 6. Average growth curve and likelihood profiles for parameters L_{∞} , K and t_0 estimated by the von Bertalanffy growth model for the Pacific sardine in the Gulf of California, during the seasons 2010–11 to 2012–13.

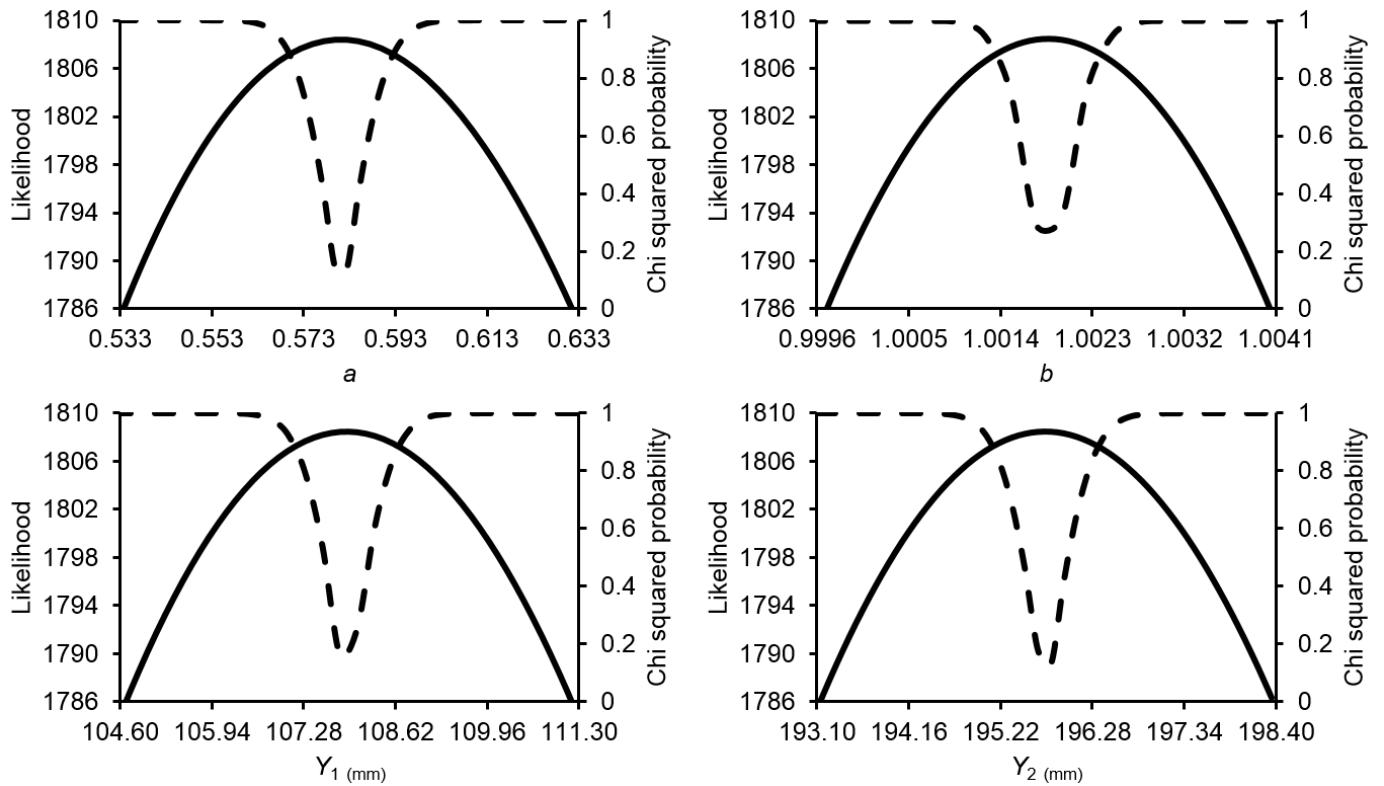


Figure 7. Likelihood profiles of parameters estimated with Schnute growth model, the second best candidate growth model for the Pacific sardine in the Gulf of California.

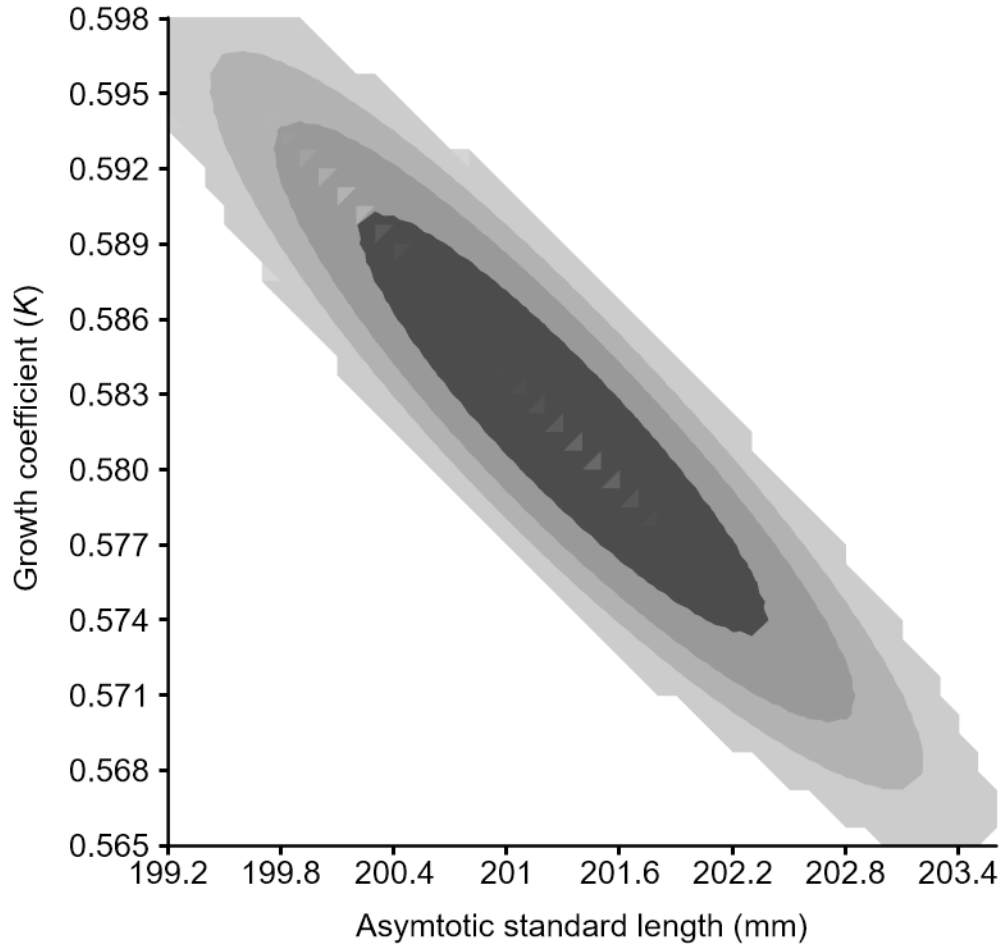


Figure 8. Likelihood contour for parameters L_{∞} and K estimated by von Bertalanffy growth model for the Pacific sardine *Sardinops caeruleus* in the Gulf of California. The area in dark gray denotes joint confidence intervals (χ^2 test, $p < 0.05$).

of choosing the correct model from the set of candidate models, given the data used (Burnham and Anderson 2002; Burnham and Anderson 2004; Burnham et al. 2011), and if we take in account that the model with the highest probability was the VBGM, we could accordingly consider it the best model. Growth parameters L_{∞} and K in the von Bertalanffy model showed the covariance characteristic; therefore, obtaining a likelihood contour for these parameters obtained in the Pacific sardine was a good way to show those regions in which the most probable parameter values are jointly found. In this study, growth parameters showed a strongly inverse correlation, so that, when one of the parameters increased its value, the other one decreased it and vice versa (fig. 8).

In previous growth studies for this species in the GC, based on age readings in otoliths and using the VBGM, Jiménez-Rodríguez (1991) and Nevárez-Martínez et al. (1996) estimated growth parameters in *S. caeruleus*, whose values compared with those obtained in our study were higher for L_{∞} (202.90 – 224.17 mm

SL) but lower for K (0.457 – 0.55). These differences in growth can reflect interannual variations in Pacific sardine growth, which could be due to density-dependent or climate factors (Checkley Jr. et al. 2017; Dorval et al. 2015; Piner et al. 2018). Quinn and Deriso (1999) support that the species uses the energy obtained by food to grow, reproduce and emigrate; thus the reason why these processes could be affected or modified in the species according to food availability, environmental conditions and density-dependent pressure, generating variation in growth.

On the other hand, Quiñonez-Velázquez et al. (2002) estimated that $L_{\infty} = 221.00$ mm SL and $K = 0.41$ when they analyzed information for the Pacific sardine in Isla de Cedros, Baja California, whereas Dorval et al. (2015) estimated the values of $L_{\infty} = 300.75$ mm SL and $K = 0.172$ in their analysis for the sardine of the coasts of California; that is, in both cases those authors found much larger values for L_{∞} and much smaller for K , based on the adjustment of

the VBGM model. In addition, Dorval et al. (2015) also made estimations with other models, but even when those models gave different results compared to the standard model of VBGM, their estimates, compared with ours, were still much higher for L_{∞} and much lower for K . This could imply that a cline exists in species growth from north to south with a more accelerated growth rate in the GC stock compared to those of Baja California or California stocks; the sardine in the coasts of California reaches around 67% at two years of age, in Isla de Cedros about 75% and in the GC about 81%.

Moreover, sardine growth studies have been performed based on the analysis of length structures in commercial catches, in which the VBGM model has been directly adjusted (Cisneros-Mata et al. 1990; De Anda-Montañez et al. 1999; Martínez-Zavala et al. 2006). In these studies, the values estimated were very different from those obtained by the VBGM and Schnute models, that is, they estimated higher values for L_{∞} and smaller values for K . Although apparently the results of this type of analysis cannot be compared directly with those obtained in this study (different methods), we want to note that if the methods based on lengths are used to analyze growth in commercial species, such as the Pacific sardine where only commercial sizes are available, and adjusted directly to the VBGM, the growth of juveniles will be poorly represented (Gamito 1998; Charnov 2008; Mercier et al. 2011). Therefore, these methods would tend to overestimate L_{∞} while underestimating K , and thus they are not suitable for use in assessment and management of fishery resources (Katsanevakis 2006).

According to the results of the inference multimodel, and strictly speaking, no clear “winning model” could be declared (that is, one with $w_i \geq 90\%$ values) within the candidates (Akaike 1998; Burnham and Anderson 2002), but two models, VBGM ($w_i = 73.11\%$) and Schnute ($w_i = 26.89\%$), were the ones that represented reliable age-length data of the Pacific sardine in the GC. In these cases, it was necessary to calculate an averaged model that weighted the asymptotic growth value of the species and performed inference on parameter L_{∞} (Burnham and Anderson 2002). The calculus of the averaged model was supported by the weighted values and weights of all the models (4) tested, following Katsanevakis and Maravelias (2008). Thus, the averaged model value had a number close to the calculus provided by a greater w_i in the analysis. If the biological point reference has been given by parameter L_{∞} , it is recommended to infer over the calculated value with the averaged model since it decreases uncertainty in the best model within those tested for a determined set of data (Burnham and Anderson 2002; Katsanevakis and Maravelias 2008). Nonetheless, if model parameters are required jointly, as well as the growth

curve form and projection, it is better to infer in von Bertalanffy, which was the one that showed the highest Akaike weight ($w_i = 73.11\%$). Recently, Mendivil-Mendoza et al. (2017) showed it was possible to obtain a true averaged model utilizing special solution cases of the Schnute (1981) model since it is versatile, capable of describing any type of growth curve according to the age-length data at hand and with interpretation bases of equivalent parameters to those obtained with VBGM. This methodology should be explored in future growth studies on the Pacific sardine.

ACKNOWLEDGMENTS

The authors thank INAPESCA-CRIP (National Fishing and Aquaculture Institute-Regional Centers for Fisheries Research) Guaymas, for materials and financial support to this research, as well as to CONACYT (Consejo Nacional de Ciencia y Tecnología) México for the financial support received throughout the project CB-2015-256477; Gustavo Padilla Arredondo for geographical work and Diana D. Fischer for editorial services in English.

LITERATURE CITED

- Akaike, H. 1998. Information theory and an extension of the maximum likelihood principle. In: Selected papers of Hirotugu Akaike (pp. 199–213). Springer, New York, NY.
- Ali, M., A. Nicieza, and R. J. Wootton. 2003. Compensatory growth in fishes: a response to growth depression. *Fish and Fisheries*, 4: 147–190.
- Barnes, J. T., and T. J. Foreman. 1994. Recent evidence for the formation of annual growth increments in the otoliths of young Pacific sardines (*Sardinops sagax*). *California Fish and Game*, 80(1), 29–35.
- Beamish, R., and G. A. McFarlane. 1983. The forgotten requirement for age validation in fisheries biology. *Transactions of the American Fisheries Society*, 112(6), 735–743.
- Beddington, J. R., and G. P. Kirkwood. 2005. The estimation of potential yield and stock status using life-history parameters. *Philosophical Transactions of the Royal Society B: Biological Sciences*, 360: 163–170.
- Beninger, P. G., I. Boldina, and S. Katsanevakis. 2012. Strengthening statistical usage in marine ecology. *Journal of Experimental Marine Biology and Ecology*, 426–427: 97–108.
- Bertalanffy von, L. 1938. A quantitative theory of organic growth. *Human Biology*, 10(2): 181–213.
- Botsford, L. W. 1981. The effects of increased individual growth rates on depressed population size. *American Naturalist*, 117, 38–63.
- Burnham, K. P., and D. R. Anderson. 2002. Model selection and multimodel inference: a practical information-theoretic approach. Springer, New York, 488 p.
- Burnham, K. P., and D. R. Anderson. 2004. Multimodel inference: understanding AIC and BIC in model selection. *Sociological methods & research*, 33(2), 261–304.
- Burnham, K. P., D. R. Anderson, and K. P. Huyvaert. 2011. AIC model selection and multimodel inference in behavioral ecology: some background, observations, and comparisons. *Behavioral Ecology and Sociobiology*, 65(1): 23–35.
- Cailliet, G. M., W. D. Smith, H. F. Mollet, and K. J. Goldman. 2006. Age and growth studies of chondrichthyan fishes: the need for consistency in the terminology, verification, validation, and growth function fitting. *Environmental Biology of Fishes*, 77: 211–228.
- Charnov, E. L. 2008. Fish growth: Bertalanffy k is proportional to reproductive effort. *Environmental Biology of Fishes*, 83(2), 185–187.
- Checkley, JR., D. M., R. G. Asch, and R. R. Rykaczewski. 2017. Climate, anchovy, and sardine. *Annual Review of Marine Science*, 9: 469–493.

- Cisneros-Mata, M. A., J. Estrada, and G. Montemayor. 1990. Growth, mortality and recruitment of exploited small pelagic fishes in the Gulf of California. *Fishbyte*, 8: 15–17.
- Clark, F. N. 1947. Analysis of populations of the Pacific sardine on the basis of vertebral counts. *Calif. Dep. Fish Game Fish Bull.* 65, 5–26.
- Clark, F. N., and J. F. Janssen. 1945. Movements and abundance of the sardine as measured by tag returns. *Calif. Dep. Fish Game Fish Bull.* 61, 7–42.
- D.O.F. 2018. Carta Nacional Pesquera. SAGARPA, CONAPECSA Diario Oficial de la Federación. Consultado el 11/06/2018.
- De Anda-Montañez, A., F. Arreguín-Sánchez, and S. Martínez-Aguilar. 1999. Length-based growth estimates for Pacific sardine (*Sardinops sagax*) in the Gulf of California, Mexico. *Calif. Coop. Oceanic Fish. Invest. Rep.* 40: 179–183.
- Demer, D. A., and J. P. Zwolinski. 2014. Optimizing fishing quotas to meet target fishing fractions of an internationally exploited stock of Pacific Sardine. *North American journal of fisheries management.* 34(6), 1119–1130.
- Dorval, E., J. D. McDaniel, B. J. Macewicz, and D. L. Porzio. 2015. Changes in growth and maturation parameters of Pacific sardine *Sardinops sagax* collected off California during a period of stock recovery from 1994 to 2010. *Journal of Fish biology.* 87(2): 286–310.
- Estrada-García, J. J., M. Cisneros-Mata, F. Páez-Barrera, and P. Santos-Molina. 1986. Informe de la temporada de pesca 1984/1985 del recurso sardina. Secretaría de Pesca. Instituto Nacional de la Pesca. Centro Regional de Investigación Pesquera-Guaymas, Son. México. 160p.
- Felin, F. E. 1954. Population heterogeneity in the Pacific pilchard. US Government Printing Office.
- Félix-Uraga, R. 1986. Edad, crecimiento y estructura poblacional de *Sardinops sagax caerulea* en Bahía Magdalena, durante 1981 a 1984 (Doctoral dissertation, Instituto Politécnico Nacional. Centro Interdisciplinario de Ciencias Marinas).
- Félix-Uraga, R., V. M. Gómez-Muñoz, C. Quiñonez-Velázquez, F. N. Melo-Barrera, K. T. Hill, and W. García-Franco. 2005. Pacific sardine (*Sardinops sagax*) stock discrimination off the west coast of Baja California and southern California using otolith morphometry. *Calif. Coop. Oceanic Fish. Invest. Rep.* 46: 113–121.
- Félix-Uraga, R., V. M. Gómez-Muñoz, C. Quiñonez-Velázquez, F. N. Melo-Barrera, and W. García-Franco. 2004. On the existence of Pacific sardine groups off the west coast of the Baja California Peninsula and southern California. *Calif. Coop. Oceanic Fish. Invest. Rep.* 45: 146–151.
- Froese, R., and D. Pauly. 2018. FishBase. World Wide Web electronic publication. www.fishbase.org, version (06/2018).
- Gallardo-Cabello, M., A. Laguarda-Figueroa, and V. Pérez-Arroyo. 1991. Determinación de los parámetros poblacionales: edad, crecimiento y mortalidad natural de la sardina Monterrey *Sardinops sagax caerulea* (Jenyns, 1842) de las poblaciones localizadas en el sur de Golfo de California (Pisces: Clupeidae). *Ciencia Pesquera* (8): 107–117.
- Gamito, S. 1998. Growth models and their use in ecological modelling: an application to a fish population. *Ecological modelling.* 113(1–3), 83–94.
- García-Rodríguez, F. J., S. A. García-Gasca, J. De La Cruz-Aguero, and V. M. Cota-Gómez. 2011. A study of the population structure of the Pacific sardine *Sardinops sagax* (Jenyns 1842) in Mexico based on morphometric and genetic analyses. *Fisheries Research*, 107(1–3), 169–176.
- Gompertz, B. 1825. On the nature of the function expressive of the law of human mortality, and on a new mode of determining the value of life contingencies *Philosophical Transactions of the Royal Society of London* 115: 513–583.
- Haddon, M. 2001. Modelling and quantitative methods in fisheries. Boca Raton, FL: Chapman and Hall/CRC. 406p.
- Haddon, M. 2011. Modelling and Quantitative Methods in Fisheries. 2nd Edition. Chapman and Hall/CRC. 465 p.
- Hilborn, R., and M. Mangel. 1997. The ecological detective: confronting models with data (Vol. 28). Princeton University Press.
- Holden, M. F., and D. F. S. Raitt. 1974—Manual of fisheries science. FAO Fish. Tech. Pap., 115, Rev. 1: 214 pp.
- Jiménez-Rodríguez, J. G., 1991. Análisis comparativo del crecimiento y la estructura poblacional de sardina Monterrey *Sardinops caeruleus* (Girard) en el Golfo de California de las temporadas 1988/89 y 1989/90. Tesis de Licenciatura. Escuela de Biología Universidad Autónoma de Guadalajara, Jalisco, México. 60 p.
- Katsanevakis, S. 2006. Modelling fish growth: model selection, multi-model inference and model selection uncertainty. *Fisheries Research.* 81(2–3): 229–235.
- Katsanevakis, S., and C. D. Maravelias. 2008. Modelling fish growth: Multi-model inference as a better alternative to a priori using von Bertalanffy equation. *Fish and Fisheries.* 9(2): 178–187.
- Lanz-Sánchez, E. E., M. O. Nevárez-Martínez, J. López-Martínez, and J. A. Dworak. 2008. Spatial distribution and species composition of small pelagic fish in the Gulf of California. *Distribución espacial y composición de especies de pelágicos menores en el Golfo de California. Biología Tropical.* 56 (2): 575–590.
- Lewison, R. L., L. B. Crowder, A. J. Read, and S. A. Freeman. 2004. Understanding impacts of fisheries bycatch on marine megafauna. *Trends in Ecology and Evolution.* 19(11): 598–604.
- Lorenzen, K. 2016. Toward a new paradigm for growth modeling in fisheries stock assessments: embracing plasticity and its consequences. *Fisheries Research.* 180: 4–22.
- Mais, K. F. 1972. Subpopulation study of Pacific sardine. *California Fish and Game.* 58(4), 296.
- Marr, J. C. 1960. The causes of major variations in the catch of the Pacific sardine (*Sardinops caerulea* (Girard)). *Proc. World Scient. Meet. Biology Sardines and Related Species.* 3:667–791.
- Martínez-Zavala, M. A., M. O. Nevárez-Martínez, M. L. Anguiano-Carrasco, J. P. Santos-Molina, and A. R. Godínez-Cota. 2006. Diagnóstico de la pesquería de pelágicos menores en el Golfo de California, temporadas de pesca 1998/99 a 2002/03. SAGARPA, Instituto Nacional de la Pesca, Centro Regional de Investigación Pesquera (Guaymas, Sonora, México). 94 p.
- Méndez-Da-Silveira, B. 1987. Edad y crecimiento de *Sardinops sagax caerulea* en el Golfo de California. Tesis Profesional. Facultad de Ciencias. Universidad de Guadalajara. México. 91 p.
- Mendivil-Mendoza, J. E., G. Rodríguez-Domínguez, S. G. Castillo-Vargasmachuca, G. G. Ortega-Lizárraga, E. A. Aragón-Noriega. 2017. Estimación de los parámetros de crecimiento de la curvina golfinia *Cynoscion othonopterus* (pisces: Sciaenidae) por medio de los casos del modelo de Schnute. *Interciencia.* 42(9).
- Mercier, L., J. Panfili, C. Paillon, A. N'diaye, D. Mouillot, and A. M. Darnaude. 2011. Otolith reading and multi-model inference for improved estimation of age and growth in the gilthead seabream *Sparus aurata* (L.). *Estuarine, Coastal and Shelf Science.* 92: 534–545.
- Neter, J., M. H. Kutner, C. J. Nachtsheim, and W. Wasserman. 1996. Applied linear statistical models. New York, NY: McGraw-Hill. 1408p.
- Nevárez-Martínez, M. O., D. Lluch-Belda, M. A. Cisneros-Mata, J. P. Santos-Molina, M. Martínez-Zavala, and S. Lluch-Cota. 2001. Distribution and abundance of Pacific sardine (*Sardinops sagax*) in the Gulf of California and their relation with the environment. *Progress in Oceanography.* 49: 565–580.
- Nevárez-Martínez, M. O., M. A. Cisneros-Mata, G. Montemayor-López, and P. Santos-Molina. 1996. Estructura por edad, y crecimiento de la sardina monterrey (*Sardinops sagax caeruleus*) del Golfo de California, México: Temporada de pesca 1990/91. *Ciencia Pesquera*, 13, 30–36.
- Nevárez-Martínez, M. O., M. A. Martínez-Zavala, M. L. Jacob-Cervantes, C. E. Coteró-Altamirano, J. P. Santos-Molina, and A. Valdez-Pelayo. 2014. Peces Pelágicos Menores *Sardinops sagax*, *Opisthonema* spp., *Scomber japonicus*, *Engraulis mordax*, *Cetengraulis mysticetus*, *Etrumeus teres*, *Trachurus symmetricus*, *Oligoplites* spp. En (Eds): Beléndez-Moreno, L. F. J., E. Espino-Barr, G. Galindo-Cortes, M. T. Gaspar-Dillanes, L. Huidobro-Campos, and E. Morales-Bojórquez. *Sustentabilidad y Pesca Responsable en México: Evaluación y Manejo.* Secretaría de Agricultura, Ganadería, Desarrollo Rural, Pesca y Alimentación. Instituto Nacional de la Pesca. México. 453 pp.
- Parma, A. M., and R. B. Deriso. 1990. Dynamics of age and size composition in a population subject to size-selective mortality: effects of phenotypic variability in growth. *Canadian Journal of Fisheries and Aquatic Sciences.* 47(2): 274–289.
- Parrish, R. H., R. Serra, and W. S. Grant. 1989. The monotypic sardines, Sardina and Sardinops: their taxonomy, distribution, stock structure, and zoogeography. *Canadian Journal of Fisheries and Aquatic Sciences.* 46(11), 2019–2036.
- Pawitan, Y. 2001. In All Likelihood: statistical modeling and inference using likelihood. Oxford: Oxford University Press. 528p.
- Phillips, J. B., 1948. Growth of the sardine *Sardinops caerulea* 1941–42 through 1945–47. *Calif. Dept. Fish and Game. Calif. Fish. Bull.* 71:33 p.
- Piner, K., J. McDaniel, H. H. Lee, K. Hill, and B. Macewicz. 2018. Evaluation of the influence of age and length on Pacific Sardine (*Sardinops Sagax*) maturation and characterization of its temporal variability. *California Cooperative Oceanic Fisheries Investigations Reports.* 59: 1–12 p.

- Quinn, J. T., and R. B. Deriso. 1999. Quantitative fish dynamics. Oxford University Press. New York. 452p.
- Quiñonez-Velázquez, C., Alvarado-Castillo, R. and R. Félix-Uraga. 2002. Relación entre el crecimiento individual y la abundancia de la población de la sardina del Pacífico *Sardinops Caenuleus* (Pisces: Clupeidae) (Girard 1856) en Isla de Cedros, Baja California, México. Revista de biología marina y oceanografía. 37(1), 1–8.
- Quiñonez-Velázquez, C., M. O. Nevárez-Martínez, and M. G. Gluyas-Millán. 2000. Growth and hatching dates of juvenile pacific sardine *Sardinops caeruleus* in the Gulf of California. Fisheries Research. 48(2): 99–106.
- Radovich, J. 1982. The collapse of the California sardine fishery. What have we learned. 56–78.
- Ramírez-Granados, R. 1958. Aspectos biológicos y económicos de la pesquería de sardina *Sardinops caerulea* (Girard, 1954) en aguas mexicanas del Pacífico. Veracruz: Sría. de Marina.
- Ricker, W. E. 1975. Computation and interpretation of biological statistics of fish populations. Bulletin of Fisheries Research Board Canada. 191: 382.
- Schnute, J. 1981. A versatile growth model with statistically stable parameters. Canadian Journal of Fisheries and Aquatic Sciences. 38(9): 1128–1140.
- Silliman, R. P., 1943. Studies on the Pacific pilchard or sardine (*Sardinops caenula*). 5: – A method of computing mortalities and replacement. Spec. Sci. Rep. U.S. Wildl. Serv. (24):10 p.
- Smith, P. E. 2005. A history of proposals for subpopulation structure in the Pacific sardine (*Sardinops sagax*) population off western North America. California Cooperative Oceanic Fisheries Investigations Report. 46, 75.
- Venzon, D. J., and S. H. Moolgavkar. 1988. A method for computing profile-likelihood-based confidence intervals. Applied statistics. 87–94.
- Vincenzi, S., A. J. Crivelli, S. Munch, H. J. Skaug, and M. Mangel. 2016. Trade-offs between accuracy and interpretability in von Bertalanffy random-effects models of growth. Ecological applications. 26(5): 1535–1552.
- Vrooman, A. M. 1964. Serologically differentiated subpopulations of the Pacific sardine, *Sardinops caerulea*. Journal of the Fisheries Board of Canada. 21(4), 691–701.
- Williams, T., and B. C. Bedford. 1974. The use of otoliths for age determination. Pp. 114–123. In: T.B. Bagenal (ed.), The Ageing of Fish. Unwin Brothers, Ltd. England.
- Yaremko, M. L. 1996. Age determination in pacific sardine, *Sardinops sagax*. NOAA Technical Memorandum NMFS, 233, pp: 1–39.
- Zar, J. H. 1999. Biostatistical Analysis. Englewood Cliffs, NJ: Prentice-Hall. 633p.

DYNAMIC HABITAT USE OF ALBACORE AND THEIR PRIMARY PREY SPECIES IN THE CALIFORNIA CURRENT SYSTEM

BARBARA MUHLING, STEPHANIE BRODIE,
OWYN SNODGRASS, DESIREE TOMMASI

University of California, Santa Cruz
Institute for Marine Science
Santa Cruz, CA
ph: (858) 546-7197
Barbara.Muhling@noaa.gov

BARBARA MUHLING, OWYN SNODGRASS,
HEIDI DEWAR, DESIREE TOMMASI, JOHN CHILDERS

NOAA Southwest Fisheries Science Center
San Diego, CA

STEPHANIE BRODIE, MICHAEL JACOX
NOAA Southwest Fisheries Science Center
Monterey, CA

MICHAEL JACOX

NOAA Earth System Research Laboratory
Boulder, CO

CHRISTOPHER A. EDWARDS

Ocean Sciences Department
University of California, Santa Cruz, CA

YI XU

Department of Fisheries and Oceans
Delta, British Columbia, Canada

STEPHANIE SNYDER

Thomas More University,
Crestview Hills, KY

ABSTRACT

Juvenile north Pacific albacore (*Thunnus alalunga*) forage in the California Current System (CCS), supporting fisheries between Baja California and British Columbia. Within the CCS, their distribution, abundance, and foraging behaviors are strongly variable interannually. Here, we use catch logbook data and trawl survey records to investigate how juvenile albacore in the CCS use their oceanographic environment, and how their distributions overlap with the habitats of four key forage species. We show that northern anchovy (*Engraulis mordax*) and hake (*Merluccius productus*) habitat is associated with productive coastal waters found more inshore of core juvenile albacore habitat, whereas Pacific sardine (*Sardinops sagax*) and boreal clubhook squid (*Onychoteuthis borealijaponica*) habitat overlaps more consistently with that of albacore. Our results can improve understanding of how albacore movements relate to foraging strategies, and why prey-switching behavior occurs. This has relevance for the development of ecosystem models for the CCS, and for the eventual implementation of ecosystem-based fishery management.

INTRODUCTION

Ecosystem-based fishery management (EBFM) aims to account for environmental and ecosystem factors within fisheries assessment and management frameworks (Link 2017). This goal can be achieved through many possible approaches of varying complexity; including explicit consideration of processes such as climate variability and change, habitat quality, predator-prey relationships in models of species productivity, distribution, and trophic structure (Pikitch et al. 2004; Link 2017). Optimal management strategies may involve trade-offs, as managers balance a desire to maximize sustainable catch of target species while preserving ecosystem function, particularly for major forage species such as clu-

peids, krill, and some cephalopods (Smith et al. 2011). Many of these forage species are fished commercially, but also support higher-order predators further up the food chain, such as other exploited species (e.g., tunas, billfish) and protected resources (e.g., marine mammals and seabirds) (Pikitch et al. 2004; Link and Browman 2014). Effectively managing marine ecosystems to preserve these trophic linkages, and improve robustness of management strategies to environmental variability, thus requires knowledge of food web structure.

Food webs of the California Current System (CCS) are comparatively well studied (e.g. Field et al. 2006; Kaplan et al. 2013; Rose et al. 2015; Koehn et al. 2016). However, it is not yet clear how the dynamic nature of the CCS in space and time impacts trophic structure and predator-prey relationships, which presents a challenge for building ecosystem models (Hunsicker et al. 2011). The diets of many large pelagic predators may vary both temporally and spatially, reflecting opportunistic feeding strategies. Some studies in the CCS have shown a near-exclusive reliance of pelagic predators such as tunas on one prey species, particularly coastal pelagic fishes such as anchovy (*Engraulis mordax*), while others show a much more diverse diet including crustaceans and cephalopods (Pinkas et al. 1971; Bernard et al. 1985; Glaser 2010). Existing studies have typically been snapshots, providing limited information on how predator-prey interactions vary at higher temporal and spatial scales. However, such variability has implications for how energy flows through the food web, as well as foraging costs and net energy gain in predators, some of which migrate long distances to reach the CCS (Childers et al. 2011; Fujioka et al. 2018). Prey-switching behavior in predators may be triggered by changes in dominant species in the ambient prey assemblage, or by active targeting of preferred or high-energy prey when these are more available (Begoña Santos et al. 2013). The importance of these behaviors to

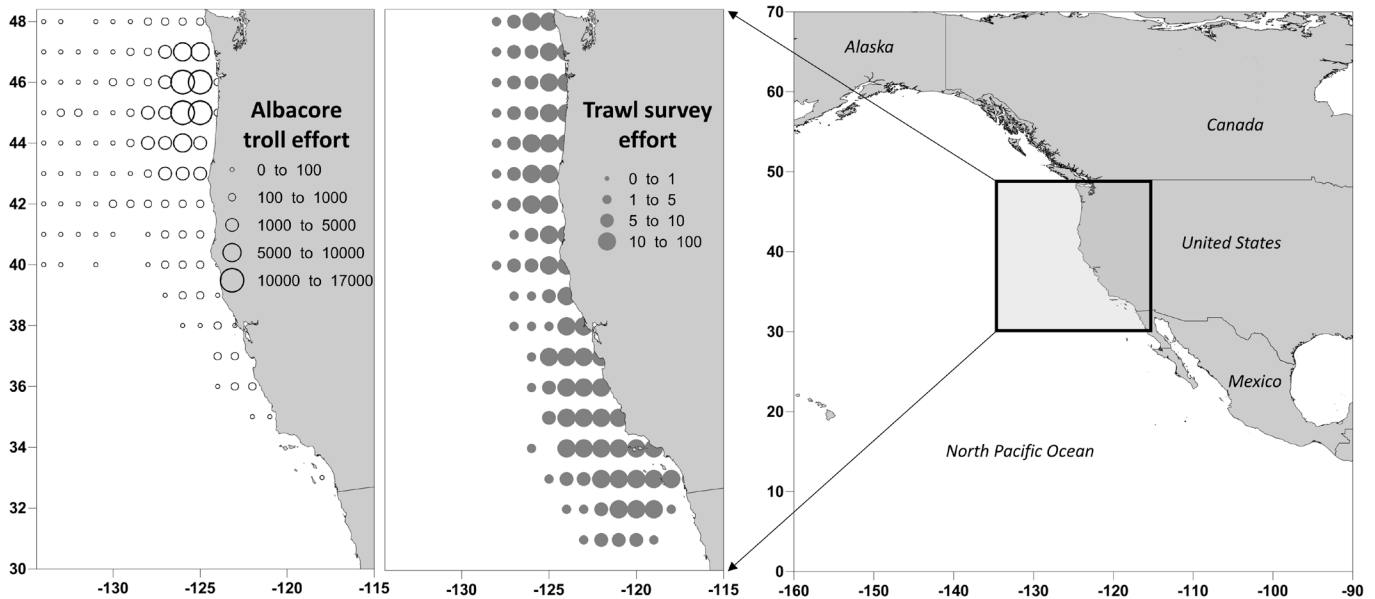


Figure 1. Map of the study area and ROMS domain. The total number of sets in the albacore surface fishery 2002–15 (left), and hauls in the NOAA SWFSC trawl surveys 2003–16 (right) are also shown. Locations with < 3 vessels reporting data for the troll fishery are not shown.

pelagic predators in the CCS is not yet well known. A first step to understanding foraging ecology is therefore to define the spatial and environmental niches occupied by interacting predator and prey species, and to assess how the degree of overlap between these varies in space and time.

Foraging behaviors in commercially important predators have implications for the fisheries that target them. Switching between shallow-living prey species and those that live deeper in the water column, or undertake diel vertical migrations, may impact the availability of predators to fishing gear. For example, commercial and recreational tuna fisheries in the CCS mostly use surface gear, which is largely deployed during daylight hours (Teo 2017; Runcie et al. 2018). Consequently, shifts in the vertical distribution of tuna in response to forage will impact gear vulnerability and catch. Improving understanding of spatiotemporal predator-prey relationships between commercially important species thus has the potential to benefit fishers, future management strategies in the CCS, and to contribute to the implementation of EBFM.

In this study, we used statistical species distribution models (SDMs) to predict the distribution of a top predator (albacore: *Thunnus alalunga*) and five key prey species (northern anchovy: *Engraulis mordax*; hake: *Merluccius productus*; boreal clubhook squid: *Onychoteuthis borealijaponica*; Pacific sardine: *Sardinops sagax*; and Pacific saury: *Cololabis saira*) in the CCS. Environmental predictors were sourced from a high-resolution, data-assimilative CCS configuration of the Regional Ocean Modeling System (ROMS), allowing examination of the impor-

tance of subsurface water column structure in species distributions. We compared results between three contrasting years with different environmental conditions: a weak El Niño year (2004), a cool La Niña year (2012), and a very warm El Niño/marine heat wave year (2015). Overall, we aimed to provide a better understanding of how these species overlap in space and time, and how environmental variability impacts their distributions.

METHODS

Biological data sources

Albacore catch per unit effort (CPUE) was defined as the number of fish recorded per vessel-day in the US pole-and-line and troll fisheries. These were obtained from logbooks from US vessels submitted to the National Oceanic and Atmospheric Administration (NOAA) National Marine Fisheries Service (NMFS). Data were available throughout the central and eastern North Pacific Ocean from 1961 through the end of 2015. However, we limited records used for SDM training to those contained within the ROMS domain (fig. 1, and see further description below), and within the time period covered by the MODIS Aqua and VIIRS ocean color missions (mid-2002 onwards). This ensured that at least two of the three ocean color satellites (SeaWiFS, MODIS Aqua, VIIRS) were available to source surface chlorophyll for most of the sets, limiting observations lost to clouds. To account for varying degrees of accuracy in fishing locations reporting in the logbooks, we removed records where fishing latitude and longitude were both reported in whole degrees ($n = 2,937$),

assuming that these were approximate locations. Locations of all remaining records were then coarsened to show catch per vessel/day at 0.25° resolution, to align with expected accuracy in location reporting, and vessel movements while fishing (see Nieto et al. 2017). These filtering criteria resulted in 129,693 spatially explicit, daily data points for environmental data extraction.

A fishery-independent data set was also available to validate albacore habitat predictions. Since 2001, NMFS and the American Fishermen's Research Foundation (AFRF) have collaborated to tag albacore in the CCS with archival tags (see Childers et al. 2011 and Snyder 2016 for more details). To date, 30 tags have been recovered; 22 between 2003 and 2008, and a further 8 from 2012 to the present. Location data for all recovered tags was processed using an unscented Kalman filter (Lam et al. 2008). 4,624 daily estimated tagged albacore locations were available within the ROMS domain, covering 11 years between 2003 and 2016. Although positional error from this type of tag can be substantial (>1 degrees), we extracted environmental variables at all daily archival tag locations in the same way as for the troll fishing locations. As a comparison, we also extracted environmental variables for the same dates as the tag locations, but at random locations throughout the ROMS domain ("pseudo-absences"). Random locations were generated using "spsample" in the "sp" package in R (Pebesma and Bivand 2005). Predicted habitat quality from the albacore SDM (see description below) was then compared between the tag locations, and the pseudo-absence locations. In addition, as tagged albacore were sometimes located in regions outside the main area of fishing operations, tag locations were added to maps of predicted albacore CPUE as a means of qualitative validation.

We used the Glaser (2010) comparative study of albacore diets to choose key prey species to model. The most important prey taxa were defined as those which had contributed >20% energetic contribution to diets in any region of the CCS, defined as north (>44°N), central (34°–44°N), and south (<34°N), in any of the four studies examined covering years 1949–2006. These criteria resulted in the selection of northern anchovy, Pacific saury, hake, and cephalopods for further analysis. We also included sardine, which is a key CCS forage species that showed moderate energetic contribution (15.3%) to albacore diets in the southern CCS in 2005–06, but was of surprisingly little importance in the other feeding studies. We narrowed the cephalopod group further by examining the results of the two studies that found them to be of greatest importance: Pinkas et al. (1971), and Glaser et al. (2015). Both studies showed that boreal clubhook squid (clubhook squid hereafter) contributed the most to albacore diets, in terms of % energetic contribution. We there-

fore proceeded with anchovy, saury, hake, sardine, and clubhook squid as the five prey species for which to construct SDMs.

Occurrence records for prey species were obtained from trawl surveys conducted by the NOAA Southwest Fisheries Science Center (SWFSC), with 1,486 hauls completed between 2003 and 2016. Sampling effort was primarily concentrated in spring (April: 460 hauls) and summer (July–August: 691 hauls), but some samples were also available from other months between March and October. The trawl net was towed near the surface at night, at a target speed of 3.5–4.0 knots. The net was fitted with an 8 mm mesh liner in the codend (more details are contained in Zwolinski and Demer 2012; Zwolinski et al. 2012, and Weber et al. 2018). Sampling was concentrated on the continental shelf and slope.

Environmental variables

Environmental predictors for the SDMs were sourced from a data assimilative CCS configuration of ROMS, with 42 terrain-following vertical levels, and a domain covering 30°–48°N, inshore of 134°W at 0.1° horizontal resolution (<http://oceanmodeling.ucsc.edu/ccsrt> version 2016a; Veneziani et al. 2009; Neveu et al. 2016). The temporal scale of the biological data covered two ROMS iterations; a historical reanalysis (1980–2010; Neveu et al. 2016) and a near real-time product (2011–present). Environmental variables used in the SDMs were limited to those that were consistent across the reanalysis products (Becker et al. 2018; Brodie et al. 2018).

The predictors extracted from the data assimilative CCS model for use in the SDMs were similar to those used previously to model distributions of large pelagic fishes and mammals in the CCS (Scales et al. 2017; Becker et al. 2018; Brodie et al. 2018) (table 1). Variables included sea surface temperature (SST), measures of mesoscale oceanographic features (sea surface height, eddy kinetic energy), and measures of current flow and wind stress (northward and eastward wind stress and current velocities, wind stress curl). These were extracted as 0.3 by 0.3 degree means for albacore fishing locations, and at 0.1 degree native resolution for trawl sampling locations, to best align with the spatial resolution of the biological data. The exception was wind stress curl, which was extracted at 0.5 degree resolution for all data sets, to account for the coarser resolution of wind forcing used to force the historical reanalysis. In addition to the surface-associated predictors, we included two indicators of subsurface water column structure, as Brodie et al. (2018) found them to be useful predictors of the distribution of other large pelagic fishes. These were isothermal layer depth, and bulk buoyancy frequency, which represents stratification and stability in the upper water column. Isothermal

TABLE 1
 Environmental variables used as predictors in SDMs for all species. “st.dev” denotes standard deviation.

Variable Name	Measured Unit	Source
Sea surface temperature	°C	ROMS
Sea surface temperature st.dev.	°C	Derived from ROMS
Sea surface height	m	ROMS
Sea surface height st.dev.	m	Derived from ROMS
Surface eastward current velocity	m/s	ROMS
Surface eastward wind stress	N/m ²	ROMS
Surface northward current velocity	m/s	ROMS
Surface northward wind stress	N/m ²	ROMS
Wind stress curl	N/m ³	ROMS
Eddy kinetic energy (log)	m ² /s ²	Derived from ROMS
Isothermal layer depth	m	Derived from ROMS
Bulk buoyancy frequency	/s	Derived from ROMS
Surface chlorophyll (4th root)	mg/m ³	SeaWiFS, MODIS Aqua, VIIRS
Moon phase	%	“lunar” R package

layer depth was calculated as the depth at which temperature deviates by 0.5°C relative to the surface, while bulk buoyancy frequency was calculated as the mean buoyancy frequency in the upper 200 m of the water column (or to the bottom in shallower water). The spatial standard deviation of both sea surface temperature and sea surface height at 0.7 degree resolution were also included as predictors, to highlight areas of high variability such as frontal zones (Hazen et al. 2018). The percent of the moon illuminated on the troll fishing or trawl sampling date was also included as a predictor, as some prey and predators have been shown to alter their vertical distributions depending on moon phase (e.g., Sepulveda et al. 2010; Drazen et al. 2011).

Surface chlorophyll concentration was extracted from the SeaWiFS (1997–2010), MODIS Aqua (2002–16), and VIIRS (2012–16) sensors, using the SWFSC Environmental Research Division’s ERDDAP server. Chlorophyll was extracted at 0.25 degree spatial resolution for albacore fishing, tagged albacore, and trawl survey locations, from 8-day composites, to minimize the number of observations lost to cloud cover. Where more than one chlorophyll product was available (64.8% of troll locations, and 77.6% of trawl locations), a mean between the two was taken. Troll locations with no chlorophyll information due to clouds were removed, leaving a total of 111,984 points for SDM training. Similarly, removing daily archival tag positions with no chlorophyll information left 3,695 locations for model validation. The trawl survey data set was much smaller than the fishery-dependent logbook data set, and so to preserve as much data as possible, monthly chlorophyll was used at sampling locations with no 8-day chlorophyll available. This impacted 65 observations, or 4.4% of the data set. A comparison of 8-day and monthly chlorophyll at the remaining 1421 stations showed them to be closely correlated ($r = 0.83$), and so this substitution likely did not impact the results substantially.

Eddy kinetic energy and surface chlorophyll were strongly right-skewed, and so as a result were \log_e and 4th root transformed, respectively, before further analysis. Cross-correlation matrices were then used to identify any collinear predictors, across all biological locations for which environmental data were extracted. Sea surface temperature was moderately and positively correlated with bulk buoyancy frequency ($r = 0.70$). However, leaving both variables in the SDMs resulted in stronger models for all species (determined by comparisons of R^2 for the albacore SDM and area under the receiver operating curve (AUC) for the prey species SDMs), and so we elected to keep both in the suite of predictors. All other correlations among variables were $< r = 0.6$.

Forage fish species may show dramatic fluctuations in stock biomass over short periods of time, and may also restrict their migration patterns at low population sizes (MacCall 1990; Demer et al. 2012; Zwolinski et al. 2012). As a result, theoretically suitable environmental habitat may be unoccupied when stocks are at low levels, impacting the probability of occurrence in trawl surveys, and potentially model performance (Weber et al. 2018). To account for these interactions, we included annual biomass indicators in the hake, sardine, and anchovy SDMs, as additional predictors. Estimates of hake biomass (in metric tons) were sourced directly from the stock assessment (Edwards et al. 2018). Recent estimates of sardine spawning biomass were also sourced from the most recent stock assessment, however this assessment model only includes output for 2006 through 2016 (Hill et al. 2018). Values for years prior to 2006 were sourced from a prior stock assessment, and should be considered more uncertain (Hill et al. 2014). As there is no current stock assessment for anchovy, we followed Zwolinski and Demer (2012) by estimating biomass from three-year running mean larval abundances from CalCOFI surveys. We calculated these by averaging larvae per m² across stations which were sampled between January and

June using standard oblique bongo net tows. We only included “core” sampling stations between 30°–40°N, east of 130°W, which were sampled in at least 15 of the 20 years between 1997–2016. We note that CalCOFI larval abundance indices are most applicable to the central anchovy stock, and that the sardine stock assessment covers only the northern sardine stock. However, trawl surveys likely capture anchovy and sardine from other subpopulations (particularly the more northern anchovy stock) at certain times of year. Saury larvae and clubhook squid paralarvae are only rarely recorded in CalCOFI surveys, and so no biomass indicators were included in the SDMs for these two species.

Similarly, the overall abundance of juvenile albacore in the CCS each year could theoretically be influenced by stock-wide recruitment strength several years earlier. We therefore included annual recruitment estimates from the North Pacific albacore stock assessment in the albacore SDM (ISC 2017). As the majority of albacore caught by the surface fleet are 2–3 years old, we used recruitment estimates from 2 and 3 years prior as two separate predictor variables. As North Pacific albacore recruitment is strongly variable from year to year, these two recruitment time series were not strongly correlated ($r = 0.19$), and so both were included in the SDM.

SDMs

SDMs were built and visualized using boosted regression trees (BRTs) in the “dismo” and “gbm” packages for R Version 3.3.2 (Elith et al. 2008; Ridgeway 2017). The BRT for albacore CPUE was constructed using a Gaussian distribution, with CPUE values transformed using $\log_{10}(x+1)$ beforehand to reduce skewness. The BRTs predicting the probability of presence for the five prey species were built using a Bernoulli distribution. The optimum tree complexity and learning rate for each SDM, to maximize skill and minimize overfitting, was determined largely following the guidelines in Elith et al. (2008). BRTs were built using 50% of the available training data, selected randomly, and then scored on the remaining 50% of the data. The configuration with the lowest error on the unseen validation data set, and which also resulted in a model with at least 2,000 trees, was assumed to be the best. This exercise resulted in a tree complexity value of 7 for the albacore SDM, and 5 for each of the prey species, with a learning rate of 0.1 for the albacore SDM, 0.0008 for the anchovy SDM, 0.0006 for the hake SDM, 0.00005 for the saury SDM, and 0.0002 for the sardine and clubhook squid SDMs, with a bag fraction of 0.6 in all cases. Overall model skill was determined using R^2 between predicted and observed values for the albacore CPUE SDM, and AUC for the prey species presence/absence SDMs. These skill metrics were calculated using only the validation data

not used for building the models. The relative influence of each predictor in the model is scored out of 100 based on the number of times each variable is used for tree splitting, weighted by the squared improvement to the model as a result of each split, and averaged over all trees (Elith et al. 2008).

SDMs were visualized using one- and two-dimensional partial plots. The marginal effect of each predictor in each SDM was shown by plotting observed and predicted abundance (for albacore) or occurrence (for prey species) against binned environmental variables, integrated across all other predictors. Additionally, two-dimensional partial relationships were visualized using plot.gbm in the “gbm” package, which shows the predicted marginal effects of two predictors simultaneously.

Initial tests of the albacore SDM showed that the model did not resolve the lower temperature limit of favorable habitat in a biologically reasonable way, with surface temperatures of $<9^{\circ}\text{C}$ predicted to be suitable. These predictions are contrary to current knowledge on the physiology of albacore, and were caused by there being very few troll sets completed in cold waters. This bias is a common issue with building SDMs using fishery-dependent data, as fishers rarely fish in strongly unsuitable habitat (Jones et al. 2012). We thus followed Muhling et al. (2017) by adding 54 “dummy” zero catch locations to the data set, located at whole degree locations from 43°–48°N, and 134°–126°W, in January and February, for each year from 2003–15. Albacore have never been recorded in this region in January and February by commercial or recreational fishers, or by archival tag locations, and we therefore assumed that these locations represented strongly unfavorable habitat. A total of 984 of these dummy locations had all environmental variables available (including chlorophyll), and were added to the 111,988 true catch records, giving 112,972 total points. The addition of this relatively small number of dummy locations forced a more biologically realistic lower temperature limit in the SDM, with negligible effect on predictions at surface temperatures $>10^{\circ}\text{C}$. However, this should be noted as a source of uncertainty in the albacore SDM.

RESULTS

Bulk buoyancy frequency was the most important variable in the albacore CPUE SDM, with a score of 17.57 (table 2). Sea surface temperature (11.70) and surface chlorophyll (10.90) were also influential to the model. Notably, recruitment strength 2 and 3 years prior were not particularly important to the albacore SDM, ranking 14th and 16th, respectively, out of the 16 total predictors. The coefficient of determination (R^2) between observed and predicted CPUE in the unseen validation portion of the data set was 0.31.

TABLE 2
 Predictor variable importance to all 5 SDMs. The top three most important variables for each SDM are shaded in gray.

Variable Name	Albacore	Anchovy	Hake	Sardine	Clubhook
Sea surface temperature	11.70	6.98	4.92	14.04	10.46
Sea surface temperature st.dev.	5.06	6.97	6.53	6.73	6.56
Sea surface height	6.00	6.23	10.53	6.19	5.92
Sea surface height st.dev.	4.62	3.59	7.46	3.45	5.56
Surface eastward current velocity	3.85	3.31	5.60	4.09	2.28
Surface eastward wind stress	4.86	4.03	3.42	6.31	7.60
Surface northward current velocity	4.17	6.66	3.16	4.95	3.24
Surface northward wind stress	4.78	15.82	3.70	5.1	9.4
Wind stress curl	4.81	2.72	4.31	5.86	7.29
Eddy kinetic energy (log)	3.73	7.27	4.37	5.37	3.64
Isothermal layer depth	6.34	9.52	9.03	3.41	10.65
Bulk buoyancy frequency	17.57	5.74	10.03	8.27	8.34
Surface chlorophyll (4th root)	10.90	12.51	17.89	10.41	6.58
Moon phase	4.83	5.01	6.86	4.78	11.44
Albacore recruits 2 years ago	3.83	—	—	—	—
Albacore recruits 3 years ago	2.93	—	—	—	—
Anchovy SSB index	—	3.64	—	—	—
Hake SSB index	—	—	2.2	—	—
Sardine SSB index	—	—	—	11.03	—
SDM AUC or R ²	R ² = 0.31	AUC = 0.82	AUC = 0.79	AUC = 0.78	AUC = 0.71

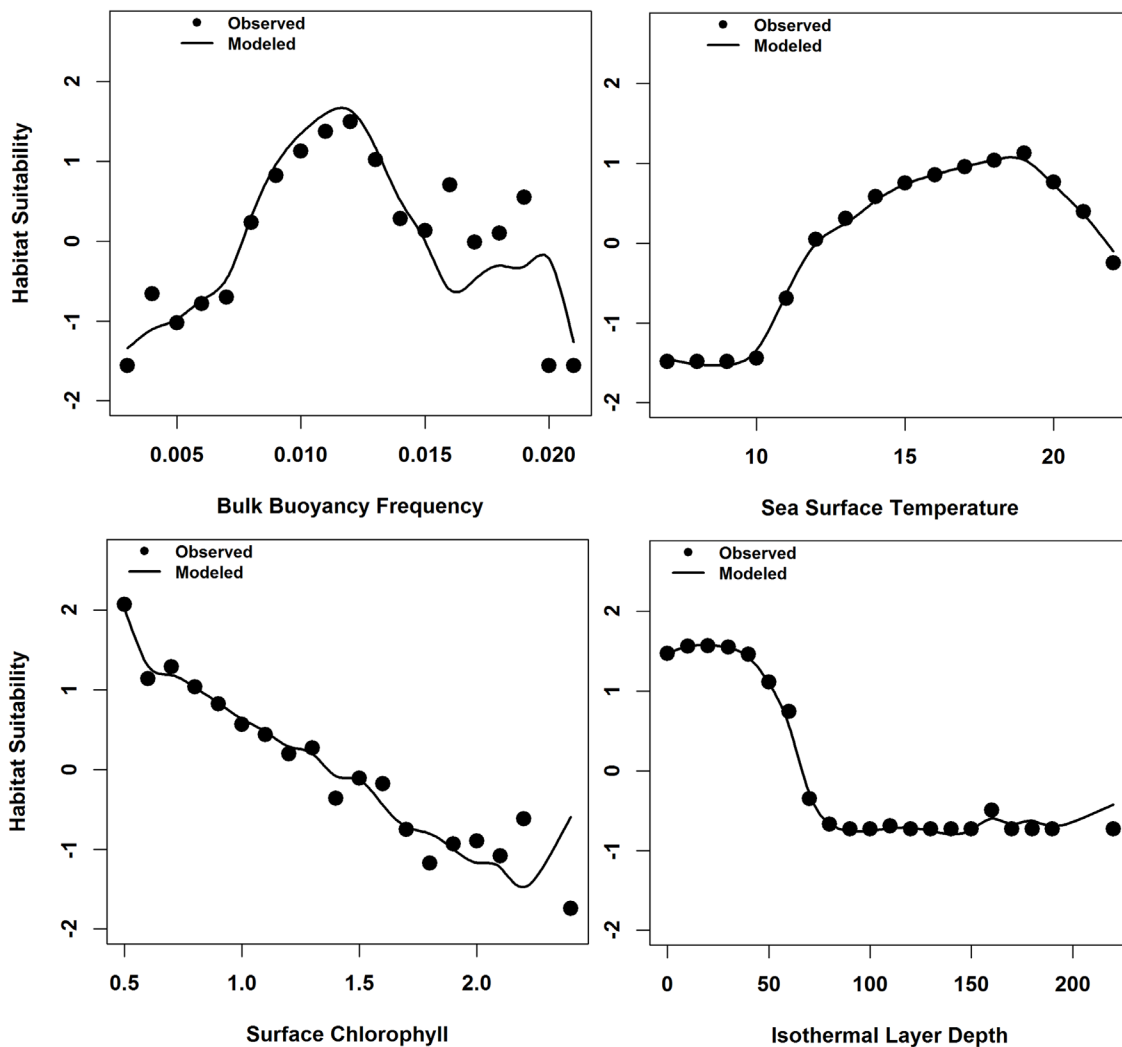


Figure 2. Partial response curves from binned observations and the SDM for albacore, for the four most influential predictors in the model.

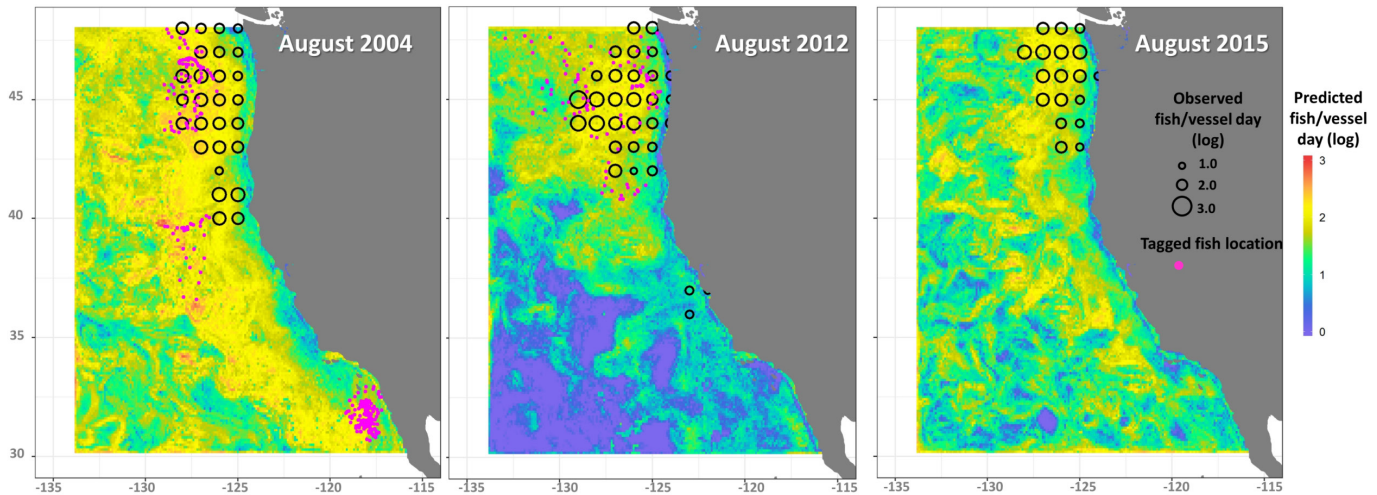


Figure 3. Predicted catch per unit effort (log CPUE) in fish/vessel/day in the albacore surface fishery during August for three example years: 2004, 2012 and 2015. Monthly means of the daily ROMS outputs are shown. Observed CPUE is shown in the black circles, with daily locations from albacore tagged with archival tags shown in pink, for the same month and year as the SDM predictions.

Partial plots suggested that albacore CPUE was generally highest at moderate values of bulk buoyancy frequency (~ 0.012 /s) and surface temperature ($\sim 15^{\circ}\text{--}20^{\circ}\text{C}$), and at lower values of surface chlorophyll and isothermal layer depth (fig. 2).

Predictions from the albacore SDM for 2004, 2012, and 2015 during the month of August (around the typical peak of the fishing season) showed some variability in habitat extent among years (fig. 3). In August 2004, predicted suitable habitat was located throughout the latitudinal extent of the study region, between Baja California in the south (30°N), and the US–Canada border in the north (48°N). In contrast, August 2012 had lower predictions of albacore habitat south of $\sim 40^{\circ}\text{N}$, with August 2015 showing an intermediate situation. There was little fishing effort south of 40°N in all three years, making it difficult to validate the interannual variability in predictions; however some albacore tagged with archival tags were located off Baja California in August 2004, suggesting that there may have been some favorable habitat present during this year (fig. 3). In all years, the extreme inshore region close to the coast was predicted to be less favorable for albacore, as was the off-shore, southwestern portion of the study area (south of 37°N , west of 123°W).

Predicted albacore CPUE was higher at the daily archival tag locations than it was at the random pseudo-absence locations in the winter and summer, but differences were minimal during spring and fall (fig. 4). Overall habitat suitability was highest during summer and lowest during winter at points throughout the ROMS model domain. However, predictions were markedly higher at the true tag locations. This result suggests that even though there is large uncertainty in

location estimates of tagged fish, making migrating versus foraging behavior difficult to distinguish, tagged fish were preferentially located in habitat predicted to be more suitable by the SDM.

The anchovy SDMs performed strongly on the unseen validation data ($\text{AUC} = 0.82$), while the hake, sardine, and clubhook squid AUCs were good to fair (0.79, 0.78, and 0.71, respectively) (Pearce and Ferrier 2000; Weber and McClatchie 2010). The saury SDM AUC (0.69) indicated the weakest model of the five. This result was likely due to the low proportion of positive occurrences of saury in the trawl data (45/1373 stations), which limited the power of the SDM for this species. As spatial predictions from the saury SDM were also patchy, and biologically implausible, this model was not considered further.

SDMs for the remaining four prey species were strongly influenced by surface chlorophyll (table 2). Surface temperature was the most important variable in the sardine SDM, and also influential in the clubhook squid SDM, where it ranked 3rd of 14 predictors. The sardine biomass index was strongly important to the sardine SDM, suggesting that sardine were more likely to be present when overall biomass was higher. In contrast, the anchovy biomass index was much less influential to the anchovy SDM (ranking 12th out of 15 predictors), and the hake biomass index was the least important of all predictors in the hake SDM.

Partial plots for the three strongest predictors in each of the prey SDMs showed that hake and anchovy were associated with moderate to high surface chlorophyll concentrations, while sardine were associated with moderate to low chlorophyll areas (fig. 5). Anchovy were also most likely to be present at weak (near-zero) north-

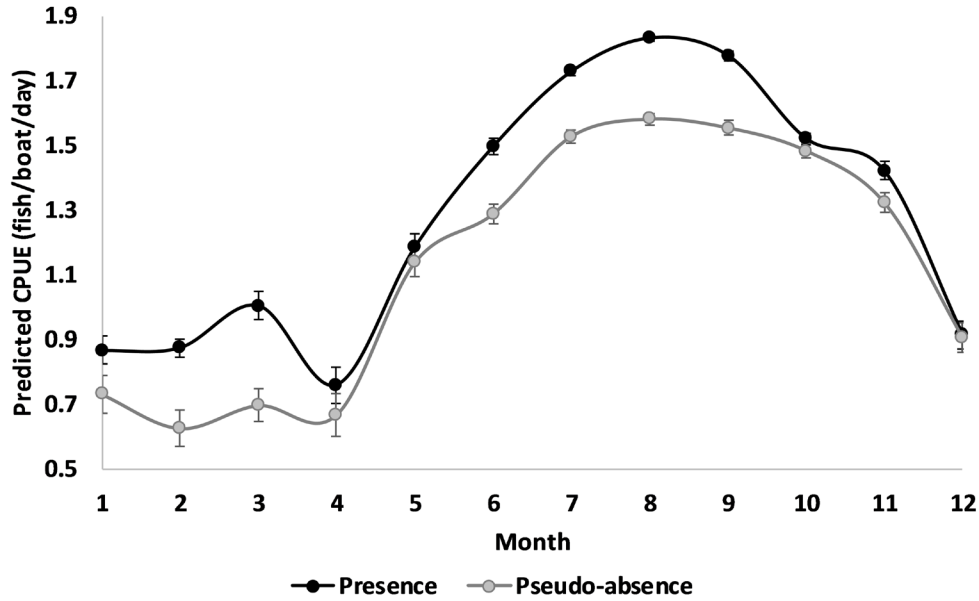


Figure 4. Predicted catch per unit effort (log CPUE) from the albacore SDM at 3,695 daily locations of tagged albacore in the ROMS domain by month, between 2003 and 2016. Predicted CPUE at 3,695 random locations in the ROMS domain sampled on the same dates as the tag locations are also shown. Error bars denote standard errors.

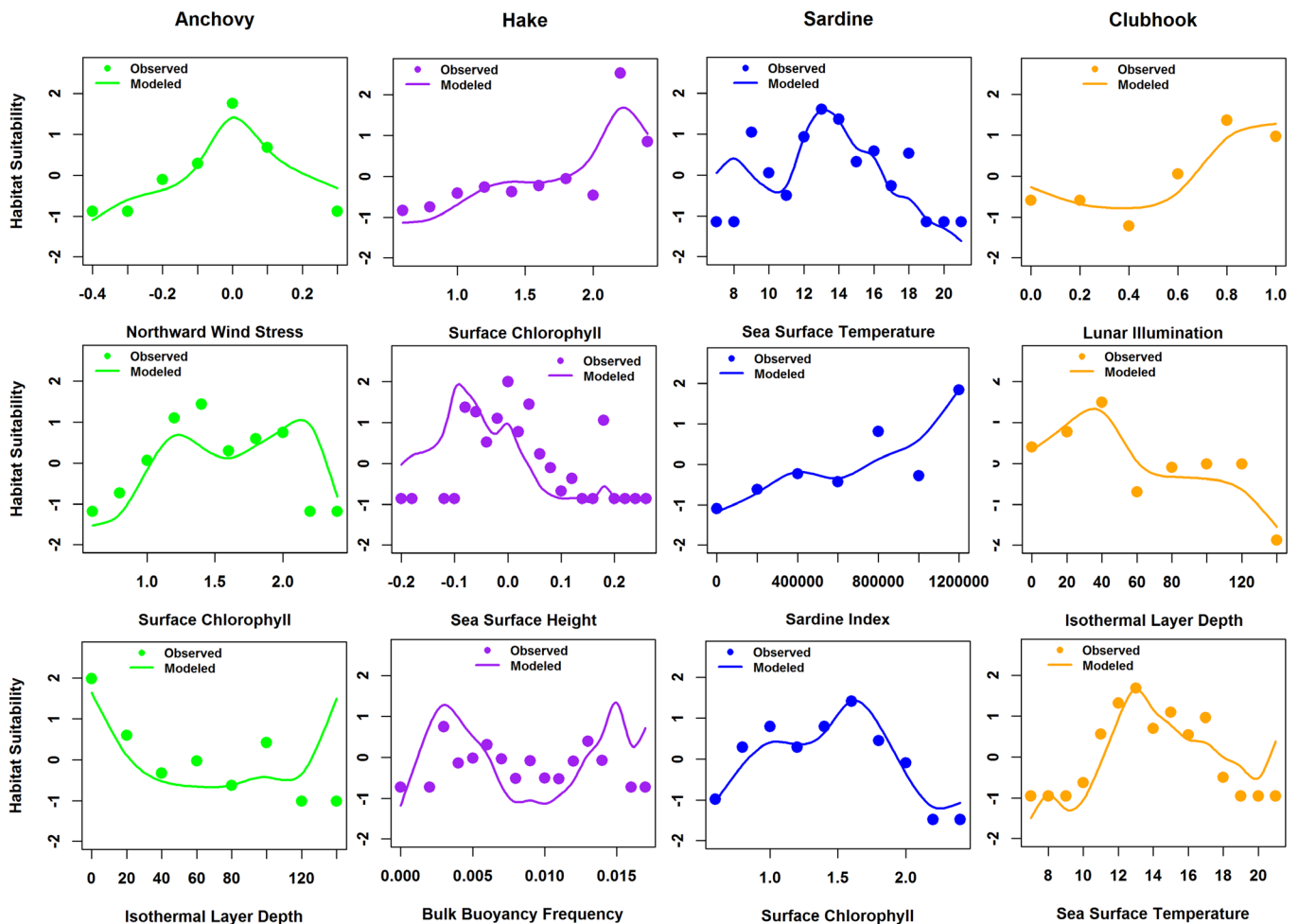


Figure 5. Partial response curves from binned observations and the SDM for four prey species, for the three most influential predictors in each model.

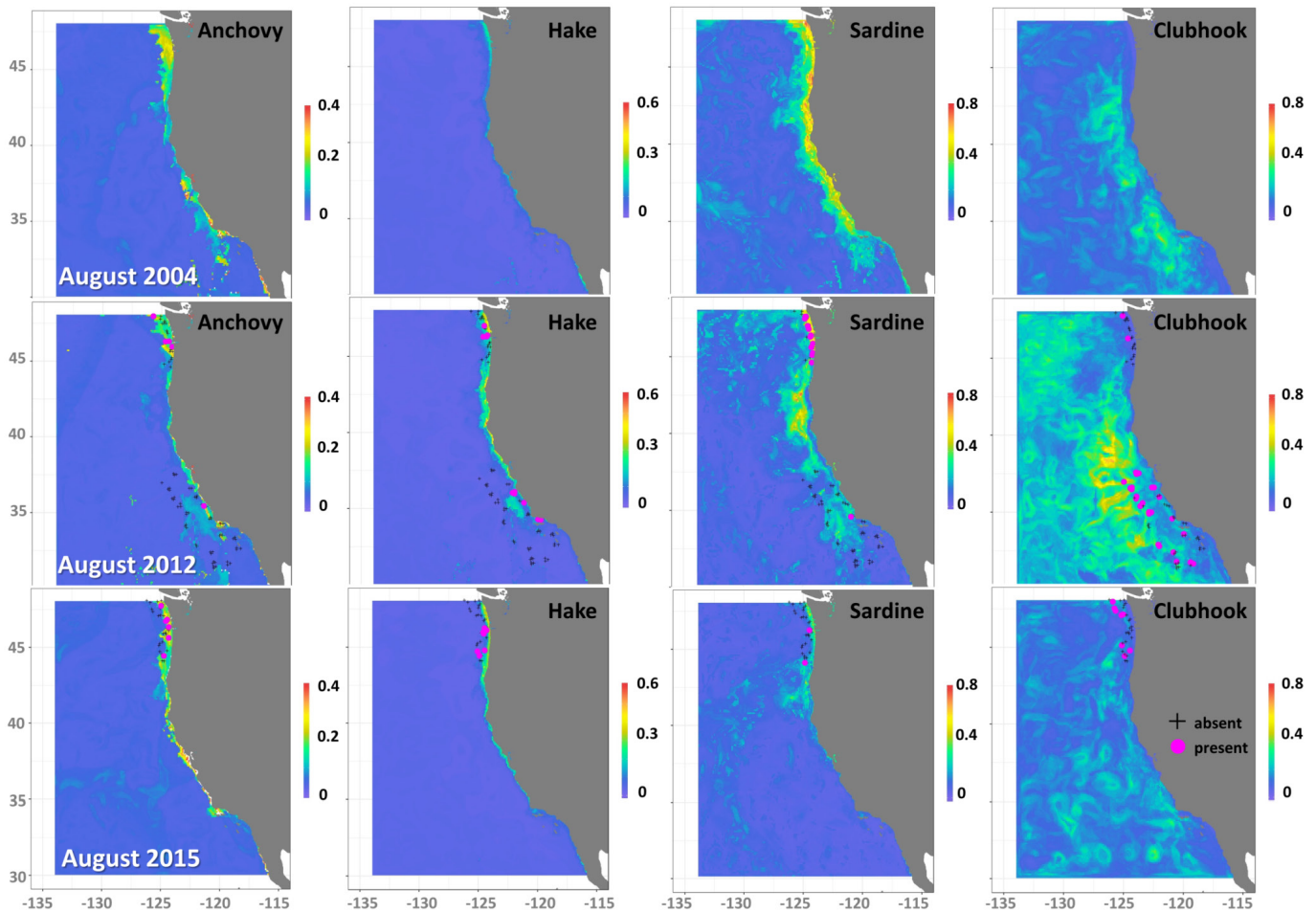


Figure 6. Predicted probability of occurrence (/1) of four prey species in the SWFSC trawl surveys during August for three example years: 2004, 2012 and 2015. Monthly means of the daily ROMS outputs are shown. Observed positive catch locations are shown in pink, with observed negative catch locations shown in black crosses, for the same month and year as the SDM predictions.

ward wind stress. Sardine were most likely to be present at moderate ($\sim 10^{\circ}$ – 17°C) sea surface temperatures, and during times of higher overall biomass. Clubhook squid were more commonly present in trawl surveys near to the full moon, at moderate to low isothermal layer depths, and moderate sea surface temperatures ($\sim 11^{\circ}$ – 18°C) (fig. 5).

Predictions of suitable habitat for the four prey species in August 2004, 2012, and 2015 highlighted the strong association of anchovy and hake with near-coastal environments (fig. 6). In contrast, sardine were associated with both inshore and continental shelf environments, while clubhook squid were associated with continental shelf and offshore mesoscale features. Favorable habitat for hake appeared to extend further south in 2012, but it was difficult to validate predictions with so few survey data available. During the “blob” marine heat wave in 2015, anchovy and hake habitat was not predicted to be strongly different from the other two years examined. However, conditions appeared less favorable over-

all for clubhook squid (fig. 6). The probability of sardine occurrence was also predicted to be low, likely driven by the low biomass of sardine during 2015, and the high importance of the sardine biomass index to the SDM for this species.

Previous studies have shown that anchovy and hake can be important to the diets of albacore. However, predictions from the SDMs (fig. 3, fig. 6) suggested somewhat minimal spatial overlap of these species with albacore. Two-dimensional representations of SDMs, showing partial relationships with surface chlorophyll and sea surface temperature averaged across all other predictors, also highlighted this separation in environmental space (fig. 7). Although surface chlorophyll and sea surface temperature were moderately to strongly important to the SDMs for albacore, anchovy, hake, sardine, and clubhook squid (table 2), the partial relationships were quite different. While albacore CPUE was predicted to be highest at low surface chlorophyll and moderate sea surface temperatures, anchovy and hake were most likely

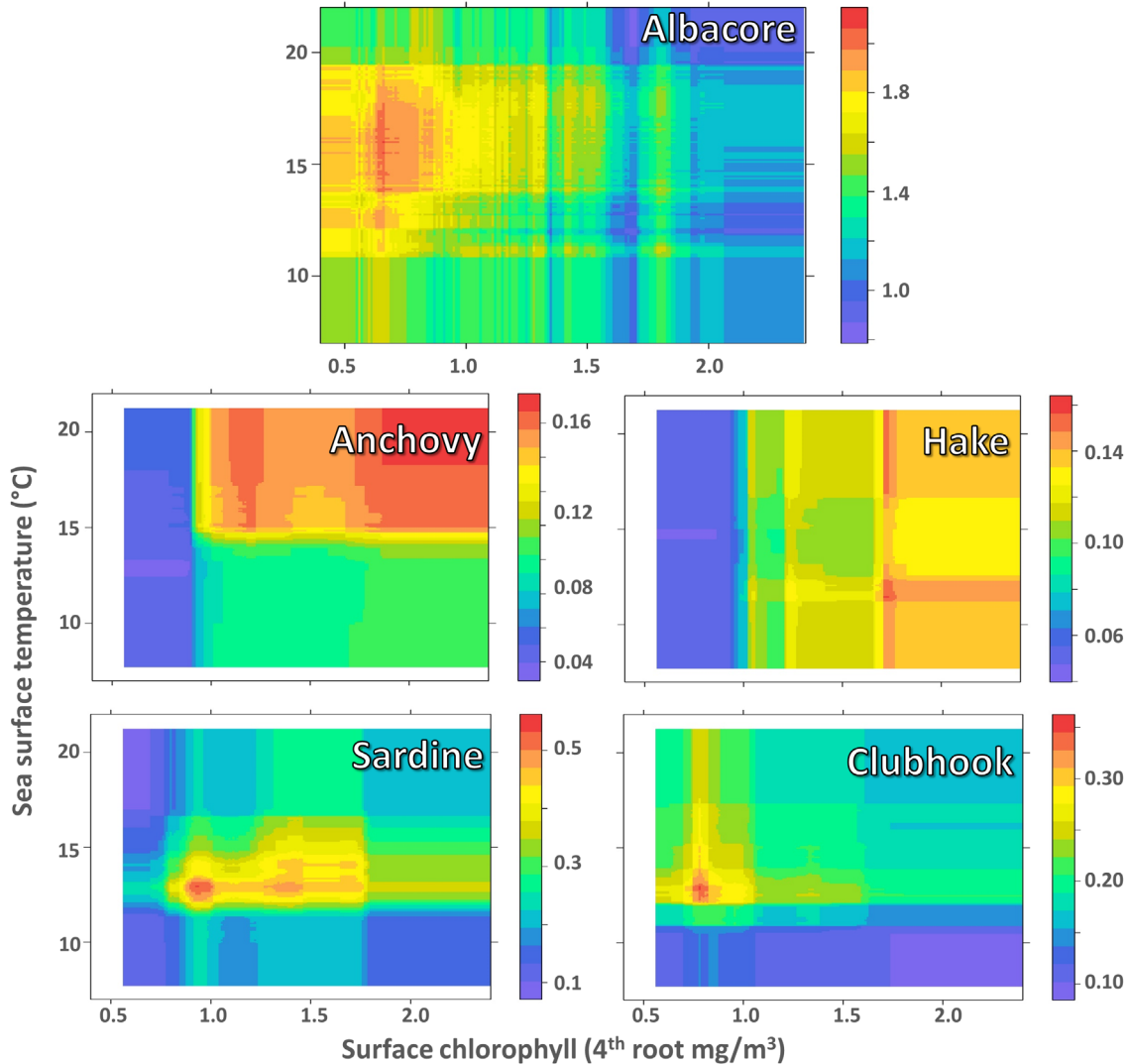


Figure 7. Two-dimensional representations of SDMs for albacore, anchovy, hake, sardine, and clubhook squid, showing the marginal effects of sea surface temperature (°C), and surface chlorophyll (4th root transformed). Colors show predicted CPUE in catch/vessel/day (albacore), or probability of occurrence /1 (anchovy, hake, sardine, clubhook squid)

to be collected where surface chlorophyll was higher, characteristic of the productive inshore waters in which they were most abundant. In contrast, sardine and clubhook squid occupied similar environmental space to albacore, reflecting the occupation of the continental shelf and slope waters by both species.

DISCUSSION

Results from the albacore SDM are generally consistent with the findings of previous habitat modeling studies that used satellite variables as predictors (e.g., Nieto et al. 2017; Xu et al. 2017). Our model outputs showed that the highest catch rates for this species were located in the transitional area offshore of the coastal upwelling zone. However, the use of data assimilative CCS ocean model output provided the advantages of relatively long,

gap-free environmental time series, and the availability of variables describing subsurface water column structure. Two of the four most influential variables in the albacore SDM were subsurface variables not available from satellite sensors: bulk buoyancy frequency and isothermal layer depth. Albacore CPUE was highest at moderate values of bulk buoyancy frequency. This variable is a measure of water column stability, with higher values indicating a more stable, stratified water column, and low values indicating highly mixed, less stable waters typical of recent upwelling (Brodie et al. 2018). In practice, habitats with moderate BBV were those located just offshore of the upwelling zone, and may provide access to a transition zone between upwelled waters richer in prey, and more stable waters offshore where fish can recover from vertical movements (Snyder et al. 2017).

Isothermal layer depth approximates the thickness of the mixed layer, below which temperature and oxygen decline sharply. Albacore CPUE was higher at shallower isothermal layer depths less than around 70 m. These conditions were mostly found in the warmer summer months, when albacore are most abundant in the CCS, and particularly off Oregon and Washington. Shallower isothermal layer depths may concentrate prey nearer to the surface, providing favorable feeding conditions for albacore, but may also concentrate albacore themselves in the upper water column, where they are more vulnerable to surface fishing gear.

Albacore CPUE was also higher at lower values of surface chlorophyll, suggesting avoidance of both colder nearshore upwelled waters, and mesoscale features moving new productivity offshore. Predictions from the SDM trained on fishery-dependent data were consistent with fishery-independent observations of tagged albacore, providing a rare opportunity to validate a distribution model with independent data. Tagged fish occupied habitat that was markedly more favorable than random during summer, the season when they are relatively resident in the CCS (Childers et al. 2011). During spring and fall, when many albacore are migrating between the CCS and the open North Pacific, they were located in habitat not much more favorable than random, likely reflecting rapid movements between seasonal foraging areas (Childers et al. 2011; Snyder 2016).

Bulk buoyancy frequency and isothermal layer depth from the ocean model were also shown to be useful for predicting swordfish (*Xiphias gladius*) habitat in the CCS in a previous study (Brodie et al. 2018). However, swordfish spend much more time at depth than albacore, particularly during the day (Sepulveda et al. 2010; Childers et al. 2011). As a result, close relationships between their occurrence and the subsurface environment may be expected. Results from the current study suggest that dynamic subsurface predictors can also be useful for modeling distribution of more epi-pelagic species such as albacore, providing a useful complement to the more widely used surface environmental variables.

Observed catch rates of albacore from the troll fishery were concentrated in the northern CCS during our study time period, just offshore of Oregon and Washington. Although our results may be partially confounded by factors such as cannery closures in southern California in the 1980s, the northern CCS also had consistently favorable spring–summer albacore habitat, as predicted by the SDM. In contrast, predicted habitat suitability off California and Baja California appeared to be more ephemeral, being highly favorable in August 2004, but much less so in 2012 and 2015. Albacore catches off southern California are strongly variable interannually, and have been so for at least the past 100 years (Clemens and

Craig 1965; Childers et al. 2011). Although larger-scale migration patterns (Childers et al. 2011; Snyder 2016) and potentially stock structure (Laurs and Lynn 1977) likely influence the availability of albacore off southern California, results from the present study suggest that habitat suitability in the southern CCS may also contribute to interannual variability in north–south catch distributions. Despite relatively high variability in recruitment in the years since 2002 (ISC 2017), we found no strong influence of year class strength on CPUE in the CCS. This apparent lack of influence of recruitment suggests that regional-scale environmental conditions may be more influential for determining catch rates, but additional examination of migration and movement patterns is likely needed to confirm this.

The 2013–16 northeast Pacific marine heat wave (including the “blob” and the 2015–16 El Niño event) resulted in much warmer waters than usual in the study region, with lower primary productivity except for within a narrow band of strong upwelling near the coast (Jacox et al. 2016; Zaba and Rudnick 2016). In August 2015, most of the CCS was at least 1°C warmer than usual, with positive temperature anomalies of >2°C off California (Gentemann et al. 2017). In contrast, summer 2012 was cooler than average in the CCS after several La Niña years, while 2004 temperatures were slightly above normal (Goericke et al. 2005; Bjorkstedt et al. 2012; Runcie et al. 2018). Anomalously warm conditions in 2015 did not result in a marked northward shift in predicted albacore habitat within the ROMS model domain. Predictions from the SDM suggested that suitable habitat was available from northern Baja California to the northern limit of the study area (48°N) during this year. However, albacore are known to extend their range northwards as far as southeast Alaska during warm years, as was observed in 2005 and in 2015 (Cavole et al. 2016; Christian and Holmes 2016). Although temperature is known to be an important determinant of albacore habitat in the North Pacific (Snyder 2016; Nieto et al. 2017; Xu et al. 2017), the ocean circulation model domain covered a relatively small portion of their geographic range, which is usually within tolerable limits from spring through fall. The study domain would therefore need to be extended northwards to best capture changes in habitat and range extensions for albacore resulting from marine heat waves and future warming. This may also be the case for the four prey species, which are also found well outside the ROMS domain (Lluch-Belda et al. 1991; Bigelow 1994; Gustafson et al. 2000).

A somewhat unexpected result of the study was the general lack of spatial overlap between albacore and some of their main prey species, particularly anchovy and hake. While albacore catch was low in highly productive coastal waters, anchovy and hake showed a strong

affinity for these areas, while sardine were most common on the continental shelf. These results are consistent with previous work on the distribution of these species (Zwolinski et al. 2012; Weber et al. 2018). Some historical diet studies conducted when anchovy biomass was high show a near-exclusive reliance of albacore on anchovy in some parts of the CCS (Glaser 2010). The spatial separation between albacore's preferred habitat and that of their prey suggests that albacore may need to move back and forth across the front separating productive coastal waters from offshore waters to feed on anchovy. Studies of tagged albacore have shown that they can employ precisely this behavior when conditions are favorable (Fiedler and Bernard 1987; Snyder et al. 2017), and that these movement patterns are likely to confer physiological advantages (Kirby et al. 2000). These observations may explain why catch rates of albacore can be higher near thermal fronts and Lagrangian coherent structures (Nieto et al. 2017; Xu et al. 2017; Watson et al. 2018). We included spatial standard deviation of sea surface temperature as an indicator of frontal activity in the SDMs, but although this variable was moderately influential to the albacore model (ranked 6th of 16), the partial relationship was negative (result not shown). However, Nieto et al. (2017) and Xu et al. (2017) show that the distance of fishing activity from thermal fronts, and the distance of the front from the coast, may be better predictors of CPUE than temperature gradient metrics, such as those used in this study. Studies on albacore (Watson et al. 2018) and other large pelagic predators (Abrahms et al. 2018; Scales et al. 2018) suggest that Lagrangian Coherent Structures, identified from surface velocity fields using finite-time or finite-size Lyapunov exponents (FTLE, FSLE), may act as hotspots of distribution and foraging activity. Further studies of how albacore forage across fronts could thus examine different indicators of frontal activity across multiple spatiotemporal scales to find the most ecologically relevant predictors, and potentially improve the modest predictive power of the albacore SDM from this study.

In contrast to targeting coastal species such as anchovy, albacore can potentially feed on sardine or cephalopods such as clubhook squid while remaining further offshore. Clubhook squid habitat, in particular, showed strong spatial and environmental overlap with albacore habitat. While sardine habitat was also spatially accessible to albacore, they were absent from albacore diets in the 1950s–60s and contributed only 5%–15% of energetic contribution by region in 2005–06 (Glaser 2010). However, sardine populations were at very low levels from the early 1950s, before recovering somewhat in the late 1990s and declining again more recently (Zwolinski and Demer 2012). Future foraging studies during periods of higher sardine abundance may provide more accurate

information on the potential importance of sardine to albacore diets.

Although saury have been shown to be important to albacore diets (Glaser 2010), the SDM for this species had poor skill, due to the rarity of this species in the trawl and larval surveys. However, the low number of positive occurrences was most likely due to low vulnerability of saury to these fishing gears, rather than an absence of saury in the region. Previous studies using more neustonic gears have recorded saury in greater numbers (e.g., Moser 2002; Brodeur et al. 2005), and so future efforts to model saury distributions should use catch records from surveys targeting near-surface environments.

It is not yet clear how albacore feeding on ecologically distinct prey species may alter their degree of aggregation near fronts, or their diel vertical distribution, depending on the species targeted. While anchovy and sardine are generally distributed in the upper water column (Robinson et al. 1995; Kaltenberg and Benoit-Bird 2009), clubhook squid may undertake more extensive diel vertical migrations, occupying much deeper depths during the day (Watanabe et al. 2006). As the main fishing methods in the US fishery are surface-based troll and pole-and-line, and fishing takes place mostly during the day, there is the potential for different foraging behaviors to impact availability of albacore to fishers.

By switching between coastal and offshore-associated prey species, albacore may exert spatiotemporally variable predation pressure on forage species, with implications for the CCS pelagic food web (Wade et al. 2007; Glaser 2010; 2011). Trophic links are dynamic, and anomalous environmental conditions can cause unexpected predator–prey relationships. For example, Glaser (2010) shows that hake formed an important component of albacore diets in 2005–06, but not in earlier studies from the 1950s–60s. This discrepancy may arise from unusually warm conditions in the mid-2000s leading to hake spawning further north than previously recorded, resulting in high abundances of young-of-the-year (YOY) in the central–northern CCS during spring and summer (Phillips et al. 2007). Spatiotemporal overlap between core albacore habitat and juvenile hake may therefore only occur sporadically under warm conditions, as hake spawning in the northern CCS was recorded again during the marine heat wave years of 2015–06 (Auth et al. 2018). However, it provides an example of an unanticipated trophic connection between an epipelagic predator and a prey species which is largely mesopelagic once mature (Childers et al. 2011; Gustafson et al. 2000), facilitated by spawning phenology responding to anomalous environmental conditions.

Previous studies of albacore diets in the CCS have shown that while they can take fish larger than 10 cm in

length, they rely strongly on YOY and juvenile life stages of prey (Glaser 2010). This preference may relate to ease of capture, maximum mouth gape in the age classes of albacore in the CCS (mostly 2–3-year-olds), or some other unknown factor (Menard et al. 2006). Although offshore samples are rare, available evidence suggests that juveniles of the four prey species examined here likely occupy similar spatial habitats to mature adults (Bigelow 1994; Gustafson et al. 2000; Demer et al. 2013; Rose et al. 2015). However, they only occur as the size classes apparently targeted by albacore for part of the year, depending on their spawning dates, and growth rates. The prey SDMs constructed in this study predicted the presence of any life stage catchable by the trawl gear, which likely includes some juveniles and some adults, depending on the species (Demer et al. 2013). Narrowing predictions of available albacore prey fields to include only the prey sizes targeted will thus require consideration of spawning phenology and growth rates for each prey species, which also likely vary interannually and spatially with oceanographic conditions (Weber and McClatchie 2010; Auth et al. 2018; Weber et al. 2018). For example, Daly et al. (2013) show that although both sardine and anchovy can occur in the northern CCS as adults, larval anchovy are collected much more commonly than larval sardine. This may result in distinct latitudinal ranges of YOY anchovy versus sardine, even though their distributions as adults are quite similar.

Additional future work should also include more consistent sampling of albacore diets and trophic ecology at higher spatial and temporal resolution, to improve understanding of the bioenergetic implications of prey switching. As albacore do not spawn in the CCS, they presumably migrate into the area as juveniles to build condition. Reliance on prey with different energy contents (Glaser 2010) may therefore have implications for trade-offs between energy spent migrating, and energy gained on foraging grounds (Kitagawa and Aoki 2017). Albacore have the potential to exert significant predation pressure on forage species (Glaser 2011), but these trophic links are likely to be highly dynamic. To advance the goals of EBFM in the CCS, a better understanding of spatiotemporal overlap and trophodynamics of predators and prey is required. In addition, improved knowledge of how oceanographic conditions and prey fields interact to influence availability of albacore to surface fisheries in the region could help industry adapt to environmental variability and future change.

ACKNOWLEDGEMENTS

We thank Deb Wilson-Vandenberg, the California Department of Fish and Wildlife, and the SWFSC for hosting the 2018 CalCOFI conference, including the symposium where this work was presented.

We also thank Yuhong Gu, Arjun Joshi, Bev Macewicz, Juan Zwolinski, Andrew Thompson, John Field, Steve Teo, Keith Sakuma, Rick Brodeur, and Toby Auth from the SWFSC for data provision, and assistance with data interpretation. Ed Weber and Elliott Hazen also provided valuable feedback on the draft manuscript. We acknowledge the staff, vessels, and crew involved in the SWFSC trawl surveys, for sample collection and processing. Elliott Hazen, Heather Welch, and Roy Mendelsohn from the SWFSC Environmental Research Division and Kylie Scales at the University of the Sunshine Coast contributed to code and analyses for habitat modeling and oceanographic data handling. The American Fisheries Research Foundation (AFRF) collaborated with the SWFSC, particularly Suzanne Kohin, to implement the albacore tagging program, and collect biological samples, along with the Sportfishing Association of California. B. M., S. B., D. T., and C. E. are partially supported by the Future Seas project, which was funded by the NOAA Climate Program Office's Coastal Oceans and Climate Applications (COCA; NA17OAR4310268) and Modeling, Analysis, Predictions, and Projections (MAPP; NA17OAR4310108) programs.

LITERATURE

- Abrahms, B., K. L. Scales, E. L. Hazen, S. J. Bograd, R. S. Schick, P. W. Robinson, and D. P. Costa. 2018. Mesoscale activity facilitates energy gain in a top predator. *Proc. Royal Soc. B* 285: <http://doi.org/10.1098/rspb.2018.1101>.
- Auth, T. D., E. A. Daly, R. D. Brodeur, and J. L. Fisher. 2018. Phenological and distributional shifts in ichthyoplankton associated with recent warming in the northeast Pacific Ocean. *Global Change Biol.* 24:259–272.
- Begoña Santos, M., I. German, D. Correia, F. L. Read, J. Martinez Cedeira, M. Caldas, A. Lopez et al. 2013. Long-term variation in common dolphin diet in relation to prey abundance. *Mar. Ecol. Prog. Ser.* 481:249–268.
- Becker, E. A., K. A. Forney, J. V. Redfern, J. Barlow, M. G. Jacox, J. J. Roberts, and D. M. Palacios. 2018. Predicting cetacean abundance and distribution in a changing climate. *Divers. Distrib.* <https://doi.org/10.1111/ddi.12867>.
- Bernard, H. J., J. B. Hedgepeth, and S. B. Reilly, S. B. 1985. Stomach contents of albacore, skipjack, and bonito caught off southern California during summer 1983. *Calif. Coop. Oceanic Fish. Invest. Rep.* 26:175–183.
- Bigelow, K. A. 1994. Age and growth of the oceanic squid *Onychoteuthis borealijaponica* in the North Pacific. *Fish. Bull.* 92:13–25.
- Bjorkstedt, E. P., S. J. Bograd, W. J. Sydeman, S. A. Thompson, R. Goericke, R. Durazo, P. Warzybok et al. 2012. State of the California Current 2011–12: Ecosystems respond to local forcing as La Niña wavers and wanes. *Calif. Coop. Oceanic Fish. Invest. Rep.* 53:41–76.
- Brodie, S., M. G. Jacox, S. J. Bograd, H. Welch, H. Dewar, K. L. Scales, K. L., S. M. Maxwell et al. 2018. Integrating dynamic subsurface habitat metrics into species distribution models. *Front. Mar. Sci.* 5: <https://doi.org/10.3389/fmars.2018.00219>.
- Brodeur, R. D., J. P. Fisher, R. L. Emmett, C. A. Morgan, and E. Casillas. 2005. Species composition and community structure of pelagic nekton off Oregon and Washington under variable oceanographic conditions. *Marine Ecology Progress Series* 298:41–57.
- Cavole, L. M., A. M. Demko, R. E. Diner, A. Giddings, I. Koester, C. M. Pagniello, M. L. Paulsen et al. 2016. Biological impacts of the 2013–2015 warm-water anomaly in the Northeast Pacific: winners, losers, and the future. *Oceanography* 29:273–285.
- Childers, J., S. Snyder, and S. Kohin, S. 2011. Migration and behavior of juvenile North Pacific albacore (*Thunnus alalunga*). *Fish. Oceanogr.* 20:157–173.
- Christian, J. R. and J. Holmes. 2016. Changes in albacore tuna habitat in the northeast Pacific Ocean under anthropogenic warming. *Fish. Oceanogr.* 25:544–554.

- Daly, E. A., T. D. Auth, R. D. Brodeur, and W. T. Peterson. 2013. Winter ichthyoplankton biomass as a predictor of early summer prey fields and survival of juvenile salmon in the northern California Current. *Marine Ecology Progress Series* 484:203–217.
- Demer, D. A., J. P. Zwolinski, K. A. Byers, G. R. Cutter, J. S. Renfree, T. S. Sessions, and B. J. Macewicz. 2012. Prediction and confirmation of seasonal migration of Pacific sardine (*Sardinops sagax*) in the California Current Ecosystem. *Fish. Bull.* 110:52–70.
- Demer, D. A., J. P. Zwolinski, G. R. Cutter Jr, K. A. Byers, B. J. Macewicz, and K. T. Hill. 2013. Sampling selectivity in acoustic-trawl surveys of Pacific sardine (*Sardinops sagax*) biomass and length distribution. *ICES J. Mar. Sci.* 70:1369–1377.
- Drazen, J. C., G. Lisa, and R. Domokos. 2011. Micronekton abundance and biomass in Hawaiian waters as influenced by seamounts, eddies, and the moon. *Deep Sea Res Part 1 Oceanogr Res Pap.* 58:557–566.
- Edwards, A. M., I. G. Taylor, C. J. Grandin, and A. M. Berger. 2018. Status of the Pacific hake (whiting) stock in U.S. and Canadian waters in 2018. Prepared by the Joint Technical Committee of the U.S. and Canada Pacific Hake/Whiting Agreement, National Marine Fisheries Service and Fisheries and Oceans Canada. 222 p.
- Elith, J., J. R. Leathwick, and T. Hastie. 2008. A working guide to boosted regression trees. *J. Anim. Ecol.* 77:802–813.
- Fiedler, P. C. and H. J. Bernard. 1987. Tuna aggregation and feeding near fronts observed in satellite imagery. *Cont. Shelf Res.* 7:871–881.
- Field, J. C., R. C. Francis, and K. Aydin. 2006. Top-down modeling and bottom-up dynamics: linking a fisheries-based ecosystem model with climate hypotheses in the Northern California Current. *Prog. Oceanogr.* 68:238–270.
- Fujioka, K., H. Fukuda, Y. Tei, S. Okamoto, H. Kiyofuji, S. Furukawa, J. Takagi et al. 2018. Spatial and temporal variability in the trans-Pacific migration of Pacific bluefin tuna (*Thunnus orientalis*) revealed by archival tags. *Prog. Oceanogr.* 162:52–65.
- Gentemann, C. L., M. R. Fewings, and M. García-Reyes. 2017. Satellite sea surface temperatures along the West Coast of the United States during the 2014–2016 northeast Pacific marine heat wave. *Geophys. Res. Lett.* 44:312–319.
- Glaser, S. M. 2010. Interdecadal variability in predator–prey interactions of juvenile North Pacific albacore in the California Current System. *Mar. Ecol. Prog. Ser.* 414:209–221.
- Glaser, S. M. 2011. Do albacore exert top-down pressure on northern anchovy? Estimating anchovy mortality as a result of predation by juvenile north Pacific albacore in the California current system. *Fish. Oceanogr.* 20:242–257.
- Glaser, S. M., K. E. Waechter, and N. C. Bransome. 2015. Through the stomach of a predator: regional patterns of forage in the diet of albacore tuna in the California Current System and metrics needed for ecosystem-based management. *J. Mar. Syst.* 146:38–49.
- Goericke, R., E. Venrick, A. Mantyla, R. Hoof, C. Collins, G. Gaxiola-Castro, S. J. Bograd et al. 2005. The state of the California current, 2004–05: still cool? *Calif. Coop. Oceanic Fish. Invest. Rep.* 46:32–71.
- Gustafson, R. G., W. H. Lenarz, B. B. McCain, C. C. Schmitt, W. S. Grant, T. L. Builder, R. D. Methot. 2000. Status review of Pacific hake, Pacific cod, and walleye pollock from Puget Sound, Washington. NOAA Technical Memorandum NMFS-NWFSC-44.
- Hazen, E. L., K. L. Scales, S. M. Maxwell, D. K. Briscoe, H. Welch, S. J. Bograd, H. Bailey et al. 2018. A dynamic ocean management tool to reduce bycatch and support sustainable fisheries. *Sci. Adv.* 4: DOI: 10.1126/sciadv.aar3001.
- Hill, K. T., P. R. Crone, D. A. Demer, J. P. Zwolinski, E. Dorval, and B. J. Macewicz. 2014. Assessment of the Pacific sardine resource in 2014 for U.S.A. management in 2014–15. US Department of Commerce. NOAA Technical Memorandum NOAA-TM-NMFS-SWFSC-531.
- Hill, K. T., P. R. Crone, and J. P. Zwolinski. 2018. Assessment of the Pacific sardine resource in 2018 for U.S. management in 2018–19. US Department of Commerce. NOAA Technical Memorandum NMFS-SWFSC-600. <https://doi.org/10.7289/V5/TM-SWFSC-600>.
- Hunsicker, M. E., L. Ciannelli, K. M. Bailey, J. A. Buckel, J. Wilson White, J. S. Link, T. E. Essington et al. 2011. Functional responses and scaling in predator–prey interactions of marine fishes: contemporary issues and emerging concepts. *Ecol. Lett.* 14:1288–1299.
- International Scientific Committee (ISC). 2017. Stock assessment of albacore tuna in the North Pacific Ocean in 2017. In: Report of the Albacore Working Group Stock Assessment Workshop. International Scientific Committee for Tuna and Tuna-like Species in the North Pacific Ocean, Vancouver, Canada, pp. 103.
- Jacox, M. G., E. L. Hazen, K. D. Zaba, D. L. Rudnick, C. A. Edwards, A. M. Moore, and S. J. Bograd. 2016. Impacts of the 2015–2016 El Niño on the California Current System: Early assessment and comparison to past events. *Geophys. Res. Lett.* 43:7072–7080.
- Jones, M. C., S. R. Dye, J. K. Pinnegar, R. Warren, and W. W. Cheung. 2012. Modelling commercial fish distributions: Prediction and assessment using different approaches. *Ecol. Model.* 225:133–145.
- Kaltenberg, A. M. and K. J. Benoit-Bird. 2009. Diel behavior of sardine and anchovy schools in the California Current System. *Mar. Ecol. Prog. Ser.* 394:247–262.
- Kaplan, I. C., C. J. Brown, E. A. Fulton, I. A. Gray, J. C. Field, and A. D. Smith. 2013. Impacts of depleting forage species in the California Current. *Environ. Conserv.* 40:380–393.
- Kirby, D. S., O. Fiksen, and P. J. B. Hart. 2000. A dynamic optimisation model for the behaviour of tunas at ocean fronts. *Fisheries Oceanography* 9:328–342.
- Kitagawa, T. and Y. Aoki. 2017. Viewpoints of high migratory tuna species ecology. Comment on; Physics of metabolic organization; by M. Jusup et al. *Phys. Life Rev.* 20:54–56.
- Koehn, L. E., T. E. Essington, K. N. Marshall, I. C. Kaplan, W. J. Sydeman, A. I. Szoboszlai, and J. A. Thayer. Developing a high taxonomic resolution food web model to assess the functional role of forage fish in the California Current ecosystem. *Ecol. Modell.* 335:87–100.
- Lam, C. H., A. Nielsen, and J. R. Sibert. 2008. Improving light and temperature based geolocation by unscented Kalman filtering. *Fish. Res.* 9:15–25.
- Laurs, M. R. and J. Lynn. 1977. Seasonal migration of North Pacific albacore, *Thunnus alalunga*, into North American coastal waters: distribution, relative abundance, and association with Transition Zone waters. *Fish. Bull.* 75:795–822.
- Link, J. 2017. A Conversation about NMFS' Ecosystem-Based Fisheries Management Policy and Road Map. *Fisheries* 42:498–503.
- Link, J. S. and H. I. Browman. 2014. Integrating what? Levels of marine ecosystem-based assessment and management. *ICES J. Mar. Sci.* 71:1170–1173.
- Lluch-Belda, D., D. B. Lluch-Cota, S. Hernandez-Vazquez, C. Salinas-Zavala, and R. A. Schwartzlose. 1991. Sardine and anchovy spawning as related to temperature and upwell in the California current system. *Calif. Coop. Oceanic Fish. Invest. Rep.* 32:105–111.
- MacCall, A. D. 1990. Dynamic geography of marine fish populations. Seattle, WA: Washington Sea Grant Program.
- Ménard, F., C. Labrune, Y. J. Shin, A. S. Asine, and F. X. Bard. 2006. Opportunistic predation in tuna: a size-based approach. *Mar. Ecol. Prog. Ser.* 323:223–231.
- Moser, H. G. 2002. Distributional atlas of fish larvae and eggs from Manta (surface) samples collected on CalCOFI surveys from 1977 to 2000 (Vol. 35). California Dept. of Fish and Game, Southwest Fisheries Science Center.
- Muhling, B. A., R. Brill, J. T. Lamkin, M. A. Roffer, S. K. Lee, Y. Liu, and F. Muller-Karger. 2017. Projections of future habitat use by Atlantic bluefin tuna: mechanistic vs. correlative distribution models. *ICES J. Mar. Sci.* 74:698–716.
- Neveu, E., A. M. Moore, C. A. Edwards, J. Fiechter, P. Drake, W. J. Crawford, M. G. Jacox et al. 2016. An historical analysis of the California Current circulation using ROMS 4D-Var: System configuration and diagnostics. *Ocean Model.* 99:133–151.
- Nieto, K., Y. Xu, S. L. Teo, S. McClatchie, and J. Holmes. 2017. How important are coastal fronts to albacore tuna (*Thunnus alalunga*) habitat in the Northeast Pacific Ocean? *Prog. Oceanogr.* 150:62–71.
- Pearce, J. and S. Ferrier, S. 2000. Evaluating the predictive performance of habitat models developed using logistic regression. *Ecol. Model.* 133:225–245.
- Pebesma, E. R. and R. S. Bivand. 2005. Classes and methods for spatial data in R. *R. news* 5 (2), <https://cran.r-project.org/doc/Rnews/>.
- Phillips, A. J., S. Ralston, R. D. Brodeur, T. D. Auth, R. L. Emmett, C. Johnson, and V. G. Wespestad. 2007. Recent pre-recruit Pacific hake (*Merluccius productus*) occurrences in the northern California Current suggest a northward expansion of their spawning area. *Calif. Coop. Oceanic Fish. Invest. Rep.* 48:215–229.
- Pikitch, E., C. Santora, E. A. Babcock, A. Bakun, R. Bonfil, D. O. Conover, P. A. Dayton et al. 2004. Ecosystem-based fishery management. *Science* 305:346–347.

- Pinkas L., M. S. Oliphant, and I. L. K. Iverson. 1971 Food habits of albacore, bluefin tuna, and bonito in California waters. *Fish. Bull.* 152:2–83
- Ridgeway, G. 2017. gbm: Generalized Boosted Regression Models. R package version 2.1.1. 2015. URL: <https://CRAN.R-project.org/package=gbm>.
- Robinson, C. J., F. V. Arenas and G. J. Gomez. 1995. Diel vertical and off-shore-inshore movements of anchovies off the central Baja California coast. *J. Fish Biol.* 47:877–892.
- Rose, K. A., J. Fiechter, E. N. Curchitser, K. Hedstrom, M. Bernal, S. Creekmore, A. Haynie et al. 2015. Demonstration of a fully-coupled end-to-end model for small pelagic fish using sardine and anchovy in the California Current. *Prog. Oceanogr.* 138:348–380.
- Runcie, R. M., B. Muhling, E. L. Hazen, S. J. Bograd, T. Garfield, and G. DiNardo. 2018. Environmental associations of Pacific bluefin tuna (*Thunnus orientalis*) catch in the California Current system. *Fish. Oceanogr.* <https://doi.org/10.1111/fog.12418>.
- Scales, K. L., E. L. Hazen, M. G. Jacox, C. A. Edwards, A. M. Boustany, M. J. Oliver, and S. J. Bograd. 2017. Scale of inference: on the sensitivity of habitat models for wide-ranging marine predators to the resolution of environmental data. *Ecography* 40:210–220.
- Scales, K. L., E. L. Hazen, M. G. Jacox, F. Castruccio, S. M. Maxwell, R. L. Lewison, and S. J. Bograd. 2018. Fisheries bycatch risk to marine megafauna is intensified in Lagrangian coherent structures. *Proc. Natl. Acad. Sci. USA* 115:7362–7367.
- Sepulveda, C. A., A. Knight, N. Nasby-Lucas, and M. L. Domeier. 2010. Fine-scale movements of the swordfish *Xiphias gladius* in the Southern California Bight. *Fish. Oceanogr.* 19:279–289.
- Smith, A. D., C. J. Brown, C. M. Bulman, E. A. Fulton, P. Johnson, I. C. Kaplan, H. Lozano-Montes et al. 2011. Impacts of fishing low-trophic level species on marine ecosystems. *Science* 333:1147–1150.
- Snyder, S. M. (2016). Navigating a seascape: physiological and environmental motivations behind juvenile North Pacific albacore movement patterns. Doctoral dissertation, University of California–San Diego.
- Snyder, S., P. J. Franks, L. D. Talley, Y. Xu, and S. Kohin. 2017. Crossing the line: Tunas actively exploit submesoscale fronts to enhance foraging success. *Limnol. Oceanogr. Lett.* 2:187–194.
- Teo, S. L. H. 2017. Relative abundance indices of juvenile albacore tuna for the US surface fishery in the north Pacific Ocean. ISC/17/ALBWG/09.
- Veneziani, M., C. A. Edwards, J. D. Doyle, and D. Foley. 2009. A central California coastal ocean modeling study: 1. Forward model and the influence of realistic versus climatological forcing. *J. Geophys. Res. Oceans* 114: <https://doi.org/10.1029/2008JC004774>.
- Wade, P. R., V. N. Burkanov, M. E. Dahlheim, N. A. Friday, L. W. Fritz, T. R. Loughlin, T. R., S. A. Mizroch et al. 2007. Killer whales and marine mammal trends in the North Pacific—a re-examination of evidence for sequential megafauna collapse and the prey-switching hypothesis. *Mar. Mammal Sci.* 23:766–802.
- Watanabe, H., T. Kubodera, M. Moku, and K. Kawaguchi. 2006. Diel vertical migration of squid in the warm core ring and cold water masses in the transition region of the western North Pacific. *Mar. Ecol. Prog. Ser.* 315:187–197.
- Watson, J. R., E. C. Fuller, F. S. Castruccio, and J. F. Samhuri. 2018. Fishermen Follow Fine-Scale Physical Ocean Features for Finance. *Front. Mar. Sci.* 5: <https://doi.org/10.3389/fmars.2018.00046>.
- Weber, E. D. and S. McClatchie. 2010. Predictive models of northern anchovy *Engraulis mordax* and Pacific sardine *Sardinops sagax* spawning habitat in the California Current. *Mar. Ecol. Prog. Ser.* 406:251–263.
- Weber, E. D., Y. Chao, and F. Chai. 2018. Performance of fish-habitat classifiers based on derived predictors from a coupled biophysical model. *J. Mar. Syst.* 186:105–114.
- Xu, Y., K. Nieto, S. L. Teo, S. McClatchie, and J. Holmes. 2017. Influence of fronts on the spatial distribution of albacore tuna (*Thunnus alalunga*) in the Northeast Pacific over the past 30 years (1982–2011). *Prog. Oceanogr.* 150:72–78.
- Zaba, K. D. and D. L. Rudnick (2016). The 2014–2015 warming anomaly in the Southern California Current System observed by underwater gliders. *Geophys. Res. Lett.* 43:1241–1248.
- Zwolinski, J. P. and D. A. Demer. 2012. A cold oceanographic regime with high exploitation rates in the Northeast Pacific forecasts a collapse of the sardine stock. *Proc. Natl. Acad. Sci. USA* 109:4175–4180.
- Zwolinski, J. P., D. A. Demer, K. A. Byers, G. R. Cutter, J. S. Renfree, T. S. Sessions, and B. J. Macewicz. 2012. Distributions and abundances of Pacific sardine (*Sardinops sagax*) and other pelagic fishes in the California Current Ecosystem during spring 2006, 2008, and 2010, estimated from acoustic-trawl surveys. *Fish. Bull.* 110:110–122.

DISTRIBUTION OF PELAGIC THALIACEANS, *THETYS VAGINA* AND *PYROSOMA ATLANTICUM*, DURING A PERIOD OF MASS OCCURRENCE WITHIN THE CALIFORNIA CURRENT

REBECCA R. MILLER

Cooperative Institute for Marine Ecosystems and Climate
University of California, Santa Cruz
1156 High Street
Santa Cruz, CA 95060
Rebecca.Miller@noaa.gov

JARROD A. SANTORA

Department of Applied Mathematics
University of California, Santa Cruz
1156 High Street
Santa Cruz, CA 95060

TOBY D. AUTH

Pacific States Marine Fisheries Commission
2030 SE Marine Science Drive
Newport, OR 97365

KEITH M. SAKUMA, BRIAN K. WELLS,
AND JOHN C. FIELD

Fisheries Ecology Division
Southwest Fisheries Science Center
National Marine Fisheries Service
National Oceanic and Atmospheric Administration
110 McAllister Way
Santa Cruz, CA 95060

RICHARD D. BRODEUR

Fisheries Ecology Division
Northwest Fisheries Science Center
National Marine Fisheries Service
National Oceanic and Atmospheric Administration
2030 SE Marine Science Drive
Newport, OR 97365

ABSTRACT

The spatial distribution, abundance, and size variability of two pelagic tunicate species, *Thetys vagina* and *Pyrosoma atlanticum*, were examined from midwater trawl surveys to assess the historical context and geographical aspects of a major mass occurrence event throughout the California Current Large Marine Ecosystem during 2012–19. Off central California, abundance of both species were significantly greater in 2012–19 compared to 1983–2001, and their recent persistent multiyear abundance peaks were unprecedented. Coastwide abundance and distribution of *T. vagina* during 2013–19 was patchy, with no discernible shifts in distribution or changes in mean length. From 2013–18, abundance and distribution of *P. atlanticum* demonstrated a temporal trend of increasing abundance from south to north, and in northern areas, average *P. atlanticum* colony length increased over time. In 2019, high abundances of *P. atlanticum* occurred south of Monterey Bay, but were not found in the northern California Current. We discuss how in situ and regional-scale environmental drivers may have contributed to this recent multiyear gelatinous mass occurrence, and potential consequences to forage community structure and ecosystem function.

INTRODUCTION

Several notable mass occurrences of gelatinous pelagic tunicates have been documented throughout the Northeast Pacific, including the California Current, since 2011 (Wells et al. 2013; Li et al. 2016; Brodeur et al. 2018; Sutherland et al. 2018). Mass occurrences of pelagic tunicates are similar to other high-profile gelatinous species, including Scyphozoans, in that blooms have significant impacts on marine ecosystem dynamics and human activities, which result in trophic alteration of epipelagic

and nearshore food webs (e.g., species diet and interactions), reduction in efficiency of fisheries operations (e.g., damaged fishing nets), and clogging cooling water intakes of coastal hydropower facilities (Brodeur et al. 2018; Brodeur et al. 2019; Iguchi and Kidokoro 2006; Gorman 2017; Eng 2012; Purcell et al. 2007; Graham et al. 2014; Uye and Brodeur 2017). While the population dynamics, spatial ecology, and environmental drivers of pelagic tunicate mass occurrences are not well understood, their rapid population increases are often attributed to anomalous ocean conditions that favor feeding and successful reproduction (Lavaniegos and Ohman 2003; Licandro et al. 2006; Lucas and Dawson 2014). Likewise, it is unclear how pelagic tunicates expand and contract within and beyond their range, or whether extensive population occurrences are a signal of increasing climate trends and variability.

There are numerous species of important, and often understudied, pelagic tunicates of the class Thaliacea, which include salps (family Salpidae) and pyrosomes (e.g., *Pyrosoma atlanticum*). Thaliacean bodies are typically larger than other zooplankton, but are generally lower in carbon relative to their mass, are often transparent, and buoyant to minimize predation risk and energetic expenditures; consequently they tend to have low caloric value relative to body size when compared to crustaceans (Alldredge and Madin 1982; Henschke et al. 2016a). Complex life-history attributes include alternating asexual (solitary forms), sexual (aggregative forms) and overlapping generations for salps; and zooid colonial growth (asexual) and budding (sexual) for pyrosomes (Bone 1998; Henschke et al. 2016a). These reproductive strategies enable pelagic thaliacean populations to persist in the water column at low densities with minimal reproduction during periods of low food supply, yet

undergo exponential population growth and develop spectacular mass occurrences during optimal environmental conditions (Silver 1975; Perissinotto et al. 2007; Loeb and Santora 2012; Henschke et al. 2016a). During periods of mass occurrence, thaliaceans can represent a substantial fraction of zooplankton biomass and organic carbon which impacts energy flow and productivity in marine ecosystems (Silver 1975; Lavaniegos and Ohman 2003; Henschke et al. 2016a), including high filter-feeding rates on very small (10 μ micron) phytoplankton and microzooplankton (Conley et al. 2018) and carbon contributions to deep-sea benthos in the form of fecal pellets and carcasses (Henschke et al. 2013; Smith et al. 2014; Archer 2018).

In the California Current Large Marine Ecosystem (CCLME), the occurrence and long-term variability of pelagic tunicates have been characterized using collections made by the California Cooperative Oceanic Fisheries Investigations (CalCOFI) program (e.g., Berner 1967; Blackburn 1979). From CalCOFI observations, Lavaniegos and Ohman (2003) found that despite representing a substantial volume of the zooplankton volume, thaliaceans represented a more modest, but highly variable, average fraction of total carbon; 5% off southern California, 13% off central California (Lavaniegos and Ohman 2003). Most of this carbon was attributed to salps, as pyrosomes are known to have a more subtropical distribution (their work documented both *P. atlanticum* and *P. aherniosum*) and were less frequently observed in southern and central California waters. In fact, no pyrosomes were documented in half of the years reported in Lavaniegos and Ohman (2003), with a few of the remaining years (5 to 10 years, depending on the region) having either trace or modest numbers. Most years of high pyrosome abundance included anomalously warm events, such as the 1957–59 El Niño, the 1983 El Niño, and the unusual warm/low productivity event in 2005 in central California (Lavaniegos and Ohman 2007). Furthermore, when previous abundance peaks of pyrosomes occurred they lasted for only a year or two, suggesting that environmental conditions were not favorable for sustained multiyear population blooms and expansions. Aside from Brodeur et al. (2018) and Sunderland et al. (2018), who documented recent *P. atlanticum* occurrence in the North Pacific, previous reports that mention thaliaceans off California, Oregon, or Washington do not explicitly document *P. atlanticum* abundance.

Lavaniegos and Ohman (2003, 2007) evaluated time series of ten frequently occurring salp species (order Salpida) in CalCOFI collections and found indications of shifts in species composition between cool- and warm-water species, and greater overall abundance in central and southern California during cool years or time periods. During 1961–64, Hubbard and Percy (1971)

conducted a study off Oregon and documented six commonly occurring salp species, also noting shifts between the one warm year (e.g., 1963) and other cooler years. Hubbard and Percy (1971) encountered *Thetys vagina* in the spring of 1963, noting this species tended to be a cosmopolitan but typically warm-water species. More recently, Peterson and Keister (2002) documented high densities of *Salpa fusiformis* off Oregon in April of 1999. Li et al. (2016) also documented unusually high abundance levels of several northern salp species, including *Salpa aspera* in the Gulf of Alaska during 2011, an event that may have contributed to the massive salp occurrence that was encountered off central and southern California in 2012 (Wells et al. 2013; Smith et al. 2014; Sakuma et al. 2016), for which *Salpa aspera* appears to have been one of the most abundant species (SIO Pelagic Invertebrates Collection Database, accessed Oct. 2019, <https://oceaninformatics.ucsd.edu/zoodb/secure/login.php>).

We investigate the spatiotemporal patterns of a recent mass occurrence of *Thetys vagina* and *Pyrosoma atlanticum* (hereafter referred to as *Thetys* and *Pyrosoma*) throughout the CCLME using data from a midwater trawl survey conducted in late spring. These species are among the largest pelagic tunicates that occur in the CCLME, such that all but the smallest individuals (<9.5 mm) can be sampled with a midwater trawl (Sakuma et al. 2016). Our study examines the distribution, abundance, and size variability of these species before, during, and after the unprecedented large marine heat wave in the eastern North Pacific Ocean of 2014–16 (Bond et al. 2015; Di Lorenzo and Mantua 2016; Jacox et al. 2018). To evaluate their spatio-temporal abundance trends, we enumerated catches in central California from 1983–2001, and coast-wide from 2013–19, allowing us to put in context the relative abundance and distribution of the recent mass occurrence to previous abundance levels. We derive a length-to-weight relationship in order to convert recent estimates of abundance and length composition (length information was not collected on these species prior to 2012) to biomass, and examined *Thetys* and *Pyrosoma* length by year and region to evaluate trends in size over space and time. We then discuss the ecosystem and food-web implications of the bloom patterns and offer possible explanations of oceanic transport mechanisms that may have allowed the *Thetys* and *Pyrosoma* mass occurrence to expand and contract throughout the entire CCLME.

METHODS

Study area

The CCLME is a temperate eastern boundary upwelling ecosystem that is influenced by subarctic and subtropical source water variability (Hickey 1979; King

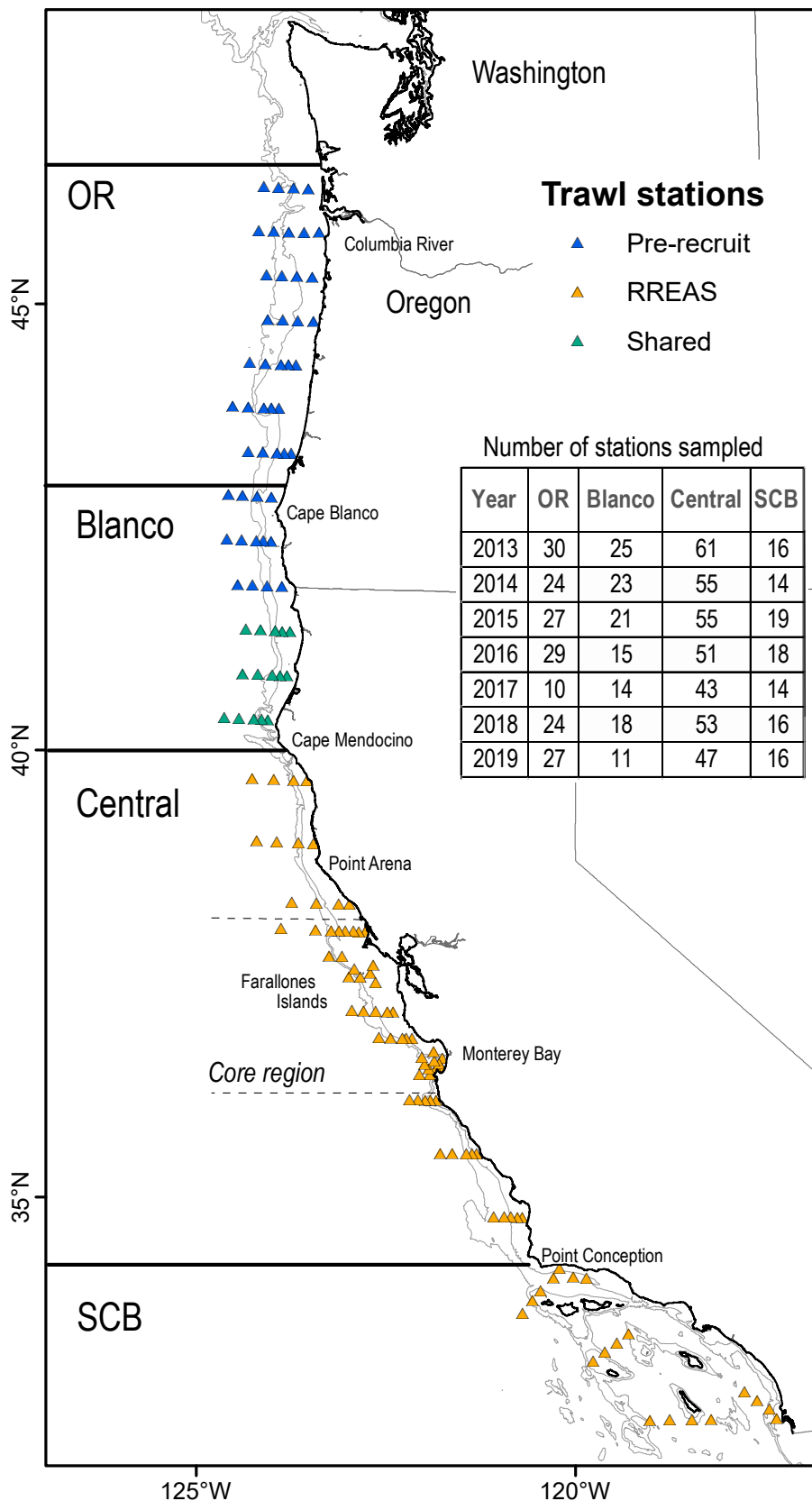


Figure 1. Fixed stations and regions sampled by the RREAS and pre-recruit juvenile rockfish surveys. Depth contours are 200 and 600 m. Table indicates the number of stations sampled for each year. Stations between the dashed line are located in the core region.

et al. 2011). Although the CCLME is highly dynamic, the structure and variability of the pelagic food-web and species assemblages are fairly well understood in terms of biogeography and coastal geomorphology. During spring and summer, southward transport of the California Current increases and physical interactions with coastal promontories influences coastal upwelling, mesoscale ocean circulation, and retention patterns (Checkley and Barth 2009). The primary geographic promontories associated with strong upwelling centers and biogeographic breaks in oceanographic conditions are Cape Blanco, Cape Mendocino, and Point Conception (Checkley and Barth 2009; Fenberg et al. 2015; Gottscho 2016; Friedman et al. 2018), with additional smaller promontories such as Point Reyes and Point Arena in central California affecting regional oceanographic dynamics (fig. 1). These capes and points are associated with upwelling jets and influence the southward and offshore movement of coastal surface waters. The area between Capes Blanco and Mendocino generally exhibits the greatest variability in offshore transport and turbulence. North of Cape Blanco the continental shelf widens and the coast is oriented straight north-south, the dominant direction of wind, such that upwelling is more laminar. South of Cape Mendocino the coast is oriented northeast-southwest and the shelf is narrower, with an increased incidence of coastal prominences resulting in the development of several upwelling centers that also influence meandering upwelling jets. South of Point Conception, the California Current interacts with complex bathymetry (e.g., deep basins and banks) and is characterized by ephemeral areas of upwelling and relaxation. We apply these biogeographic breaks within the CCLME for estimating regional spatiotemporal indicators of *Thetys* and *Pyrosoma* abundance, distribution, and size.

Ecosystem surveys

Micronekton catch data were derived from the combined efforts of the National Oceanic and Atmospheric Administration (NOAA) Rockfish Recruitment and Ecosystem Assessment Survey (RREAS) operated by the Southwest Fisheries Science Center (SWFSC) for California waters, and the pre-recruit survey operated by the Northwest Fisheries Science Center (NWFSC) in waters off Oregon and Washington. The surveys occur annually in May–July during the season of ocean upwelling and increased southward transport. Since 1983, the RREAS has conducted midwater trawls quantifying micronekton species assemblages and regional hydrographic conditions (Ralston et al. 2015; Sakuma et al. 2016; Santora et al. 2017). The RREAS originally sampled the central California coast (Monterey to Point Reyes; Region C fig. 1) and expanded in 2004 to cover the entire California coast. The pre-recruit survey, initiated in 2011

off of Oregon and Washington, has the same objectives and trawl methodology as the RREAS (Brodeur et al. 2019a), and data have been pooled for evaluating spatial distribution and abundance patterns of juvenile rockfish (Field et al. 2017) and epipelagic micronekton forage communities (Friedman et al. 2018). The combination of these surveys provides full spatial coverage of nearly all of the US waters of the entire CCLME (excluding the coastal areas off of Northwest Washington State) for the 2013–19 time period (fig. 1).

Trawls were conducted at fixed sample stations (fig. 1) using a modified Cobb midwater trawl with a target headrope depth of 30 m and a tow speed of ~2 knots. Most RREAS stations are sampled 1–3 times per year (Sakuma et al. 2016), while the pre-recruit stations are sampled once per year (Brodeur et al. 2019). Trawls are typically 15 min in duration and conducted at night to reduce net avoidance by visually-dependent agile organisms and allow for the capture of organisms that exhibit Type I diel vertical migration (i.e., up at night, down during the day). For the RREAS, in instances where pre-trawl visual observations indicate large numbers of jellyfish or other gelatinous zooplankton a 5-minute trawl is conducted and the catch are expanded based on an expansion factor developed from an analysis of coupled 5- and 15-minute trawls (N. Grunloh and K. Sakuma unpublished data). Under very high abundance levels of gelatinous zooplankton, stations are abandoned entirely to avoid significant damage to the sampling gear. Until 2012, either abandoning or reducing trawl durations was done only in response to high abundance levels of scyphozoans (e.g., the Pacific sea nettle, *Chrysaora fuscescens*, and the moon jellyfish, *Aurelia* spp.). However, in 2012 the extraordinarily high number of salps throughout the survey area resulted in several trawls that substantially damaged trawl nets, and a high proportion of the 2012 trawls were shortened to 5 minutes in order to minimize gear damage throughout the survey. Salps and *Pyrosoma* had previously been enumerated from the start of the survey in 1983, with *Thetys* distinguished from all other Salpidae (which were not identified to the species level), and with improved and standardized subsampling methods standardized beginning in 1990 (Ralston et al. 2015; Sakuma et al. 2016). Due to competing priorities and time constraints, enumeration of salps and *Pyrosoma* was halted in 2002, however, the increased abundance of salps in 2012 led to a decision to return to the enumeration of salps and *Pyrosoma* as part of the survey catch analysis.

The number of *Thetys* and *Pyrosoma* captured in trawls are expressed as a standardized catch per unit effort (CPUE), with standardized trawl being the unit of effort. Within the long-term central California study area (core area), the 1983–2001 and 2012–19 sampling periods provided a total of 1,714 trawls averaged by 698

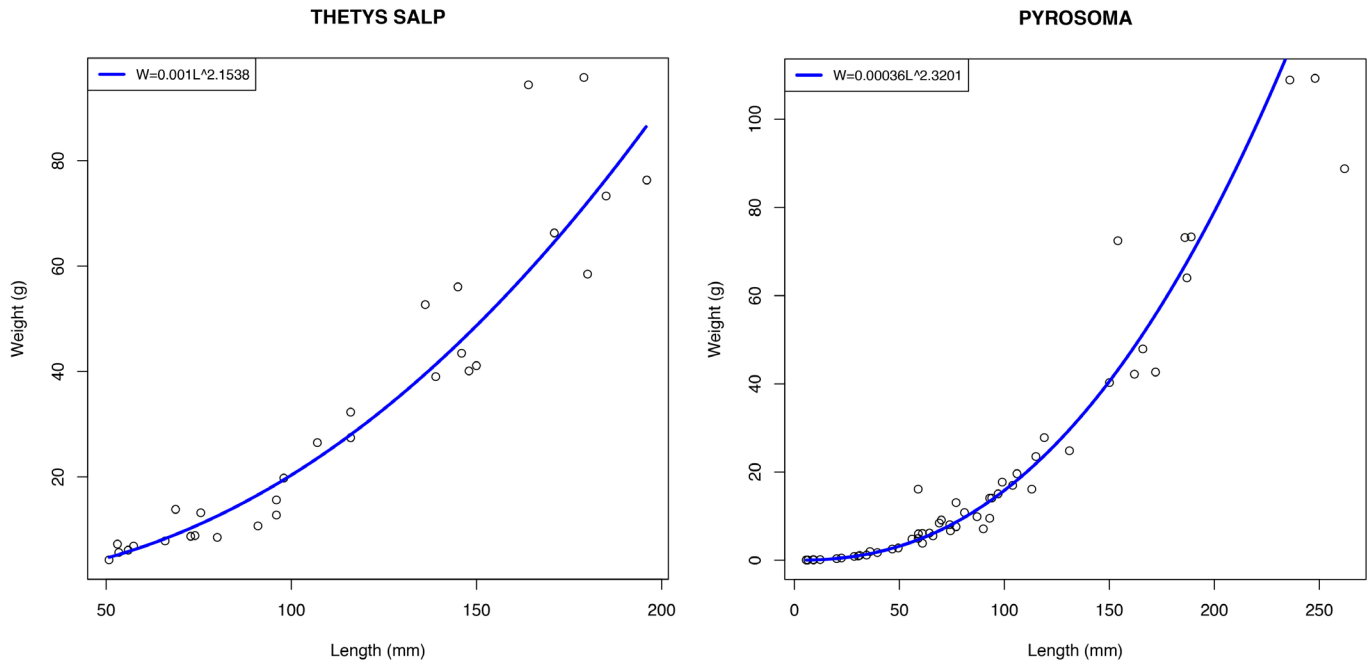


Figure 2. Length-to-weight relationships for *Thetys vagina* and *Pyrosoma atlanticum*.

station-year observations. For the coastwide study, the catches and lengths of *Thetys* and *Pyrosoma* were evaluated for 2013–19 (with 2013 the first year of complete coastwide coverage) using a total of 1,145 trawls averaged by 776 station-year observations. Catches for trawls aborted due to the high prevalence of *Pyrosoma* (2 trawls in 2017) were included by assigning the maximum catch recorded in a trawl for the respective taxa.

Length to biomass conversions of *Thetys vagina* and *Pyrosoma atlanticum*

Estimates of *Thetys* and *Pyrosoma* biomass are presented because length frequency and colony counts are highly variable whereas biomass is comparable among survey regions. For each trawl, length measurements (mm) were taken for a random subset of up to 30 *Thetys* and *Pyrosoma*. Both of these gelatinous species have a sufficiently rigid body structure to allow for reliable length measurements. For length analyses, stations that were sampled once during the year and had a species count of only one *Thetys* individual or *Pyrosoma* colony were removed. Combined, both surveys measured lengths of 6,790 *Thetys* (ranging 8–315 mm) and 13,170 *Pyrosoma* (ranging 3–540 mm), resulting in a total of 419 and 559 positive station-year observations, respectively. We derived a length-to-weight conversion from 30 *Thetys* samples (lengths = 51–196 mm, wet weights = 4.2–95.8 g) and 55 *Pyrosoma* samples (lengths = 5.6–262 mm, wet weights = 0.1–109.3 g) during the 2016 and 2019 survey. We applied the following allometric growth length-to-weight equation to determine relationships: *Thetys*,

Weight = $0.001\text{Length}^{2.1538}$, and *Pyrosoma*, Weight = $0.00036\text{Length}^{2.3201}$ (fig. 2). Relative biomass was calculated by multiplying the average catch (CPUE) by the average weight for each taxa by haul (in g wet weight).

Distribution of *Thetys vagina* and *Pyrosoma atlanticum*

Catch data for *Thetys* and *Pyrosoma* were assessed for spatial variability and presence of regional maxima (i.e., hot spots) for the core region (1983–2001; 2012–19), and coastwide (2013–19). Catches (core area) and standardized relative biomass estimates (coastwide) were spatially interpolated using kriging with inverse distance weighting (Geostatistical Analyst toolbox in ArcMap 10.3; ESRI 2015). For kriging, a spatial neighborhood of five stations was chosen due to the approximate number of stations per survey transect (fig. 1), and interpolated surfaces were buffered at approximately 40 km from each station. For each year, we calculated the mean latitude of the coastwide biomass and denote the station with the maximum catch. Off central California, mean catches for the early years of the survey (1983–2001) were compared to the later survey years (2012–19) using a paired samples t-test. For the coastwide analysis, we calculated Moran's *I* to assess the relative spatial intensity (i.e., degree of spatial clustering of accumulations), of *Thetys* and *Pyrosoma* per year (Santora et al. 2011; Wells et al. 2017). To assess interannual regional variability, CPUE and length data were evaluated using ANOVA, and a post-hoc Tukey's HSD was used to determine mean differences within each biogeographic region by year (R. Core, 2018).

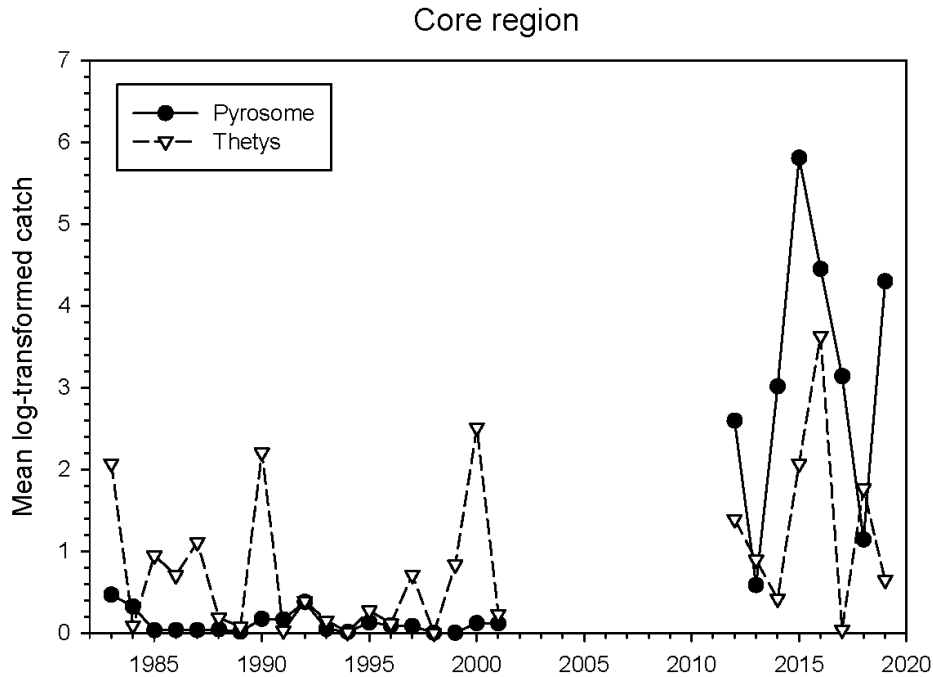


Figure 3. Time series of the annual mean log-transformed catch, $\ln(\text{catch}+1)$, for *Pyrosoma atlanticum* and *Thetys vagina* within the core region for the years 1983–2001 and 2012–19.

RESULTS

Temporal variability off central California

The time series of annual mean catches (CPUE) from 1983–2019 within the core region showed a moderate increase of *Thetys* during the 2012–19 time period, while *Pyrosoma* catches in 2012–19 increased by several orders of magnitude (fig. 3). *Thetys* abundance was variable from 1983–2001, with large peaks in 1983, 1990, 2000, and moderate multiyear peak during 1985–87. The average catch of *Thetys* during 1983–2001 compared to 2012–19 was significantly greater (0.608 ± 0.31 SD and 1.31 ± 0.70 SD, respectively; $p < 0.0001$; fig 3). Particularly noteworthy is the significant difference, by several orders of magnitude, of *Pyrosoma* catches during the 1983–2001 and 2012–19 time periods (0.098 ± 0.07 SD and 2.94 ± 1.37 SD, respectively; t-test $p < 0.0001$; fig. 3). Although *Pyrosoma* catches had low abundances during 1983–2001, they were present in 17 of 19 years, with zero catches 1998 and 1999. Abundance peaks of *Pyrosoma* occurred in 2012, 2014–16, and in 2019; the sustained multiyear peaks in abundance. Comparison of the spatial mean abundance during each time period indicates a greater spatial intensity of catches of both species (fig. 4). Despite the magnitude and variability of catches during the different time periods, both *Thetys* and *Pyrosoma* catches were greater offshore, with lower abundance at inshore stations near Point Reyes, Gulf of

Farallones, and southern Monterey Bay (fig. 4). During the later time period (2012–19) the offshore station at 37.6°N had the regional maximum catches for both *Thetys* and *Pyrosoma* (fig. 4).

Interannual spatial variability within the CCLME

During 2013–19, relative biomass estimates of *Thetys* exhibited enhanced mesoscale variability throughout the CCLME (fig. 5), with the highest catch rates (peaking at 58,729 grams wet weight per haul) from central Oregon through northern-central California (44°–38°N) in 2013. The catch data indicate reduced biomass coastwide in 2014, increasing but patchy coastwide biomass in 2015, and during 2016 the greatest biomass was focused in central California (between Cape Mendocino and Point Conception; peaking at 37,330 grams wet weight per haul; fig 5). *Thetys* biomass was lower in 2017 and 2018, except for in southern California in 2018 (fig 6). *Thetys* biomass in 2019 was reduced in all regions relative to 2018, but biomass was only significantly lower in the southern California region (Tukeys p -value < 0.001) (fig. 6). Stations with maximum *Thetys* biomass were located in central California for four of the seven years evaluated. *Thetys* maximum biomass in 2015 and 2016 occurred offshore at 38.5°N, while in 2014 and 2017 the maximum biomass was offshore at 40.5°N. Moran's I analysis of *Thetys* coastwide biomass indicate significant and

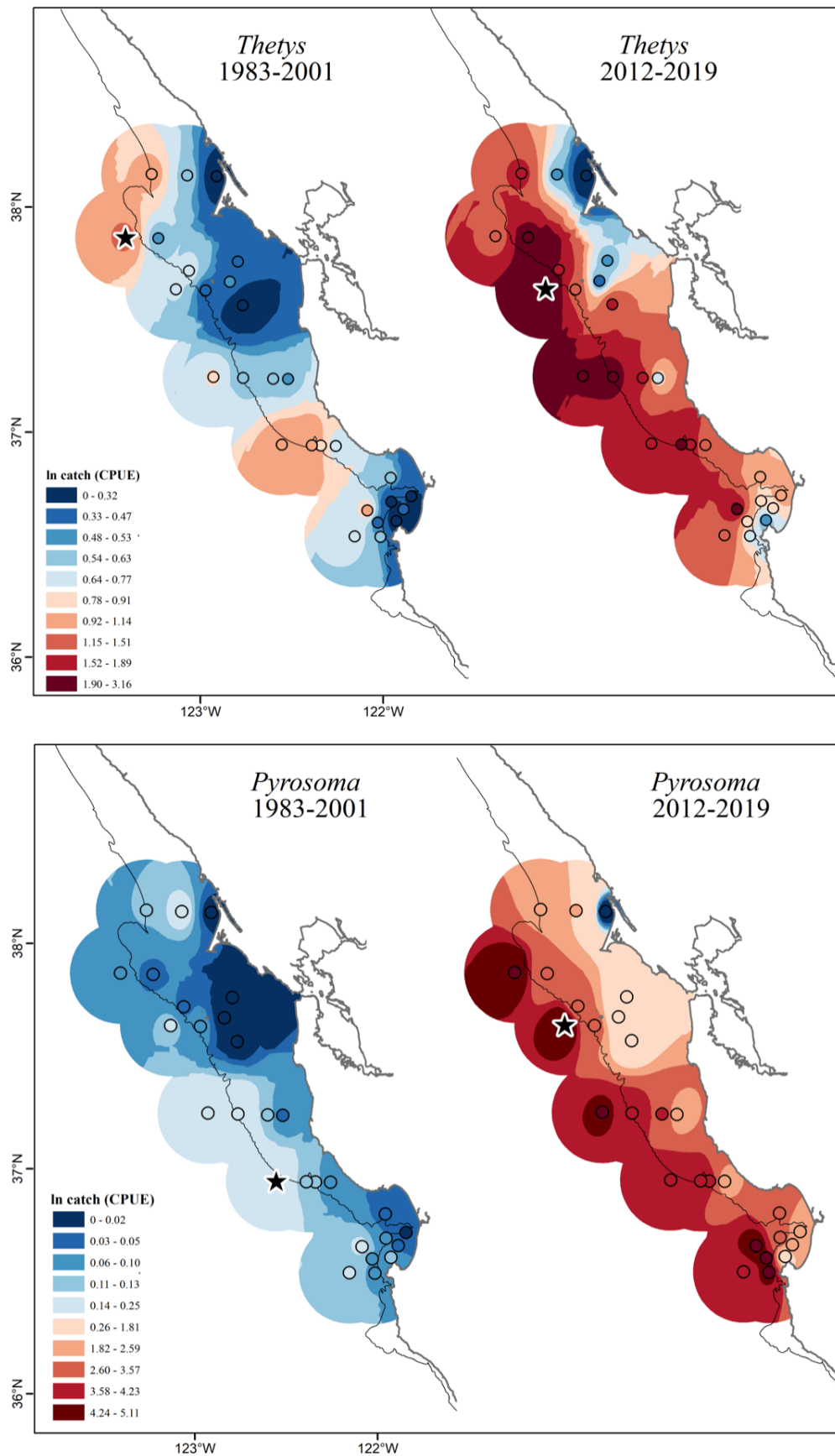


Figure 4. Top panel shows core region spatial mean catches (CPUE) of *Thetys vagina* for two time periods (1983–2001; 2012–19). Bottom panel shows core region spatial mean catches (CPUE) of *Pyrosoma atlanticum* for two time periods (1983–2001; 2012–19). The star represents the station with the maximum catch. The 200 m depth contour is shown. Classification is based on 10% quantiles.

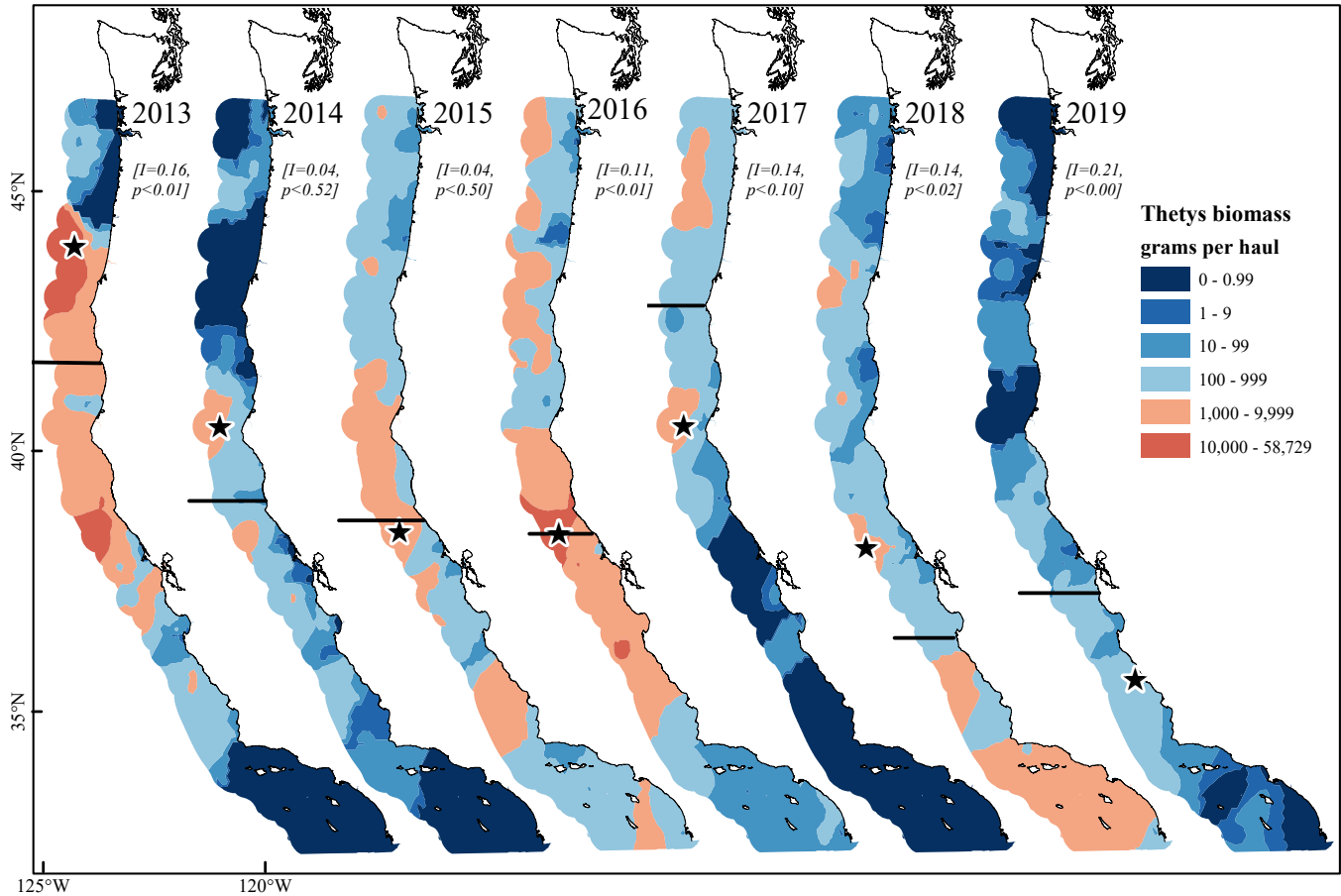


Figure 5. *Thetys vagina* biomass (grams of wet weight per haul) during the May–June period in the California Current Large Marine Ecosystem in 2013–19. The solid line represents the latitude at which the coastwide biomass mean occurred for each year. The star represents the station with the maximum catch. The Moran's *I* and *p*-value are presented for each year, where Moran's *I* value of 0–1 suggests spatial clustering, 0 spatial randomness, –1–0 suggests spatial dispersion.

greater spatial intensity (or clustering), in 2013, 2016, 2018, and 2019 (fig. 5). During those years, the mean latitudinal biomass showed a sequentially increasing pattern from north to south. Moran's *I* values during 2014, 2015, and 2017 indicated less spatial intensity and consistent with a randomly distributed pattern (fig. 5). *Thetys* median lengths were between 100–150 mm and were consistent among regions and years (fig. 7). In the Oregon region, *Thetys* median lengths decreased from 135 mm in 2013 to 114 mm in 2018, but the trend over time was not significant ($p = 0.66$). Lengths for *Thetys* from southern California, central California and Blanco regions had no discernible trend; however, median lengths from the central California region were significantly larger ($p < 0.001$) in 2016 and 2019 when compared to the preceding years.

Pyrosoma relative biomass trends demonstrated a distinct temporal trend of increasing abundance within the CCLME from south to the north during 2013–18, while in 2019 abundance was vastly reduced in northern regions and predominately located in the central region (37°–35°N); (fig. 6, fig. 8). *Pyrosoma* biomass in

2013–14 had a patchy, southern distribution, and were significantly less abundant ($p < 0.0001$) in the central region, when compared to 2015. *Pyrosoma* biomass during the 2015–16 marine heatwave were centered near Monterey Bay in 2015 (mean latitude 36.7°N), while in 2016 the mean latitude was centered in the Cape Blanco region (41.3°N) with biomass abundant in both the central region and the Oregon offshore stations. In 2017 and 2018 *Pyrosoma* biomass was significantly greater ($p < 0.0001$) in the Oregon and Blanco regions, reaching peak relative abundance levels in the waters off of Washington, Oregon, and Northern California (fig. 6, fig. 8). By 2019 only one small pyrosome (19 mm) was found in the Oregon region, while *Pyrosoma* biomass was greatest in the central region and notably the median biomass was slightly larger in this region than it was in 2015 (fig. 6). The stations with *Pyrosoma* maximum catches were located in the Oregon region immediately after the marine heat wave (catches peaking at 73,179 grams wet weight per haul in 2016, 1,655,032 in 2017 and 927,988 in 2018, respectively). The highest catch rates for pyrosomes for both 2015 and 2019 were off-

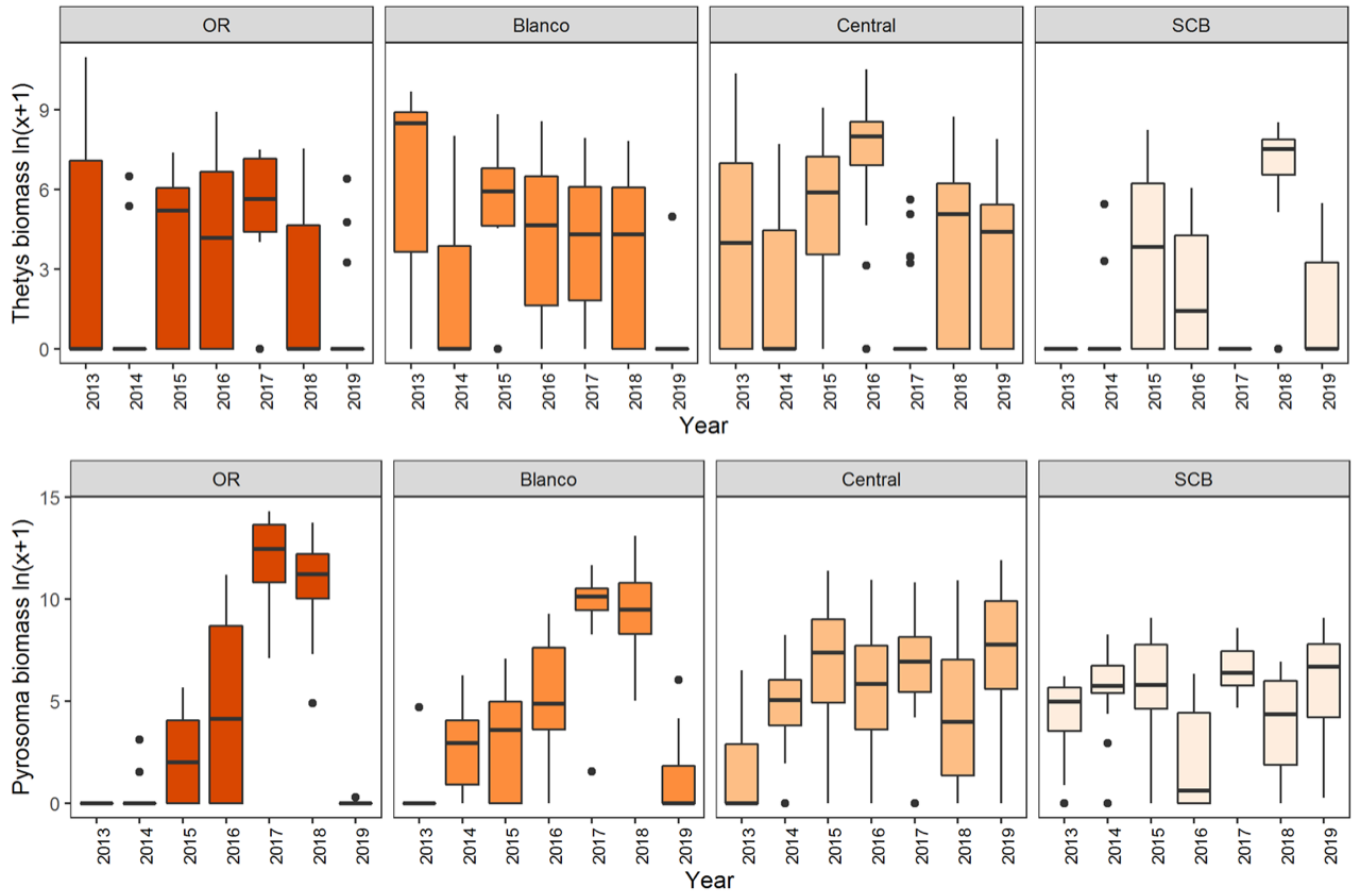


Figure 6. Boxplots of *Thetys vagina* and *Pyrosoma atlanticum* biomass by region and year in the California Current Large Marine Ecosystem during the May–June period. Boxplots show the median, interquartile range (Q25, Q75), whiskers show highest or lowest value, dots represent extreme values.

shore waters of central California (35.7°N). Throughout this time period of increasing abundance there was also an increase in the spatial autocorrelation, or clustering, of *Pyrosoma* which were significantly clustered during and after the marine heat wave from 2015–19, with the highest Moran's *I* value observed in 2019 (0.32; $p < 0.0001$).

Coincident with the positive abundance trends were increasing colony size in northern regions over time and decreasing colony sizes in the SCB region (fig 7). In the SCB region *Pyrosoma* median lengths trended smaller from 2013–17, from 67 mm in 2013 to 19 mm with a low variance ($p < 0.012$) in 2017; while in 2018–19 median lengths were larger (50 and 69 mm, respectively). Off central California, median *Pyrosoma* lengths were similar (53, 35, 45, and 38 mm) during the period from 2013 to 2016, while from 2017–19, lengths increased to 111, 79 and 112 mm, respectively ($p < 0.0001$). In the Blanco region, *Pyrosoma* lengths significantly increased from a median of 49 mm in 2014 to 138 mm in 2018 ($p < 0.0001$), while in 2019 median lengths were slightly smaller (113 mm). Off Oregon, *Pyrosoma* colony median lengths increased by a factor of three, from 40 to 125 mm ($p < 0.03$) from 2014 to 2017.

An unusual, rarely encountered *Pyrosoma* species in the RREAS survey, was caught in 2019 off of Davenport, California, (lat 37.0° N) with a station bottom depth of 128 m. It was identified as *Pyrosomella verticillata*, based on the keys in vanSoest 1981 and Bone 1998 (L. Sala, Scripps Institution of Oceanography, pers. comm.). *Pyrosomella verticillata* is known to occur in the warm Indo–West Pacific waters (vanSoest 1981), however in 2008 a colony was found in the southwest Atlantic Ocean (Carvalho and Bonecker 2008) indicating the potential for greater oceanic distribution.

DISCUSSION

Our study described the spatial and temporal aspects of the extraordinarily large mass occurrence of two pelagic thaliacean taxa, *T. vagina* and *P. atlanticum* throughout the CCLME. As observed in our long-term monitoring area off central California, both species had significantly greater catches during 2012–19 compared to the 1983–2001 time period. Although *T. vagina* displayed 3 strong abundance peaks during 1983–2001, they were largely ephemeral, but their abundance persisted and increased in frequency during 2012–19. On the other

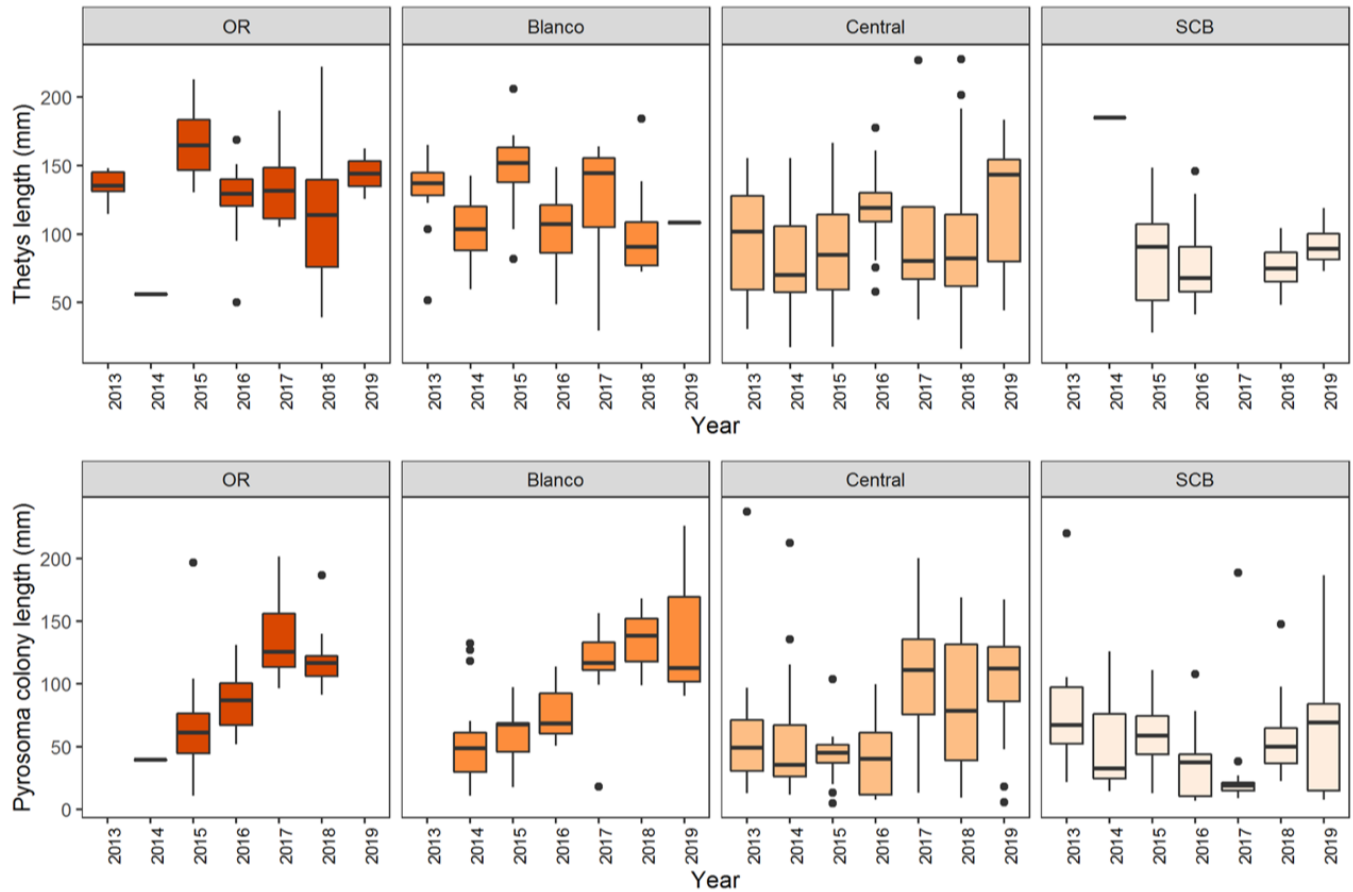


Figure 7. Boxplots of *Thetys vagina* and *Pyrosoma atlanticum* lengths (mm) in the California Current Large Marine Ecosystem by region and year during the May–June period. Boxplots show the median, interquartile range (Q25, Q75), whiskers show highest or lowest value, dots represent extreme values.

hand, *P. atlanticum* displayed no peaks until 2012 and were then persistent for 8 years. Although oceanographic variables were not formally evaluated in this study, these strong interdecadal differences suggest that ocean conditions played some role in facilitating the recent multiyear persistent blooms of these species. Ocean and climate conditions within the central–northern California Current during 1983–2001 were characterized by several strong ENSO events and largely considered a positive (warm) phase of the Pacific Decadal Oscillation, which generally leads to above average ocean temperatures in the California Current and Northeastern Pacific ocean (Peterson and Schwing 2003; Checkley and Barth 2009). Ocean conditions during 2012–19 were variable, having a mixture of both strong upwelling conditions and sustained warming events (Wells et al. 2013; Bond et al. 2015; Di Lorenzo and Mantua 2016; Thompson et al. 2018), suggesting that temperature alone is likely not responsible for driving mass occurrence. Given the passive movement and nature of these organisms, it seems more likely that anomalous ocean current transport, combined with food availability (e.g., phytoplankton species and particle size), may have supported and sus-

tained the persistent multiyear blooms (Lavaniegos and Ohman 2003; Henschke et al. 2016).

Our study provides novel insight on the extent of the sustained mass occurrence event across the extent of a large marine ecosystem. Coastwide catch patterns from 2013–19 generally demonstrate a patchy distribution for *Thetys* and an increase in northward distribution, abundance, and significant clustering for *Pyrosoma*. There were notable latitudinal clines in size observed for *Pyrosoma* over space and time, with no such patterns in size observed for *Thetys*. Oceanographic conditions varied substantially within the California Current during 2013–19, ranging from one of the strongest upwelling years on record (2013), a multiyear marine heat wave (2014–16), a strong El Niño (2016), and a return to near average upwelling conditions (2017–19), but with pronounced differences in sea temperature and upwelling between northern and southern regions (Wells et al. 2013; Thompson et al. 2018). The northward and onshore expansion of biomass and size variability of *Pyrosoma* may be in response to the large marine heatwave of 2015–16 (Brodeur et al. 2019a). Importantly, other species of salps appeared in unprecedented

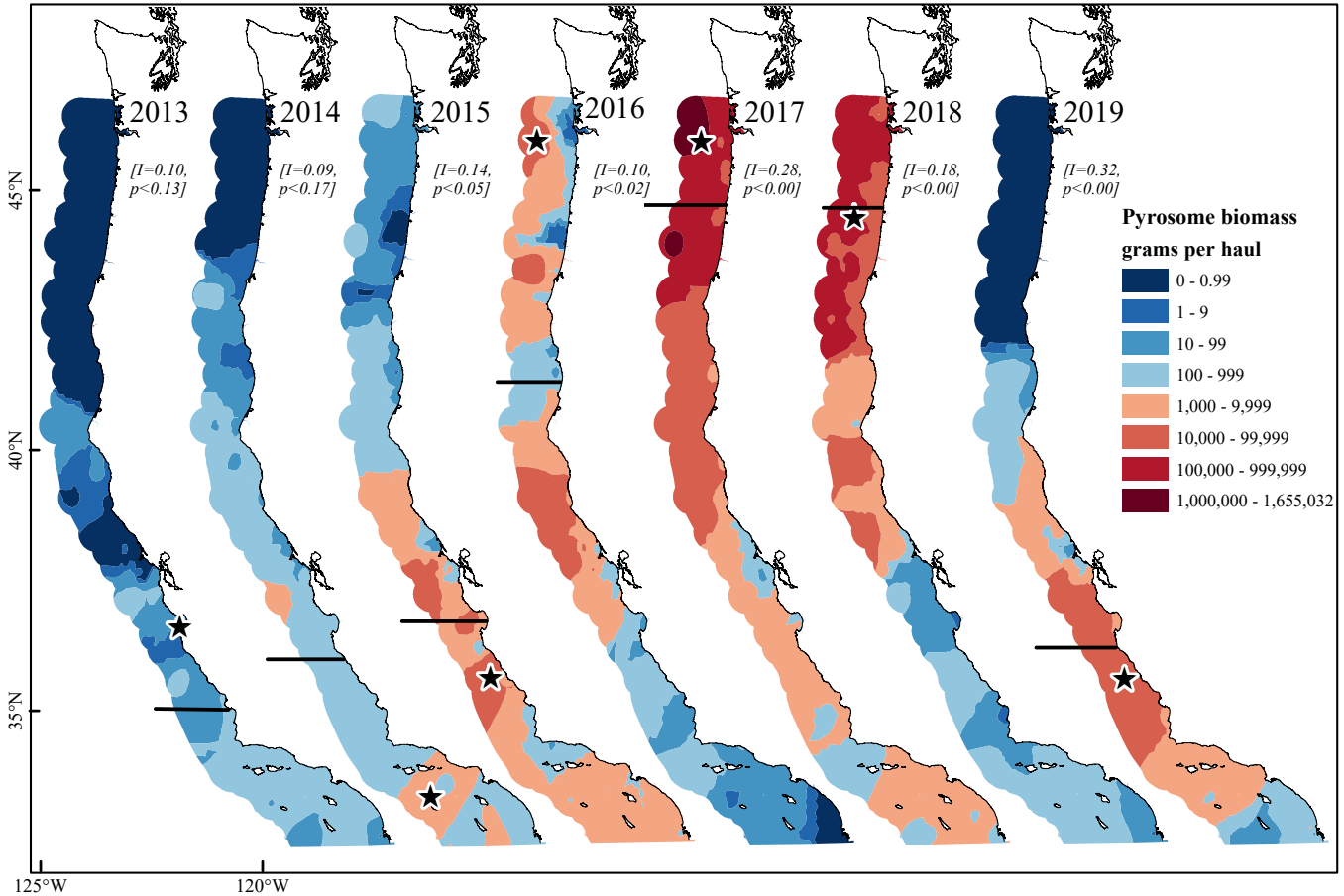


Figure 8. *Pyrosoma atlanticum* biomass (grams of wet weight per haul) during the May–June period in the California Current Large Marine Ecosystem from 2013–19. The solid line represents the latitude at which the coastwide biomass mean occurred for each year. The star represents the station with the maximum catch. The biomass hotspot indicates a chronological south to north progression. The Moran's *I* and *p*-value are presented for each year, where Moran's *I* value of 0–1 suggests spatial clustering, 0 spatial randomness, –1–0 suggests spatial dispersion.

numbers throughout the northeast Pacific Ocean since 2011 (Wells et al. 2013; Smith et al. 2014; Li et al. 2016; Thompson et al. 2018), therefore the mass occurrence of pelagic thaliaceans were clearly not limited to these two taxa alone throughout this time period.

The persistent multiyear high abundance of several taxa of gelatinous zooplankton within the CCLME during this seven year period is unusual. There is limited information on what conditions promote mass occurrence of pelagic tunicates in the CCLME, which tend to exhibit episodic population peaks between longer time periods of lower abundance. Other pelagic tunicate blooms around the world have episodic duration and timing over days (Deibel 1985), months (Boero et al. 2013), or years (Lavaniegos and Ohman 2007; Loeb and Santora 2012), and such blooms could be indicators of the prevailing oceanographic conditions. Although both *Thetys* and *Pyrosoma* blooms appear to have preceded the 2014–16 marine heat wave in the Northeast Pacific Ocean, which was one of the strongest and most prolonged events on record (Hobday et al. 2018), the

question of what effect the marine heat wave may have had in enhancing or extending the ongoing mass occurrence is worthy of consideration. For example, it is likely that some of the salps described in the 2012 bloom off California (Wells et al. 2013) originated from the 2011 mass occurrence described in the Gulf of Alaska (Li et al 2016). Similarly, the tremendous abundance and apparently historically unprecedented spatial expansion of *Pyrosoma* were largely concurrent with the onset of the large marine heat wave, which could have facilitated the northward expansion of these organisms. By 2017, Brodeur et al. (2018) reported *Pyrosoma* in anomalously high abundance throughout the Northeast Pacific, including the west coast of Vancouver Island and into the northern Gulf of Alaska. *Pyrosoma* are thought to be associated with advection of offshore warm water into coastal waters (Brodeur et al. 2018; 2019, Sutherland et al. 2018). Due to the consistency of our sampling, we were able to track this northward expansion first into northern California and eventually up to the northern end of our sampling area (i.e., southern Washington),

with concurrent decreases in populations off central and southern California.

We provide an assessment of size-related life-history characteristics for *Thetys* and *Pyrosoma* throughout the CCLME (from 32° to 46°N). While *Thetys* lengths were generally similar in space and time throughout the CCLME, their lengths were significantly larger within the central California region in 2016. This was towards the end of the marine heat wave which had the highest *Thetys* catches within central California, possibly indicating favorable ocean conditions suited for *Thetys* reproduction and growth. *Pyrosoma* sizes off southern California became progressively smaller from 2013–17, perhaps indicating that ocean conditions were ideal for reproductive sexual budding and seeding in these areas. On the other hand, north of central California, *Pyrosoma* lengths increased during the 2015–18 mass occurrence, possibly indicating that sufficient food resources allowed for zooid colonial growth (asexual). For example, although *Pyrosoma* lengths in the northern California Current were of literature-based estimates of sexual reproductive size (e.g., >40 mm; van Soest 1981), the variance of the lengths in 2016–18 were not below 40 mm, possibly indicating younger, newly seeded *Pyrosoma* were not as prevalent. While it is unknown what the life span of *Pyrosoma* colonies are or whether colony size is related to age, Henschke et al. (2019) reported that food availability contributes to the sustained growth and development of *Pyrosoma* mass occurrences. These species have particular filter feeding efficiencies, and although phytoplankton size and composition is not available with this data set, the species composition and size structure of phytoplankton and zooplankton communities could be influencing the population dynamics of these species.

Other unknowns are whether the catch, lengths, and lifecycle stage of these taxa differ throughout the water column, and specifically whether trawl sampling at night (target depth layer 30 m) was optimal for collecting these taxa. *Pyrosoma* are known to undertake large diel vertical migrations of up to 1,000 m (Henschke et al. 2019), with the depth and timing of migration related to colony size (Andersen and Sardou 1994). Daytime video observations off Oregon show that *Pyrosoma* was most abundant at a depth of between 25 and 35 m during the day but this species is known to migrate closer to the surface at night (Sutherland et al. 2018; Blondheim et al. unpublished data). Although the survey trawls fished near the surface during the short recovery period, we believe that the majority of catches were made at the target depth layer, and the trawls may have missed a substantial part of the biomass (and other size classes) of both *Thetys* and *Pyrosoma* at other depth layers. While this analysis is the largest spatial scale of *Thetys* catches on the US West Coast that we are aware of, the lifecycle stage of *Thetys*

were not identified as solitary or aggregate forms. Not distinguishing between the reproduction forms could be a contributing factor as to why no discernible patterns were found for *Thetys* biomass and lengths.

An important next step in quantifying the determinants of coastwide variability and potential interactions of thaliaceans within the forage assemblage is to identify the connection between source water variability and their occurrence and distribution (Schroeder et al. 2019). There is some regional work to provide a foundation for this endeavor. Lavaniegos and Ohman (2007) showed that the decline in thaliaceans inferred from CalCOFI observations was associated with an increase in water column density stratification, supporting the need to look more closely at source waters and transport trends to resolve abundance and seeding/distribution patterns relative to oceanographic drivers. To further support the oceanographic connectivity between the southern and central California sectors of the CCLME, Lavaniegos and Ohman (2007) noted that a large fraction of the interannual variability of zooplankton is shared between sectors. However, the CalCOFI data for most years cannot be used for trends in fine scale distribution or patchiness for either central or southern California, as station-specific zooplankton are pooled into a single large grouping, enumerated and aggregated (Lavaniegos and Ohman 2003).

Given the magnitude of the recent thaliacean mass occurrence compared to past abundance trends, it is likely that during the 2012–19 time period, thaliaceans represented a far greater percentage of total productivity and standing carbon than the 5%–8% that was previously estimated by Lavaniegos and Ohman (2007) for the southern and central sectors of the CCLME. For example, *Thetys vagina* is poorly sampled in typical plankton sampling gear; the species was identified only twice (1955 and 1964) in the CalCOFI time series through 2003, despite being encountered at relatively high abundances during the years 1983, 1990, and 1999 within midwater trawls reported in this study. Other previous studies of *Thetys vagina* occurrences have been based on data collected from larger sampling devices, such as other midwater trawl (10 meter diameter otter trawls) surveys (Iguchi and Kidokoro 2006) or larger (1 m²) plankton net surveys (Henschke et al. 2016b). Although our results are informative regarding the relative abundance and spatial distribution patterns of *Thetys* and *Pyrosoma* from 2013–19 throughout the CCLME, some type of analysis or calibration to enable robust estimates of abundance per unit area (e.g., cubic meters sampled or square meters of water column) will be necessary to evaluate the potential impact of these mass occurrences quantitatively, and to compare our abundance estimates to those available from other time series. Such estimates could not be developed in this analysis, for despite the fact that there are estimates

of net opening and area swept by our gear, it is highly unlikely that these low motility pelagic tunicates are fully selected by the total mouth opening of the trawl. Rather, the selectivity of the gear is likely to vary substantially with the size of the target organism, as net mesh sizes are fairly large (15.2 cm, or 6 inches) at the net opening, and are reduced to 6.7 cm (3 inches) and 3.8 cm (1.5 inches) as the net tapers to the fine (0.95 cm, 3/8 inch) cod-end liner. Thus, as with many other micronekton, the selectivity of the target species will vary by size, presumably to a much greater extent for the highly variable (by size) *Pyrosoma* colonies relative to *Thetys*, which generally have a more limited size range. Consequently, future efforts to estimate the absolute (rather than relative) biomass of thaliaceans over time and space using trawl survey data will require careful evaluation of selectivity and catchability patterns, which may require calibration with survey gear that is more typically used for sampling gelatinous zooplankton (Kwong et al. 2018).

Ecosystem implications of the gelatinous pelagic tunicate mass occurrence

Pelagic tunicate mass occurrence are known to alter macro-zooplankton communities and functioning of marine food webs (Allredge and Madin 1982, Drits et al. 1992; Perissinotto et al. 2007). *Pyrosoma* are aggregate filter feeders with each zooid rapidly consuming pico- and microplankton. Areas with high *Pyrosoma* biomass have been demonstrated to cause the depletion of chlorophyll-*a* standing stocks (Drits et al. 1992; Perissinotto et al. 2007, Décima et al. 2019). However, these studies were generally conducted in oceanic, low productivity regions, therefore the impact of *Pyrosoma* grazing in highly productive regions like the California Current is not well known. Similarly, there is limited information on feeding in *Thetys* populations. Based on a small sample size of individuals collected in the Japan Sea, Iguchi and Kidokoro (2006) determined that *Thetys* feed mainly on small phytoplankton and tintinnids, but also consumed a small number of copepods. Overall, large salp blooms have been shown to have negative effects on lower trophic level productivity in many ecosystems (Allredge and Madin 1982; Perissinotto and Pakhomov 1998; Henschke et al. 2016b).

Due to their large individual size and relatively low energy content, persistent thaliacean mass occurrence may have major implications for mid- and higher-trophic level predators in marine food webs, as these gelatinous organisms may not be appropriate prey items for mobile predators that require high lipid or high caloric values (e.g., salmon, seabirds, and marine mammals). However, they may be suitable for many other predators, such as leatherback turtles (*Dermochelys coriacea*; Hays et al. 2009; Jones et al. 2012) and many

species of rockfish (*Sebastes* spp.; Adams 1987; Lee and Sampson 2009; Chiu 2018). For example, both Adams (1987) and Lee and Sampson (2009) found that widow rockfish (*S. entomelas*) off California and Oregon preyed heavily on salps, which represented from 30% to >90% of diet volume in those studies depending on year and season. Lee and Sampson (2009) found that yellowtail rockfish (*S. flavidus*) also preyed heavily on gelatinous zooplankton off Oregon, and Chiu (2018) found the same for yellowtail rockfish in central California during 2013 and 2014. The Chiu (2018) study was the only study known to the authors to include substantial rockfish predation on *Pyrosoma* as well as salps, which comprised >5% of the diet by number and nearly 8% by weight, as might be expected given the relative rarity of *Pyrosoma* prior to the recent mass occurrence. Several small pelagic fishes such as northern anchovies (*Engraulis mordax*), Pacific sardines (*Sardinops sagax*), and Pacific herring (*Clupea pallasii*) consumed a mainly gelatinous diet during the recent marine heat wave, relative to their normal diet of mostly crustaceans during cooler year (Brodeur et al. 2019b). Zuercher and Galloway (2019) demonstrated that pelagic tunicates and other offshore macrozooplankton represent important energetic subsidies to nearshore kelp forests. Given these findings, it seems likely that thaliaceans represent a fairly important source of forage for many rockfish and other predators during periods of high abundance.

A substantial fraction of the carbon associated with thaliacean mass occurrence is likely to be exported to other food webs to be used by non-pelagic, benthic predators (Lebrato and Jones 2009; Archer et al. 2018; Brodeur et al. 2018). Specifically, Smith et al. (2014) showed that the 2012 salp mass occurrence, and subsequent die-off in Monterey Bay was an unprecedented event with respect to carbon export to deep water benthic habitats. It has also been noted that the fecal pellets and carcasses of larger salps (such as *Thetys*) and *Pyrosoma* tend to sink considerably faster than those of smaller species or individuals (Smith et al. 2014; Henschke et al. 2016a; Henschke et al. 2016b). Pelagic tunicates also provide shelter for species during certain life stages, including juvenile medusa fish (*Icichthys lockingtoni*), juvenile small-eye squaretail (*Tetragonurus cuvieri*), hyperiid amphipods (*Phronima*), and tuberculate octopus (*Ocythoe tuberculata*) (Love 2011, and as observed on RREAS survey). Thus, the role of these gelatinous organisms with respect to both their position in the food web, in the overall carbon cycle and community structure warrants continued investigation into both the oceanographic drivers and consequences of their distribution and population dynamics through effective monitoring efforts. Given the projections

of increased warming and expectations of larger and more sustained marine heat waves in the California Current and the global ocean in general (Joh and Di Lorenzo 2017; Frölicher and Laufkötter 2018), we may anticipate that these mass occurrences may continue and perhaps intensify in the coming decades, with unknown consequences.

ACKNOWLEDGEMENTS

We would like to thank the captains, crew, and participating scientists on all of the research vessels (e.g., RV *Bell M. Shimada*, RV *Reuben Lasker*, RV *Ocean Starr*) used for the juvenile rockfish surveys. We especially thank I. Iglesias who wrote the R code for the allometric growth length-to-weight relationship curve, and L. Sala who identified *Pyrosomella verticillata*. V. J. Loeb, J. Bizzarro, M. Monk, and 2 anonymous reviewers provided helpful comments and insight in improving the quality of this manuscript.

LITERATURE CITED

- Adams, P. B. 1987. Diet of widow rockfish (*Sebastes entomelas*) in northern California. In: Lenarz, W. H., and D. R. Gunderson (Eds.) *Widow rockfish: proceedings of a workshop*. NOAA Technical Report, NMFS 48, pp. 37–41.
- Allredge, A. L., and L. P. Madin. 1982. Pelagic tunicates: unique herbivores in the marine plankton. *BioScience*. 32(8):655–663.
- Andersen, V., and J. Sardou. 1994. *Pyrosoma atlanticum* (Tunicata, Thaliacea): diel migration and vertical distribution as a function of colony size. *J. Plankton Res.* 16:337–349.
- Archer, S. K., A. S. Kahn, S. P. Leys, T. Norgard, F. Girard, C. Du Preez, and A. Dunham. 2018. Pyrosome consumption by benthic organisms during blooms in the NE Pacific and Gulf of Mexico. *Ecology*. 99:981–984.
- Berner, L. O. 1967. Distributional atlas of Thaliacea in the California Current Region. Calif. Coop. Ocean. Fish. Invest. Rep. Atlas 8.
- Blackburn, M. 1979. Thaliacea of the California Current region: relations to temperature chlorophyll, currents and upwelling. Calif. Coop. Ocean. Fish. Invest. Rep. 20:184–194.
- Boero, F., G. Belmonte, R. Bracale, S. Fraschetti, S. Piraino, and S. Zampardi. 2013. A salp bloom (Tunicata, Thaliacea) along the Apulian coast and in the Otranto Channel between March–May 2013. *F1000Research*, 2:181.
- Bond, N. A., M. F. Cronin, H. Freeland, and N. Mantua 2015. Causes and impacts of the 2014 warm anomaly in the NE Pacific. *Geophys. Res. Lett.* 42:3414–3420, doi:10.1002/2015GL063306.
- Bone, Q. 1998. *The Biology of Pelagic Tunicates*. Oxford Univ. Press, Oxford.
- Brodeur, R., I. Perry, J. Boldt, L. Flostrand, M. Galbraith, J. King, J. Murphy, K. Sakuma, and A. Thompson. 2018. An unusual gelatinous plankton event in the NE Pacific: The Great Pyrosome Bloom of 2017. *PICES Press*. 26(1):22–27.
- Brodeur, R. D., T. D. Auth, and A. J. Phillips. 2019a. Major shifts in pelagic community structure in an upwelling ecosystem related to an unprecedented marine heatwave. *Front. Mar. Sci.* 6:212, doi:10.3389/fmars.2019.00212.
- Brodeur, R. D., M. E. Hunsicker, A. Hann, and T. W. Miller. 2019b. Effects of warming ocean conditions on feeding ecology of small pelagic fishes in a coastal upwelling ecosystem: a shift to gelatinous food sources. *Mar. Ecol. Prog. Ser.* 617–618:149–163.
- Carvalho, P. F., and S. L. Bonecker. 2008. Tunicata, Thaliacea, Pyrosomatidae, *Pyrosomella verticillata* (Neumann, 1909): first record from the Southwest Atlantic Ocean. *Check List* 4(3):272–274.
- Checkley, D. M., and J. A. Barth. 2009. Patterns and processes in the California Current system. *Prog. Oceanogr.* 83:49–64.
- Chiu, J., 2018. Diets and stable isotope signatures of yellowtail rockfish (*Sebastes flavidus*) in Central California. Masters of Science Thesis, Moss Landing Marine Laboratory, San Jose State University.
- Conley, K. R., F. Lombard, and K. R. Sutherland. 2018. Mammoth grazers on the ocean's minuteness: a review of selective feeding using mucous meshes. *Proc. R. Soc. B.* 285:20180056, doi:org/10.1098/rspb.2018.0056.
- Décima, M., M. R. Stukel, L. López-López, and M. R. Landry. 2019. The unique ecological role of pyrosomes in the Eastern Tropical Pacific. *Limnol. Oceanogr.* 64:728–743.
- Deibel, D. 1985. Dolioids Blooms of the pelagic tunicate, *Doliolletta gegenbaui*: Are they associated with Gulf Stream frontal eddies? *J. of Marine Res.*, 43(1) 211–236.
- Di Lorenzo, E., and N. Mantua. 2016. Multi-year persistence of the 2014/15 North Pacific marine heatwave. *Nat. Clim. Chang.* 6:1042–1047, doi:10.1038/nclimate3082.
- Drits, A. V., E. G. Arashkevich, and T. N. Semenova. 1992. *Pyrosoma atlanticum* (Tunicata, Thaliacea): grazing impact on phytoplankton standing stock and role in organic carbon flux. *J. Plankton Res.* 14:799–809.
- Eng, James. “Diablo Canyon Nuclear Plant in California Knocked Offline by Jellyfish-Like Creature Called Salp.” *NBC News*. April 27, 2012. http://usnews.nbcnews.com/_news/2012/04/27/11432974-diablo-canyon-nuclear-plant-in-california-knocked-offline-by-jellyfish-like-creature-called-salp?lite. Accessed September 23, 2019.
- ESRI. 2015. ArcGIS 10.3 Environmental Systems Research Institute. Redlands, Calif.
- Field, J. C., E. J. Dick, N. Grunloh, X. He, K. Sakuma, and S. Ralston. 2018. Coastwide Pre-Recruit Indices from SWFSC and NWFS/PWCC Midwater trawl Surveys (2001–16). Appendix B in He, X. and J. C. Field. Stock assessment update: Status of bocaccio, *Sebastes paucispinis*, in the Conception, Monterey and Eureka INPFC areas for 2017. Pacific Fishery Management Council, Portland, Oregon. 224 p. <https://www.pcouncil.org/groundfish/stock-assessments/by-species/bocaccio-rockfish/>.
- Friedman, W. R., J. A. Santora, I. D. Schroeder, D. D. Huff, R. D. Brodeur, J. C. Field, and B. K. Wells. 2018. Environmental and geographic relationships among salmon forage assemblages along the continental shelf of the California Current. *Mar. Ecol. Prog. Ser.* 596:181–198.
- Frölicher, T. L., and C. Laufkötter. 2018. Emerging risks from marine heat waves. *Nature Communications* 9, Article number: 650.
- Gorman, Steve. “Jellied sea creatures confound scientists, fisherman on U.S. Pacific Coast.” *Reuters*. June 27, 2017. <https://www.reuters.com/article/us-environment-pyrosomes/jellied-sea-creatures-confound-scientists-fishermen-on-u-s-pacific-coast-idUSKBN191145>. Accessed September 23, 2019.
- Gottscho, A. D. 2016. Zoogeography of the San Andreas Fault system: Great Pacific Fracture Zones correspond with spatially concordant phylogeographic boundaries in western North America. *Biol. Rev.* 91: 235–254. doi:10.1111/brv.12167.
- Graham, W. M., S. Gelcich, K. L. Robinson, C. M. Duarte, L. Brotz, J. E. Purcell, L. P. Madin, H. Mianzan, K. R. Sutherland, S. Uye, K. A. Pitt, C. H. Lucas, M. Boegeberg, R. D. Brodeur, and R. H. Condon. 2014. Linking human well-being and jellyfish: ecosystem services, impacts and societal responses. *Front. Ecol. Environ.* 12:515–523.
- Hays, G. C., M. R. Farquhar, P. Luschi, S. L. Teo, and R. M. Thys. 2009. Vertical niche overlap by two ocean giants with similar diets: Ocean sunfish and leatherback turtles. *J. Exp. Mar. Biol. Ecol.* 370(1–2):134–143.
- Henschke N., D. A. Bowden, J. D. Everett, S. P. Holmes, R. J. Kloser, R. W. Lee, and I. M. Suthers. 2013. Salp-falls in the Tasman Sea: a major food input to deep-sea benthos. *Mar. Ecol. Prog. Ser.* 491:165–175. <https://doi.org/10.3354/meps10450>.
- Henschke, N., J. D. Everett, A. J. Richardson, and I. M. Suthers. 2016a. Re-thinking the role of salps in the ocean. *Trends Ecol. Evol.* 31(9):720–733.
- Henschke, N., J. D. Everett, and I. M. Suthers. 2016b. An observation of two oceanic salp swarms in the Tasman Sea: *Thetys vagina* and *Cyclosalpa affinis*. *Mar. Biodiv., Rec.*, 9(1), 21.
- Henschke, N., E. A. Pakhomov, L. E. Kwong, J. D. Everett, L. Laiolo, A. R. Coghlan, and I. M. Suthers. 2019. Large vertical migrations of *Pyrosoma atlanticum* play an important role in active carbon transport. *J. Geophys. Res.: Biogeosci.* 124, 1056–1070. <https://doi.org/10.1029/2018JG004918>
- Hickey, B. M. 1979. The California Current system—hypotheses and facts. *Progress in Oceanography*, 8(4), pp.191–279.
- Hobday, A. J., E. C. J. Oliver, A. Sen Gupta, J. A. Benthuisen, M. T. Burrows, M. G. Donat, N. J. Holbrook, P. J. Moore, M. S. Thomsen, T. Wernberg, and D. A. Smale. 2018. Categorizing and naming marine heatwaves. *Oceanography*. 31:162–173.

- Hubbard Jr., L.T., and W.G. Percy. 1971. Geographic distribution and relative abundance of Salpidae off the Oregon coast. *J. Fish. Res. Board Can.* 28(12):1831–1836.
- Iguchi, N. and H. Kidokoro. 2006. Horizontal distribution of *Thetys vagina* Tilesius (Tunicata, Thaliacea) in the Japan Sea during spring 2004. *Journal of Plankton Research*, 28(6), pp.537–541.
- Jacox, M. G., M. A. Alexander, N. J. Mantua, J. D. Scott, G. Hervieux, R. S. Webb, and F. E. Werner. 2018. Forcing of multiyear extreme ocean temperatures that impact California Current living marine resources in 2016. *Bull. Am. Meteorol. Soc.* 99:S27–S33.
- Joh, Y., and E. Di Lorenzo. 2017. Increasing coupling between NPGO and PDO leads to prolonged marine heatwaves in the Northeast Pacific. *Geophys. Res. Lett.* 44:11,663–11,671, doi:10.1002/2017GL075930.
- Jones, T. T., B. L. Bostrom, M. D. Hastings, K. S. Van Houtan, D. Pauly, and D. R. Jones. 2012. Resource requirements of the Pacific leatherback turtle population. *PLoS One*. 7(10):e45447.
- King, J. R., V. N. Agostini, C. J. Harvey, G. A. McFarlane, M. G. G. Foreman, J. E. Overland, E. Di Lorenzo, N. A. Bond, and K. Y. Aydin. 2011. Climate forcing and the California Current ecosystem. *ICES J. Mar. Sci.* 68:1199–1216.
- Kwong, L. E., E. A. Pakhomov, A. V. Suntsov, M. P. Seki, R. D. Brodeur, L. G. Pakhomova, and R. Domokos. 2018. An intercomparison of the taxonomic and size composition of tropical micronekton based upon several sampling gears. *Deep-Sea Res. I* 135:34–45.
- Lavaniegos, B. E., and M. D. Ohman. 2003. Long-term changes in pelagic tunicates of the California Current. *Deep-Sea Res. II*. 50(14–16):2473–2498.
- Lavaniegos, B. E., and M. D. Ohman. 2007. Coherence of long-term variations of zooplankton in two sectors of the California Current System. *Prog. Oceanogr.* 75(1):42–69.
- Lebrato, M., and D. O. B. Jones. 2009. Mass deposition event of *Pyrosoma atlanticum* carcasses off Ivory Coast (West Africa). *Limnol. Oceanogr.* 45:1197–1209.
- Lee, Y.W., and D. B. Sampson. 2009. Dietary variations in three co-occurring rockfish species off the Pacific Northwest during anomalous oceanographic events in 1998 and 1999. *Fish. Bull.* 107(4):510–522.
- Li, K., A. J. Doubleday, M. D. Galbraith, and R. R. Hopcroft. 2016. High abundance of salps in the coastal Gulf of Alaska during 2011: A first record of bloom occurrence for the northern Gulf. *Deep-Sea Res. Part II*. 132:136–145.
- Licandro, P., F. Ibañez, and M. Etienne. 2006. Long-term fluctuations (1974–99) of the salps *Thalia democratica* and *Salpa fusiformis* in the northwestern Mediterranean Sea: Relationships with hydroclimatic variability. *Limnol. Oceanogr.* 51(4):1832–1848.
- Loeb, V. J., and J. A. Santora. 2012. Population dynamics of *Salpa thompsoni* near the Antarctic Peninsula: Growth rates and interannual variations in reproductive activity (1993–2009). *Proces. Oceanogr.* 96:93–107.
- Love, M. S. 2011. Certainly more than you want to know about the fishes of the Pacific Coast. Santa Barbara. Really Big Press.
- Lucas, C. H., and M. D. Dawson. 2014. What are jellyfishes and Thaliaceans and why do they bloom? In: Pitt, K.A., and Lucas, C.H. (Eds.) Chapter 2, Jellyfish Blooms. Springer, Dordrecht, Netherlands, pp. 9–44, doi:10.1007/978-94-007-7015-7_2.
- Perissinotto, R., and E. A. Pakhomov. 1998. The trophic role of the tunicate *Salpa thompsoni* in the Antarctic marine ecosystem. *J. Mar. Syst.* 17:361–374.
- Perissinotto, R., P. Mayzaud, P. D. Nichols, and J. P. Labat. 2007. Grazing by *Pyrosoma atlanticum* (Tunicata Thaliacea) in the south Indian Ocean. *Mar. Ecol. Prog. Ser.* 330:1–11.
- Peterson, W. T., and J. E. Keister. 2002. The effect of a large cape on distribution patterns of coastal and oceanic copepods off Oregon and northern California during the 1998–99 El Niño-La Niña. *Prog. Oceanogr.* 53(2–4):389–411.
- Peterson, W. T., and F. B. Schwing. 2003. A new climate regime in northeast Pacific ecosystems. *Geophysical research letters*, 30(17).
- Purcell, J. E., S.-I. Uye, and W.-T. Lo. 2007. Anthropogenic causes of jellyfish blooms and their direct consequences for humans: a review. *Mar. Ecol. Prog. Ser.* 350: 153–174.
- R Core Team. 2018. R: a language and environment for statistical computing [online]. In R Foundation for Statistical Computing, Vienna, Austria.
- Ralston, S., J. C. Field, and K. M. Sakuma. 2015. Long-term variation in a central California pelagic forage assemblage. *J. Mar. Syst.* 146:26–37.
- Sakuma, K.M., J. C. Field, N. J. Mantua, S. Ralston, B. B. Marinovic, and C. N. Carrion. 2016. Anomalous epipelagic micronekton assemblage patterns in the neritic waters of the California Current in Spring 2015 during a period of extreme ocean conditions. *Calif. Coop. Ocean. Fish. Invest. Rep.* 57:163–183.
- Santora, J.A., S. Ralston, and W. J. Sydeman. 2011. Spatial organization of krill and seabirds in the central California Current. *ICES J. Mar. Sci.*, 68(7), 1391–1402.
- Santora, J. A., J. C. Field, I. D. Schroeder, K. M. Sakuma, B. K. Wells, and W. J. Sydeman. 2012. Spatial ecology of krill, micronekton and top predators in the central California Current: Implications for defining ecologically important areas. *Prog. Oceanogr.* 106:154–174.
- Santora J.A., E. L. Hazen, I. D. Schroeder, S. J. Bograd, K. A. Sakuma, and J. C. Field. 2017. Impacts of ocean climate variability of pelagic forage species in an upwelling ecosystem. *Mar Ecol Prog Ser.* 580:205–220.
- Schroeder, I. D., J. A. Santora, S. J. Bograd, E. L. Hazen, K. M. Sakuma, A. M. Moore, C. A. Edwards, B. K. Wells, and J. C. Field. 2019. Source water variability as a driver of rockfish recruitment in the California Current Ecosystem: implications for climate change and fisheries management. *Can. J. Fish. Aquat. Sci.* 76(6):950–960.
- Silver, M.W. 1975. The habitat of *Salpa fusiformis* in the California Current as defined by indicator assemblages 1. *Limnol. Oceanogr.* 20(2):230–237.
- SIO Pelagic Invertebrates Collection. CalCOFI Database. Accessed October 2019. San Diego. <https://oceaninformatics.ucsd.edu/zoodb/secure/login.php>.
- Smith Jr., K.L., A. D. Sherman, C. L. Huffard, P. R. McGill, R. Henthorn, S. Von Thun, H. A. Ruhl, M. Kahru, and M. D. Ohman. 2014. Large salp bloom export from the upper ocean and benthic community response in the abyssal northeast Pacific: day to week resolution. *Limnol. Oceanogr.* 59(3):745–757.
- Sutherland, K. R., H. L. Sorensen, O. N. Blondheim, R. D. Brodeur, and A. W. Galloway. 2018. Range expansion of tropical pyrosomes in the northeast Pacific Ocean. *Ecology*. 99(10):2397–2399.
- Thompson, A. R., I. D. Schroeder, S. J. Bograd, E. L. Hazen, A. Leising, B. K. Wells, J. L. Largier, J. L. Fisher, K. Jacobson, S. Zeman, E. P. Bjorkstedt, R. R. Robertson, F. P. Chavez, M. Kahru, R. Goericke, S. McClatchie, C. E. Peabody, T. R. Baumgartner, B. E. Lavaniegos, J. Gomez-Vales, R. D. Brodeur, E. A. Daly, C. A. Morgan, T. D. Auth, B. J. Burke, J. Field, K. Sakuma, E. D. Weber, W. Watson, J. Coates, R. Schoenbaum, L. Rogers-Bennett, R. M. Suryan, J. Dolliver, S. Lored, J. E. Zamon, S. R. Schneider, R. T. Golightly, P. Warzybok, J. Jahncke, J. A. Santora, S. A. Thompson, W. Sydeman, and S. R. Melin. 2018. State of the California Current 2017–18: Still not quite normal in the north and getting interesting in the south. *Calif. Coop. Ocean. Fish. Invest. Reports* 59:1–66.
- Uye, S. I., and R. D. Brodeur, (Eds.). 2017. Report of Working Group 26 on jellyfish blooms around the North Pacific Rim: Causes and consequences. *PICES Sci. Rep.* 51:1–221.
- van Soest, R. W. M. 1981. A monograph of the order Pyrosomatida (Tunicata, Thaliacea). *Journal of Plankton Research*, 3(4), 603–631.
- Wells, B. K., I. D. Schroeder, J. A. Santora, E. L. Hazen, S. J. Bograd, E. P. Bjorkstedt, V. J. Loeb, S. McClatchie, E. D. Weber, W. Watson, A. R. Thompson, W. T. Peterson, R. D. Brodeur, J. Harding, J. Field, K. Sakuma, S. Hayes, N. Mantua, W. J. Sydeman, M. Losekoot, S. A. Thompson, J. Largier, S. Y. Kim, F. P. Chavez, C. Barceló, P. Warzybok, R. Bradley, J. Jahncke, R. Goericke, G. S. Campbell, J. A. Hildebrand, S. R. Melin, R. L. DeLong, J. Gomez-Valdes, B. Lavaniegos, G. Gaiola-Castro, R. T. Golightly, S. R. Schneider, N. Lo, R. M. Suryan, A. J. Gladics, C. A. Horton, J. Fisher, C. Morgan, J. Peterson, E. A. Daly, T. D. Auth, and J. Abell. 2013. State of the California Current 2012–13: No such thing as an ‘average’ year. *California Cooperative Oceanic Fisheries Investigations Reports*. 54:37–71.
- Wells, B. K., J. A. Santora, M. J. Henderson, P. Warzybok, J. Jahncke, R. W. Bradley, D. D. Huff, I. D. Schroeder, P. Nelson, J. C. Field, and D. G. Ainley. 2017. Environmental conditions and prey-switching by a seabird predator impact juvenile salmon survival. *J. Mar. Syst.* 174:54–63.
- Zuercher, R., and A. W. Galloway. 2019. Coastal marine ecosystem connectivity: pelagic ocean to kelp forest subsidies. *Ecosphere*. 10(2):e02602.

SPATIAL PATTERNS IN NEARSHORE JUVENILE FISH ABUNDANCE THROUGHOUT THE CALIFORNIA NETWORK OF MARINE PROTECTED AREAS AS REVEALED BY SEABIRD FORAGING RATES

DAN P. ROBINETTE*, NADAV NUR, AND JAIME JAHNCKE

Point Blue Conservation Science
3820 Cypress Drive Suite 11
Petaluma, CA 94954
ph: (805) 757-0838
drobinette@pointblue.org

ABSTRACT

The successful adaptive management of marine protected areas (MPAs) requires knowledge of spatial variability in the rates of juvenile fish recruitment to recovering fish populations. We used the foraging rates of two piscivorous seabirds (Brandt's cormorant and pelagic cormorant) to index juvenile fish abundance at 46 sites throughout California's MPA network. We used mixed effects negative binomial regression to develop models relating seabird foraging rates to coastal geography and annual upwelling strength and variability. The best models for both species included upwelling variability among years (i.e., persistent versus pulsed upwelling). The effects of upwelling variability differed depending on coastal geography. In the lees of headlands, foraging rates were highest and more stable with respect to upwelling variability. For all other coastal configurations, pulsed upwelling was associated with higher foraging rates. Thus, periods of relaxation in upwelling appear to be important for these sites. Our results suggest that coastal geography should be considered when establishing realistic expectations for the performance of individual MPAs.

INTRODUCTION

In 2012, the State of California finished implementing a network of 124 marine protected areas (MPAs) throughout state waters (Kirlin et al. 2013). One goal for resource managers is to adaptively manage the network in order to recover fish populations that have been depressed by intensive historic fishing throughout California (see Ainley et al. 2018 for an overview of California's fishing history and management actions taken to rebuild stocks). Successful adaptive management of the network will require establishing realistic expectations for the performance of individual MPAs as not all MPAs are equal in their potential for population recovery rates. In other words, managers need to be able to distinguish between an individual MPA that is underperforming versus one that needs more time. The network itself resides within the California Current System, an eastern boundary current where high interannual variability in wind-driven coastal upwelling leads to high

variability in primary productivity and the survival of early-life stages of many fish species (Ryckaczewski and Checkley 2007). As a result, the growth of nearshore fish populations within the CCS tends to be recruitment-limited (Morgan et al. 2011). Thus, variability in the strength of juvenile recruitment is an important determinant of recovery rates for fish populations protected within California MPAs.

The placement of individual MPAs along California's geographically complex coastline has direct implications for establishing expectations about variability in recruitment rates. The California coastline is dotted with headlands that create eddies in their lee during coastal upwelling events and influence the distribution of fish larvae at scales of 10–100 km (Sponaugle et al. 2002). Several studies over the past 25 years have demonstrated that these coastal headlands accumulate larvae and enhance year class recruitment to leeward habitats (e.g., Wing et al. 1998). Most of these studies have investigated individual headlands and have not looked at interactions between coastal geography and coastal upwelling by comparing multiple headlands throughout California.

Here, we investigate the role of coastal upwelling and coastal geography in determining spatiotemporal variability in community-level juvenile fish recruitment throughout California's MPA network and whether the effects of upwelling differ among sites with different coastal geographic characteristics. We define recruitment as the settlement of juvenile age classes into adult habitat. We target the community of fishes that have pelagic egg and larval stages that can be redistributed by ocean currents and that can settle as juveniles into a variety of nearshore habitats (e.g., kelp forest, sandy bottom, rocky reef) within one km of shore (e.g., many species of rockfishes, *Sebastes* sp., and sanddabs, *Citharichthys* sp.; see Robinette et al. 2018). We investigate juvenile fish abundance within one km of shore because this is the extent of our visual shore-based surveys. However, our results can be used to infer patterns of relative juvenile fish abundance within several km (but likely <10 km) of shore.

We used the foraging rates of two coastally breeding seabirds, Brandt's cormorant (*Phalacrocorax penicillatus*) and pelagic cormorant (*Phalacrocorax pelagicus*), to index

relative juvenile fish abundance at 46 sites throughout California's MPA network using data collected over nine years. While both species can take a variety of prey from nearshore habitats, studies have shown that relatively few species dominate the diets of each species (Ainley et al. 1981; Elliott et al. 2018). Pelagic cormorants feed heavily on post-settlement age juvenile fishes in mostly rocky habitats and, while Brandt's cormorants can prey heavily on schooling fishes in pelagic environments, they also take post-settlement age juvenile fishes from habitats associated with both rocky and soft bottom substrates. We use foraging behavior to identify when the cormorants are taking post-settlement age fishes in midwater and bottom habitats as those are the fishes we consider recruited into the nearshore habitats protected by MPAs. Both species are pursuit divers and can easily access all depths of the water column found within one km of shore. As such, they are good at sampling juvenile fish abundance throughout a variety of nearshore habitats.

Numerous studies conducted over the past four decades have shown that seabirds respond predictably to changes in prey abundance and can thus be used as reliable indicators of change in prey populations (see Cairns 1992; Hatch and Sanger 1992). Seabirds are highly visible and easily enumerated and many of the coastally breeding species (e.g., Brandt's and pelagic cormorants) prey heavily on juvenile age classes of multiple fish species. The use of seabirds to index temporal variability in juvenile fish abundance has been well established (e.g., Mills et al. 2007; Roth et al. 2007). More recently, seabirds have been used to investigate spatial variability in juvenile fish abundance on scales relevant to MPA management. Robinette et al. (2007) used measures of seabird diet, fish larval abundance, and coastal upwelling to compare juvenile sanddab recruitment in the lee of a coastal headland to that at an exposed site. Recruitment to the leeward site was overall greater and less variable among years than at the exposed site. Robinette et al. (2012) investigated foraging rates of four juvenile-fish-eating seabird species around the same headland over six years and found that all four species consistently foraged in the lee of the headland where juvenile fish recruitment was presumably higher. In addition, Robinette et al. (2018) compared seabird foraging rates to independent measures of juvenile fish abundance in kelp forests at 11 sites within three distinct regions of the Southern California Bight. Seabird and fish distributions were similar at the regional scale but less similar at the site-specific scale. At the site level, seabirds were sampling a broader array of habitats than the kelp forest fish surveys and thus providing an index of community-level juvenile fish abundance over multiple habitats within a site. Here, we use seabird foraging rates as a proxy for juvenile fish abundance in midwater and bottom habitats. While there are

many post-settlement factors (e.g., predation on juveniles) that dictate the recruitment of individuals into adult fish populations, understanding the conditions that lead to high juvenile fish abundance will allow MPA managers to better understand where fish recruitment is likely to occur in a given year.

Spatiotemporal variability in juvenile fish abundance is largely determined by survival at the early larval stage (Rothschild 2000). Wheeler et al. (2016) found that even subtle changes in larval condition can lead to orders-of-magnitude differences in year-class strength. Coastal upwelling plays a significant role in larval survival as it is a major source of variability in both primary productivity and the offshore distribution of larvae (Ryckaczewski and Checkley 2007). The offshore advection of surface waters that drives coastal upwelling can also displace larvae from important nearshore settlement habitat. In fact, studies have shown that juvenile recruitment can be higher during periods of relaxation in upwelling when larvae are distributed more onshore (Wing et al. 1995a, 1995b; Ottman et al. 2018). However, results from other studies on the advection of larvae have been less convincing (e.g., Wilson et al. 2008) and some have shown no relationship between coastal upwelling and larval distribution (e.g., Kinlan and Gaines 2003; Morgan et al. 2009, 2018). These studies attribute the lack of clear relationships between upwelling and larval distribution to ontogenetic and species-specific differences in larval behavior and vertical distribution allowing larvae to take refuge from offshore surface currents. These differing responses of larvae to coastal upwelling make it challenging to understand the impacts of upwelling on fish recruitment at the community level and at spatial scales relevant to MPA management.

Despite the varying responses of different ages and species of larvae to coastal upwelling, multiple studies have consistently shown that eddies formed in the lee of headlands accumulate larvae and their planktonic prey, thereby increasing larval survival and juvenile recruitment to these habitats (Wing et al. 1998; Roughan et al. 2005; Mace and Morgan 2006a, 2006b; Morgan et al. 2011). This retention creates recruitment hot spots and appears to happen in the lee of both large headlands (e.g., Wing et al. 1998) and small headlands (e.g., Roughan et al. 2005; Mace and Morgan 2006a), though the role of headland size and shape in creating retention has not been thoroughly investigated. Understanding how coastal upwelling and coastal geography interact to impact larval survival and distribution will allow MPA managers to make basic predictions about the conditions under which individual MPAs are likely to experience high recruitment events. This, in turn, will allow managers to establish realistic expectations for the performance of individual MPAs.

Here, we ask 1) what is the role of coastal upwelling in determining annual juvenile fish abundance in nearshore habitats, 2) does the size and shape of a headland determine its impact on annual juvenile fish abundance, and 3) does the effect of coastal upwelling differ with respect to coastal geography? We test the hypotheses that 1) variability in upwelling (i.e., more periods of relaxation in upwelling) will have a greater impact on annual juvenile fish abundance than overall upwelling strength, 2) larger, pointier headlands will have a greater impact on annual juvenile fish abundance than smaller, broader headlands, and 3) the impacts of coastal upwelling on annual fish recruitment will vary among exposed, windward, and leeward stretches of coast. We test for both linear and curvilinear impacts of upwelling and headland characteristics. Additionally, in an effort to better understand the mechanisms for how upwelling impacts juvenile fish recruitment, we compared results using two different upwelling indices: 1) Coastal Upwelling Transport Index (CUTI) and 2) Biologically Effective Upwelling Transport Index (BEUTI). The CUTI estimates vertical transport and is a good measure of the potential for offshore transport during upwelling (Jacox et al. 2018). The BEUTI estimates vertical nitrate flux due to upwelling and is a good measure of the potential biological response (e.g., primary productivity) to upwelling (Jacox et al. 2018). Finally, we compare our foraging observations to upwelling during both the current year when juvenile fish have already settled into adult habitats and the year prior to our foraging observations when the fish are newly hatched larvae in order to understand when in the early fish life history stage upwelling is having the biggest impact on juvenile fish abundance.

METHODS

Indicator Species

We used the foraging rates of Brandt's and pelagic cormorants to index relative juvenile fish abundance at individual sites throughout the MPA network. Pelagic cormorants breed in small groups (often <100 individuals) usually on ledges of coastal cliffs and take mostly juvenile bottom fishes in rocky reef habitats, though they will also take bottom fishes from flat sand and mud habitats (Hobson 2013). In California, Ainley et al. (1981), found the dominant prey of pelagic cormorants to be sculpins (family Cottidae) and various species of nearshore rockfishes. Brandt's cormorants breed in large colonies (100s to 1,000s of individuals) usually on offshore rocks. The feeding niche of Brandt's cormorants is broader in both diet and foraging habitat than that of pelagic cormorants, taking approximately equal biomass of schooling fishes (e.g., anchovies and pre-

settlement rockfishes) and midwater and bottom fishes (e.g., post-settlement rockfishes and sanddabs; Ainley et al. 1981; Elliott et al. 2015). In our study, we distinguish between birds forming large flocks to forage on schooling fishes versus isolated dives by individual birds foraging on post-settlement juvenile fishes in midwater and bottom habitats (Thiebault et al. 2014) as we are interested only in the latter (see section on Seabird Foraging Surveys below). In central California, Elliott et al. (2015) found that Brandt's cormorants can switch dominant prey types between years, foraging heavily on either anchovies, rockfishes, or sanddabs in a given year. At the southern California islands, Ainley et al. (1981) found that anchovies were again the dominant schooling prey while rockfishes and blacksmith (*Chromis punctipinnis*) were the dominant midwater prey. Robinette (unpublished data) found that, in addition to anchovies and rockfishes, sanddabs and sculpins were the dominant bottom prey at a mainland southern California colony. Thus, while there is some overlap in the niches of Brandt's and pelagic cormorants, they are also sampling different components of the ecosystem. Our sampling approach therefore provides broad sampling coverage over multiple components of nearshore fish communities.

Survey Site Characteristics

We conducted seabird foraging surveys at 46 sites throughout the California MPA network (table 1, figs. 1 and 2). We divided the network into four bioregions to control for known latitudinal gradients in marine community composition. We used the geographic boundaries used by Blanchette et al. (2008) but included an additional break at Cape Mendocino as studies have shown this to be a biogeographic barrier (Sivasundar et al. 2010). However, we did not divide the Southern California Bight at Santa Monica bay as was done in Blanchette et al. (2008) due to a low representation of sites throughout the bight. Thus, our four bioregions are 1) North (north of Cape Mendocino), 2) North Central (between Cape Mendocino and Monterey Bay), 3) South Central (between Monterey Bay and Point Conception), and 4) South (south of Point Conception). The majority of sites were included in baseline monitoring programs for California's Marine Life Protection Act Initiative and were surveyed for two consecutive years (table 1). In addition, we surveyed six sites within South Central for seven to eight years (2007–14) as part of a long-term coastal seabird monitoring project. We controlled for differences among years surveyed in our statistical models.

We defined coastal geography around each site in three ways. First, we categorized each site as located along an exposed section of coast (exposed), within 30 km windward of a headland (windward), or within

TABLE 1
 Names, years surveyed, coastal geography categories, length of nearest headland, and coastal direction
 of the 46 sites surveyed throughout the four bioregions of coastal California. Site codes are used in Figures 1 and 2.
 Coastal direction values of 66° to 134° represent south-facing coastlines, values of 135° to 224° represent
 west-facing coastlines, and values of 225° to 277° represent north-facing coastlines.

Bioregion	Survey Site (site codes)	Survey Years	Coastal Geography	Headland Length (km)	Coastal Direction (Deg)
North					
	Pyramid Point (py)	2014–15	Windward	6.8	184
	Crescent City (cc)	2014–15	Exposed	6.8	160
	Patrick's Point (pp)	2014–15	Exposed	5.5	174
	Trinidad Bay (tb)	2014–15	Leeward	5.5	141
	South Cape Mendicino (sc)	2014–15	Exposed	3.0	169
	Devil's Gate (dg)	2014–15	Leeward	3.0	169
North Central					
	Kibesillah (ki)	2014–15	Exposed	0	173
	Ten Mile (tm)	2014–15	Exposed	0	173
	Point Cabrillo (ca)	2014–15	Exposed	0	162
	Mendocino Headlands (mh)	2014–15	Exposed	0	162
	Bodega SMCA (bc)	2010–11	Exposed	3.7	147
	Bodega SMR (br)	2010–11	Exposed	3.7	147
	McClure's Beach (mb)	2010–11	Windward	15.4	153
	Point Reyes (po)	2010–11	Leeward	15.4	96
	Drakes Bay (db)	2010–11	Leeward	15.4	110
	Miller Point (mi)	2010–11	Leeward	15.4	141
	Montara (mr)	2010–11	Exposed	5.0	151
	Pillar Point (pi)	2010–11	Exposed	5.0	151
	Pescadero (pe)	2010–11	Windward	6.7	186
South Central					
	La Cruz Rock (lc)	2011–12	Exposed	5.9	137
	Pt Piedras Blancas (pb)	2011–12	Exposed	5.9	178
	San Simeon (ss)	2011–12	Leeward	5.9	119
	Cayucos Point (cp)	2011–12	Leeward	6.7	87
	Spooner's Cove (sp)	2011–12	Windward	12.5	200
	PG&E Trail (pg)	2011–12	Exposed	12.5	143
	Fossil Point (fp)	2011–12	Leeward	12.5	104
	Dinosaur Caves (dc)	2011–12	Leeward	12.5	74
	Lion's Head (lh)	2007–12	Leeward	5.3	128
	Purisima Colony (pr)	2007–14	Leeward	3.0	150
	Cabrillo Beach (cb)	2007–14	Leeward	3.0	150
	Lompoc Landing (ll)	2009–14	Leeward	3.0	150
	Vantage Point (vp)	2007–14	Exposed	9.1	143
	Boathouse (bh)	2007–14	Exposed	9.1	96
	Sudden Ranch (su)	2007–14	Leeward	9.1	121
South					
	Northwest Point (nw)	2012–13	Windward	10.4	277
	Painted Cave (pc)	2012–13	Windward	10.4	277
	Scorpion (sc)	2012–13	Windward	10.4	232
	Scorpion SMR (sr)	2012–13	Windward	10.4	265
	South Beach (sb)	2012–13	Exposed	10.4	124
	Gull Island (gi)	2012–13	Exposed	10.4	66
	Point Vicente (pa)	2012–13	Exposed	17.9	159
	White Point (ps)	2012–13	Exposed	17.9	114
	North La Jolla (ln)	2012–13	Windward	6.2	267
	South La Jolla (ls)	2012–13	Exposed	6.2	143
	Sunset Cliffs (sn)	2012–13	Exposed	6.2	184
	Cabrillo Monument (cm)	2012–13	Exposed	6.2	161

30 km in the lee of a headland (leeward). We categorized sites that were on the tips (west-facing portion) of headlands as exposed. Second, we defined the coastal orientation of a site by measuring coastal direction which we defined as the direction (degrees) of a straight line drawn

parallel to the coast in the poleward direction. Coastal direction values ranged from 66° to 277° with smaller values (66° to 134°) representing south-facing coastlines, intermediate values (135° to 224°) representing west-facing coastlines, and larger values (225° to 277°) repre-

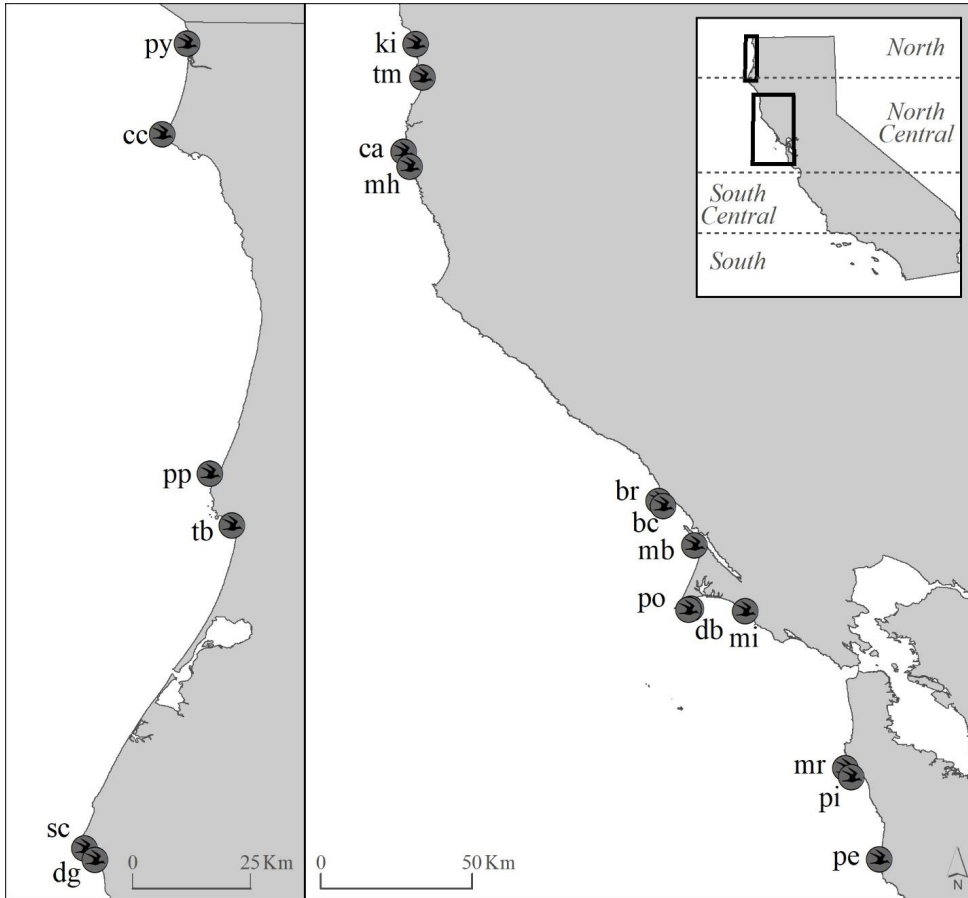


Figure 1. Locations of seabird foraging survey sites within the North and North Central bioregions of California. See Table 1 for site code definitions and years surveyed.

senting north-facing coastlines. Finally we defined the size and shape of the nearest headland to a given site. We used existing literature on nearshore larval retention (e.g., Mace and Morgan 2006a; Wing et al. 1995a) to define a headland as any coastline that projects into the ocean at least three km but less than 20 km and distinguish headlands from the two large capes along California’s coast (Cape Mendocino and Point Conception) which project approximately 35–40 km into the ocean. Capes influence ocean currents on large scales and can create breaks in biogeography (Sivasundar et al. 2010). They can also create eddies but these tend to influence large areas and lead to latitudinal rather than nearshore retention (Sponaugle et al. 2002). Additionally, we treated Santa Cruz Island as a headland for the purposes of our analysis. For each headland, we measured headland size, headland length, and headland aspect ratio. We measured headland size as the distance the headland projects into ocean. If there was no headland within 30 km (e.g., at some exposed sites), then headland size was equal to zero. We calculated headland width as the linear along-shore distance from where a headland begins to project into the ocean to where it returns to the predominant

direction of the coast. We used aspect ratio (headland size divided by headland length) to define the overall shape of a headland, with larger values indicating a more abrupt or “pointy” change in coastline.

Finally, we measured a site’s distance to the nearest headland in order to investigate whether proximity to a headland impacted fish recruitment rates. We measured this as the straight-line distance from the survey site to the nearest tip of the nearest headland. We recorded distances measured from sites windward of a headland as negative values and distances from sites leeward of a headland as positive values. We recorded distance as zero for sites on the west-facing portion of a headland. For island sites, we measured the distance from the site to the nearest western tip of the island. For sites farther than 30 km from a headland, we recorded a maximum distance of 30 km as these were considered exposed and likely not influenced by the headland.

Seabird Foraging Surveys

We conducted weekly seabird foraging surveys from April through July at each of the 46 sites during the years listed in Table 1. We conducted surveys during one

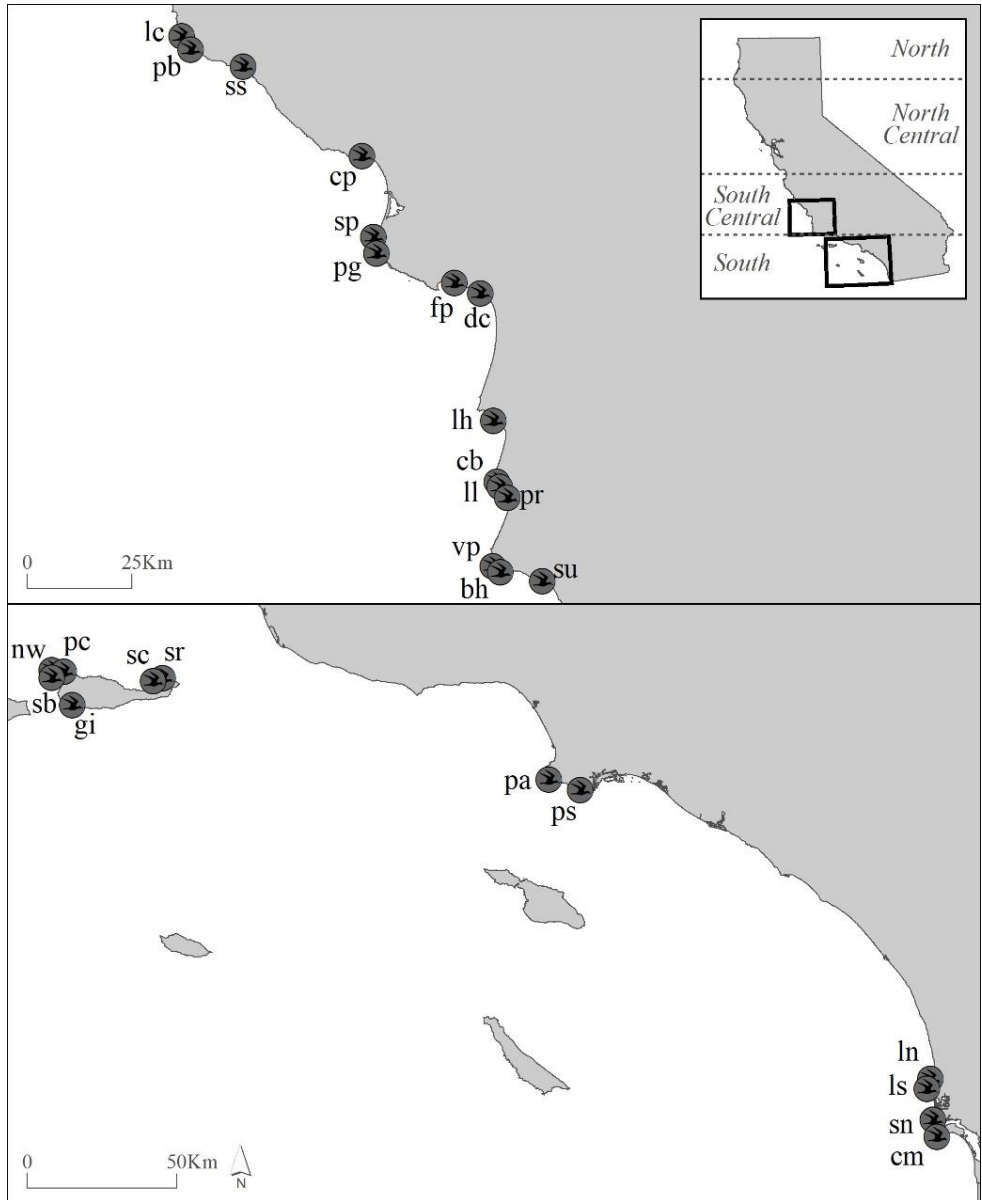


Figure 2. Locations of seabird foraging survey sites within the South Central and South bioregions of California. See Table 1 for site code definitions and years surveyed.

of the following time periods: 0600–0900, 0900–1200, 1200–1500, or 1500–1800, rotating sites among the four time periods per week to develop a complete 12-hour assessment of foraging activity. We made observations from a single observation point, using binoculars and a 20–60x spotting scope. We divided each three-hour period into 15-minute blocks. During each 15-minute block, we scanned all water within a one-kilometer radius of our observation point and recorded the numbers of actively diving individuals for all seabird species. We collected data on birds foraging in flocks separately from birds foraging independently in order to distinguish the general prey types (i.e., schooling and pre-settlement juvenile fishes versus post-settlement juvenile fishes)

being taken. We defined a foraging flock as an aggregation of five or more birds foraging on an aggregation of prey (e.g., a shoal of anchovies). We defined independent foragers as birds that were not aggregated and not diving for aggregated prey. Thus, there could be more than five individual foragers within our one km radius, but they were all foraging independent of one another. In this study, we use only data on independent foragers as that behavior indicates foraging on non-schooling juveniles that have settled into adult habitat. We recorded only birds that were observed actively diving as foraging. We calculated a foraging rate by averaging all 15-minute blocks over the three-hour survey to produce the mean number of diving birds per survey. Thus, our sample unit

is each three-hour survey, and our total sample size for all sites and years is 1,797 surveys. We did not pool data from multiple years for a given site. Rather, we treated site-year as a random effect in order to control for correlated responses among surveys within a site, within a year, and allow the models to assess interannual and spatial variability in juvenile fish abundance.

Data Analysis

We used mixed effects negative binomial regression to investigate how coastal geography and coastal upwelling contributed to annual variability in the foraging rates of Brandt's cormorants and pelagic cormorants, our proxies for juvenile fish abundance, using Stata 14 (StataCorp. 2015). We analyzed six variables describing coastal geography and four variables describing coastal upwelling to generate statistical models accounting for variability in foraging rates. Site-year was treated as a random effect.

In addition, we used bioregion, time of day, season, local breeding population size, and percent rocky bottom substrate to control for variation in foraging rates not related to coastal geography and/or upwelling. We did not include wind speed, wave height, or tide as control variables as we found that those variables did not significantly affect cormorant foraging rates (see Robinette et al. 2012). Categories for biogeography are defined above. Time of day is the three-hour period during which observations were made (integer ranging from 1 to 4) and season is the week during which observations were made (integer ranging from 14 to 35); we fit both as polynomials up to second order. Breeding population size is the number of birds for either Brandt's or pelagic cormorants breeding within 10 km of our foraging observation site. Both species typically forage within 10 km of their breeding sites (Kotzerka et al. 2011; Peck-Richardson et al. 2018). We used annual breeding population numbers recorded during ground-based surveys conducted as part of the same monitoring projects contributing the foraging data, ln-transformed. Percent rocky bottom substrate is the percentage of our foraging observation area (1 km radius from our observation site) that contained rocky bottom substrate. We obtained bottom substrate data from California Department of Fish and Game (ftp://ftp.dfg.ca.gov/R7_MR/HABITAT/) and calculated percent rocky bottom using ArcGIS 10.5.1.

Calculations of Indices Used in the Models We used geographic category, coastal direction, headland size, headland length, headland aspect ratio, and distance to headland as defined above for our coastal geography variables. For coastal upwelling, we calculated annual upwelling strength and variability across the settlement season (April through August) separately for the CUTI and BEUTI indices. We obtained monthly values for both indices from the M. Jacox website (<http://mjacox.com/upwelling-indices/>).

We calculated annual upwelling strength as the sum of monthly upwelling values across all five months and annual upwelling variability as the standard deviation in monthly values across all five months. We calculated upwelling strength and variability for the year during which observations were made (current year) to define oceanographic conditions when the seabirds were foraging and for the year prior to when observations were made (year-1) to define oceanographic conditions during the period when their prey were likely developing from larvae into juveniles and settling into nearshore habitats. We calculated values for all four coastal upwelling variables separately for each of the two upwelling indices. We tested linear and quadratic relationships for all non-categorical variables except coastal direction.

Mixed Effects Models For each seabird species, we created two separate base models—one using the CUTI values for coastal upwelling and the other using the BEUTI values. For each model, we used a backwards stepwise approach to select the best model describing variability in foraging rate. We loaded each model with all the variables and removed non-significant ($p > 0.05$) variables from model iterations, one at a time, to produce a model containing only significant variables ($p < 0.05$). The exception was that linear terms were included if the quadratic term was significant.

We then tested for interactions between coastal geographic category (windward, exposed, or leeward) and coastal upwelling variables to determine if the effect of these variables differed by coastal geographic category. We did this using only the BEUTI base models as initial model results for both indices were similar, and the BEUTI model was the superior predictive model. We used likelihood ratio tests (LRTs) to test for differences among models containing or not containing interactions; the likelihood ratio statistic (LRS) provides a measure of the variation in the dependent variable accounted for by a single variable or an entire model. We first examined interactions one at a time, and then considered models with two interactions. Where models were not nested, we used Akaike information criterion (AIC) to select the best model with interactions.

We used AIC to confirm that all variables in the final models should be retained. Note that main effects were always included if the respective interaction was included.

RESULTS

CUTI and BEUTI Models without Interactions

Brandt's Cormorants Table 2 shows the variables that had significant relationships with Brandt's cormorant foraging rate in the initial CUTI and BEUTI models. The results from the CUTI model were similar to

TABLE 2

Best models describing variability in Brandt's cormorant foraging rates using either the CUTI or BEUTI index to quantify upwelling strength and variability. Each model was selected using a backwards stepwise approach. The table shows only variables that were significant ($p < 0.05$) and therefore included in the model. Dashed lines identify variables that were not included in a given model. Linear and quadratic expressions are delineated by "L" and "Q", respectively. For categorical variables (Cat), each category listed is being compared to a base category (North category for Region and Windward category for Geography). Likelihood ratio statistics (LRS) are shown for each model.

Factor	CUTI		BEUTI	
	Coeff	p	Coeff	p
CUTI AIC = 5782.60 LRS(15) = 129.09 n = 1,797, $p < 0.001$				
BEUTI AIC = 5781.47 LRS(18) = 144.66 n = 1,797, $p < 0.001$				
<i>Control Variables</i>				
Region (Cat)				
North Central	-0.737	0.034	1.389	<0.001
South Central	1.121	0.006	1.030	0.004
South	1.286	0.006	0.693	0.125
Time of Day (L)	0.459	<0.001	0.441	<0.001
Time of Day (Q)	-0.084	<0.001	-0.080	<0.001
Within Season (L)	-0.113	0.007	-0.119	0.005
Within Season (Q)	2.8 e-3	0.002	2.9 e-3	0.001
Population (L)	—	—	0.0003	0.006
<i>Coastal Geography</i>				
Geography (Cat)				
Exposed	0.202	0.294	0.068	0.500
Leeward	0.606	0.009	0.471	0.010
Headland Size (L)	0.396	<0.001	0.198	0.001
Headland Size (Q)	-0.012	0.002	-0.007	0.011
Headland Length (L)	-0.036	0.009	—	—
Headland AR (L)	-2.863	<0.001	—	—
<i>Upwelling</i>				
Cumulative (L)	—	—	-0.001	0.001
Stan Dev (L)	—	—	0.139	0.005
Cumulative Y-1 (L)	—	—	-0.003	<0.001
Cumulative Y-1 (Q)	—	—	7.0 e-7	<0.001
Stan Dev Y-1 (L)	-2.218	0.059	0.348	0.001
Stan Dev Y-1 (Q)	-2.406	0.037	-0.010	0.001

those from the BEUTI model, but the BEUTI model was substantially superior to the CUTI model (AIC = 5781.47 vs AIC = 5782.60, respectively). Thus, while we continue to compare both models in this section, we only show model outputs for the superior BEUTI model when illustrating relationships between foraging rate and upwelling and coastal geography variables.

Both models showed significant relationships for all control variables except local breeding population size. Only the BEUTI model included a significant relationship between foraging rate and population size. There were differences in mean foraging rate among bioregions, curvilinear relationships between foraging rate and time of day and season, and a linear relationship between foraging rates and local population size (BEUTI model only). There was no significant relationship between foraging rates and bottom substrate for either model. Additionally, both models showed differences among geographic categories, with mean foraging rates highest at leeward sites (fig. 3).

Both CUTI and BEUTI models showed curvilinear relationships between foraging rates and headland size, with foraging rates increasing with headland size and plateauing as headland size increased past 10 km (fig. 4). The CUTI model also showed linear relationships between foraging rate and headland length and headland aspect ratio. Coastal direction and distance to headland did not make significant contributions to either model. Both models showed curvilinear relationships between foraging rates and prior year upwelling variability, with an intermediate maximum. Only the BEUTI model showed curvilinear relationship with prior year upwelling strength, with an intermediate maximum, and linear relationships with current year upwelling strength and upwelling variability. We explore these relationships further in the interactions section below.

Pelagic Cormorants Table 3 shows results from the initial CUTI and BEUTI models for pelagic cormorants. As with Brandt's cormorants, the CUTI model was similar to the BEUTI model, but the BEUTI model

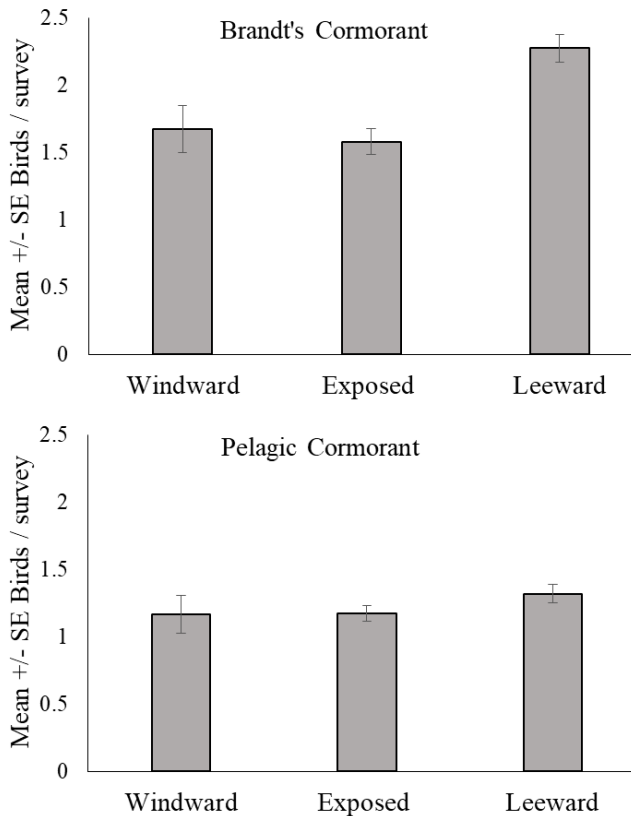


Figure 3. Mean +/- Standard Error (SE) foraging rates for Brandt's cormorants and pelagic cormorants for three categories of coastal geography: windward, exposed, and leeward.

was substantially superior to the CUTI model (AIC = 4457.09 vs AIC = 4461.34, respectively). We therefore only show model outputs for the superior BEUTI model when illustrating relationships between foraging rate and upwelling and coastal geography variables.

There were no differences in mean foraging rates among bioregions and curvilinear relationships between

foraging rates and time of day, season, and local breeding population size. Similar to Brandt's cormorants, there was no significant relationship between foraging rate and bottom substrate with either model.

Unlike Brandt's cormorants, mean foraging rates for pelagic cormorants were only slightly higher at leeward sites (fig. 3) and only the BEUTI model showed significant differences among coastal geography categories. Both models showed a curvilinear relationship between foraging rates and headland length, with very short and very long headlands leading to higher foraging rates (fig. 4). Additionally, both models showed a linear relationship between foraging rates and coastal direction, with lower coastal direction values (i.e., south-facing coastlines) leading to higher foraging rates (fig. 4). Both models showed curvilinear relationships between foraging rates and current year upwelling strength and prior year upwelling variability, with intermediate maximums. We explore these relationships further in the interactions section below.

Interactions between Coastal Upwelling and Coastal Geography

Brandt's Cormorant For the Brandt's cormorant BEUTI model, we found significant interactions between geography category and upwelling strength, upwelling variability, and prior year upwelling variability, considered one at a time. Both upwelling strength and upwelling variability interactions were significant when included in a single model as were upwelling strength and prior year upwelling variability interactions. However, the interaction with upwelling variability was not significant when the interactions with upwelling strength and prior year upwelling variability were included in the model. AIC showed that the model including interactions with upwelling strength and prior year upwelling variability was superior to a model that included

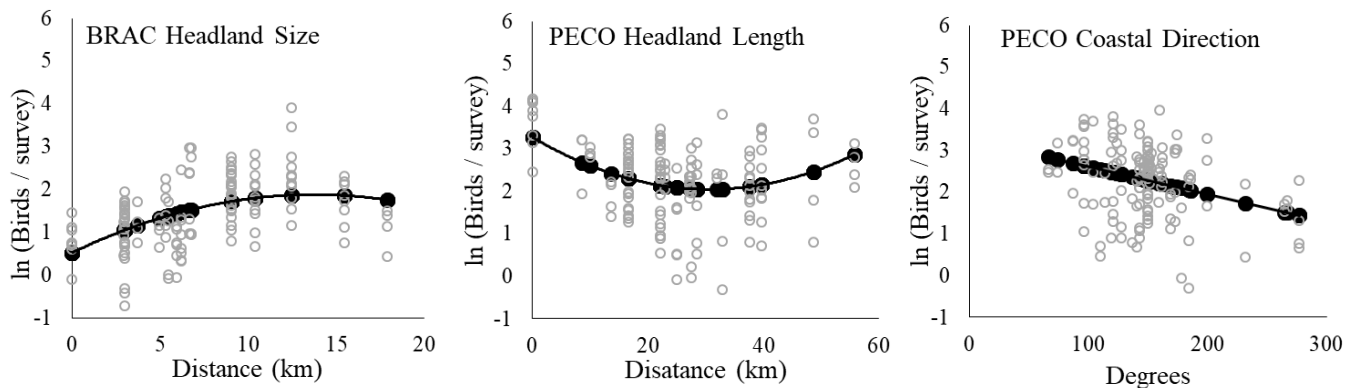


Figure 4. Effects of headland size on Brandt's cormorant (BRAC) foraging rates and the effects of headland length and coastal direction on pelagic cormorant (PECO) foraging rates. Black points represent predicted values based on BEUTI model outputs and open gray circles represent raw observations for a given site from a given year controlled for the effects of all independent variables except that displayed on the x-axis. Controlled raw observations were derived by removing the effects of all independent variables used in the BEUTI model except the variable displayed on the x-axis.

TABLE 3

Best models describing variability in pelagic cormorant foraging rates using either the CUTI or BEUTI index to quantify upwelling strength and variability. Each model was selected using a backwards stepwise approach.

The table shows only variables that were significant ($p < 0.05$) and therefore included in the model.

Dashed lines identify variables that were not included in a given model. Linear and quadratic terms are delineated by “L” and “Q”, respectively. For categorical variables (Cat), each level listed is being compared to a base level (Windward category for Geography). Likelihood ratio statistics (LRS) are shown for each model.

Factor	CUTI		BEUTI	
	Coeff	p	Coeff	p
CUTI AIC = 4461.34 LRS(15) = 192.17 n = 1,797, $p < 0.001$				
BEUTI AIC = 4457.09 LRS(15) = 209.21 n = 1,797, $p < 0.001$				
<i>Control Variables</i>				
Time of Day (L)	0.641	<0.001	0.650	<0.001
Time of Day (Q)	-0.126	<0.001	-0.128	<0.001
Week (L)	-0.267	<0.001	-0.275	<0.001
Week (Q)	5.4 e-3	<0.001	5.6 e-3	<0.001
Population Size (L)	0.009	<0.001	0.008	<0.001
Population Size (Q)	-3 e-5	0.001	-2 e-5	0.004
<i>Coastal Geography</i>				
Geography (Cat)				
Exposed	-0.488	0.100	-0.537	0.059
Leeward	0.039	0.900	-0.062	0.834
Coastal Direction (L)	-0.007	0.004	-0.007	0.003
Headland Length (L)	-0.059	0.004	-0.080	<0.001
Headland Length (Q)	0.001	0.002	0.001	0.001
<i>Upwelling</i>				
Cumulative (L)	0.109	0.009	0.002	0.001
Cumulative (Q)	-4 e-4	0.012	-9 e-7	<0.001
Stan Dev Y-1 (L)	9.729	0.009	0.245	<0.001
Stan Dev Y-1 (Q)	-5.467	0.036	-0.004	0.033

TABLE 4

Comparison of two models for Brandt’s cormorants with interactions between geography category and upwelling variables: in addition, interaction results from the best model as determined by AIC (model including interactions between geography category and upwelling strength and prior year upwelling variability).

Model	AIC			
Cum BEUTI & Std Dev BEUTI Year -1	5769.23			
Cum BEUTI & Std Dev BEUTI	5770.26			
Cum BEUTI & Std Dev BEUTI Year-1: LRS (24) = 180.53, n = 1,797, $p < 0.001$				
		Coeff	Std Error	P
Cum BEUTI (linear)	Windward	8.9 e-4	8.0 e-4	0.268
	Exposed	-9.2 e-4	4.7 e-4	0.049
	Leeward	-2.0 e-3	4.6 e-4	<0.001
Std Dev BEUTI Year -1 (linear)	Windward	-0.129	0.166	0.437
	Exposed	0.311	0.104	0.003
	Leeward	0.319	0.119	0.007
Std Dev BEUTI Year -1 (quadratic)	Windward	-2.2 e-3	4.1 e-3	0.593
	Exposed	-0.010	3.0 e-3	0.001
	Leeward	-9.2 e-3	4.1 e-3	0.023

interactions with upwelling strength and upwelling variability (table 4). Likelihood ratio tests confirmed the significance of the interaction with prior year upwelling variability, when the interaction with upwelling strength was included (LRS = 9.91, $df = 4$, $p = 0.042$), and conversely, the significance of the interaction with upwelling strength, when the interaction with prior year upwell-

ing variability was included (LRS = 12.87, $df = 2$, $p = 0.002$). The final model with interactions for upwelling strength and prior year upwelling variability showed significant relationships between foraging rates and both upwelling variables for exposed and leeward sites, but not for windward sites (table 4). Foraging rates showed negative linear relationships with upwelling strength at

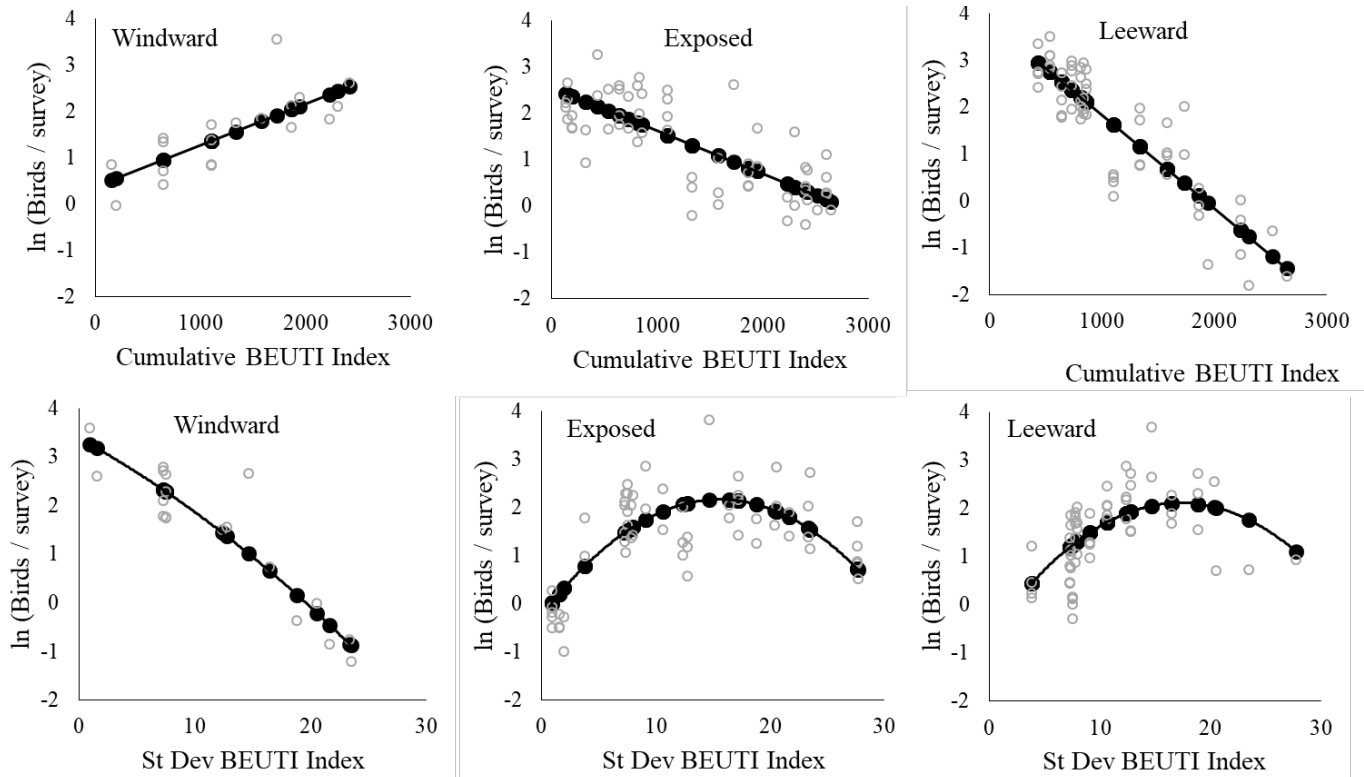


Figure 5. Effects of upwelling strength and prior year upwelling variability on Brandt's cormorant foraging rates at windward, exposed, and leeward study sites. Black points represent predicted values based on BEUTI model outputs and open gray circles represent raw observations for a given site from a given year controlled for the effects of all independent variables except that displayed on the x-axis. Controlled raw observations were derived by removing the effects of all independent variables used in the BEUTI model except the variable displayed on the x-axis.

exposed and leeward sites, though foraging rates were more variable at leeward sites (fig. 5). Furthermore, foraging rates at were highest at exposed and leeward sites with intermediate values of prior year upwelling, though foraging rates at leeward sites were less variable overall.

Pelagic Cormorant For pelagic cormorant BEUTI models, we found significant interactions between geography category and upwelling strength and prior year upwelling variability. However, the interaction with upwelling strength was not significant when the interaction with prior year upwelling variability was included in the model. AIC showed that the model including the interaction with prior year upwelling variability was an improvement over the model including the interaction with upwelling strength (table 5). A likelihood ratio test showed that this model differed significantly from the model that did not include interactions (LRS = 28.04, $df = 4$, $p < 0.001$). The final model with interaction for prior year upwelling variability showed significant relationships between foraging rates and upwelling for windward and exposed sites, but not for leeward sites (table 5). Foraging rates at the windward sight peaked at intermediate values of prior year upwelling variability and then decreased slightly (fig. 6). Foraging rates at the

exposed sights plateaued at higher values of prior year upwelling variability and did not decrease.

DISCUSSION

We found that the effects of coastal upwelling on seabird foraging rates differed by coastal geography. This was especially true for prior year upwelling. Foraging rates were higher at exposed sites when prior year upwelling was more variable. This is likely because variability in upwelling reduces offshore transport thereby increasing retention of larvae to nearshore habitats where they settle as juveniles into midwater and bottom habitats. Ainley et al. (1993) found similar results when using the common murre (*Uria aalge*) to sample juvenile rockfish abundance within the Gulf of the Farallones, with pelagic juvenile rockfish more abundant within the gulf in years when upwelling was pulsed during the rockfish larval stage. Foraging rates at leeward habitats were more stable and did not change drastically with changes in prior year upwelling variability. These results are supported by Wing et al. (1995b) who reported continuous post-larvae settlement in the lee of Point Reyes in central California compared to more episodic settlement at exposed habitats.

TABLE 5
 Comparison of two models for pelagic cormorants with interactions between geography category and upwelling variables: in addition interaction results from the best model as determined by AIC (model including interactions between geography category and prior year upwelling variability).

Model		AIC		
Std Dev BEUTI Year -1		4437.05		
Cum BEUTI		4440.96		
Std Dev BEUTI Year -1: LRS (19) = 210.86, n = 1,797, p <0.001				
		Coeff	Std Error	P
Std Dev BEUTI Year -1 (linear)	Windward	0.587	0.171	0.001
	Exposed	0.370	0.068	<0.001
	Leeward	0.073	0.076	0.338
Std Dev BEUTI Year -1 (quadratic)	Windward	-0.017	5.7 e-3	0.003
	Exposed	-6.8 e-3	2.0 e-3	0.001
	Leeward	-6.9 e-3	2.7 e-3	0.796

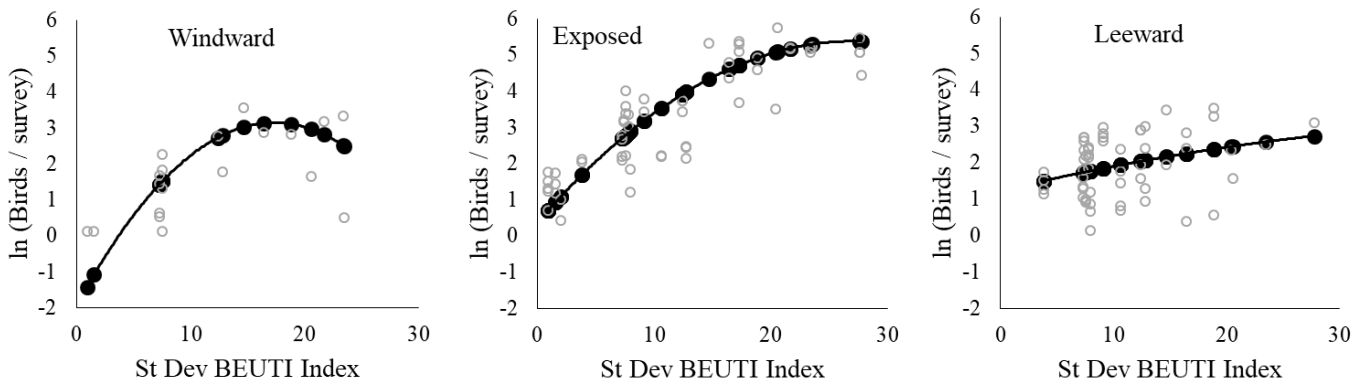


Figure 6. Effects of prior year upwelling variability on pelagic cormorant foraging rates at windward, exposed, and leeward study sites. Black points represent predicted values based on BEUTI model outputs and open gray circles represent raw observations for a given site from a given year controlled for the effects of all independent variables except that displayed on the x-axis. Controlled raw observations were derived by removing the effects of all independent variables used in the BEUTI model except the variable displayed on the x-axis.

In contrast to what we expected, Brandt’s cormorant foraging rates were lower at exposed and leeward habitats when current year upwelling was more intense. This may be more of a result of prey switching in Brandt’s cormorants as current year upwelling conditions change rather than an indicator of juvenile fish abundance at exposed and leeward habitats. Brandt’s cormorants regularly switch from midwater and bottom fishes to anchovies when anchovy favorable conditions occur (Elliott et al. 2015, 2016; Warzybok et al. 2018). Intense coastal upwelling supports blooms of the larger phytoplankton species that northern anchovies prey upon (Rykaczewski and Checkley 2007). Furthermore, there is evidence that intense upwelling causes swarming behavior in schooling fishes that would make them more available to cormorants, whereas these species are more dispersed and less available during relaxation in upwelling (Benoit-Bird et al. 2018). Thus, Brandt’s cormorants may be foraging more on anchovies away from shore during intense upwelling years. Diet studies of pelagic cormorants have shown that they are likely not switching to pelagic prey like anchovies (Ainley et al. 1981).

We found that the overall relationship between cormorant foraging rates and prior year upwelling variability was not linear but curvilinear. Foraging rates were overall higher with intermediate values of prior year upwelling variability. Thus, there appears to be an optimal window of coastal upwelling conditions that increases larval survival and leads to peak juvenile fish abundance. Cury and Roy (1989) found a curvilinear relationship between upwelling strength and larval survival that suggests larval survival is highest with intermediate levels of coastal upwelling. Roy et al. (1992) described an “optimal environmental window” of wind speeds that promote larval survival. If upwelling is too weak, there is not enough primary productivity to support larval survival. However, if upwelling is too strong, larval mortality can occur as larvae are displaced from water masses favorable to larval survival. Our results showing that BEUTI-based models were superior to CUTI-based models suggest that larval survival due to increased primary productivity is also important as the delivery of larvae to nearshore habitats in determining juvenile fish abundance. Finally, Robinette et al. (2007)

found that upwelling variability was more important than upwelling strength in determining regional survival and delivery to nearshore habitats. Our results here support that conclusion and the idea of an optimal environmental window for larval survival. Intermediate variability in coastal upwelling allows for primary productivity to support larval survival but reduces offshore transport away from nearshore habitats. Ultimately, upwelling variability translates into more relaxation events that allow larvae to return to exposed and windward habitats. Retention of larvae in the lee of headlands can provide more stable recruitment rates among years by decreasing the advection of larvae during years of persistent upwelling.

We found evidence that the size and shape of headlands can impact cormorant foraging rates. There was some evidence that headlands projecting further into the ocean lead to higher juvenile fish abundance as indicated in the Brandt's cormorant models. Additionally, the pelagic cormorant models indicated that both long and short headlands lead to higher juvenile fish abundance. The longer headland length may indicate that very large headlands enhance larval retention while the shorter headland length may indicate that pointier headlands with higher aspect ratios also enhance larval retention. Additionally, coastal orientation was an important determinant of juvenile fish abundance as indicated by pelagic cormorants regardless of whether a headland was present. Pelagic cormorant foraging rates were higher at south-facing coasts than other coastal orientations. Offshore advection due to coastal upwelling is not as strong along south-facing coasts and eddies can form in the lee of the south facing coasts of embayments (e.g., Graham and Largier 1997).

Understanding the mechanisms that dictate larval survival and distribution along the coast and having a cost-effective means by which to measure the abundance of juveniles settling into nearshore habitats will allow managers to set realistic expectations for the performance of individual MPAs. Seabirds can help determine when and where larval accumulation and juvenile settlement are likely to occur and whether recruitment hot spots are being adequately represented within the MPA network. For example, MPAs that are not in the lees of coastal headlands or not along southward-facing sections of coastline may not receive similar numbers of juvenile recruits as those in leeward habitats, especially if multiple years of persistent upwelling have pushed fish larvae away from these MPAs. These MPAs may never achieve the same fish population levels as MPAs in leeward habitats. Managers should therefore establish unique expectations for individual MPAs based on their potential for juvenile fish recruitment. Additionally, seabirds offer a community-level perspective of juvenile fish recruitment

because each species samples multiple fish species across multiple habitats. Finally, using multiple seabird species that differ in their diet and foraging habitat use will provide a broad community-level perspective (see Robinette et al. 2018).

ACKNOWLEDGMENTS

Funding for data collection was provided by US Department of Defense (Contract numbers: F4D3D36298MG01, F4D3D38336M001, F4D3D3002M001, F4D3D30307M001, FA4610-10-D-0004-0040, and FA4610-13-D-004), California Sea Grant (Grant numbers: 09-015, C0100100, and MPA 10-049), and US Bureau of Land Management cooperative agreement L11AC20073. We greatly appreciate the assistance of D. Barton, C. Boser, K. Faulkner, R. Golightly, J. Howar, and G. McChesney. This work would not have been possible without the dedication of many Point Blue staff and interns. Point Blue Contribution Number 2263.

LITERATURE CITED

- Ainley, D. G., D. W. Anderson, and P. R. Kelly. 1981. Feeding ecology of marine cormorants in southwestern North America. *Condor* 83: 120–131.
- Ainley, D. G., W. J. Sydeman, R. H. Parrish, and W. H. Lenarz. 1993. Oceanic factors influencing distribution of your rockfish (*Sebastes*) in central California: a predator's perspective. *CalCOFI Reports* 34: 133–139.
- Ainley, D. G., J. A. Santora, P. J. Capitolo, J. C. Field, J. N. Beck, R. D. Carle, E. Donnelly-Greenane, G. J. McChesney, M. Elliott, R. W. Bradley, K. Linquist, P. Nelson, J. Roletto, P. Warzybok, M. Hester, and J. Jahncke. 2018. Ecosystem-based management affecting Brandt's cormorant resources and populations in the central California Current region. *Biological Conservation* 217: 407–418. doi:10.1016/j.biocon.2017.11.021.
- Benoit-Bird, K. J., C. M. Waluk, and J. P. Ryan. 2019. Forage species swarm in response to coastal upwelling. *Geophysical Research Letters* 46: 1537–1546. doi:10.1029/2018GL081603.
- Blanchette, C. A., C. M. Miner, P. T. Raimondi, D. Lohse, K. E. K. Heady, and B. R. Broitman. 2008. Biogeographical patterns of rocky intertidal communities along the Pacific coast of North America. *Journal of Biogeography* 35(9): 1593–1607. doi:10.1111/j.1365-2699.2008.01913.x.
- Cairns, D. K., 1992. Bridging the gap between ornithology and fisheries science: use of seabird data in stock assessment models. *Condor* 94: 811–824.
- Curry, P. and C. Roy. 1989. Optimal environmental window and pelagic fish recruitment success in upwelling areas. *Canadian Journal of Fisheries and Aquatic Sciences* 46: 670–680.
- Elliott, M. L., R. W. Bradley, D. P. Robinette, and J. Jahncke. 2015. Changes in forage fish community indicated by the diet of the Brandt's cormorant (*Phalacrocorax penicillatus*) in the central California Current. *Journal of Marine Systems*, 146, 50–58.
- Elliott, M. L., A. E. Schmidt, S. Acosta, R. W. Bradley, P. Warzybok, K. M. Sakuma, J. C. Field, and J. Jahncke. 2016. Brandt's cormorant diet (1994–2012) indicates the importance of fall ocean conditions for northern anchovy in central California. *Fisheries Oceanography* 25(5): 515–528. doi:10.1111/fog.12169.
- Graham, M. M., and J. L. Largier. 1997. Upwelling shadows as nearshore retention sites: the example of northern Monterey Bay. *Continental Shelf Research* 17(5): 509–532.
- Hatch, S. A., and G. A. Sanger. 1992. Puffins as samplers of juvenile Pollock and other forage fish in the Gulf of Alaska. *Marine Ecology Progress Series* 80: 1–14.
- Hobson, Keith A. 2013. Pelagic Cormorant (*Phalacrocorax pelagicus*). In: Poole A. (Ed), *The Birds of North America Online*. Ithaca: Cornell Lab of Ornithology. Retrieved from the Birds of North America Online: <http://bna.birds.cornell.edu.bnaproxy/birds.cornell.edu/bna/species/282>. doi:10.2173/bna.282.

- Jacox, M. G., C. A. Edwards, E. L. Hazen, and S. J. Bograd. 2018. Coastal upwelling revisited: Ekman, Bakun, and improved upwelling indices for the U.S. west coast. *Journal of Geophysical Research*: doi:10.1029/2018JC014187.
- Kinlan, B. P., and S. D. Gaines. 2003. Propagule dispersal in marine and terrestrial environments: a community perspective. *Ecology* 84(8): 2007–2020.
- Kirlin, J., M. Caldwell, M. Gleason, M. Weber, J. Ugoretz, E. Fox, and M. Miller-Hensona. 2013. California's Marine Life Protection Act Initiative: Supporting implementation of legislation establishing a statewide network of marine protected areas. *Ocean & Coastal Management* 74: 3–13.
- Kotzerka, J., S. A. Hatch, and S. Garthe. 2011. Evidence for foraging-site fidelity and individual foraging behavior of pelagic cormorants rearing chicks in the Gulf of Alaska. *The Condor* 113(1): 80–88. doi:10.1525/cond.2011.090158.
- Mace, A. J., and S. G. Morgan. 2006a. Larval accumulation in the lee of a small headland: implications for the design of marine reserves. *Marine Ecology Progress Series* 318: 19–29.
- Mace, A. J., and S. G. Morgan. 2006b. Biological and physical coupling in the lee of a small headland: contrasting transport mechanisms for crab larvae in an upwelling region. *Marine Ecology Progress Series* 324: 185–196.
- Mills K. L., T. Laidig, S. Ralston, and W. J. Sydeman. 2007. Diets of top predators indicate pelagic juvenile rockfish (*Sebastes* spp.) abundance in the California Current System. *Fisheries Oceanography* 16(3): 273–283.
- Morgan, S. G., J. L. Fisher, A. J. Mace. 2009. Larval recruitment in a region of strong, persistent upwelling and recruitment limitation. *Marine Ecology Progress Series* 394: 79–99. doi: 10.3354/meps08216.
- Morgan, S. G., J. L. Fisher, and J. L. Largier. 2011. Larval retention, entrainment, and accumulation in the lee of a small headland: Recruitment hot spots along windy coasts. *Limnology and Oceanography* 56(1): 161–178.
- Morgan, S. G., S. H. Miller, M. J. Robart, and J. L. Largier. 2018. Near-shore larval retention and cross-shelf migration of benthic crustaceans at an upwelling center. *Frontiers in Marine Science* 5(161). doi:10.3389/fmars.2018.00161.
- Ottmann, D., K. Grorud-Colvert, B. Huntington, S. Sponaugle. 2018. Inter-annual and regional variability in settlement of groundfishes to protected and fished nearshore waters of Oregon, USA. *Marine Ecology Progress Series* 598: 131–145. doi:10.3354/meps12616.
- Peck-Richardson, A. G., D. E. Lyons, D. D. Roby, D. A. Cushing, and J. A. Lerczak. 2018. Three-dimensional foraging habitat use and niche partitioning in two sympatric seabird species, *Phalacrocorax auritus* and *P. penicillatus*. *Marine Ecology Progress Series* 586: 251–264. doi:10.3354/meps12407.
- Robinette, D. P., J. Howar, W. J. Sydeman, and N. Nur. 2007. Spatial patterns of recruitment in a demersal fish as revealed by seabird diet. *Marine Ecology Progress Series* 352: 259–268.
- Robinette, D. P., N. Nur, A. Brown, and J. Howar. 2012. Spatial distribution of nearshore foraging seabirds in relation to a coastal marine reserve. *Marine Ornithology* 40: 111–116.
- Robinette, D. P., J. Howar, J. T. Claisse, and J. E. Caselle. 2018. Can near-shore seabirds detect variability in juvenile fish distribution at scales relevant to managing marine protected areas? *Marine Ecology*: doi:10.1111/maec.12485.
- Roth J. E., K. L. Mills, and W. J. Sydeman. 2007. Chinook salmon (*Oncorhynchus tshawytscha*)—seabird covariation off central California and possible forecasting applications. *Canadian Journal of Fisheries and Aquatic Sciences* 64: 1080–1090.
- Rothschild, B. J. 2000. “Fish stocks and recruitment”: the past thirty years. *Journal of Marine Science* 57: 191–201.
- Roughan, M., A. J. Mace, J. L. Largier, S. G. Morgan, J. L. Fisher, and M. L. Carter. 2005. Subsurface recirculation and larval retention in the lee of a small headland: A variation on the upwelling shadow theme. *Journal of Geophysical Research* 110: C10027. doi:10.1029/2005JC002898.
- Roy, C., P. Cury, and S. Kifani. 1992. Pelagic fish recruitment success and reproductive strategy in upwelling areas: environmental compromises. *South African Journal of Marine Science* 12: 135–146.
- Rykaczewski, R. R., and D. M. Checkley, Jr. 2007. Influence of ocean winds on the pelagic ecosystem in upwelling regions. *Proceedings of the National Academy of Sciences* 105(6): 1965–1970. doi:10.1073/pnas.0711777105.
- Sivasundar, A., and S. R. Palumbi. 2010. Life history, ecology and the biogeography of strong genetic breaks among 15 species of Pacific rockfish, *Sebastes*. *Mar Biol* (2010) 157:1433–1452. doi:10.1007/s00227-010-1419-3123
- Sponaugle, S., R. K. Cowen, A. Shanks, S. G. Morgan, J. M. Leis, J. Pineda, G. W. Boehlert, M. J. Kingsford, K. C. Lindeman, C. Grimes, and J. L. Munro. 2002. Predicting self-recruitment in marine populations: biophysical correlates and mechanisms. *Bulletin of Marine Science* 70(1) SUPPL.: 341–375.
- Thiebault, A., R. H. E. Mullers, P. A. Pistorius, and Y. Tremblay. 2014. Local enhancement in a seabird: reaction distances and foraging consequences of predator aggregations. *Behavioral Ecology* 25(6): 1302–1310. doi:10.1093/beheco/arv132
- Wallace, E. A. H., and G. E. Wallace. 1998. Brandt's Cormorant (*Phalacrocorax penicillatus*). *The Birds of North America Online* (A. Poole, Ed.). Ithaca: Cornell Lab of Ornithology: <http://bna.cornell.edu/bna/species/362>. doi:10.2173/bna.362.
- Warner, R. R., S. E. Swearer, and J. E. Caselle. 2000. Larval accumulation and retention: implications for the design of marine reserves and essential fish habitat. *Bulletin of Marine Science* 66(3): 821–830.
- Warzybok, P., J. A. Santora, D. G. Ainley, R. W. Bradley, J. C. Field, P. J. Capitolo, R. D. Carle, M. Elliott, J. N. Beck, G. J. McChesney, M. M. Hester, and J. Jahncke. 2018. Prey switching and consumption by seabirds in the central California Current upwelling ecosystem: Implications for forage fish management. *Journal of Marine Systems* 185 (2018) 25–39. doi:10.1016/j.jmarsys.2018.04.009.
- Wheeler, S. G., T. W. Anderson, T. W. Bell, S. G. Morgan, and J. A. Hobbs. 2016. Regional productivity predicts individual growth and recruitment of rockfishes in a northern California upwelling system. *Limnology and Oceanography* doi:10.1002/lno.10458.
- Wilson, J. R., B. R. Broitman, J. E. Caselle, and D. E. Wendt. 2008. Recruitment of coastal fishes and oceanographic variability in central California. *Estuarine, Coastal and Shelf Science* 79: 483–490. doi:10.1016/j.ecss.2008.05.001.
- Wing, S. R., J. L. Largier, L. W. Botsford, and J. F. Quinn. 1995a. Settlement and transport of benthic invertebrates in an intermittent upwelling region. *Limnology and Oceanography* 40(2): 316–329.
- Wing, S. R., L. W. Botsford, J. L. Largier, and L. E. Morgan. 1995b. Spatial structure of relaxation events and crab settlement in the northern California upwelling system. *Marine Ecology Progress Series* 128: 199–211.
- Wing, S. R., L. W. Botsford, S. V. Ralston, and J. L. Largier. 1998. Meroplanktonic distribution and circulation in a coastal retention zone of the northern California upwelling system. *Limnology and Oceanography* 43(7): 1710–1721.

REARING AND INDUCING SPAWNING IN CAPTIVE PACIFIC SARDINE (*SARDINOPS SAGAX*)

EMMANIS DORVAL, PATRICK APPEL, MEGAN H. HUMAN

Ocean Associates Inc (OAI), under contract to
Southwest Fisheries Science Center
4007 N. Abingdon Street
Arlington, VA 22207
emmanis.dorval@noaa.gov
pvappel@gmail.com
megan.human@noaa.gov

BEVERLY J. MACEWICZ, WILLIAM WATSON

National Oceanic and Atmospheric Administration
National Marine Fisheries Service
Southwest Fisheries Science Center
8901 La Jolla Shores Drive
La Jolla, CA 92037
beverly.macewicz@noaa.gov
william.watson@noaa.gov

ABSTRACT

From 2014 to 2018, we conducted laboratory experiments to develop methods for inducing spawning in Pacific sardine (*Sardinops sagax*). Wild caught immature *S. sagax* were acclimatized for three months, reared until they were fully mature, and then induced to spawn. Fish reared at 14.5°–18°C and 4–12 h day-light, and fed a vitamin-enriched diet, were mature by 27 months. Fish treated with hormones prior to 24 months of rearing did not spawn, but those injected at 27 and 39 months spawned and naturally fertilized their eggs. The successful induction method consisted of human chorionic gonadotropin injections followed by a combination of carp pituitary extract and Domperidone injections 24 h later. Spawning occurred approximately 20 h after the second hormonal treatment. Eggs collected at 27 months and incubated at 11°, 13°, and 15°C produced healthy larvae, but those spawned at 39 months did not survive to the larval stage. Ovaries were fully matured in February, but their oocytes regressed by May, suggesting that under controlled environment conditions *S. sagax* followed a seasonal maturity cycle similar to that of the naturally spawning population off California.

INTRODUCTION

The Pacific sardine, *Sardinops sagax* (Jenyns 1842), is one of the most important commercial and forage fishes in the California Current Ecosystem (CCE) (Hill et al. 2016; Nieto et al. 2014). The species is distributed from British Columbia, Canada, to the Gulf of California, Mexico, and is managed based on a three stock hypothesis, namely cold, temperate, and warm stocks (Félix-Uraga et al. 2005). The three stocks migrate almost synchronously, and thus their geographic locations along the Pacific coast differ seasonally (Demer and Zwolinski 2013). In most years the northern stock undergoes a migration in late spring to feed in waters off the Pacific Northwest (PNW) during summer and fall, and it returns south in late fall and winter to spawn in or near the Southern California Bight (SCB) during spring (Lo et al. 2011; Demer et al. 2012).

S. sagax is a fast-growing, short-lived and highly productive coastal pelagic species. Individuals may live up

to 15 years (Dorval et al. 2015; Hill et al. 2016), but they accomplish most of their growth by their second year of life. During spring spawning season in the SCB, maximum lengths average 273 mm (SL) (Dorval et al. 2015). Annual recruitments fluctuate highly and are correlated with environmental conditions such as sea surface temperature (SST) and chlorophyll *a* (Reiss et al. 2008; Zwolinski and Demer 2013). Ontogenetic development, feeding, and reproduction requirements determine the magnitude of seasonal migration and the distribution of *S. sagax* along the Pacific coast (Hargreaves et al. 1994; Smith 1978; Zwolinski and Demer 2013). Young and small *S. sagax* (<200 mm) remain inshore off California, but larger, older fish (>200 mm, age 2+) begin the northern feeding migration (Lo et al. 2011). By late winter or early spring most fish have migrated back to the SCB, but occupy offshore spawning habitats (Zwolinski and Demer 2013). In the SCB 50% of females reach sexual maturity at 0.56 years old and 150.9 mm (SL), and all are mature by age 2 and 175 mm (SL) (Dorval et al. 2015). Northern stock fish spawn from January to July, but in the SCB peak spawning is in late March–April (Lo et al. 2010a; Dorval et al. 2014).

S. sagax eggs, larvae and post recruits have been studied in the CCE (Nieto et al. 2014; Smith and Moser 2003), but additional research remains to be conducted on the adaptive ecology of late larval and early juvenile stages. These life stages are critical in determining annual recruitment strengths into the fishery (Butler et al. 1993; Takahashi and Checkley 2008; Takahashi et al. 2009). Early juveniles recruit into nearshore waters where they are harvested by the California live-bait fishery (SAFE 2017), but remain inaccessible to most traditional surveys until the late juvenile and early adult stages (Ralston et al. 2015).

Although recent studies have shown that laboratory experiments can play a critical role in understanding adaptive divergence of fish in the wild as well as the evolution of life history traits that control their growth, recruitment, and productivity (Conover and Baumann 2009), very few such studies have been conducted on juvenile *S. sagax* (Pribyl et al. 2016). The absence of reliable methods to rear and induce spawning in cap-

tive *S. sagax* has made it difficult to develop controlled experiments on early life stages of this species. Because environmental cues play a critical role in regulating reproduction in teleost fish, under laboratory conditions these stimuli may be absent or weak, leading to physiological barriers that may prevent the initiation of reproductive processes (Stacey 1984).

Hormonal therapies have been used to alleviate these physiological blocks and accelerate vitellogenesis in fish species (Zohar and Mylonas 2001), although with various degrees of success in small pelagic fish. Consistent methods were developed to induce spawning in northern anchovy, *Engraulis mordax*, reared for several months in the laboratory (Leong 1971; 1989). Olmedo et al. (1990) applied similar methods to induce spawning in recently captured mature European pilchard, *Sardina pilchardus*, but these methods did not work after fish were acclimatized for one month in the laboratory. Shiraishi et al. (1996) used chronic hormone therapies to induce Japanese pilchard, *Sardinops melanostictus*, to spawn after one year in captivity by implanting mature females with luteinizing hormone releasing hormone (LHRH) pellets. However, no reliable methods have been reported to induce spawning in *S. sagax*.

In this paper, we report on the first steps in a series of exploratory experiments to establish a method for predictably inducing spawning in *S. sagax*, and as exploratory, the primary goal here was simply to determine whether spawning could be induced in a laboratory stock. A secondary goal was to determine the viability of experimentally spawned eggs and their potential usefulness in developing future studies on larval development and mortality, physiology, and adaptive behavior of *S. sagax* to environmental changes during the larval and juvenile stages. As the application of the daily egg production method (DEPM) to *S. sagax* has partly relied on egg-development rates at-temperature derived for *S. melanosticta* (Lo et al. 1996), a third goal was to start acquiring new data so that the calibration of DEPM models can be solely based on *S. sagax* age and stage parameters.

MATERIAL AND METHODS

Gonad classification

S. sagax gonads were initially categorized using gross anatomical observations, following a classification method established by Lo et al. (2010b). This method has been applied to classify gonads collected during spring surveys conducted by the SWFSC off California for selecting maturing and mature females for histological analyses of spawning rates. Gonads were evaluated visually, and then ovaries were preserved in 10% formalin

solution. In addition to the visual evaluation, the formalin-preserved ovaries were processed and prepared as hematoxylin and eosin histological (H&E) slides. These slides were analyzed, and their oocytes, atresia, and postovulatory follicles categorized using descriptions in Macewicz et al. (1996), based on the Hunter and Macewicz (1985) classification methods. In addition, the maximum oocyte diameter (MOD) of the most developed oocyte type was recorded to determine how close mature fish were to spawning. Subsequently, the histological analyses were used to determine the phase in the reproductive cycle of each female using standardized terminology developed by Brown-Peterson et al. (2011). Females were either assigned to the immature phase or to one of four mature phases: developing (including the early developing subphase); spawning capable; regressing; and regenerating. Since *S. sagax* are batch spawners, and postovulatory follicle complexes can be identified (aged) as to time since spawning, the spawning capable phase includes the following subphases: actively spawning (that night); past-spawner (one night ago); and past-spawner (two nights ago) (Macewicz et al. 1996).

Broodstock

Young of the year (YOY) *S. sagax* were collected from stocking cages at the Mission Bay bait barge (Everingham Bros. Bait Co.) in San Diego in December 2014 and January 2015. Fish were transferred to the SWFSC aquarium, and were acclimated for 2–3 months in 2,800 L oval tanks. Before acclimation, randomly selected fish ($n = 43$) averaged 157.8 mm (SE = ± 1.3) in fork length (FL; hereafter, fish lengths always are FL) and 35.8 g (SE = ± 0.8) in weight. Ovaries were collected from 21 of the YOY females. Ageing from whole otoliths confirmed that all fish were less than 1 year old (age=0). After acclimation, all individual fish ($N = 367$) were measured for length and weight, and then stocked in a single 4,500 L circular broodstock tank (BST) on March 5 and 6, 2015. In all tanks, water depth was set to 0.9 m, and flow rate was maintained at 23 L/min, allowing the BST to turn over 7.4 times per day.

Broodstock fish were reared at approximately ambient temperature and fixed photoperiod until August 2016. Ambient temperatures approximated daily oceanic conditions off the Scripps Institution of Oceanography (SIO) pier in San Diego (Dorval et al. 2011), varying from 12° to 21°C. The photoperiod consisted of 12 h light (260–300 lx) and 12 h dark cycle. Light intensity was measured with a digital light meter (Extech Instrument, LT 300). Thereafter, with environmental controls, the temperature in the BST was maintained at about 14.7°C ($\pm 0.11^\circ\text{C}$) and light level was reduced to 4–16 lx until May 2017 to simulate the cooler water and reduced light in the natural environ-

TABLE 1
 Photoperiod and temperature conditions for all experimental trials prior and during hormonal injection.
 Duration is expressed in months (mo) and weeks (w).

Experiment	Tank	Period	Duration	Photoperiod	
				Hours of light (lx)	Temperature (SE)
I	BST	Mar 2015–Aug 2016	15 mo	12 (270–300)	17.7°C (±0.11)
I	A, B, C, D	Apr–May 2016	1 mo	12 (270–300)	16°C
I	A, B, C, D	May–Jun 2016	1 mo	8 (150)	14°C
I	A, B, C, D	Jun–Jul 2016	1 mo	10 (58)	12°C
I	A, B, C, D	Jul 2016	1 w	10 (58)	13°C
II	BST	Aug 2016–May 2017	10 mo	12 (4–16)	14.7°C (±0.02)
II	E	Jan 9–Jan 13, 2017	1 w	8 (58)	14.5°C
II	F	Jan 9–Jan 13, 2017	1 w	8 (58)	14.5°C
II	G	Jan 30–Feb 2, 2017	1 w	4 (58)	14.5°C
II	H	Feb 27–Mar 3, 2017	1 w	4 (58)	14.5°C
II	I	May 15–May 19, 2017	1 w	4 (58)	14.5°C
III	BST	Jun 12–Sep 7, 2017	3 mo	12 (270–300)	16.67°C (±0.08)
		Sep 8–Feb 12, 2018	5 mo	12 (4–16)	15.8°C (±0.10)
III	J	Feb 12–Feb 16, 2018	1 w	4 (58)	14.5°C
III	K	Feb 21–Feb 25, 2018	1 w	4 (58)	14.5°C

ment during winter. Note that mature *S. sagax* reside in waters as deep as 30–70 m (Dorval et al. 2011; Stieroff et al. 2019), and off southern California the euphotic depth, where light is 1% of surface value, tends to range slightly deeper than 30 m to a little over 50 m on average (Aknes and Ohman 2009). Therefore, *S. sagax* spend considerable amount of time in near to full darkness during daytime, before emerging at night in surface waters for feeding or spawning. In June 2017, temperature and illuminance in the BST were incrementally increased to reach 17.8°C and 300 lx, respectively. From September 2017 to February 2018, these parameters were progressively decreased to fixed values of 14.5°C and 58 lx, respectively (table 1). In the BST, environmental conditions were monitored daily during the whole study, and percent saturation of dissolved oxygen (DO) was measured as a proxy for water quality.

Throughout this study *S. sagax* were fed an experimental diet comprising 30% of high energy feeds (Oregon BioTrout) and 70% of protein and vitamin enriched gel cubes (Mazuri® Aquatic Gel Diet, MAG). The MAG primarily contained fish and krill protein and oil, essential vitamins including stabilized vitamin C (Stay-C®), vitamins E, K, D3, and B12, and required trace minerals. The MAG was prepared from a mixture of 40% of dried powder (Mazuri® Gel diet Formula Code-5B0C) to 60% water, heated near to boiling, by weight. Hence, the experimental feed approximately comprised 29.2% protein, 11.4% oil (fat), 1.2% crude fiber, 2.6% carbohydrate, 8.1% ash, 44.6% moisture, and at least 0.6% phosphorous, 0.2% selenium, 0.9% vitamins, 1.1% calcium, and 0.3% sodium. Fish were fed throughout the day and provided a daily ration equivalent to 1.5% of their body mass.

Prior to any biological measurement, tagging or hormonal injection, *S. sagax* were anesthetized by immersion in a solution bath of tricaine methanesulfonate (MS-222). Concentration of the solution bath (50 ppm) was similar across trials and, depending on their weight, fish were treated for two to five minutes. For euthanizing fish prior to gonad and otolith extraction, the concentration of MS-222 solution was nearly tripled (140 ppm).

Experimental trials

As fish grew in the BST, occasionally a few were removed for visual examination of gonad maturation. All gonads examined were identified as clearly immature, intermediate, active, or hydrated based on the visibility of yolk-oocyte developmental stages or visible milt (Lo et al., 2010b). Experimental trials were initiated in March 2016 when gonad stage was intermediate or active. The BST fish were sequentially removed from the tank for three experiments to evaluate the effects of photoperiod, light intensity, temperature, hormone combination, and concentration on the gonad maturation. The three experiments were divided into several trials, where fish were reared under varying levels of environmental factors. Because gender cannot be reliably determined based on external examination of *S. sagax*, the number of each sex in the experimental trials was unknown. Prior to each experiment, small samples of fish (2–10) were sacrificed to visually evaluate gonads. In addition, samples of 5–20 were sacrificed 2, 3, or 5 days after hormone injection, except in the last trial where all fish (46) were sacrificed. These samples were dissected to visually evaluate gonads and ovary tissues were collected for histological analyses. Experimental trials were completed in

TABLE 2
Combination of hormone and concentration of solution injected per mean fish body length and weight during each trial.

Experiment	Trial	Hormone	Concentration ^a	Injection date	Dose per fish	Volume injected per fish (ml)	Location	Fish (N)	Sex ratio ^b	Mean weight (g. ±S.E.)	
I	I.1	HCG	600 IU/9 ml	7/12/16	30 IU	0.45	Muscular/	20	1	104.78 (5.58)	
	I.1	CPE	72.4 mg/13.5 ml	7/13/16	1.21 mg	0.20	Dorsal fin				
	I.2	I.2	HCG	600 IU/9 ml	7/12/16	30 IU	0.45	Dorsal fin	20	2.2	109.42 (8.69)
		I.2	SPE	72.12 mg/13.5 ml	7/13/16	1.21 mg	0.20				
		I.2	D122	3.65 mg/13.5 ml	7/13/16	0.06 mg	0.20				
		I.2									
	I.3	I.3	HCG	1,800 IU/22.5 ml	7/19/16	30 IU	0.50	Dorsal fin	28		108 (4.80)
		I.3	CPE	72.31 mg/13.5 ml	7/20/16	2.58 mg	0.50				
	I.4	I.4	HCG	1,800 IU/22.5 ml	7/19/16	30 IU	0.50	Dorsal fin	27		108 (4.80)
		I.4	SPE	72.07 mg/13.5 ml	7/20/16	2.58 mg	0.50				
		I.4	D122	5.08 mg/18 ml	7/20/16	0.14 mg	0.50				
		I.4									
II	II.1	HCG	18,000 IU/12 ml	1/9/17	300 IU	0.20	Peritoneal/	17	1	138.74 (6.88)	
		CPE	125 mg/12 ml	1/10/17	5 mg	0.50					Pelvic fin
	II.2	II.2	HCG	18,000 IU/12 ml	1/9/17	300 IU	0.20	Dorsal fin	16	1	132.58 (6.82)
		II.2	SPE	125 mg/12 ml	1/10/17	5 mg	0.50				
		II.2	D122	1.6 mg/12 ml	1/10/17	0.064 mg	0.30				
		II.2									
	II.3	II.3	HCG	10,000 IU/8 ml	1/30/17	250 IU	0.20	Dorsal fin	32	0.67	149.68(16.59)
		II.3	SPE	200 mg/ 12 ml	1/31/17	6 mg	0.40				
	II.4	II.4	HCG	10,000 IU/8 ml	2/27/17	250 IU	0.20	Dorsal fin	40		174.98 (9.08)
		II.4	CPE + D122	((400 mg CPE) + 11 mg D122)/24ml	2/28/17	8.33 mg CPE + 0.23 mg D122	0.50				
	II.5	II.5	HCG	10,000 IU/8 ml	5/15/17	250 IU	0.20	Dorsal fin	38		160.95 (9.70)
		II.5	CPE + D122	((400 mg CPE) + 11 mg D122)/24ml	5/15/17	8.33 mg CPE + 0.23 mg D122	0.50				
II.5											
II.5											
III	III.1	HCG	10,000 IU/8 ml	2/12/18	313 IU	0.25	Peritoneal/	30	1.14	193.82 (6.44)	
		CPE + D122	((360 mg CPE) + 9.44 mg D122)/24ml	2/13/18	10.5 mg CPE + 0.28 mg D122	0.70					Pelvic fin
	III.2	III.2	HCG	15,454 IU/12.5 ml	2/21/18	309 IU	0.25	Dorsal fin	46	0.77	167.64 (5.12)
		III.2	CPE + D122	((490 mg CPE) + 13.04 mg D122)/38.8ml	2/22/18	8.84 mg CPE + 0.24 mg D122	0.70				
		III.2									
		III.2									

^aConcentrations are in IU/ml for HCG and mg/ml for all other hormones. IU is the international unit used to indicate the amount of biological activity of a substance, e.g. the hormone HCG.

^bSex ratio = Female/male

2840 L oval tanks located in an enclosed section of the aquarium, where light intensity and photoperiod were controlled. In all trials, fish were not fed the day prior to the start of hormonal injections.

Experiment I: This experiment was designed to simulate environmental conditions that *S. sagax* may experience during the last three months prior to their spring spawning in the SCB. These conditions, decreasing temperature, and photoperiod followed first by increasing photoperiod and then increasing temperature, simulate conditions that would be experienced during migration, beginning in the fall and early winter to spring, from feeding areas off the PNW to spawning in the SCB (Lo et al. 2010a; Dorval et al. 2014). In April 2016, 120 fish were subsampled from the BST and assigned randomly to four trial tanks (A, B, C, D) at a density of 30 fish per tank. For three months the fish in all four tanks were reared under the same changing photoperiod and temperature conditions (table 1). At the end of the three-month period, the fish in each tank were treated with a different hormone combination, potentially to induce spawning, as described for trials I.1 to I.4 in Table 2.

Experiment II: The aim of this experiment was to maintain the BST within a range of temperatures that varied little from the mean temperature (14.5°C) measured from plankton (pairovet net) tows that captured *S. sagax* eggs during summer surveys in 1986 and 1987 and spring surveys in 1994 and 2004–13 in the SCB (Dorval et al. 2014). Thus, temperature in the BST was decreased from an average ambient temperature of 17.7°C to a mean of 14.7°C from August 2016 to May 2017. Photoperiod in the BST was set at a 12 h cycle and light intensity during the day was lowered to 4–16 lx to approximate environmental condition during winter and up to the spawning season. Trials began when a sampled female was classified as having an active ovary with yolked oocytes visible. Randomly selected fish samples (20–40) from the BST were apportioned among five tanks, and trials (II.1–II.5) were conducted using five combinations of hormones (table 2). Trials II.1 to II.4 were conducted at the beginning of the normal spawning season (January–February), whereas II.5 was conducted near the end of the season (May).

Experiment III: The objective of this experiment was to determine whether fish that were previously treated or not with hormones could again mature their gonads in the laboratory the following year, and whether trial II.4 could be replicated. In June 2017, all surviving fish from Experiment II were mixed with the remaining fish in the BST. Temperature in the BST was then progressively increased from 14.5°C to 18°C by the end of August 2017, before being decreased to 14.5°C by mid-December and held at that level through Feb-

ruary 2018. From June to August 2017, light intensity ranged from 270 to 300 lx to simulate summer environmental conditions, and from September 2017 to February 2018 it was lowered to <5 lx, approximating winter conditions (table 1). Two experimental trials were conducted (III.1 and III.2) using the same combinations of hormones and the same number of injections as in trial II.4 (table 2).

Hormone Induction

Hormones used in trials were selected based on previously successful spawning experiments of small pelagic fish (Leong 1971; Leong 1989; Olmedo et al. 1990), and other cultured species (Zohar et al. 2001). Four types of hormones were used: (1) human chorionic gonadotropin (HCG, Sigma-Aldrich®), prepared as a lyophilized powder from human pregnancy urine; (2) carp pituitary extract (CPE, Argent Aquaculture®), purified from the pituitary gland of *Cyprinus* spp.; (3) salmon pituitary extract (SPE, Argent Aquaculture®), purified from the pituitary gland of salmonid species; and (4) Domperidone (D122-100MG, Sigma-Aldrich®) a dopamine antagonist prepared as dried powder.

HCG solutions were prepared less than 1 h before injection, whereas solutions of CPE, SPE, and D122 were prepared 2–3 h prior to injection. Hormonal powders were weighed using a dual range analytical balance (Mettler Toledo XS205) with a repeatability of 0.1 mg. All hormonal powders were dissolved in sterilized 0.9% saline water (Teknova®). For all trials, the induction method consisted of: HCG injections during the first day followed by CPE, SPE, and Domperidone 24 h later. The combinations and concentrations of these hormones for each trial are provided in Table 2. Solutions of HCG were injected using #23 gauge needles, whereas for all other hormones #22 gauge needles were used. After each day of injection, the photoperiod was set according to the objective of the experiment (table 2). During the first experiment, hormones were injected intramuscularly below the dorsal fin, whereas during the second and third experiments, hormones were injected in the peritoneal cavity about half way between the pelvic fins and the anal pore.

Egg Incubation

After spawning, eggs were collected and incubated to verify their viability and development up to hatching and early larval stage through yolk absorption. The incubation system consisted of three Cole-Parmer® (Polystat R6L) incubators, each of which controlled temperature in a separate bath. Each bath consisted of a Styrofoam box containing fresh water and a copper coil connected via plastic tubing to the incubator. A 6-L beaker containing approximately 5 L of seawater was placed within

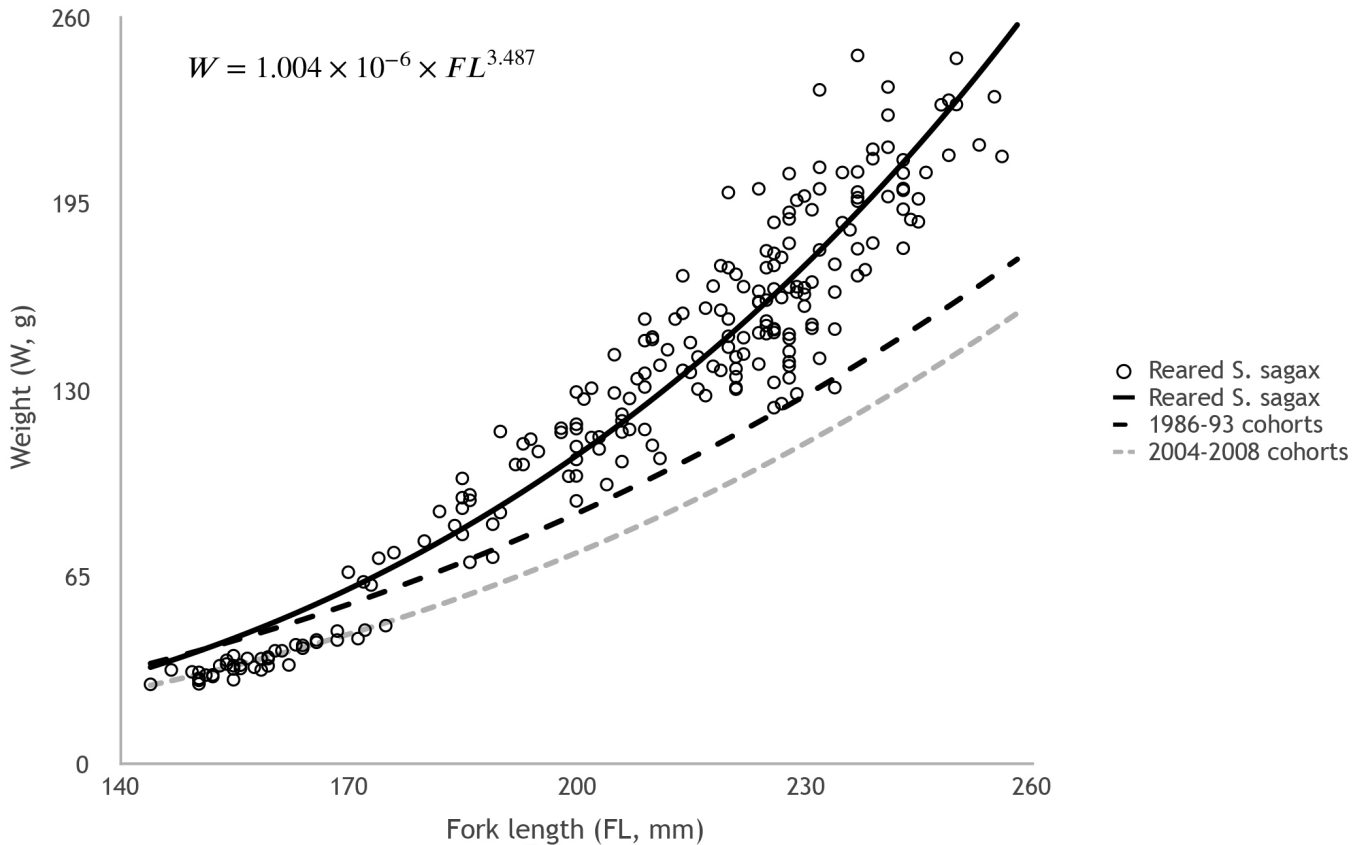


Figure 1. Comparison of predicted weight-at-length of *S. sagax* reared over 39 months during the spawning experiment and wild caught fish (1986–93 and 2004–08 cohorts) collected off California during spring surveys. The equation shown on the plot is for laboratory-reared *S. sagax*. Predicted curves for the two aggregated cohorts were derived from weight-length relationships in Dorval et al. (2015).

each coil and maintained at a constant preset temperature ($\pm 0.1^\circ\text{C}$). Prior to egg collection, the incubators were set at 11° , 13° , and 15°C , respectively, to represent the range of oceanic temperatures likely experienced by *S. sagax* eggs in the SCB during spring.

Eggs were collected in an egg trap consisting of a five-gallon bucket with drainage holes covered by $150\ \mu\text{m}$ mesh. The trap was connected to the drainage system of the spawning tank. Recently spawned eggs were pipetted from the egg trap and transferred to the 6-L beakers, at a density of approximately 400 eggs per beaker, but remaining eggs in the trap were not counted. Because relatively few eggs were spawned in experiment III, only the 15°C bath was used for that experiment. At the start of the incubation five eggs from each beaker were sampled and preserved in 3% formalin, and the time of preservation was recorded as sample 1. Eggs were initially sampled every hour for the first 3 h of the incubation. Thereafter, egg samples were collected every 2 h in each beaker until the completion of hatching. After hatching, yolk-sac stage larvae were collected daily until their eyes were fully pigmented and the yolk reserve was depleted.

RESULTS

Rearing and growth

In the laboratory-controlled environment, juvenile *S. sagax* grew and matured following a different growth trajectory than in wild-caught fish (fig. 1). Body weight was nonlinearly related to length with an allometric coefficient of 3.487 and an intercept of 1.004×10^{-6} ($SE = 0.52 \times 10^{-6}$). The fish nearly quintupled in average weight from the time of capture ($35.8\ \text{g} \pm 0.8$) to the end of the experiment ($178.0\ \text{g} \pm 4.2$). Mature *S. sagax* averaged 216 mm ($SE = \pm 2.3$) and 234 mm ($SE = \pm 1.3$) at 27–30 and 39 months, respectively (fig. 2). The fish experienced low mortalities ($<35\%$ in 30 months) during the course of the experiment. The ratio of females to males ranged from 0.6 to 2.2 in the trials. Percent saturation of DO averaged 100% ($SE = \pm 0.27$), indicating high level of water quality was maintained throughout the experiment.

Gonad development

S. sagax collected at the San Diego bait barge in December 2014 and January 2015 were largely domi-

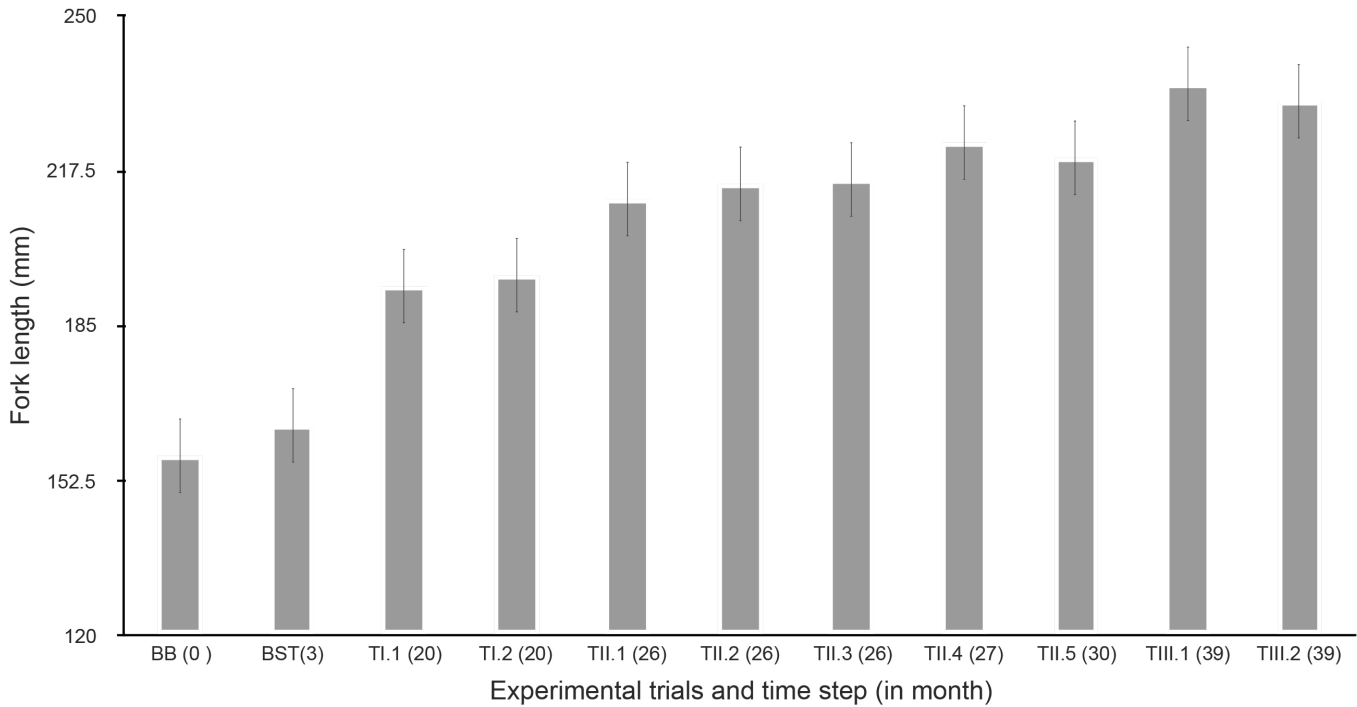


Figure 2. Mean fork length of *Sardinops sagax* sampled from the San Diego bait barge (BB) and from the broodstock tank (BST) during each experimental trial. Values in parenthesis are number of months since initial fish collection. Error bars are \pm 1SD.

nated by immature individuals or individuals entering sexual maturity for the first time. Histological analysis of ovarian tissue showed that 38% of these females were immature (table 3). Mature females (62%) were in the developing phase, with most in the early developing sub-phase ($n = 11$), and their ovaries contained non-yolking oocytes less than 0.3 mm in diameter. In gross anatomical evaluation of testes, most males (71%) were identified as clearly immature.

After 20 months of rearing, less than 18% of females were categorized as immature, suggesting that the broodstock was largely comprised of sexually mature fish. Although the mature females were in the developing phase, less than 50% were in the early developing sub-phase, and 20% had begun vitellogenesis (table 3). By 25 months (January 2017), all *S. sagax* were mature with all females producing yolking oocytes and 20% were spawning capable. In late February, 2017, 50% of observed ovaries contained hydrated oocytes, and milt was present in all testes. Females sampled in February 2017 had substantially larger gonads than those collected in January (table 3). In May 2017, most females had reduced gonads, which weighed less than 1.6 g. Most male testes were still secreting milt, but 10% had regressed to the intermediate category (table 4).

In February 2018, all observed males but one were secreting milt and all females had mature ovaries. Nine out of 15 females from trial III.1 were spawning capa-

ble, including five that had postovulatory follicles, indicating past spawning (table 3). Five out of 18 females were spawning capable in trial III.2, with two females exhibiting postovulatory follicles. Most of the developing and all of the spawning capable females had moderate to major atresia of vitellogenic oocytes.

Induced spawning

Neither females nor males injected in experiment I responded to hormonal induction. The fish were relatively small, with mean weights ranging from 105 to 113 g. The means of realized concentrations of HCG ranged from 27 to 29 IU per 100 g of body weight, and those for CPE and SPE ranged from 1.07 to 2.11 g per 100 g of body weight. In trial I.2 fish were injected with a separate dose of Domperidone at a concentration of 0.05 mg per 100 g of fish, but this hormone apparently had no effects.

Concentrations of hormone solutions were increased in experiment II (table 2). During trials II.1–II.3, mean realized concentrations of HCG ranged from 116 IU to 216 IU per 100 g of body weight, whereas 3.6 g to 4 g of CPE or SPE were injected per 100 g of body weight. Domperidone was separately injected in fish from trial II.2 at a concentration of 0.05 mg per 100 g of body weight. Although female *S. sagax* did not respond to hormonal treatment during these trials, 88% of males in trial II.1 and 50% males in trial II.2 secreted milt.

TABLE 3
Sardinops sagax reproductive cycle phases and range of ovary wet weight (g) and maximum oocyte diameters (MOD in mm) observed from ovaries of fish collected at the San Diego bait barge (BB) and during each experimental trial.

Experiment	Trial	Sample date	Ovary N	Ovary wet weight ^a	Immature phase		Mature phases			
					n	MOD	Developing		Spawning capable	
							n	MOD	n	MOD
BB		12/04/2014 or 01/15/2015	21		8	0.13–0.15	13	0.15–0.27		
I	I.1	7/18/16	12		2	0.16–0.16	10	0.19–0.37		
	I.2	7/18/16	11		2	0.13–0.15	9	0.21–0.40		
II	II.1	1/11/2017 or 1/13/2017	5	2.60–3.60			5	0.35–0.44		
	II.2	1/11/2017 or 1/13/2017	9	1.50–5.30			7	0.29–0.56	2	0.61–0.63
	II.3	2/3/17	2	1.60–3.00			2	0.30–0.48	1 ^b	0.67
	II.4	3/3/17	9	2.30–7.90			3	0.35–0.58	6 ^c	0.48–0.63
	II.5	5/19/17	3	1.00–1.50			3	0.21–0.47		
III	III.1	2/15/18	15	3.22–13.85			6	0.30–0.48	9 ^c	0.49–0.65
	III.2	2/23/2017 or 2/26/18	18	1.82–7.99			13	0.18–0.51	5 ^c	0.50–0.57

^aSpawning female ovary weight ranged from 6.4 to 7.9 g and their body weight ranged from 143–170 g.

^bOvaries were dissected before hormonal injection.

^cNumber of females that spawned after hormonal injection: 5 in II.4 and III.1, and 2 in III.2

TABLE 4
 Gross anatomical evaluation of *Sardinops sagax* testes after hormonal injections during experiment II and III.

Experiment	Trial	Percentage of testes in each category		
		Clearly immature	Intermediate	Active
II	II.1	0	20	80
	II.2	0	43	57
	II.4	0	0	100
	II.5	0	10	90
III	III.1	0	0	100
	III.2	0	0	100

In trial II.4, within 24 h after the second injection, *S. sagax* spawned and newly spawned eggs were observed in the traps. On the first day of the trial, fish were injected with 143 IU of HCG per 100 g of body weight on average. On the second day, fish were treated with a mixed solution of CPE and D122 at a dosage of 4.76 g and 0.13 mg per 100 g of fish, respectively. Spawning and fertilization occurred naturally. Nineteen *S. sagax* were sacrificed from this trial, two days after spawning, comprising nine females and ten males. Based on visual and histological analyses, five females did spawn two nights prior to sampling, whereas six males were actively secreting milt.

Hormonal induction had no effects on females injected during trial II.5. Although fish were not sampled between trials II.4 and II.5, ovaries of mature females were in the developing phase which indicated that within two months ovaries could pass through the regressing phase and be back in the developing phase of

the reproductive cycle. In contrast, 90% of males were still oozing milt.

Mature *S. sagax* treated with hormones in trials III.1 and III.2 successfully spawned. Similarly to trial II.4, spawning occurred 20 h after the second injection. On average, fish were injected with 161–184 IU of HCG, and 5.35 mg of CPE plus 0.14 mg of Domperidone per 100 g of body weight, respectively, during the first and second day of these trials. Histological analyses showed that five females in trial III.1 and two in trial III.2 did spawn prior to sampling (table 3).

Egg rearing

Live fertilized eggs siphoned in trial II.4 from the egg-trap were at the 2- and 4-cell stage of embryogenesis, approximately 4–8 h post-fertilization, at the time of collection and transfer to the incubation baths. The rate of subsequent embryonic development and time until hatching was a function of incubation temperature, with eggs reared at 15°C hatching approximately 63 h to 77 h after fertilization, and those at 11°C developing much more slowly, hatching approximately 111 h to 127 h after fertilization (table 5). Egg samples collected every 2 h up to hatching showed no obvious visual morphological differences from those collected in the wild.

Duration of the yolk-sac stage of larval development was, like the rate of embryonic development, a function of water temperature, with larvae at 15°C completing yolk absorption within seven days after hatching, those at 13°C completing yolk absorption within nine days after hatching, and those at 11°C not completing yolk absorption by ten days after hatching, when the experiment was terminated.

TABLE 5
 Estimated hours following fertilization to hatching and yolk absorption at 11°, 13°, and 15°C during the egg rearing experiment.

Temperature (°C)	Hatching		Yolk sac absorption
	Start time (h*)	End time (h*)	End time (h*)
11	111	127	> 167**
13	83	97	239
15	63	77	167

*Estimated number of hours were approximate due to the intervals of egg collection.

**Few embryos survived to hatching and yolk-sac larvae were not collected after 167 hours although a very few, still in yolk-sac stage, found in the final collection at termination of the experiment may have survived until then.

In trial III.1 far fewer eggs were available for collection compared with trial II.4, and in trial III.2 even fewer were available. Although eggs initially appeared to be viable in both trials, in trial III.1 most eggs apparently were not fertilized and embryos did not develop. The few eggs that did begin embryogenesis mostly developed abnormally and did not survive past the first few cleavages, dying after 16 h; none survived through the morula stage of development. In trial III.2, although there were fewer eggs, a larger proportion were fertile and began normal embryogenesis; however, few survived past the morula stage and none survived through the blastula stage of development. Most of these eggs died after 23 h of incubation, although one stage-3 egg, showing the segmentation cavity between the blastodisc and the yolk mass, was collected alive in the final sampling.

DISCUSSION

For the first time YOY *S. sagax*, reared over two years, were induced to spawn under experimentally controlled temperature, diet, photoperiod, and hormonal treatments. Female *S. sagax*, fully spawning capable after 27 months of rearing, were induced to spawn using a combination of HCG, CPE, and Domperidone. Eggs were fertilized naturally, and were reared through hatching and the yolk-sac larval stage. This study demonstrated that *S. sagax* can be induced to spawn in captivity, and can produce healthy eggs and larvae, although repeated hormonal treatments on the same broodstock may affect egg quality. These experiments establish a basis for designing a subsequent experiment series to refine the technique so that spawning can be efficiently and reliably induced, and for developing laboratory studies to enhance the understanding of *S. sagax* early life history strategies and adaption to changes in environmental conditions.

Fish rearing and growth

Compared to past experiments, *S. sagax* reared in this study were healthier, lived longer, and reached similar length-size to wild-caught spawning fish in the SCB

(Dorval et al. 2015; Dorval et al. 2011; Javor and Dorval 2016). Although the experiment was not set to specifically contrast the effects of biological and environmental parameters, several factors contributed in improving the quality of rearing conditions. In this study, we transitioned from a high-energy feed (BioTrout pellets) to a more balanced diet combining these pellets with the MAG, which provided additional proteins and oils from fish and krill and essential vitamins and minerals. The experimental feed contained nearly 24% less fat than BioTrout pellets. It also contained stabilizing vitamin C (Stay-C), and at least 2% of essential minerals, including selenium. Stay-C is more digestible than other ascorbic acid polymorphs, and has been shown to enhance growth rates, survival rates, and immune responses of juvenile fish (Liang et al. 2017; Khan et al. 2017; Zhou et al. 2012). Selenium can improve lysozyme activity, hence boosting the immunity of fish (Burk et al. 2003). One potential direct impact of these nutrients on *S. sagax* health was the near disappearance of the puffy snout syndrome (eye and mouth occlusion which limits feeding), which was frequently observed in *S. sagax* and other pelagic fish reared during past experiments that lacked these supplements. No puffy snouts were observed during the first three years of experiments, and only three fish exhibited this syndrome during the last two experimental trials.

Beyond the reduction in fat content and availability of essential vitamins, the experimental feed also provided proteins and oils from a more diverse source of marine animals, including different fish and krill species, than is available in the high-energy feed. During the 30 months of the experiment, *S. sagax* more than quadrupled their growth. The weight and length relationship had an allometric coefficient (3.5 ± 0.1 , fig. 1) higher than observed in wild-caught spawning fish (2.8 ± 0.01) suggesting that fish reared in this study accumulated more mass per unit length than those from the natural population (Dorval et al. 2015). Hence, using a diet formulation that contains nearly all essential nutrients facilitated the maintenance of a healthy broodstock during the experiment. Further, compared to Dorval et al. (2011) daily ration was reduced from 5% body weight to only 1.5%, leading to significantly reduced accumulation of wastes and improved water quality in rearing tanks.

To optimize growth rate while minimizing the risk of diseases, YOY *S. sagax* were reared at an average temperature of 17.7°C (± 0.11). However, for stimulating gonad development and maturation, older *S. sagax* were raised in water averaging 14.7°C. These experimental temperatures simulated the average SSTs likely to be experienced by the northern stock, which mostly resides in water below 17°C. Dorval et al. (2011) found that at 17°C *S. sagax* grew faster than at 13°C, and achieved

better survival rates than at 21°C. However, the stock appears to have adapted to spawn primarily between 13° and 15°C. From 1994 to 2013 *S. sagax* eggs were collected in the SCB in surface waters ranging from 13.4° to 18.9°C on average, but mean temperature exceeded 15°C in only two (1986 and 1987) of 12 years of surveys (Dorval et al. 2014).

Controlling photoperiod levels was also critical to *S. sagax* growth, particularly before they fully reached sexual maturity. YOY were reared at 12-h-day light intensity ranging from 270 lx to 300 lx during the first year. To simulate winter environmental conditions light intensity was set to 4–16 lx; whereas prior to hormonal induction illuminance was set to be equal or less than 4 lx in the successful trials. Previous studies have demonstrated that photoperiod can determine the optimal temperature of growth for juvenile *Gadus morhua* and *Hippoglossus hippoglossus* (Imstrand et al. 2007; Jonassen et al. 2000). However, the effect of light intensity is less predictable as it may greatly vary with species and environmental conditions (Boeuf and Le Bail 1999). To our knowledge no studies have determined the optimal combination of photoperiod and temperature for juvenile *S. sagax* growth, warranting the development of new growth experiments in this area.

Gonad development and maturation

S. sagax reared during this experiment appeared to follow similar seasonal patterns in maturation and regression of their gonads as in wild-caught fish. The patterns of gonad development and regression followed closely those of the northern stock of *S. sagax* that develop in late winter and early spring in the SCB, spawn from March to late April, and begin gonadal regression by early May when little spawning occurs off California (Dorval et al. 2014; Macewicz et al. 1996). Further, these results demonstrated that the development of gonads in *S. sagax* is strongly tied to their natural biological clock and environmental conditions, and that hormonal induction played little role until the near completion of this process when they were in the spawning capable phase. Similar to other pelagic fish such as *E. mordax*, *Sardina pilchardus*, and *S. melanostictus*, it appeared that hormones only act as a stimulator of final oocyte maturation (FOM) and ovulation in *S. sagax*. Finally, these results showed that photoperiod does play a role in *S. sagax* maturation, although its optimal level and interactions with temperature and other environmental parameters remain to be quantified.

Induced-spawning

In this study, various exploratory experimental trials (I.1–I.4, II.1–II.3) were conducted, prior to determining the timing of hormonal induction and the combi-

nation of hormones that could be replicated to induce spawning in *S. sagax*. Three spawning trials, II.4, III.1, and III.2, successfully induced *S. sagax* to spawn using a combination of HCG, CPE, and Domperidone injections (table 2). Doses of HCG (143–184 IU) and CPE (4.8–5.5 g) per 100 g of body weight used in the three trials were within the range of concentrations used for *E. mordax* (Leong 1971, 1989). HCG was also within the range administered to most captive fish, which may vary from 10 to 400 IU per 100 g of body weight (Zohar and Mylonas 2001). Single treatments with HCG can stimulate FOM and ovulation in many cultured fish, for example cobia (*Rachycentron canadum*) at very low dose (i.e., 27.5 IU per 100 g) (Caylor et al., 1994), and mangrove red snapper (*Lutjanus argentimaculatus*) at very high dose (i.e., 1,500 IU per 100 g) (Emata et al. 1994). The potency of HCG in fish species is likely due to its long retention time in blood vessels (Ohta and Tanaka 1997; Zohar and Mylonas 2001). However, for small pelagic fish such as *E. mordax* and *S. sagax*, its effectiveness seems to depend on the addition of other hormones. HCG did not work alone in *E. mordax* (Leong 1971), and its combination with CPE and pregnant mare serum was necessary to induce spawning in *Sardina pilchardus* (Olmedo et al. 1990). Similarly, in the successful trials of this study, fish were injected with a mixed solution of CPE and Domperidone, 24 h after the HCG injection. The CPE used in this study provided additional gonadotropins purified from carp pituitary (Yaron 1995). The Domperidone, a dopamine antagonist, injected at 0.13–0.14 mg per 100 g of body weight, helped remove the inhibition on gonadotropins and thus further enhanced the effects of HCG and CPE on FOM and ovulation (Zohar and Mylonas 2001).

It is difficult to identify the exact causes for lack of FOM and ovulation in trial II.3, which combined HCG, SPE, and Domperidone injections in fish with closely similar gonad maturation as in trial II.4. However, poor handling in trial II.3 might have increased stress levels, and consequently reduced the effectiveness of the hormones. There could be also species specificity for these hormones. If so, it is possible that SPE gonadotropins may not be useful for *S. sagax*. The timing of injections might be a determining factor as well. For example, it has been shown that the effects of dopamine antagonists, such as Domperidone, may change over the course of the reproductive cycle, and the magnitude of changes may be species-specific (Peter et al. 1986; Trudeau and Peter 1995). Finally, it is important to note that the determination of optimal hormone combinations, dosages, and species-specificity was beyond the scope of this study. However, experiments are being planned to determine their optimal levels for inducing spawning in *S. sagax*.

Egg incubation

Reared eggs and yolk-sac stage larvae from trial II.4 were qualitatively similar to wild-caught eggs and larvae, and appear to have developed normally. Rates of embryogenesis that we observed were consistent with findings from previous studies. For example, Lasker (1964) found that at 11°C hatching may occur 140 h after spawning, whereas at 21°C it took only 34 h for eggs to hatch post-spawning. Yolk-sac stage larvae at 11°C were largely inactive and did not complete yolk absorption before the experiment ended, while those at 15°C became increasingly active after the first day post-hatching, which undoubtedly contributed to their higher rate of yolk utilization and completion of the yolk-sac stage within seven days after hatching.

We made no attempt to quantify mortality rates during embryonic and larval development following trial II.4, but visual inspection during sample collections suggested that mortality rates of eggs and larvae reared at 11°C were somewhat higher than those of eggs reared at 15°C and 13°C, however, they were not noticeably different from rates observed during rearing of wild-caught eggs and larvae in other experiments (unpublished data). Given that *S. sagax* batch fecundity may range from 17,662 to 60,916 oocytes for females averaging 67 to 192 g (Dorval et al. 2016), the relative paucity of eggs resulting from trials III.1 and III.2 was not likely due to the sex ratio or the number of females that spawned in either trial. Although there were more males than females in trial III.2 (table 2), histological analysis of observed samples showed 2 females (out of 5 spawning capable) spawned during this trial. Further, the number of spawned females in trials II.4 and III.1 was similar, i.e. $n = 5$ (table 3). The preponderance of unfertilized eggs resulting from trial III.1 is also difficult to explain because all males collected from that trial were actively secreting milt, and environmental conditions were similar to trial III.2. Although initially viable eggs resulted from both trials, the abnormal development and very early complete mortality of embryos in trial III.1, and apparently normal development but complete mortality of embryos by only a few hours later in embryogenesis during trial III.2, suggests the possibility that repeated hormone-induced spawning of *S. sagax* will not yield viable progeny. Additional induced spawning and egg incubation trials will be required to explore this possibility. In the future, we also plan to attempt rearing larvae resulting from induced spawning experiments through a complete life cycle to maturity. Furthermore, the temperature-dependent embryogenesis experiment conducted here is part of a separate, larger study of the relationship of temperature with the rate of embryonic development in *S. sagax* over a much broader temperature

range (9°–21°C) to which the northern stock is likely adapted (Pribyl et al. 2016). This study will be treated in a separate paper, which will provide new data to calibrate and improve the parametrization of the daily egg production method for *S. sagax*.

ACKNOWLEDGMENTS

We thank Erin Lyman (Monterey Bay Aquarium) for her advice on pelagic fish diets. We also thank Helena Aryafar and Julianne Taylor for their assistance with fish collection and sample processing, and Noelle Bowlin for helping with fish rearing and spawning induction. We are grateful to Barbara Javor, whose comments have greatly improved the manuscript. This study was conducted at the SWFSC Aquarium under Fish and Invertebrate Protocol # SW1601.

LITERATURE CITED

- Akness, D. L., and M. D. Ohman. 2009. Multi-decadal shoaling of the euphotic zone in the southern sector of the California Current System. *Limnol. Oceanogr.*, 54:1272–1281.
- Boeuf, G., and P. E. Le Bail. 1999. Does light have an influence on fish growth? *Aquaculture* 177: 129–152.
- Brown-Peterson, N. J., D. M. Wyanski, F. Saborido-Rey, B. J. Macewicz, and S. K. Lowerre-Barbieri. 2011. A standardized terminology for describing reproductive development in fishes. *Mar. Coast. Fish.* 3: 52–70.
- Butler, J. L., P. E. Smith, and N. C. H. Lo. 1993. The effect of natural variability of life-history parameters on anchovy and sardine population growth. *Calif. Coop. Oceanic Fish. Invest. Rep.* 34:104–111.
- Burk, R. F., K. E. Hill, and A. K. Motley. 2003. Selenoprotein metabolism and function: Evidence for more than one function for selenoprotein. *J. Nutr.* 133: 1517–1520.
- Caylor, R. E., P. M. Biesiot, and J. S. Franks. 1994. Culture of cobia (*Rachycentron canadum*) cryopreservation of sperm and induced spawning. *Aquaculture* 125: 81–92.
- Conover, D. O., and H. Baumann. 2009. The role of experiments in understanding fishery-induced evolution. *Evol. Appl.* 2: 276–90.
- Demer, D. A., and J. P. Zwolinski. 2013. Corroboration and refinement of a method for differentiating landings from two stocks of Pacific sardine (*Sardinops sagax*) in the California Current. *ICES J. Mar. Sci.* 71: 328–335.
- Demer, D. A., J. P. Zwolinski, K. A. Byers, G. R. Cutter, J. S. Renfree, T. S. Sessions, and B. J. Macewicz. 2012. Prediction and confirmation of seasonal migration of Pacific sardine (*Sardinops sagax*) in the California Current Ecosystem. *Fishery Bulletin* 110, 52–70.
- Dorval, E., B. J. Macewicz, D. A. Griffith, and Y. Gu. 2014. Spawning biomass of Pacific sardine (*Sardinops sagax*) estimated from the daily egg production method off California in 2013. NOAA-TM-NMFS-SWFSC-535.
- Dorval, E., B. J. Macewicz, D. A. Griffith, and Y. Gu. 2016. Spawning biomass of Pacific sardine (*Sardinops sagax*) estimated from the daily egg production method off California in 2015. NOAA-TM-NMFS-SWFSC-560.
- Dorval, E., J. D. McDaniel, B. J. Macewicz, and D. L. Porzio. 2015. Changes in growth and maturation parameters of Pacific sardine *Sardinops sagax* collected off California during a period of stock recovery from 1994 to 2010. *J. Fish. Biol.* 87: 286–310.
- Dorval, E., K. Piner, L. Robertson, C. S. Reiss, B. Javor, and R. Vetter. 2011. Temperature record in the oxygen stable isotopes of Pacific sardine otoliths: Experimental vs. wild stocks from the Southern California Bight. *J. Exp. Mar. Biol. Ecol.* 397: 136–143.
- Emata, A. C., B. Eullaran, and T. U. Bagarinao. 1994. Induced spawning and early life description of the mangrove red snapper, *Lutjanus argentimaculatus*. *Aquaculture* 121: 381–387.
- Félix-Uraga, R., C. Quiñónez-Velázquez, K. T. Hill, V. M. Gómez-Muñoz, F. N. Melo-Barrera, and W. García-Franco. 2005. Pacific sardine (*Sardinops sagax*) stock discrimination off the west coast of Baja California and southern California using otolith morphometry. *Calif. Coop. Oceanic Fish. Invest. Rep.* 46: 113–121.

- Hargreaves, N. B., D. M. Ware, and G. A. McFarlane. 1994. Return of Pacific sardine (*Sardinops sagax*) to the British Columbia coast in 1992. *Can. J. Fish. Aquat. Sci.* 51: 460–463.
- Hill, K. T., P. R. Crone, E. Dorval, and B. J. Macewicz. 2016. Assessment of Pacific sardine resource in 2016 for U.S. Management. NOAA-TM-NMFS-SWFSC-562.
- Hunter, J. R., and B. J. Macewicz. 1985. Rates of atresia in the ovary of captive and wild northern anchovy, *Engraulis mordax*. *Fish. Bull.* 83: 119–136.
- Imsland, A. K., A. Foss, T. Alvseike, A. Folkvord, S. O. Stefansson, and T. M. Jonassen. 2007. Interaction between temperature and photoperiod on growth and feeding of Atlantic cod (*Gadus morhua*): possible secondary effects. *Can. J. Fish. Aquat. Sci.* 64: 239–248.
- Javor, B., and E. Dorval. 2016. Stability of trace elements in otolith of juvenile Pacific sardine, *Sardinops sagax*. *Calif. Coop. Oceanic Fish. Invest. Rep.* 57: 109–123.
- Jonassen, T. M., A. K. Imsland, S. Kadowaki, and S. O. Stefansson. 2000. Interaction of temperature and photoperiod on growth of Atlantic halibut *Hippoglossus hippoglossus* L. *Aquac. Res.* 31: 219–227.
- Khan, K. U., A. Zuberi, S. Nazir, I. Ullah, Z. Jamil, and H. Sarwar. 2017. Synergistic effects of dietary nano selenium and vitamin C on growth, feeding, and physiological parameters of mahseer fish (*Tor putitora*). *Aquac. Rep.* 5: 70–75.
- Lasker. 1964. An experimental study of the effect of temperature on the incubation time, development, and growth of Pacific sardine embryos and larvae. *Copeia* 1964: 399–405.
- Leong, R. 1971. Induced spawning of the northern anchovy, *Engraulis mordax* Girard. *Fish. Bull.* 69: 357–360.
- Leong, R. J. H. 1989. Sperm concentration and fertilization rate during spawning of captive anchovy, *Engraulis mordax*. *Calif. Coop. Oceanic Fish. Invest. Rep.* 30: 136–139.
- Liang, X. P., Y. Li, Y. M. Hou, H. Qiu, and Q. C. Zhou. 2017. Effect of dietary vitamin C on the growth performance, antioxidant ability and innate immunity of juvenile yellow catfish (*Pelteobagrus fulvidraco* Richardson). *Aquac. Res.* 48: 149–160.
- Lo, N. C. H., B. J. Macewicz, and D. A. Griffith. 2010a. Spawning biomass of Pacific sardine (*Sardinops sagax*) off the US in 2010. NOAA-TM-NMFS-SWFSC-463.
- Lo, N. C. H., B. J. Macewicz, and D. A. Griffith. 2010b. Biomass and reproduction of Pacific sardine off the Pacific northwestern United States, 2003–2005. *Fish. Bull.* 108: 174–192.
- Lo, N. C. H., B. J. Macewicz, and D. A. Griffith. 2011. Migration of Pacific sardine (*Sardinops sagax*) off the west coast of the United States in 2003–05. *Bull. Mar. Sci.* 87: 395–412.
- Lo, N. C. H., Y. A. Green-Ruiz, M. J. Cervantes, H. G. Moser, R. J. Lynn. 1996. Egg production and spawning biomass of Pacific sardine (*Sardinops sagax*) in 1994, determined by the daily egg production method. *Calif. Coop. Oceanic Fish. Invest. Rep.* 37: 160–174.
- Macewicz, B. J., J. J. Castro-Gonzalez, C. E. Cotero-Altamirano, and J. R. Hunter. 1996. Adult reproductive parameters of Pacific sardine (*Sardinops sagax*) during 1994. *Calif. Coop. Oceanic Fish. Invest. Rep.* 37: 140–151.
- Nieto, K., S. McClatchie, E. D. Weber, and C. E. Lennert-Cody. 2014. Effect of mesoscale eddies and streamers on sardine spawning habitat and recruitment success off southern and central California. *J. Geophys. Res.* doi/10.1002/2014JC010251.
- Ohta, H., and H. Tanaka. 1997. Relationship between serum levels of human chorionic gonadotropin (hCG) and 11-ketotestosterone after a single injection of hCG and induced maturity in the male Japanese eel, *Anguilla japonica*. *Aquaculture* 153: 123–134.
- Olmedo, M., J. Iglesia, J. B. Peleteiro, R. Forés, and A. Miranda. 1990. Acclimatization and induced spawning of sardine, *Sardina pilchardus* Walbaum in captivity. *J. Exp. Mar. Biol. Ecol.* 140: 61–67.
- Peter, R. E., J. P. Chang, C. S. Nahorniak, R. J. Omeljaniuk, M. Sokolowska, S. H. Shih, and R. Billard. 1986. Interaction of catecholamines and GnRH of Gonadotropin secretion in teleost fish. *Rec. Prog. Horm. Res.* 42: 513–548.
- Pribyl, A. L., J. R. Hyde, L. Robertson, and R. Vetter. 2016. Defining an ideal temperature range for the northern subpopulation of Pacific sardine, *Sardinops sagax caeruleus*. *Envir. Biol. Fish.* 99: 275–291.
- Ralston, S., J. C. Field, and K. M. Sakuma. 2015. Long-term variation in a central California pelagic forage assemblage. *J. Mar. Syst.* 146: 26–37.
- Reiss, C. S., D. M. Checkley Jr., and S. J. Bograd. 2008. Remotely sensed spawning habitat of Pacific sardine (*Sardinops sagax*) and Northern anchovy (*Engraulis mordax*) within the California Current. *Fish. Oceanogr.* 17: 126–136.
- SAFE. 2017. Status of the Pacific coast coastal pelagic species fishery and recommended acceptable biological catches, stock assessment and fishery evaluation 2016. Pacific Fisheries Management Council, PFMC, Portland, OR 97220. pp. 1–92 http://www.pcouncil.org/wp-content/uploads/2017/05/CPS_SAFE_FINAL_May-2017.pdf.
- Shiraishi, M., N. Azuma, and I. Aoki. 1996. Large schools of Japanese sardine, *Sardinops malanostictus*, mate in single pair units at night. *Envir. Biol. Fish.* 45: 405–409.
- Smith, P. E., 1978. Biological effects of ocean variability: time and space scale ocean response. *Rapport-Exploration de conservation et d'exploration de la mer* 173: 117–127.
- Smith, P. E., and H. G. Moser, 2003. Long-term trends and variability in the larvae of Pacific sardine and associated fish species of the California Current region. *Deep Sea Research Part II: Topical Studies in Oceanography* 50: 2519–2536.
- Stacey, N. E., 1984. Control of the timing of ovulation by exogenous and endogenous factors. *In: Potts, G. W., Wootton, R. J. Z. Eds., Fish Reproduction: Strategies and Tactics.* Academic Press, London, pp. 207–222.
- Stierhoff, K. L., J. P. Zwolinski, and D. A. Demer. 2019. Distribution, biomass, and demography of coastal pelagic fishes in the California Current Ecosystem during summer 2018 based on acoustic-trawl sampling. NOAA-TM-NMFS-SWFSC-613.
- Takahashi, M., and D. M. Checkley Jr. 2008. Growth and Survival of Pacific sardine (*Sardinops sagax*) in the California Current Region. *J. North. Atl. Sci.* 41: 129–136.
- Takahashi, M., Y. Watanabe, A. Yatsu, and H. Nishida. 2009. Contrasting responses in larval and juvenile growth to a climate–ocean regime shift between anchovy and sardine. *Can. J. Fish. Aquat. Sci.* 66: 972–982.
- Trudeau, V. L., and R. E. Peter. 1995. Functional interaction between neuroendocrine systems regulating GtH-II release. *In Reproductive physiology of fishes*, Goetz, F. W., Thomas, P. (Eds). *Fish Symposium 95*, Austin, Texas, pp. 44–48.
- Yaron, Z. 1995. Endocrine control of gametogenesis and spawning induction in the carp. *Aquaculture* 129: 49–73.
- Zhou, Q., L. Wang, H. Wang, F. Xie, and T. Wang. 2012. Effect of dietary vitamin C on the growth performance and innate immunity of juvenile cobia (*Rachycentron canadum*). *Fish. Shellfish Immunol.* 32: 969–75.
- Zohar, Y., and C. C. Mylonas. 2001. Endocrine manipulations of spawning in cultured fish: from hormones to genes. *Aquaculture* 197: 99–136.
- Zwolinski, J. P., and D. A. Demer. 2013. Environmental and parental control of Pacific sardine (*Sardinops sagax*) recruitment. *ICES J. Mar. Sci.* 71: 2198–2207.

INSTRUCTIONS TO AUTHORS

CalCOFI Reports is a peer-reviewed journal. Papers submitted for publication in the “Scientific Contributions” section are read by two or more referees and by arbiters when necessary; “Symposium” papers are invited by the convener of the annual symposium and are reviewed and edited at the convener’s discretion. The “Reports, Review, and Publications” section contains newsworthy information on the status of stocks and environmental conditions; the papers in this section are not peer reviewed; the CalCOFI Editorial Board will not consider unsolicited review papers.

The CalCOFI Editorial Board will consider for publication in the “Scientific Contributions” section manuscripts not previously published elsewhere that address the following in relation to the North Pacific, the California Current, and the Gulf of California: marine organisms; marine chemistry, fertility, and food chains; marine fishery modeling, prediction, policy, and management; marine climatology, paleoclimatology, ecology, and paleoecology; marine pollution; physical, chemical, and biological oceanography; and new marine instrumentation and methods.

Submission Guidelines

Submissions are open year-round. Please submit manuscripts as MS word documents in electronic format via email to: calcofi_coordinator@coast.ucsd.edu. (use Word; see “Manuscript Guidelines” below for more details on preparing tables and figures). Include one complete file with all tables and figures for reviewers.

The manuscript should contain the following parts:

1. A title page containing the manuscript’s title, your name, your institutional affiliation and contact information (address, telephone and fax numbers, e-mail address), and a word count
2. An abstract of no more than 150 words that succinctly expresses only the manuscript’s most central points, using the active voice
3. Body of the text, including any footnotes
4. Literature cited, in alphabetical order
5. Acknowledgments, if any
6. Tables
7. Figures and captions

Manuscript Guidelines

Length. Unless previously approved by the Scientific Editor, manuscripts should not exceed 6,000 words, including title page, abstract, text body, footnotes, acknowledgments, and literature cited but excluding figures and tables.

Text. Double-space all elements of the text, allow margins of at least 1 inch on all sides, and use a standard font (such as Times or Times New Roman) no smaller than 12 points. Number the pages consecutively. Eliminate all nonessential formatting. Indi-

cate subordination of heads consistently; for example, use all caps for the main heads, boldface for the next level, and italics for the third level. To indent paragraphs, use the tab key, not the space bar or a “style” feature of any sort. Never use letters for numbers or vice versa; in other words, do not type the lowercase “el” for the number “one” or the capital letter “oh” for zero. Use your word-processor’s automatic footnoting feature to insert footnotes. Acknowledgments, if included, should be placed at the end of the text and may include funding sources. Place the entire text (title page, abstract, text body, footnotes, acknowledgments, and literature cited) in one document file, and label it with your name—for example, “Smith text.doc.”

Tables. Use your word-processor’s *Table* feature, rather than spaces or tabs, to create the columns and rows. Use *minimal* formatting, and do not insert vertical or horizontal rules. Double-space the tables and use a standard font, such as Times or Times New Roman. Number the tables consecutively, and provide a brief title for each. Place explanatory material and sources in a note beneath the table. Be sure each table is specifically referred to in the text.

Figures. Figures should be in black and white or color. Submit figures—whether drawings, graphs, or photographs—as separate, high-resolution electronic files (preferably 300 ppi for better printing purposes). Label the files, for example, “Smith fig 1” and “Smith fig 2.” If you are submitting as a PDF, please embed all fonts. If your figures are embedded in your Word docs, please create separate high-resolution PDF files of each figure from the original art file. Please review your files after saving them as PDFs, to make sure all your figures translated correctly. Contributors are advised to make a trial reduction of complex figures to ensure that patterns, shading, and letters will remain distinct when reduced. Include a north arrow and latitude and longitude lines on maps. Use consistent labels and abbreviations and the same style of lettering for all figures if possible. Number figures consecutively, and specifically refer to each in the text. Provide a caption for each figure. Gather the captions together, and place them at the end of the electronic text file, following the “Literature Cited” section.

Editorial Style

For matters of editorial style, contributors should consult recent editions of *CalCOFI Reports*. Contributors may also refer to *The Chicago Manual of Style*, 15th ed. Whenever possible, write in the first person, and use active verbs. Use the full name of a person, organization, program, or agency when mentioning it for the first time in your manuscript. Double-check the spelling of non-English words, and include special characters such as accents and umlauts. Use correct SI symbols for *units of measure* in figures, tables, and text (other units may be given in parentheses). Prepare *equations* in accordance with similar expressions in the printed literature.

Cite *sources* in the text as Smith (1999) or Smith and Jones (2000) or (Gabriel et al. 1998; Smith and Jones 2000) (the latter when there are three or more authors). There should be no comma between author and date. References should be cited in chronological order from the oldest to the most recent.

In the “Literature Cited” section, show sources alphabetically by the first author’s surname, and secondarily in chronological order with earliest dates first. Provide surnames and first initials of all authors; do not use “et al.” for multi-authored works. No source should appear in the “Literature Cited” section unless it is specifically cited in the text, tables, or figure captions. *Personal communications* and *unpublished documents* should not be included in the “Literature Cited” section but may be cited in the text in parentheses; use footnotes only when parentheses will not suffice. Abbreviate journal titles to match BIOSYS usage. Each source must be complete according to the following guidelines. Please note that initials follow the primary author’s surname, but for secondary authors initials come before the surnames:

ARTICLE IN A JOURNAL:

Barnes, J. T., L. D. Jacobson, A. D. MacCall, and P. Wolf. 1992. Recent population trends and abundance estimates for the Pacific sardine (*Sardinops sagax*). Calif. Coop. Oceanic Fish. Invest. Rep. 33:60–75.

BOOK:

Odum, E. P. 1959. Fundamentals of ecology. 2nd ed. Philadelphia: Saunders. 546 pp.

CHAPTER IN A BOOK:

Wooster, W. S., and J. L. Reid Jr. 1963. Eastern boundary currents. *In* The sea, M. N. Hill, ed. New York: Interscience Pub., pp. 253–280.

If your manuscript is accepted for publication, we will provide further guidance regarding preparing it for editing.

